Analysis of Physical Constraints in an Optical Burst Switching Network

vorgelegt von
Diplom-Ingenieurin
Hao Buchta
aus Berlin

von der Fakultät IV - Elektrotechnik und Informatik
der Technischen Universität Berlin
zur Erlangung des akademischen Grades

Doktor der Ingenieurwissenschaften
- Dr.-Ing. -

genehmigte Dissertation

Promotionsausschuss:

Vorsitzender:	Prof. Dr. Peter Pepper
1. Gutachter:	Prof. Dr.-Ing. Klaus Petermann
2. Gutachter:	Prof. Dr.-Ing. Peter Meissner

Tag der wissenschaftlichen Aussprache: 8. April 2005

Berlin 2005
D 83

Danksagung

Die vorliegende Arbeit entstand während meiner Tätigkeit als wissenschaftliche Mitarbeiterin am Fraunhofer-Institut für Nachrichtentechnik, Heinrich-Hertz-Institut Berlin. An dieser Stelle möchte ich mich zuerst bei allen Kollegen der Abteilung Optische Netze bedanken, die mich während der vergangenen Jahre unterstützt haben. Herrn E. Patzak gilt mein besonderer Dank. Seine stetige fachliche Hilfe und menschlicher Rat waren ganz entscheidendend für das Gelingen dieser Arbeit. Mein herzlicher Dank geht ebenfalls an Herrn G. Walf und allen HHI-Kollegen, die mit Interesse den Fortgang der Arbeit begleitet und mich stets mit Spezialwissen bei Problemlösungen aller Art unterstützt haben. Besonders J. Saniter, M. Schlosser, O. Brox, G. Bader, K. Schweers, J. Daase, K. Habel, E. Schulze, G. Reise, K. Peters, Ch. Casper, L. Molle, J. Bachus, R. Ludwig, H. Weber, V. Marembert, C. Schubert, A. Forck und R. Freund danke ich für Ihre tatkräftige Unterstützung. Hervorheben möchte ich insbesondere die Unterstützung von Herrn F. Raub bei der experimentellen Arbeit. Für ihre Mitwirkung im Rahmen ihrer studentischen Arbeiten danke ich den Herren R. Elschner und M. Nöller.

Mein besonderer Dank gilt vor allem meinem Doktorvater Herrn Prof. K. Petermann. Die zahlreichen Anregungen sowohl in persönlichen Gesprächen als auch im Rahmen von Vorträgen in seinem Seminar zur Optischen Nachrichtentechnik hat viel zum Substanzgewinn dieser Arbeit beigetragen. Seine großartige Unterstützung bei der Fertigstellung gab mir den Mut, diese Arbeit noch vor der Geburt meines Sohnes abzuschließen. Bei Herrn Prof. P. Meissner bedanke ich mich herzlich für die stetige Hilfsbereitschaft und die Übernahme des Zweitgutachtens. Für die Bereitschaft der Übernahme des Prüfungsvorsitzes bedanke ich mich bei Herrn Prof. P. Pepper. Frau G. Ernst danke ich für ihr freundliches Entgegenkommen. Sie haben alle entscheidend dazu beigetragen, daßich die wissenschaftliche Aussprache noch vor der Geburt meines Sohnes schaffen konnte.

Außerdem gilt mein Dank allen Kollegen innerhalb des BMBF-Verbundvorhabens TransiNet und der europäischen Projekte Nobel und E-Photon ONE. Besonders die Photonik-Gruppe vom Institut für Kommunikationsnetze und Rechnersysteme (IKR) an der Universität Stuttgart, vor allem Herrn Ch. Gauger, S. Junghans und K. Dolzer, danke ich für die exzellente und erfolgreiche Zusammenarbeit in den Jahren. Anschließend danke ich dem BMBF und der Europäischen Union für die finanzielle Unterstützung für die Förderung zahlreicher Forschungsprojekte.

Ferner gilt mein Dank meinen Eltern für den jahrelang tatkräftigen Beistand. Meinen Freunden danke ich für die Hilfe alle Art, insbesondere Karl Holdik. Schlußendlich möchte ich mich bei meinem Mann für seine unermüdliche Fürsorge und moralische Unterstützung während der ganzen Zeit bedanken. Und meinem Sohn Felix danke ich für seine Geduld und Verständnis in Mama's Bauch!

Zusammenfassung

Die vorliegende Arbeit leistet einen Beitrag zu den Untersuchungen von optischen „Burst“-vermittelten Netzen (Optical Burst Switching (OBS)). Die Leistungsfähigkeit, die technische Realisierbarkeit und die entstehende Komplexität solcher Netze wird eingehend untersucht.

Die optische Burst-Mode-Übertragung stellt besondere Anforderungen an die beteiligten Netzelemente, sowohl an die Übertragungsstrecke als auch an die Netzknoten. Die experimentellen und numerischen Untersuchungen des dynamischen Verhaltens der Erbium-dotierten Faserverstärker (EDFAs), die in den Übertragungsstrecken eingesetzt werden, zeigen die Notwendigkeit einer aktiven Regelung der Verstärker in OBS-Netzen. Die Reaktionszeit der Regelschleife muss im μs-Bereich liegen.

Unter Berücksichtigung vorhandener Komponenten und in naher/weiterer Zukunft zu erwartender Technologien für optische Netzknoten werden Knotenarchitekturen, die für OBS geeignet sind, entworfen und bewertet. Als Basis-Schaltelement eignet sich der optische Halbleiterverstärker (SOA) am besten dafür, große und schnelle, im μs-Bereich schaltende Netzknoten aufzubauen. Der Einflußverschiedener Signaldegradationsmechanismen auf die maximale Größe der Netzknoten wird anhand eines charakteristischen optischen Signalpfads innerhalb eines OBS-Netzes untersucht. Speziell für den sog. „Tune-and-Select“ (TAS)-Knoten lässt sich dabei feststellen, dass die Knotengröße eines SOA-basierten Netzknoten hauptsächlich durch das SOA-Rauschen, die Sättigung und die Dynamik der SOA-Verstärkung bestimmt sind. Durch den Einsatz der Verstärkungsstabilisierung und von rauscharmen optischen Halbleiterverstärkern kann ein maximaler Knotendurchsatz von mehreren Tbit/s erreicht werden.

Dieser theoretisch mögliche, maximale Knotendurchsatz kann aber in einem dynamischen OBS-Netz nie erreicht werden. Bei einer zu hohen Auslastung steigen die Burstverluste aufgrund der Burstkollisionen stark an. Der erreichbare effektive Durchsatz hängt deshalb von der tolerierbaren Burstverlustrate ab und diese hängt wiederum von den Burstreservierungsmechanismen und den Strategien zur Blockierungsauflösung im Netz ab. Die Untersuchungen der Leistungsfähigkeit verschiedener SOA-basierten Netzknoten zeigen, dass ihre technische Realisierung und die tatsächlich erreichbare Burstverlustrate miteinander gekoppelt sind. Eine abschließende Aussage über die Leistungsfähigkeit der OBS-Netzen erst dann möglich, wenn wie es in der vorliegenden Arbeit durchgeführt wird, sowohl die physikalischen bzw. technologischen als auch die verkehrstheoretischen Aspekte gemeinsam betrachtet werden.

Contents

List of symbols and abbreviations

Mathematical symbols

α_g ..... Damping constant of the Bragg region in the GC-SOA, page 104
α_H ..... Henry-factor, page 101
α_s ..... Scattering loss, page 100
α_{total} ..... Total loss in the GC-SOA, page 103
$\bar{P}_s$ ..... Averaged signal power, page 100
$\bar{P}_{laser}$ ..... Averaged laser power in the GC-SOA, page 102
$\bar{P}_{signal}$ ..... Averaged signal power in the GC-SOA, page 102
η ..... Gain cross saturation factor, page 102
Γ ..... Confinement factor, page 99
κ ..... Coupling coefficient, page 104
κ_{nl} ..... Gain compression factor, page 101
λ ..... Wavelength, page 62
μ_0 ..... Mean level of spaces, page 117
μ_1 ..... Mean level of marks, page 117
ν_{max} ..... Frequency for the maximum gain, page 105
ν_{tr} ..... Transparent frequency, page 105
ω ..... Angular frequency, page 102
ρ_{ASE} ..... Power spectral density, page 120
σ^2 ..... Variance, page 119
$\sigma^2_{ASE,\ ASE}$ ..... Variance of the ASE-ASE beat noise, page 119
σ^2_{shot} ..... Variance of the shot noise, page 119
$\sigma^2_{signal,\ ASE}$ ..... Variance of the signal-ASE beat noise, page 119
$\sigma^2_{thermal}$ ..... Variance of thermal noise, page 119
σ_0 ..... Standard deviations of spaces, page 117
σ_1 ..... Standard deviations of marks, page 117
τ_e ..... Effective carrier lifetime, page 102
τ_{pr} ..... Total processing delay for the reservation request, page 10
τ_{tr} ..... One-way propagation delay, page 10
A ..... The offered traffic load, page 143
B ..... Burst loss probability, page 143
b ..... Channel bit rate, page 10
B_r ..... Resolution bandwidth used for OSNR measurement, page 116

B_{ele} ..... Electrical Bandwidth, page 117
B_{opt} ..... Optical bandwidth, page 117
c ..... Light speed in vacuum, page 99
D ..... Decision threshold, page 119
d ..... Height of active zone of the SOA, page 168
D_{SSMF} ..... Chromatic dispersion of SSMF, page 137
D_{DCF} ..... Chromatic dispersion of DCF, page 137
e ..... Elementary charge, page 99
G ..... Gain of the amplifier, page 120
$g(n)$ ..... Material gain, page 99
g_{eff} ..... Effective gain coefficient, page 100
g_{max} ..... Maximum gain, page 105
g_{nl} ..... Nonlinear SOA gain, page 102
g_{th} ..... Gain at the threshold, page 103
$h\nu$ ..... Photon energy, page 116
I ..... Bias current, page 99
L ..... Length of transmission line, page 116
L_{SSMF} ..... Length of SSMF, page 137
L_{DCF} ..... Length of DCF, page 137
L_{gr} ..... Length of the Bragg region in the GC-SOA, page 104
M ..... Number of wavelength channel on a fibre, page 52
N ..... Number of fibres, page 56
n ..... Carrier density, page 99
n_{eff} ..... Effective refraction index, page 99
N_{dop} ..... Dopant density, page 165
n_{sp} ..... Spontaneous emission factor, page 120
P_N ..... Optical noise power, page 116
P_s ..... Optical signal power, page 100
$P_{receiver}$ ..... Receiver input power, page 93
P_{ASE} ..... ASE noise power, page 116
$P_{average,con}$ ..... EDFA Output power with a continuous input signal, page 34
$P_{in,sat}$ ..... Input saturation Power, page 74
$P_{out,sat}$ ..... Output saturation Power, page 74
Q ..... Q-factor, page 117
R ..... Carrier recombination rate, page 99
r ..... Reflection coefficient, page 104
R_{st} ..... Stimulated emission rate, page 99
S_s ..... Photon number in the active region of the SOA, page 99
V ..... Volume of the active region of the SOA, page 99
w ..... Width of active zone of the SOA, page 168
X_{Demux} ..... Crosstalk of the DeMux, page 129
X_{SOA} ..... Extinction ratio of the SOA, page 129

Abbreviations

AC ..... **A**ccess **C**ontrol
AC-DBR ..... **A**bsorption **C**hange DBR
AR ..... **A**nti-**R**eflection
ASE ..... **A**mplified **S**pontaneous **E**mission
ASK ..... **A**mplitude **S**hift **K**eying
ATM ..... **A**synchronous **T**ransfer **M**ode
AWG ..... **A**rrayed **W**aveguide **G**rating
BAS ..... **B**roadcast **A**nd **S**elect switching node
BAU ..... **B**urst **A**ssembly **U**nit
BER ..... **B**it **E**rror **R**ate
BHP ..... **B**urst **H**eader **P**acket
CapEx ..... **Cap**ital **Ex**penditure
CH ..... **C**arrier **H**eating
CR ..... **C**ompensation **R**atio
CW ..... **C**ontinuous **W**ave
CWDM ..... **C**oarse WDM
DBR ..... **D**istributed **B**ragg **R**eflector
DBR-SOA ..... The GC-SOA from AVANEX, page 78
DFG ..... **D**ifference **F**requency **G**eneration
DPSK ..... **D**ifferential **P**hase **S**hift **K**eying
DQPSK ..... **D**ifferential **Q**uadrature **P**hase **S**hift **K**eying
EAM ..... **E**lectro-**A**bsorption **M**odulator
ECL ..... **E**xternal **C**avity **L**aser
EDFA ..... **E**rbium **D**oped **F**ibre **A**mplifier
FDL ..... **F**ibre **D**elay **L**ine
FWM ..... **F**our **W**ave **M**ixing
GC-SOA ..... **G**ain -**C**lamped SOA
GCSR ..... **G**rating assisted **C**oupler with **S**ampled **R**eflector
GMPLS ..... **G**eneralised **M**ulti-**P**rotocol **L**abel **S**witching
IBT ..... **I**n **B**and **T**erminator
IM ..... **I**ntensity **M**odulation
IP ..... **I**nternet **P**rotocol
IPDR ..... **I**nput **P**ower **D**ynamic **R**ange
ISI ..... **I**nter **S**ymbol **I**nterference
IWC ..... **I**nterferometric **W**avelength **C**onverter
JET ..... **J**ust-**E**nough-**T**ime
JIT ..... **J**ust-**I**n-**T**ime
LAUC ..... **L**atest **A**vailable **U**nscheduled **C**hannel
MEMS ..... **M**icro-**E**lectro-**M**echanical **S**ystem
MI ..... **M**ichelson **I**nterferometer
MQW ..... **M**ulti **Q**uantum **W**ell
MZI ..... **M**ach **Z**ehnder **I**nterferometer

NF ..... **N**oise **F**igure
NRZ ..... **N**on **R**eturn-to-**Z**ero
OADM ..... **O**ptical **A**dd/**D**rop **M**ultiplexer
OBS ..... **O**ptical **B**urst **S**wichting
OCS ..... **O**ptically **C**ircuit **S**witching
OEO ..... **O**ptical-**E**lectronic-**O**ptical
OFS ..... **O**ptical **F**low **S**witching
OpEx ..... **Op**eration **Ex**penditure
OPS ..... **O**ptical **P**acket **S**witching
OSNR ..... **O**ptical **S**ignal-**T**o-**N**oise **R**atio
OXC ..... **O**ptical Cross-**C**onnect
PDF ..... **P**robability **D**ensity **F**unction
PMD ..... **P**olarization **M**ode **D**ispersion
PPNL ..... **P**eriodically **P**oled $LiNbO_3$
PRBS ..... **P**seudo **R**andom **B**it **S**equence
QD ..... **Q**uantum **D**ot
QoS ..... **Q**uality **o**f **S**ervice
RAM ..... **R**andom **A**ccess **M**emory
RFD ..... **R**eserve a **F**ixed **D**uration
RLD ..... **R**eserve a **L**imited **D**uration
RSP ..... **R**eceiver **S**ensivity **P**enalty
SCDT ..... **S**eparate **C**ontrol and **D**elayed **T**ransmission
SFBG ..... **S**ampled **F**ibre **B**ragg **G**rating
SGDBR ..... **S**ampled **G**rating DBR
SHB ..... **S**pectral-**H**ole **B**urning
SMSR ..... **S**ide **M**ode **S**uppression **R**atio
SOA ..... **S**emiconductor **O**ptical **A**mplifier
SSG-DBR ..... **S**uper **S**tructure **G**rating DBR
SSMF ..... **S**tandard **S**ingle **M**ode **F**ibre
TAS ..... **T**une **A**nd **S**elect switching node
TAS-dFDL .... **TAS** node with **d**edicated **FDL** buffer
TAS-LTR ..... **TAS** node with wavelength converters of **L**imited **T**uning **R**ange
TAS-shFDL ... **TAS** node with **sh**ared **FDL**
TE ..... **T**ransversal **E**lectric
TM ..... **T**ransversal **M**agnetic
TW ..... **T**ravelling **W**ave
VC ..... **V**irtual **C**ircuits
VCSEL ..... **V**ertical **C**avity **S**urface **E**mitting **L**aser
WDM ..... **W**avelength **D**ivision **M**ultiplexing
WLAN ..... **W**ireless **L**ocal **A**rea **N**etwork
WR-OBS ..... **W**avelength **R**outed OBS
XGM ..... Cross **G**ain **M**odulation
XPM ..... Cross **P**hase **M**odulation

Chapter 1

Introduction

The Internet and thus the Internet Protocol (IP) are currently the basis for most of the information exchange all over the world. Sending e-mails for short private messages as well as for rapid transmission of large business documents, obtaining updated information with search engines, doing home shopping and so on are almost a natural part of people's lives. Over the last decades the data traffic has been grown exponentially. Despite the telecom industry crisis in the beginning of the century, there is no indication that this exponential data traffic growth will stop. Two main drivers for this growth could be the broadband access (e.g. Gigabit Ethernet technology in fixed access networks, wireless local area networks (WLANs) in mobile access networks) and the new sophisticated, bandwidth-hungry services such as video telephony, online gaming, remote education, dynamic navigation systems in the automobile, and so on. Such new services require high bandwidth, and new applications will appear as soon as higher bandwidth will be provided. A conservative estimate predicted that Internet traffic will approximately double every year. Consequently, the telecommunication networks must be capable of providing huge and increasing capacities.

In order to accommodate this capacity requirement, efficient and cost-effective wavelength division multiplexing (WDM) point-to-point connections can be used between network nodes. Another and very important advantage of WDM is that it is relatively simple to upgrade the network by adding extra wavelength channels. This is essential due to the rapid increase in capacity requirement. Today up to several Tbit/s traffic can be carried by the optical links over long distances. E.g. in an ultra-dense WDM transmission experiment transmission of the total capacity of 10.92 Tbit/s have already been demonstrated [1].

In such high capacity point-to-point links the information is transmitted in the optical domain but converted to the electrical domain at the nodes for switching and signal processing. However, the huge bandwidth carried by the optical fibres leads to a mismatch with the current electronic switching technologies. To achieve

throughput capacities above 1 - 2 Tbit/s electronically, the main hurdles for their practical realization are the robustness of high speed interconnections, power dissipation of integrated circuits, and the need for multicard switching fabrics and eventually multiple racks [2]. This boundary may naturally move with time but the point is that above a certain throughput capacity, optical solutions appear superior. It is advantageous to route and switch at granularity levels adapted to these high-capacity links. In this context, WDM also opens the possibility of utilising the wavelength domain for switching and routing purposes in the optical domain.

Based on the above facts, the intelligent optical network seems to be the only solution that can not only provide large capacity links in a flexible, dynamic, and cost-effective way, but also be capable to overcome any bottlenecks and limitations arising from the electronic processing. Therefore today the WDM optical communication systems are evolving from simple optical point-to-point links to complex network architectures, which will enable dynamic optical networking. The first step towards a dynamic optical network is achieving networking in the wavelength-routed networks by using the optical add/drop multiplexers (OADM) and optical cross-connect (OXC) nodes. These nodes can provide provisioning capabilities as well as protection and restoration in the optical layer. Routing and management of the traffic demands is likely to be applied through the generalised multi-protocol label switching (GMPLS), a control plane offering intelligence in the optical layer. Whether optical or electronic switching technologies will be deployed is still a major issue. However, transparent solutions e.g. optically circuit switching (OCS) networks offer attractive features associated with reducing unnecessary Optical-Electronic-Optical (O/E/O) conversions, supporting transparent networks with reduced capital expenditure (CapEx) and operation expenditure (OpEx).

However, it is also expected that the data traffic will soon constitute the major part of the total traffic compared to the traditional voice traffic, which only has experienced a small and constant increase over the last years. Therefore, a paradigm shift in the telecommunications industry from voice-optimised to IP centric networks is the result. The growth of Internet traffic and related services do not only require an optical network which is able to deliver large capacity links in a flexible, dynamic way, but also the change from voice traffic to IP sets up some new network requirements due to the nature of IP traffic, e.g. the burstiness of the connection durations, self-similarity and asymmetry [3]. That means the traffic load in the network does not become constant in time when many bursty IP sources are combined and the required bandwidth is not the same in both directions. A highly dynamic connection pattern results in large variation of the mean traffic load and very short-term traffic demand can be caused. Also the requirement of broadband access and new services prohibit a static allocation of bandwidth or a configuration which cannot be changed on demand within a very short interval in time. Hence a network based on wavelength switching, e.g. OCS, where the available optical

bandwidth is switched in the wavelength domain, can just offer an coarse granularity which may not be able to fulfill the desired flexibility and efficiency [4]. To avoid excessive delay and extensive buffering at the ingress router, large numbers of connections and of the bandwidth reservation of each connection would be required. Also the range of future services will be very diverse in terms of required channel capacity, channel occupancy, duration set-up time and frequency.

Therefore a new IP-centric transport network architecture is required. A dynamic optical layer with requirements for smaller connection set-up times and fine switching granularity should be inserted. The promising solutions in this context are the optical packet based networks. E.g. optical packet switching (OPS) like its electronic counter part has been suggested as a switching paradigm that will efficiently utilise the available fibre bandwidth, by statistically multiplexing information from different sources on the same channel. Although a lot of research works on OPS have been performed in the past, its realisation is still far in the future. This is mainly because of the costly realisation of sophisticated optical buffers, the need of synchronisation of packet header and payload, and the fact that header processing still cannot be performed all-optically at reasonable cost. Therefore, alternative IP-centric transport network architectures are required to overcome this technological challenges but still use the bandwidth more flexible and efficiently than OCS. To account for this, a hybrid approach Optical Burst Switching (OBS) has been proposed as a compromise between OCS and OPS [5, 6].

To realise an OBS network, a new optical layer is mandatory. Only the ability to provide huge link capacities and to transmit optical signals over long-distance without regeneration are insufficient now. The current WDM system has to be upgraded to be able to support optical burst mode transmission. The signal power of the single channels in the WDM links will no longer be constant and will change according to the burst length and the gaps between them. Also the bursts could have different signal powers. This results e.g. in dynamic gain changes in the erbium-doped fibre amplifiers (EDFAs) in the transmission links, which in turn leads to possibly large variations of the output power of the data channels. That means some modifications must be introduced even on the transmission link. Also advanced photonic components and subsystems are needed. E.g. the burst mode receivers are needed to receive the incoming bursts. They must recover the clock in a small fraction of the burst length, and need to dynamically compensate for the power fluctuations along the transmission links.

Furthermore, an OBS network will be only possible if fast and large switching nodes can be built. To constitute the OBS network nodes several key components are needed, e.g. optical space switches, tunable filters/lasers, wavelength converters etc. Even though some techniques are commercially available now, improvement of their performance is still essential. Their physical and technological constraints

will have strong impact on the choice of the node architecture. Signal degradation will be caused and could lead to an increased bit error rate (BER), which limits the maximum size and the maximum throughput of the nodes.

Goal of the Work

The intention of this thesis is to investigate the required complexity and technical feasibility of an OBS network. Different physical and technological constraints in an OBS network are analysed by considering available and expected technologies in short and long term. This investigation is performed in three steps:

- First the impact of OBS on the optical transmission is analysed. The focus here is on an experimental and numerical investigation of the dynamic behavior of the EDFAs in a burst switching environment. Also the optimum method for the gain stabilisation of the EDFAs is assessed.

- Second, different OBS core node architectures are designed. In an OBS core node the semiconductor optical amplifier (SOA) is the key component. Therefore different state-of-the-art SOAs are evaluated through both experimental work and modelling. To evaluate the maximum size of the different OBS core nodes, characteristic of optical signal paths within such nodes are investigated by considering different signal degradation mechanisms.

- The final part of the work combines the physical and traffic considerations. Depending on the OBS core node architectures, burst losses can occur in case of contention at the output of the nodes. Therefore both signal degradation and burst losses must be considered to evaluate the effective throughput of such nodes. To provide a better and more balanced view on the design of OBS nodes an analysis by considering the physical and the traffic performance is performed for different node architectures.

This work is organized as follows: at the beginning of the work, a short overview of the recent status and future challenges of optical network is given to motivate the network evolution towards a dynamic optical switched network. Furthermore, the currently discussed transport network architectures such as Optical Circuit Switching (OCS), Optical Packet Switching (OPS) and Optical Burst Switching (OBS) are presented and classified in **Chapter 2**. According to the fact that the scope of this work lies particularly in the technical feasibility of an OBS network, the OBS network architecture is described in detail. Afterwards the basic requirements for the physical layer of an OBS network are derived.

Then this work deals with the analysis of the impact of OBS on optical transmission and the required key building blocks to upgrade the current WDM systems. In **Chapter 3** first a short overview of the existing prototypes and demonstrators for fast tunable transmitters and burst mode receivers represents the state-of-the-art

technologies. The main focus in this chapter is the experimental and numerical investigation of the dynamic behaviour of erbium-doped fibre amplifiers (EDFAs) in a burst switching environment. Different methods for the gain stabilisation are categorized and their advantages and disadvantages particularly with regard to the OBS networks are discussed.

The following three chapters represent the second part of the work. In **Chapter 4** the key components required for enabling OBS core nodes such as optical space switches, wavelength converters, passive splitters/combiners and so on are discussed and the main requirements for them are identified. To build large OBS core nodes fast optical space switches with a switching time less than 1 μs are essential. The choice of today's commercially available optical space switches is extremely limited. SOAs seem to be the most promising ones to be used as on/off gates in the OBS core nodes, where the gain is switched on and off electronically. Therefore two "broadcast and select" OBS core nodes based on the SOA gates are selected for the comprehensive investigation in the following chapters.

In **Chapter 5** the basic characteristics of the state-of-the-art SOA gates are presented, including both modelling and experimental investigations. First the main requirements for SOAs as on/off gates are identified. The following review of the recent developments in SOA technology shows that only two gain-clamped SOAs (GC-SOAs) can fulfill all these requirements and are presently commercially available. Therefore the experimental investigations in this chapter are concentrated on these two GC-SOAs. The static as well as dynamic characteristics of these two GC-SOAs are compared with a convectional SOA experimentally. Important parameters such as the on/off ratio, the input saturation power, and the dynamic range for the input power are investigated. Finally, simple models of the conventional SOA and GC-SOA are developed and validated experimentally.

Using the models developed in Chapter 5, a physical evaluation of the two "broadcast and select" OBS core nodes based on the SOA gates, which were selected in Chapter 4, is performed in **Chapter 6**. First a power budget analysis is done. Compared to the so-called "Broadcast-and-Select" (BAS) switching node the so-called "Tune-and-Select" (TAS) switching node is the more promising architecture for OBS applying SOAs. So the investigation in this chapter is focused on the TAS nodes. Contrary to digital electronic switches, photonic switches are analogue and signal regeneration is not implicitly performed. Several impairments like noise, crosstalk of WDM channels, SOA gain saturation and dynamics, and so on lead to signal degradation and an increased bit error rate (BER). These effects limit the maximum node size and the maximum throughput of the nodes. Therefore different signal degradation mechanisms and their impacts on the maximum size of the TAS nodes are then analysed and discussed step by step.

In an OBS network, bursts are sent without an acknowledgement of successful path set-up (one-pass reservation) and burst loss can occur in case of contention. So the effective throughput of an OBS core node is not only limited by the signal degradation but also by the burst losses. Physical and traffic considerations should be integrated. Based on the results of the physical evaluation, in **Chapter 7**, the final part of this work, the effective throughput of TAS nodes is calculated by additionally considering the traffic characteristics. To show the benefit of such integrated evaluation the analysis is then extended to different variations of TAS nodes. To increase the maximum throughput of the node, a TAS node with wavelength converters of limited tuning range (TAS-LTR) is designed. On the other hand to improve the effective throughput of the node, the fibre delay lines (FDLs) can be used. They could be provided either per output (TAS-dFDL) or per node (TAS-shFDL). This part of the work was performed in collaboration with Christoph Gauger from the Institute of Communication Networks and Computer Engineering (IKR), University Stuttgart.

Finally, **Chapter 8** concludes the thesis with a summary of the results presented in this work.

Chapter 2

Optical Network Architectures

Over the last years, several switching techniques have been proposed in the literature for supporting IP traffic over WDM-based optical networks. According to the classical definition in the voice and data communications all of them can be classified into circuit-, packet-, and burst-switching. While the first two have been used for many years for the voice and data communications, the burst switching is less popular. Therefore concepts like optical circuit switching (OCS) and optical packet switching (OPS) have also been adapted to optical networks and investigated intensively for quite a while. In contrast, optical burst switching (OBS) was introduced only recently for WDM-based optical networks, and is thus not as well understood as OCS and OPS. Accordingly, questions such as what are the differences and similarities between burst switching and circuit/packet-switching in general, and specifically, between OBS and OCS/OPS have been raised.

Fig. 2.1 depicts a possible evolution scenario of optical networks against time. The deployment of WDM technology started with static point-to-point links. Later, ring and meshed networks followed which increased the functionality compared to static circuit switched networks. More dynamics in the networks can be reached then with dynamic fast circuit switching, burst switching, and packet switching, which all are not yet applied today.

Comparing the characteristics of these three different switching technologies, the circuit switching has the coarsest granularity with respect to the switching granularity. In a WDM based optical circuit switching network fibres, wavelength bands or wavelengths can be switched by using different optical cross-connects (OXCs). The packet switching has the finest granularity and in an OPS network the packets e.g. in the KByte range are switched optically. The burst switching has a granularity between circuit and packet switching. In an OBS network aggregated packets, the so-called bursts with e.g. several tens of Kbytes are switched optically. In contrary to OCS, OPS and OBS are both expected to better support dynamic traffic patterns and improve the utilisation of the network resources. The required

switching complexity (e.g. switching time, optical signal processing) of OBS is between OCS and OPS. The limits between those architectures are not sharp and - depending on the applied definition - they even overlap.

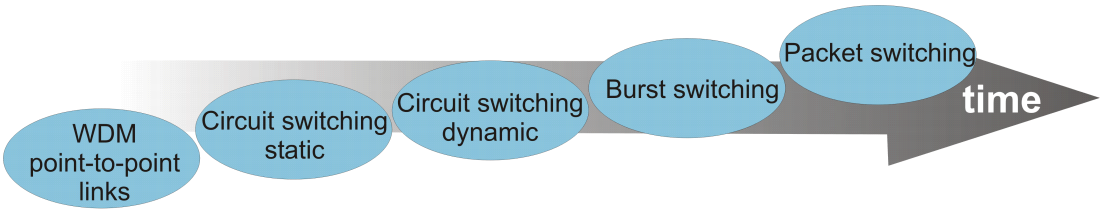

Switching technology	Granularity	Utilisation	Complexity
Ciruit switching	Coarse	Poor	Low
Burst switching	Moderate	Moderate	Moderate
Packet switching	Fine	High	High, not mature

Figure 2.1: A possible evolution scenario of optical networks.

In this chapter these three optical network architectures are introduced and compared. In Section 2.1 the main characteristics of OCS approach are described and their advantages and disadvantages are given. In Section 2.2 the main challenges of OPS approach are discussed. Finally, Section 2.3 the hybrid approach OBS is defined and described in detail, which can be considered as a compromise between OCS and OPS.

2.1 Optical Circuit Switching (OCS) - Wavelength Routing in WDM Networks

In general, circuit switching has three distinct phases, circuit set-up, data transmission and circuit tear-down. One of the main features of circuit-switching is its two-way reservation process in phase 1, where a source sends a request for setting up a circuit and then receives an acknowledgment back from the corresponding destination. A circuit is set-up by reserving a fixed bandwidth channel on each link along a path from the source to its corresponding destination. Another feature of the circuit-switching is that all the intermediate switches will be configured to connect the channels on the adjacent links in order to form a circuit, and remain so for the duration of the call. This feature also implies that no buffering of data is needed at any intermediate node.

In WDM networks, circuit-switching takes the form of wavelength routing, where an all-optical wavelength path is established between edges of the network. This optical path is called a lightpath and is created by reserving a dedicated wavelength channel on every link along the path. This lightpath is then released after the data transmission. Such wavelength routing networks can be built with fixed or tunable optical add-drop multiplexer (OADM) as well as optical cross connect (OXC) nodes connected by point-to-point fiber links in an arbitrary topology. As a result, the data transmissions between the endpoints of a lightpath require no processing, no E/O conversion, and no buffering at intermediate nodes. While the (tunable or reconfigurable) OADMs only add or drop one or more specific WDM channels in the network and do not reconfigure the through traffic, using reconfigurable WDM OXC nodes the input channels can be switched to the output channels optionally. The basic building blocks in the OXC nodes are the space switches, which provide the connectivity between the channels on the input ports and the channels on the output ports. Some vendors have already announced various OXC nodes, mostly incorporating optical Micro-Electro-Mechanical Systems (MEMS) switches, with the throughput capacities above 2.07 Petabit/s [7]. Additionally such systems have been already successfully demonstrated in several network experiments, e.g. [8–10].

In addition to providing high-speed, high-bandwidth lightpaths that are transparent to the bit rate and the modulation format, wavelength routing is especially suitable for supporting Synchronous Optical Network/Synchronous Digital Hierarchy (SONET/SDH) communication. The reasons for this are [11]:

- SONET/SDH switches communicate with each other at a constant bit rate that matches the bandwidth of a wavelength (e.g. 2.5 Gbit/s or OC-48).
- The connection duration is long relative to the path set-up time.
- The number of expensive SONET switches can be reduced with proper traffic grooming and wavelength assignment algorithms.
- The optical switches (wavelength routers) based on e.g. MEMS are currently available.

In the OCS networks three different switching granularities can be defined generally: optical fibre, wavelength band, and wavelength [12], where a wavelength is the finest switching granularity. The wavelength routing can be performed either statically or dynamically. In a static wavelength routing network, given a limited number of wavelengths, only a limited number of wavelength paths can be established at the same time. Some data may still need to go through O/E/O conversions. In a dynamic wavelength routing network wavelength paths are established (and released) dynamically to alleviate the above problems. For such fast dynamic circuit switching networks, the synonyms like optical flow switching (OFS) [13] and wavelength routed OBS (WR-OBS) [14–16] can be found in the literature. Here a wavelength is only allocated for the duration of the call and

released afterwards. Two-way reservation and an end-to-end (two-way) signaling, respectively, is performed for reserving a wavelength before the transmission of the first Byte starts. It guaranties a free optical path between the source and the destination. Its advantage is that losses cannot occur after a connection is established. The only service degradation is the (call) blocking probability at establishing a connection or by grooming to a wavelength. The disadvantage of this approach is the wasted bandwidth in the networks, i.e., the amount of Bytes which can be transmitted during an end-to-end signaling. It increases with increasing channel bit rate b in Gbit/s. The offset time T in ms between a reservation request and the data transmissions is at least as long as $2 \cdot \tau_{tr} + \tau_{pr}$, where τ_{tr} is the one-way propagation delay and τ_{pr} is the total processing delay encountered by the reservation request along the path. Therefore the wasted bandwidth B_{wasted} in MByte can be calculated according to

$$B_{wasted}[MByte] = T[ms] \cdot \frac{b[Gbit/s]}{8} = (2 \cdot \tau_{tr}[ms] + \tau_{pr}[ms]) \cdot \frac{b[Gbit/s]}{8} \quad (2.1)$$

In Fig. 2.2 the wasted bandwidth by using optical circuit switching versus the distance between source and destination are shown for different channel bit rates. A processing delay $\tau_{pr} = 10\ ms$ is assumed.

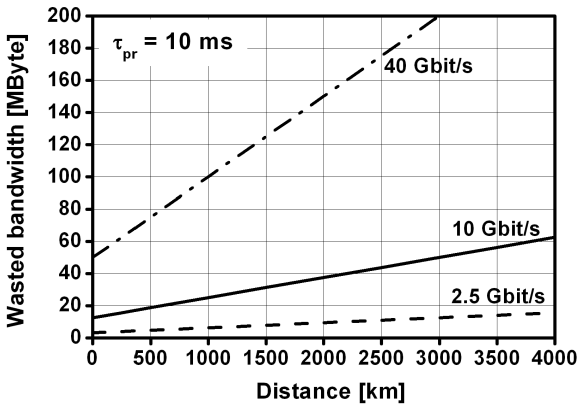

Figure 2.2: The wasted bandwidth by using OCS versus the distance between source and destination for different channel bit rates, with a processing delay $\tau_{pr} = 10\ ms$.

It can be seen that already for a one-way distance of 1000 km, e.g., Flensburg - Stuttgart, a considerable amount of the bandwidth cannot be used due to waiting for the acknowledgment of the connection. In case of, e.g., 10 Gbit/s, 25 MByte are wasted with a processing delay $\tau_{pr} = 10\ ms$. The amount of wasted bandwidth increases proportional to the channel bit rate. That means, in a wavelength routed network, the bandwidth cannot be used during the circuit set-up and circuit teardown. This might lead to a poor utilization of the network resources if the mean data transmission time of the data is not significantly greater than the time for

signalling. Furthermore, large buffers are required at the network ingress to buffer the packets which wait for the acknowledgment of the connection. Additionally, another waste of bandwidth is caused by the time to detect the end of a data transmission in order to release the allocated resources.

However, as a form of circuit switching networks, wavelength routed networks do not use statistical sharing of resources and therefore provide a low bandwidth utilization if the traffic to be supported is bursty. Since Internet traffic is self-similar (or bursty at all time scales), this means that providing wavelength paths between two remote IP routers may not be efficient. On every channel, a large amount of bandwidth has to be over-allocated in order to be also able to transport traffic peaks. Thus, most of the time this amount of bandwidth is not used. To use the networks more efficiently, packet-based optical networks are required.

2.2 Optical Packet Switching (OPS)

In a packet switching network, the length of each packet can be either fixed or variable. For the voice communications, fixed-length packets e.g. digitized voice packets are used, but for the data (computer) communications, variable-length packets e.g. IP packets are used. A disadvantage of using small, fixed-length packets is that the percentage of control overhead is higher (due to a relatively larger header in each packet) and the bandwidth utilization is lower (due to both headers and possible paddings, that means fill the packets with dummy data to achieve the fixed-length) than using variable-length packets.

Such packets can be switched either based on virtual-circuits (VCs) or datagrams. In VC-based packet switching (used by Asynchronous Transfer Mode (ATM)), a VC is established first (implying that routing is already done) and hence, each packet's header carries a label (e.g. a VC identifier). At every intermediate node the packets are forwarded (or switched) on the basis of their labels (layer 2 forwarding). In datagram-based packet-switching (used by IP), a packet header contains the destination address of the packet. At every intermediate node the packets are forwarded (or routed) on the basis of their destination addresses (layer 3 forwarding). IP traffic is processed and switched at every IP router on a packet-by-packet basis. An IP packet contains a header and a payload. The packet header contains the information required for routing the packet, while the payload carries the actual data. A main feature of both variations of packet-switching is the store-and-forward. That is, a packet needs to be completely assembled (and received) by a source (at each intermediate node) before it can be forwarded. One of the implications of this feature is that a packet will experience a delay which is proportional to its length at each node. In addition, a buffer of the size at least equal to maximum length of the packet is needed at each intermediate node.

To realise such packet based networks in optical WDM networks, optical packet switching (OPS) like its electronic counter part has been proposed [12, 17–20]. In the OPS networks a packet is the finest switching granularity. OPS is suitable for supporting bursty traffic since it allows statistical sharing of the channel bandwidth among packets belonging to different source and destination pairs. Therefore, better bandwidth utilisation can be achieved compared to optical circuit switching (OCS). During the last 15 years several European research projects have been carried out with a main focus on OPS [4, 21–24]. At the beginning of these projects the OPS concept was switching individual optical packets from one node to another without any O/E/O conversions. Packet header recognition, header processing and control would all be performed all-optically on a packet-by-packet basis. However, this pure form of OPS requires technologies that are not available as products. The efficiency of this approach is indeed questionable, at least in the foreseeable future. Therefore within these projects the notion of OPS is evolving very rapidly and the recent trends and challenges of OPS can be summarised as follow:

- **Packet length and aggregation degree**
  In general, IP packets have a length between 40 to 1500 bytes [25]. While 40 bytes is a typical length for the control packets, 1500 bytes is not a principle upper limit for IP packets but given by the lengths of Ethernet packets. In most OPS proposals a fixed packet length is assumed. E.g. in [19,22,26] each packet is inserted in a time slot of a fixed duration (1.646 μs, it corresponds to 128 bytes including 14 bytes for header at 622 Mbit/s). It includes a 14 bytes header with a fixed bit rate (e.g., 622 Mbit/s, compatible with electronic processing) and a payload that corresponds to a fixed time duration, where information is carried regardless of the bit rate (e.g., from 155 Mbit/s up to 10 Gbit/s). A guard time is inserted before and after the payload of the packet to allow the setup of the photonic devices during the switching operations and to allow for some payload phase jitter [17,19,22]. A larger packet length is proposed in [27] with 122 bit header and 3050 bit payload at 2.5 Gbit/s. Concepts with variable packet length can also be found [28, 29]. Therefore OPS typically requires a very low degree of IP packet assembly, at a bit rate above 10 Gbit/s (1500 bytes corresponds to 4.8 μs at 2.5 Gbit/s and 1.2 μs at 10 Gbit/s). However, the aggregation degree needed for the same packet length, increases with the bit rate. Furthermore, using fixed packet length fragmentation of IP packets and/or padding of packets could be necessary depending on the packet length, which would increase the overhead (waste of bandwidth) and egress node complexity. Additionally the mean packet length determines how fast switching has to be carried out, as the time for switching has to be significant shorter than the time to transmit a packet. For a packet length in the range of few μs switching time has to be in the nano-second range.

- **Position and processing of packet header**
  In OPS, the packet header can be sent "in-band" either with the same wavelength just ahead of the payload (serial header) or in parallel to the payload at a lower frequency by subcarrier multiplexing. It can also be sent "out-band" on a different wavelength. The header processing can be done transparently in the optical domain or opaquely requiring an O/E/O conversion in every node. Concepts where the headers are processed in the optical domain are still far away from implementation. However, if the header is transported at a lower bit-rate than the payload, low-cost electronics can be used for processing. Subcarrier multiplexing has the disadvantage that routing decisions can only be carried out after receiving the packet. This may cause longer delays in the case if packets are very long. If the packet header is sent on a separate wavelength, it is easy to demultiplex the header at every node. But more effort is required in order to ensure realignment between header and payload. Finally, serial transmission requires more bandwidth for header extraction.

- **Synchronisation of packet header and payload**
  In general, OPS networks can be divided into two categories: synchronous (slotted) and asynchronous (unslotted). As packet length can be fixed or variable, four potential cases can be classified according to synchronization and packet length: synchronous (slotted) and fixed length packet mode, asynchronous (unslotted) and fixed length packet mode, synchronous (slotted) and variable length packet mode, asynchronous (unslotted) and variable length packet mode. The most studied case in the literature is the synchronous (slotted) and fixed length packet mode [21, 30, 31] and it is considered to be the best choice for OPS in general. In this mode a switch matrix will have less contention than when operating in asynchronous (unslotted) mode [32]. The disadvantages of synchronous (slotted) operation are the needs for optical synchronizers at the switch interfaces and a global network clock. More recently, work on variable length packets have also been studied for OPS, with both asynchronous (unslotted) [28, 29, 33] and synchronous (slotted) operation (typically trains of packets) [34]. Among both the asynchronous (unslotted) and variable length packet mode is the more promising one. It has less overhead and avoids the needs for a network global clock and an optical synchronisation, and it reduces the edge node assembly complexity [28].

- **The need of large optical buffer**
  One of the biggest challenges of OPS is that there is no optical equivalence of the random access memory (RAM). Accordingly, an optical signal can only be delayed for a limited amount of time via the use of fibre delay lines (FDLs). Furthermore, the length of each packet cannot exceed that of the available FDL in order for the optical packet to be "stored". Therefore

such FDL based buffer can be designed and managed much simpler for fixed than for variable length packets. To perform more sophisticated buffering, methods like cascading FDLs of different lengths have been already proposed in [28, 35]. However, it is still difficult to apply fine-grain optical buffers, e.g. large fiber delay line buffers.

Despite much research works on OPS, its realization is still far in the future. This is mainly because of the costly realization of sophisticated optical buffers, the need of synchronisation of packet header and payload, and the fact that header processing still cannot be performed all-optically at reasonable costs. Therefore, alternative IP-over-WDM optical network architectures are required to overcome these technological challenges but still use the bandwidth more flexible and efficient than optical wavelength switching. To account for this a hybrid approach Optical Burst switching (OBS) has been proposed [5, 6].

2.3 Optical Burst Switching (OBS)

Although the concept of burst switching has been already known since the 1980s [36, 37], it has never been a big success in electrical networks. The main reason is that its complexity and realization requirements are comparable to that of more flexible electronic packet switching techniques. However, with the introduction of very high capacity WDM optical transmission techniques, the discrepancy between optical transmission capacity and electronic switching capability increases. Moreover, due to cost and complexity aspects, it is advantageous to keep data in the optical domain and to avoid bit-level signal processing. As already mentioned in previous sections, OCS does not support fine switching granularity on the packet-level. Only a poor bandwidth utilisation is obtained due to the absence of statistical multiplexing. On the other hand, OPS is still too complex to be realised in the near future. Therefore, a hybrid approach like burst switching seems promising for the WDM-based optical networks.

Optical burst switching (OBS) was proposed in the late 1990ies [5, 6] and it tries to combine the advantages of both OCS and OPS approaches and avoid a part of their drawbacks. During the past years, there are large efforts to realise OBS. Their main focus were important topics like new reservation mechanisms [6, 11, 29, 38, 39], assembly mechanisms [38, 40–43], prototypes [44, 45] and network architectures [43, 46–50]. At the moment, due to the fast development of this new approach and the large number of new proposals, OBS is still at its definition phase and no common definition of OBS can be found. However, among several different definitions two main directions can be found. One is more oriented towards fast wavelength switching. Synonyms like optical flow switching (OFS) [13] and wavelength routed OBS (WR-OBS) [14–16] can be found in the literature. Here, an acknowledged two-way reservation is generally used. A burst

will be only transmitted after having received a positive acknowledgement of its reservation request. The advantage of such a scheme is that no burst is lost in the network core. However, blocking of the network has to be considered which leads to either additional delay or to buffer overflow (and thus losses) at the network ingress. Additionally, acknowledged two-way reservation could result in large wasted bandwidth for long distance and high link bit rates as shown in Fig. 2.2 on page 10.

Another most widely-used definition for OBS is more packet oriented and was proposed by Qiao and Turner [5, 6, 11] and will be considered in this thesis. The main characteristics of this OBS type can be summarised as follows (the definition is given in [39, 51]):

- Client layer data (IP-Packet) is aggregated and assembled into variable length optical bursts in edge nodes. OBS assumes more extensive burst aggregation, to realize bursts with payloads typically carrying tens of KBytes.
- There is a separation between control information (header) and user information (data) in space and in time. Control header packets are sent on a separate wavelength (out-of-band) and processed electronically in all OBS core nodes to set up the switch matrix before the data bursts arrive.
- Data bursts are asynchronously switched in core nodes and stay in the optical domain until they reach their destination edge node. Only wavelength conversion and/or some degree of regeneration is applied to the signal.
- Resources are allocated by using one-pass reservation, i.e., burst transmission is not delayed until an acknowledgment of successful end-to-end path setup is received but is initiated after the burst was assembled and the control packet was sent out.
- Burst switching does not require buffering inside the core network.

In the following, the OBS network architecture based on this more packet oriented definition is discussed in Subsection 2.3.1. The requirements for the physical layer defined by such a network are derived in Subsection 2.3.2.

2.3.1 OBS Network Architecture

As depicted in Fig. 2.3, an OBS network has a meshed topology, WDM links, and two types of nodes: the *edge nodes* and the *core nodes*.

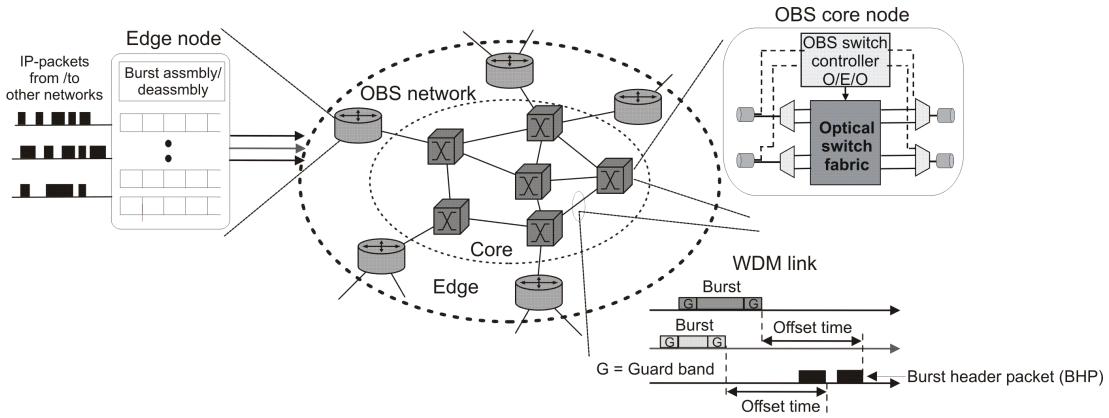

Figure 2.3: Principle of an optical burst switching network.

2.3.1.1 Edge Nodes: Burst Assembly and Disassembly

The (ingress/egress) edge nodes are the interface between IP network and the OBS network. The main functionality of an ingress edge node is burst assembling. Here a number of small transport units, e.g. several IP packets are aggregated electronically into one larger transport unit, the so-called *burst*.

The principle structure of an ingress edge node is shown in Fig. 2.4. The symbols *a, b, c* illustrate e.g. different destinations of the IP-packets. In the Burst Assembly Unit (BAU) the IP-packets will be separated according to the destination and/or Quality of Service (QoS) class and stored in Access Control (AC) Block until a control criterion is achieved and a channel of the outgoing WDM links is free. Then all packets in an assembly queue will be forwarded to the network as one burst.

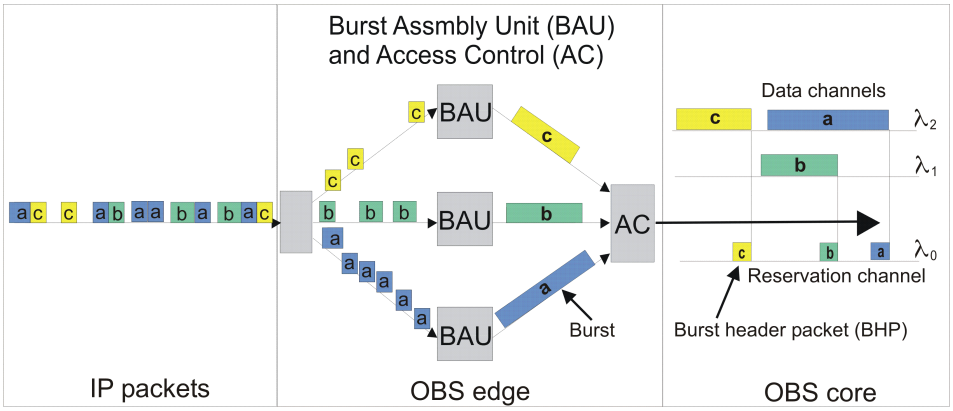

Figure 2.4: Principle structure of an OBS ingress edge node with Burst Assembly Unit (BAU) and integrated Access Control (AC).

For each *optical data burst* a *burst header packet (BHP)* is generated. The BHP contains informations like, e.g., burst length, current wavelength, service class and information on the destination. In the most OBS approaches a hybrid approach is used for transmission of BHPs and data bursts, that means: For each burst a BHP is sent out of band on a separate *reservation channel* at a different wavelength. Through an OBS network, *BHPs* will be processed electronically by an OBS controller at each OBS core node (see Fig. 2.3). This separate control approach allows sophisticated electronic processing of the control information. The reservation channel can operate with a lower bit rate than the data channels and even different modulation formats can be used. Lower bit rate for the reservation channel makes the electronic processing easier. By using such BHPs the network resources (wavelength channels respectively) are reserved for a limited time period (transmission duration of each individual burst). Therefore the network utilization is increased and statistical multiplexing between the bursts can be achieved like OPS. At the other edge of the OBS network the egress edge nodes read the encoded control information, disassemble the arriving bursts, and forward the client packets to the client layer.

Since multiple packets are assembled into a burst, the burst traffic is expected to have different statistical characteristics from those of the input packet traffic [52]. The burst assembly mechanism in the edge nodes directly influences almost all traffic characteristics in an OBS network. Different burst assembly mechanisms will lead to different burst length distributions, number of IP packets per burst and inter-arrival time between bursts, which in turn have major impact on the OBS network performance in terms of multiplexing gain, burst loss rate, throughput and delay. As it determines the nature of the traffic in the optical domain, i.e. its statistical properties, a specific traffic characteristic can be achieved by using a certain burst assembly mechanism. So, choosing the right assembly mechanism for the edge nodes and configuring it correctly is one of the most important tasks in dimensioning of an OBS network. In the literature, various burst assembly mechanisms have been proposed [38, 40, 53]. Their impact on the optimum burst size and burst arrival rate are investigated [54–56]. In addition burst assembly can also be used for service differentiation to support Quality of Service (QoS) [57–60], that means different services can be provided with different qualities. A possible technical realisation of such electronic burst assembly unit has been also published in [61].

However, the focus of this thesis is the investigation of the impact of OBS on the optical layer and the technical feasibility of such an OBS core network. Therefore, the above mentioned issues like burst assembly mechanisms, burst scheduling, QoS and so on are beyond the scope of this thesis and are not considered here. Details can be found in [52, 59, 60]. Nevertheless, the aggregation degree in the burst assembly unit at the edge of the network determines the burst length and has a direct impact on the required switching technology.

Fig. 2.5 presents the context between the switching granularity, circuit/burst/packet length, and required switching technology for fast OCS, OBS and OPS. The required end-to-end signaling times for different networks (metro, nation, world etc.) are depicted, too.

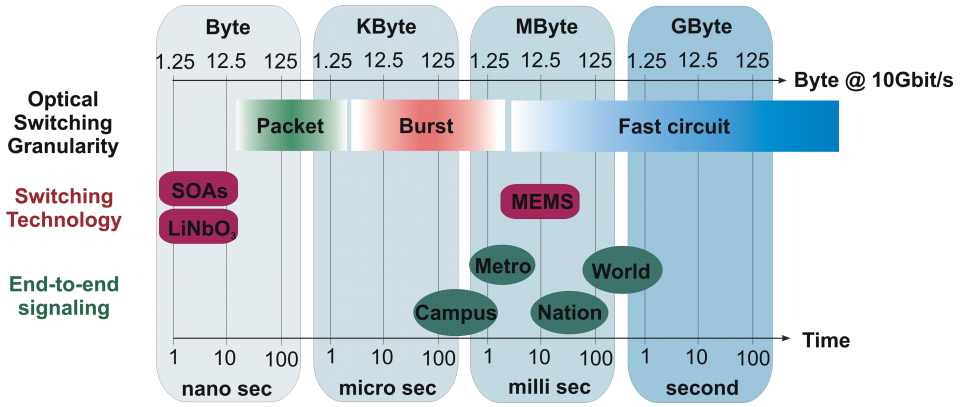

Figure 2.5: Relationships between the circuit/burst/packet granularity, required switching technologies, and signaling scheme.

Here the following dependencies and relationships between the circuit/burst/packet granularity (in terms of bytes and time duration) and the characteristics like required switching technologies and reservation schemes (one-pass reservation vs. end-to-end signaling) can be derived:

- The switching granularity (black colored in Fig. 2.5) determines the required switching technology (red) and vice versa as switching time has to be significantly shorter than the typical granularity switched.
- The switching granularity (black) and network size (round-trip-time in green) determine whether one-pass reservation or end-to-end signaling is advantageous. End-to-end signaling time defined by network size should be less than the typical granularity transported, otherwise, one-pass reservation should be preferred.

From those arguments and characteristic, it can be derived that optical bursts for one-pass reservation have variable length in the order of several tens of KBytes typically. It corresponds to a burst duration between a few μs and several 100 μs depending on channel bit rate. In contrast, if end-to-end signaling is used, optical bursts should have a duration in the ms range. The switching granularity and required switching technology of an OBS network are between OCS and OPS networks. Comparing to OCS, OBS has a finer granularity and more bandwidth flexibility can be provided, i.e. it can be better adapted to changes in the traffic pattern. The other major difference is the one-pass reservation for OBS

in contrary to end-to-end signaling for OCS. Regarding OPS, OBS has a coarser granularity and requires only a moderate switching time (μs in contrary to ns in OPS). Furthermore, a switch has to handle less requests to switch the same amount of information. This is especially important as the number of processed requests per time unit can be a limiting factor.

2.3.1.2 Burst Signaling and OBS Core

As already mentioned above, in most common OBS approaches the so-called *one-pass reservation* scheme is used to set up a burst transmission path through the OBS network from an ingress edge node to an egress edge node. This means the network resources are reserved for each individual burst but are not acknowledged before sending the data [62]. The advantage is the higher efficiency with respect to the throughput as there is no delay by overhead. An example may illustrate this: the transmission time of a 100 KByte burst on a 10 Gbit/s link is 80 μs while the propagation delay over a distance of 200 km is about 1 ms at 10 Gbit/s. Hence, during 2 ms of waiting for the acknowledgement to arrive, 25 bursts could have been transmitted. By including processing time or assuming higher bit rates, the number of not transmitted bursts even increases.

Inside the OBS core network, a burst is moved as a basic transport unit from one ingress edge node to one egress edge node and switched at intermediate core nodes. Like OCS, there is no need for buffering and electronic processing of data at the core nodes. Therefore no bit-level signal processing of the data (bursts) is needed at intermediate core nodes. To achieve this, the so-called *separate control and delayed transmission (SCDT)* method is used. In contrast to systems with immediate transmission, which send control information together with the burst, the network with delayed transmission can perform header processing without buffering data burst in each OBS core node along the path. In the most common approach of OBS, the actual transmission of the data burst is delayed by a certain basic offset time. This basic offset time enables intermediate core nodes to process the burst header packets (BHPs) electronically and to reconfigure the optical switch fabric before the data bursts arrive. The basic offset time has to compensate the sum of processing times in all intermediate OBS core nodes. This approach assumes the knowledge of the number of traversed nodes along the path prior to reservation at the edge node. In each OBS core node, offset information in the BHPs has to be reduced by the actual processing delay as illustrated in Fig. 2.6a.

Another solution is the input fibre delay line (FDL) approach as illustrated in Fig. 2.6b. Here the *burst header packets* and the bursts both are sent at the same time on different wavelengths and the bursts are delayed at the input of every OBS core node in an FDL while the BHPs are being processed. Here only an additional short fibre span at each input fibre of OBS core node is needed, in

opposite to complex FDL buffer architectures, proposed in the context of optical packet switching (OPS) in which each packet has to be stored during processing. For a time offset of 10 μs, e.g., a 2 km optical FDL for data bursts is needed per input in each OBS core node. In case of successful burst reservation a new BHP is generated and sent to the next node.

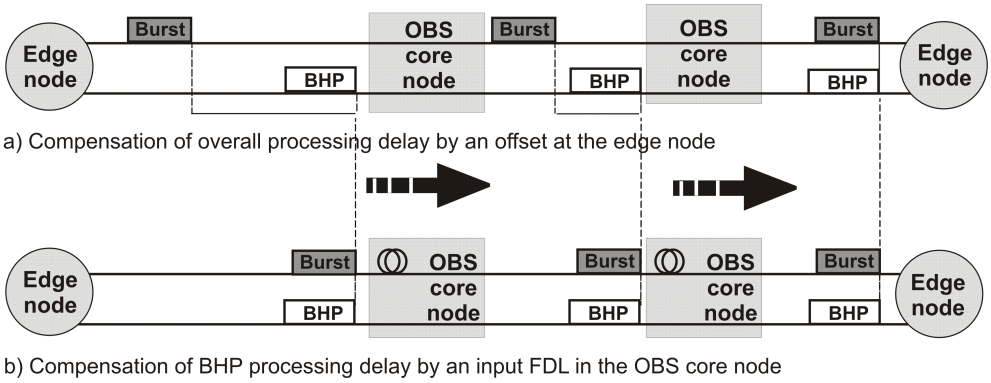

Figure 2.6: Comparison of two different approaches for realisation of separate control and delayed transmission. a) compensation of overall processing delay by a offset at edge node, b) compensation of BHP processing delay by an input FDL in OBS core node.

The most critical issue in an OBS core is that contention can occur, when two or more bursts try to leave the OBS core node at the same time on the same output fibre and the same wavelength. In electronic packet switched networks this kind of contention is resolved by the store and forward technique. The packet is stored as long as contention exists. This is not possible in optical networks because no optical random access memory (RAM) exists. An OBS core node cannot employ large and flexible random access buffers. By using the one-pass reservation scheme in addition, burst loss can be severe during such contention situations and the network performance of the OBS network becomes worse. In Fig. 2.7 the principle of burst transmission through an OBS core node and a typical contention situation is shown schematically.

As mentioned above an input FDL is used to delay the data burst while the burst header packet (BHP) is being processed. When the burst (*burst 1*) in the Fig. 2.7 arrives at the optical switch fabric the reconfiguration of the switch is already performed. Therefore *burst 1* can be directly forwarded to the output and a new burst header packet (*BHP 1*) is generated. If another burst like *burst 2* in the figure wants to go to the same output fibre (*fibre 1*) at almost the same time as *burst 1*, *burst 2* has to change its wavelength. If now a *burst 3* arrives and wants to go to the same output fibre and this output fibre is still occupied by other bursts (*burst 1, 2*), this burst has to be discarded and the reservation process is finished. As shown in Fig. 2.7, the wavelength channels in an OBS core node are reserved

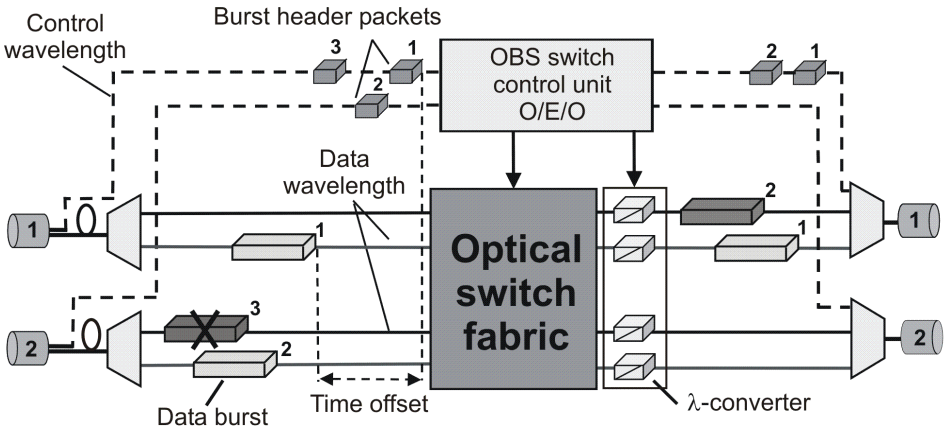

Figure 2.7: The principle of burst transmission through an OBS core node.

only for a limited duration for transmitting each data burst. To do this efficiently, several reservation mechanisms have been proposed recently in the literature [6,11]. Different OBS reservation mechanisms lead to different utilisation of the output wavelength channels per fibre, which could have strong impact on the traffic performance of the OBS core nodes and consequently on OBS node design. The most important parameter here is the burst loss rate (or blocking probability). Therefore a detailed description of different reservation mechanisms for OBS networks will be given in Chapter 7, where the effective throughput of different OBS core nodes is calculated.

Furthermore, to keep the burst loss rate as low as possible, a suitable contention resolution scheme is one of the most important issue in an OBS network [63–66]. E.g. as shown for *burst 2* in Fig. 2.7 the burst loss rate due to failed reservation can be kept low by applying many wavelengths per fiber in combination with wavelength conversion. Different contention resolution schemes do not only lead to different traffic performances of the OBS networks, but also could have several consequences for the physical implementation of the OBS core nodes. Therefore in Chapter 4 different contention resolution schemes will be compared in their performance and the consequence for implementation in the optical layer will be also discussed.

2.3.2 Technological Requirements defined by OBS

OBS will only be a feasible switching solution if the essential optical technologies and building blocks are available. From the characteristics of OBS, which are discussed above, the following requirements, especially on the physical layer can be deduced:

1) WDM Technology and Wavelength Conversion
Wavelength can be considered as a shared resource for an OBS network. In contention situations, to reduce burst losses, wavelength conversion can be used effectively allowing bursts to change their wavelength if needed. Large numbers of wavelengths transmitted on a fibre greatly improves the statistical multiplexing gain. However, this hardware requirement could increase the complexity of the switching node drastically, if very large numbers of wavelengths are required.

As the different signals enter the OBS node they have been transmitted over different distances and amplified by a different number of EDFAs. Signal degradations will then be accumulated and will cause an increasing bit error rate (BER) and limit the transmission distance. The bursts have to pass wavelength converters and depending on the characteristics of these wavelength converters the signal is either degraded or regenerated at the output. In this way the wavelength converters have essential impact on the physical layer characteristics of an optical burst switching network and a wavelength converter which could also provide the same degree of regenerative capability becomes desirable.

Furthermore, the wavelength conversion must be tunable to achieve arbitrary wavelength switching. Depending on the OBS core node architecture fast tunable lasers and/or filters are required. Their tuning speed must be in the same order of magnitude as the desired speed of the space switch (μs for OBS). The operational wavelength of a tunable wavelength converter/laser should cover the overall wavelength region of the WDM system to ensure arbitrary switching between WDM channels. Also high output power and high side mode suppression ratio are required. The key features of tunable optical filters are low insertion loss, narrow bandwidth, high side mode suppression, large dynamic range, fast tuning speed, a simple control mechanism, small size, and cost effectiveness. Wavelength stability is also an important issue. It is difficult to achieve the stability necessary for a narrow frequency grid.

2) Burst Capable Receiver
To receive optical bursts at the egress edge node, burst mode receivers are needed. Large dynamic range, fast adjustment of receiver decision threshold and fast clock recovery are required for efficiency reasons (also in the range of 1 μs for OBS). If the input wavelength varies, it might be sufficient that the receiver is broadband enough to operate at any input wavelength.

3) Optical Amplification
Erbium-doped fiber amplifiers (EDFAs) have large gain and the ability to amplify many WDM channels simultaneously without bit-by-bit crosstalk. Therefore, they are presently used in the transmission links in general. Here low noise, high but polarisation independent gain and high output power are required. Burst mode

transmission results in dynamic gain changes in EDFA, which in turn lead to possibly large variations of the output power of the data channels. So, a fast electronic/optical gain control of the amplifiers is needed. The speed of the control must be in the order of the speed of the space switches (μs for OBS).

4) Simple and Efficient FDL Buffer Structures
In the context of OBS only simple FDL buffer structures are considered for contention resolution. A requirement is that only low additional losses should be introduced. No additional dispersion or polarization mode dispersion (PMD) compensation at the receiver side and no additional optical amplifiers should be needed. In addition, OBS core nodes could require also some kind of FDL in order to guarantee a constant distance between burst header packet (BHP) and burst (offset time, see Fig. 2.6 on page 20).

5) O/E/O Conversion for BHP Processing
For OBS using one-path reservation each burst header packet (BHP) has to be processed in each OBS core node electronically. Therefore O/E/O conversion in order to process the BHPs in the electrical domain is needed. So if there is one dedicated path for signaling, the number of O/E and E/O conversion is at least equal to the number of neighbour nodes (node degree) and the number of input/output fibres respectively.

6) Suitable Optical Switch Fabrics
The optical switch fabrics for OBS should have the following performance:

- *Large size:*
  The size of switching fabrics for OBS depends on the kind of network (core or metro, close or coarse meshed) and the applications carried over OBS. About 128 x 128 ports (e.g. 4 fibres and 32 wavelengths each fibre) are regarded as typical. To realise such large switching fabrics low signal degradation is required. Therefore, switches with low loss and low crosstalk are needed. To avoid high insertion loss, large cascading structures of small switching elements in order to increase the number of input/output ports are not preferred.

- *Fast switching time:*
  For OBS using one-path reservation, optical space switches with a switching speed in the order of μs or less are needed. Here insertion loss, noise, and crosstalk should be low and polarization independence is required. Since optical space switches are in fact analogue devices, there are no digital regeneration functions automatically accomplished by switching as it is in electronic switching. To avoid accumulation of signal degradation the number of cascaded switches in the signal path must be as low as possible. So one-stage

switch architectures are preferred. Furthermore, non-blocking architectures are preferred to avoid additional burst losses caused by the node architecture.

- *High reliability and low cost:*
  Finally, the cost plays also an important role for selecting a switching technology. OBS core nodes will have O/E/O converters for the control units, wavelength converters for contention resolution, and possibly FDLs for keeping the offset times between BHP and burst constant. All of them will increase the cost, so the switching fabric should not worsen this too much.

Chapter 3

Analysis of Impact of OBS on Optical Transmission

As mentioned in the previous chapter, to transmit optical bursts, additional requirements on optical WDM transmission links have to be fulfilled. A typical optical transmission link in such an OBS network is shown schematically in Fig. 3.1. Four key building blocks are required to retrofit the current WDM systems.

1. Edge nodes with fast tunable lasers (not absolutely necessary)
2. Gain-stabilised EDFAs in the transmission links as well as at the in-/output of the OBS core nodes
3. In an OBS core node fast reconfigurable switch fabrics and wavelength converters in combination with fast tunable lasers are required
4. Burst mode receivers at the egress edge

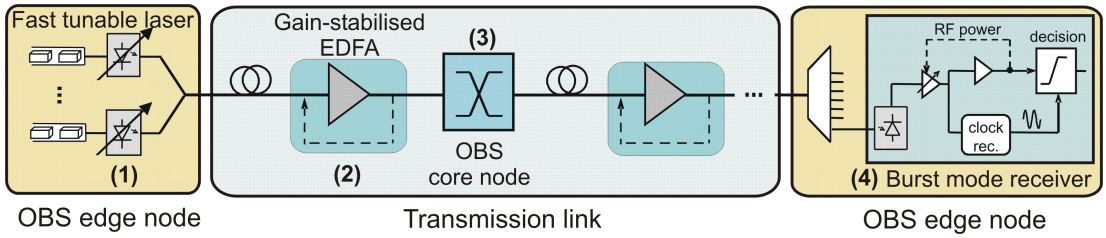

Figure 3.1: Typical optical transmission link in an OBS network, with 1) fast tunable lasers at the edge for mapping wavelengths to bursts, 2) gain-stabilised EDFAs to prevent power fluctuations, 3) OBS core node with fast optical switches to forward bursts, and 4) a burst mode receiver at the egress.

In the following the impact of OBS on optical transmission is investigated in detail. First a short overview of the existing prototypes and demonstrators for a fast

tunable transmitter and a burst mode receiver are given in Section 3.1. Then in Section 3.2 the dynamic behavior of EDFAs in a burst switching environment is investigated experimentally and numerically. Different methods for gain stabilisation are categorized and their advantages and disadvantages particularly with regard to OBS networks are discussed.

3.1 Fast Tunable Transmitters and Burst Mode Receivers

3.1.1 Fast Tunable Transmitters

Fast tunable transmitters are key components for OBS networks. As mentioned in Section 2.3 fast tunable lasers are required in the edge routers, which can tune the wavelength across the used wavelength band for sending bursts on different wavelengths. Furthermore fast tunable lasers in combination with wavelength converters can be used as the most effective method for the contention resolution. For OBS a tuning time in the range of μs is required.

Generally, the wavelength of a semiconductor laser can be changed either by changing the refractive index of the cavity medium (by means of temperature variations or current injection) or by varying the cavity length (mechanically, using micro-electro-mechanical systems (MEMS)). Due to the large time constant for the temperature or the mechanical mirror control only the lasers tuned by currents are suitable for fast tuning. During the last years several fast tuneable lasers have been proposed by using a number of different technologies and assemblies. Only few of them are commercially available at the present and the others have only been experimentally demonstrated recently.

All reported fast tunable lasers can be divided into two classes: first, and also the majority of them are multi-section Distributed Bragg Reflector (DBR) lasers, where the wavelength is tuned by current injection in the Bragg reflector. The second type are external cavity lasers (ECLs). Among the multi-section DBRs, the Grating assisted Coupler with Sampled Reflector (GCSR) laser, is the most recent development. In a GCSR laser a modulated Bragg Reflector provides a comb of peaks from which a co-directional coupler selects a peak for coarse tuning. Fine tuning is done by adjusting the current of the phase section. The speed of the tuning control loop is the determining time constant for the achievable tuning speed. The commercially available “Anywave Tunable Lasers NYW-50-D and NYW-60-B” from ADC [67] are built around a monolithic four-section GCSR laser. Another implementation of multi-section DBR is the Sampled Grating DBR (SGDBR) laser, in which a second grating is added (at the opposite end of the gain section with respect to the first grating), with a slightly different setup. This results in having

two wavelength combs, with a slight offset, in which a small tuning of the combs results in a significant change in the resonant wavelength. As in standard DBRs, the variation in refractive index (tuning the wavelength comb) is obtained varying the current flowing into the front and rear gratings and phase section. The "Agility 4235 Widely Tunable Laser Transmitter (TLT)" from Agility Communications [68] is a commercially available SGDBR laser monolithically integrated with an Electro-Absorption Modulator (EAM) and Semiconductor Optical Amplifier (SOA). The SOA enables higher output power as well as constant power level for all channels, and no output power during the tuning process can be achieved. It can be employed up to a data rate of 2.5 Gbit/s with externally integrated modulator for C-band channels (35 nm operating range, 1528 - 1563 nm). A schematic of the seven section photonic IC transmitter of Agility consisting of a full band tunable four-section SGDBR laser integrated with a monitor detector, optical amplifier and modulator is shown in Fig. 3.2a.

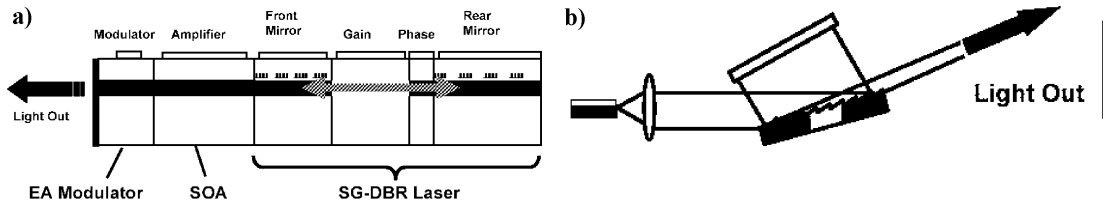

Figure 3.2: Two common structures to realise fast tunable laser. a) Agility monolithically integrated SGDBR laser, b) External cavity laser.

The external cavity lasers (ECLs), as shown in Fig. 3.2b, use a standard Fabry Perot laser chip and one or two mirrors, external to the chip, to reflect light back into the laser cavity. To tune the laser output wavelength a grating or another type of narrow-band tunable mirror is adjusted in a way that it generates the desired wavelength. This type of tuning usually involves physically moving the grating or the mirror. Typical ECL implementations are using diffraction gratings and movable reflectors, using a sampled fibre Bragg grating (SFBG) or integrating an amplifier array with a wavelength selective element such as a passive arrayed waveguide grating (AWG) router. In SFBG external cavity lasers the wavelength can be tuned in a very simple way using only one current. ECLs have extremely good characteristics, such as wide tuning ranges and high output power and spectral purity, although mechanical tuning involves low reliability and tuning speed.

In Tab. 3.1 the key parameters of such tunable lasers like: the tuning range (numbers of available channels), the tuning speed (the time giving the command for changing the wavelength and setting the desired wavelength with certain accuracy), the output power and power variation, and the minimum side mode suppression ratio (SMSR) are compared.

Design	performance					Ref.
	Tuning range	Tuning speed	Output Output	Power variation	Min. SMSR	
GCSR (4 section)	32 nm	2 ms	3 dBm		35 dB	ADC [67]
SGDBR (4 section)	35 nm	10 ms	3 dBm	± 0.5 dB	35 dB	Agility [68]
Integrated modules	35 - 80 nm	50 - 200 ns	< 9 dBm	± 1 dB	35 dB	Intune [69]
GCSR	40 nm	< 45 ns	1.5 dB	1 dB	25 dB	[70,71]
SGDBR (active locking)	> 35 nm	5 ns	0 dBm	1 dB	40 dB	[72]
SSG-DBR	> 30 nm	< 400 ns	-3 dBm	1 dB	35 dB	[73]
AC-DBR	2.5 nm	< 1 ns	13 dBm	1.2 dB	30 dB	[74]
External cavity (SFBG)	15 nm	< 50 ns	6 dBm	0.6 dB	40 dB	[75]
External cavity (grating)	12 nm	20 ns	> 7 dBm	1 dB	40 dB	[76]

Table 3.1: Summary of demonstrations for different types of tunable lasers

The first three tunable lasers in Tab. 3.1 are commercially available at present. But due to their low switching times (10 ms and 2 ms), the first two cannot be used for OBS. Only the third one, the fully integrated tunable laser with control electronics from Intune Technologies is well suitable for OBS [69]. With AltoNet1200 switching times in the range 50 ns to 200 ns can be achieved with integrated external modulator for 10 and 40 Gbit/s. Depending on the configuration the wavelength can be switched inside the C-and/or L-band. However, no information about the internal structure of this laser can be found.

The other lasers listed in Tab. 3.1 are tunable lasers which have been demonstrated in the lab recently and have a tuning time suitable for OBS. A major class of such tunable lasers are those which are shown in Fig. 3.2a. Most of them are multi-section DBR lasers formed by integrating a gain section and one or multiple tunable grating sections: sampled grating distributed Bragg reflector (SGDBR), super structure grating distributed Bragg reflector (SSG-DBR), absorption change distributed Bragg reflector (AC-DBR) or grating assisted coupler with sampled reflector (GCSR). These lasers are tuned by current injection and require calibration and complex control of three or more tuning currents.

3.1.2 Burst Mode Receivers

To receive an incoming burst, burst mode receivers are needed at the egress edge. They must recover the clock in a small fraction of the burst length, and need to dynamically compensate for power fluctuations along the transmission line. Over the last years several burst mode receivers have been demonstrated for 10 Gbit/s [77,78] and for 40 Gbit/s [79].

Burst mode receivers should have the capability to handle the following parameters:

1) Different burst format
Current commercially available transmission systems are based on non-return to zero (NRZ) intensity modulation and on direct detection of the data signal. However, it is well known that advanced phase modulation formats (e.g. differential-phase-shift keying (DPSK)) provide higher sensitivity and an increased tolerance against physical system impairments. Therefore, for OBS these modulation formats could be also used and burst mode receivers which are able to handle such modulation formats are required.

2) Variable burst length
Here the synchronization time is the critical point. It is necessary for the receiver to synchronize itself with every incoming burst. Fast adjustment of receiver decision threshold and fast clock recovery are required. The range of desired settling times here is about μs or even ns. Once the receiver has synchronized there is then no difference to the continuous transmission regime. So variable burst lengths do not cause additional problems.

3) Variable gap between bursts
As the receiver is capable to operate in continuous transmission, there is no need for a (physical) gap between bursts at all - if and only if the bursts come from the same transmitter. In case the bursts originate from different transmitters a gap for re-synchronization is needed. It can be assumed that the minimum required gap will not exceed the synchronization time. The other extreme is an unlimited long gap. In principle the receiver must be able to receive a single burst after e.g. a week of silence.

4) Variable burst power
The different bursts experience different losses and amplifications on their way through the network. One major feature of a burst mode receiver is, to survive a step in power level from one burst to the next. Depending on the receiver realization, the exposure to fast changing burst powers might be accompanied by sensitivity degradation due to saturation and other effects.

3.2 Dynamic Behavior of EDFAs in an OBS Network

In today's optical transport networks Erbium-doped fiber amplifiers (EDFAs) are generally used as in-line amplifiers to compensate the fibre losses. They are usually operated in saturation. The gain of EDFAs is reduced by an increase of stimulated emission when the optical input power rises. In the strong saturation region, the

output power is nearly constant independent of the input power. High bit rate intensity modulated light is regarded by the amplifier as constant optical power. Therefore, EDFAs with multi-wavelength input signals are immune to bit-by-bit crosstalk, i.e. they show no cross gain modulation on the bit level.

The situation changes if EDFAs are used in an OBS network as in-line amplifier as well as at the in-/output of the OBS core nodes. In an OBS network not only the number of used channels in a fibre will change randomly like in dynamic wavelength switching, even the power of a single channel will no longer be constant. It changes on a time scale corresponding to the length of the bursts and the gaps between the bursts. Transmitting optical bursts through a chain of EDFAs results in dynamic gain changes according to the variation of input power, which in turn lead to possibly large variations in output power of the data channels. Gain variations over the amplification bandwidth should be reduced to limit the gain and optical signal to noise ratio discrepancies between the different channels. EDFAs with controllable gain and output power are also necessary in order to optimize the signal-to-noise ratio and manage nonlinear interactions. Because of the fast response time in cascaded optical amplifiers (in comparison with the single EDFA), fast gain control is one of the key issues related to dynamically switched WDM networks. Especially for OBS networks, fast gain stabilization of EDFAs on a time scale of microseconds is required.

In the following the dynamics of an EDFA in a burst switching environment is investigated. The experimental setup and the simulation model used to calculate the transient responses of EDFAs are described and the results are presented for a single EDFA as well as for EDFA cascades. Then a detailed description of various gain control schemes for a single EDFA is given, followed by a characterization of gain control methods for EDFA cascades. The advantages and disadvantages of the different approaches are discussed particularly with regard to OBS networks.

3.2.1 Analysis of EDFA Gain Dynamics

To investigate the dynamic behaviour of EDFAs in an OBS network, the time-dependent output power of single EDFAs and EDFA cascades are treated experimentally and numerically. The input signal of each channel is modeled as a sequence of data transmission and silence periods to simulate optical bursts.

3.2.1.1 Experimental Investigations of EDFA Dynamic Behaviour

The experimental setup used for measurements is shown in Fig. 3.3. To generate the burst traffic the 2.5 Gbit/s signal of a BER-Transmitter is switched on and off controlled by a square wave generator. The burst and gap length can be adjusted arbitrarily. The signal is used to directly modulate a laser. The average input

power $P_{in,average}$ is 0 dBm. The 20 dB-attenuators between the EDFAs are used to simulate the loss of optical fiber links. The optical power is detected after an EDFA or at the end of the EDFA cascade and the transient response is measured by a digital communication analyzer.

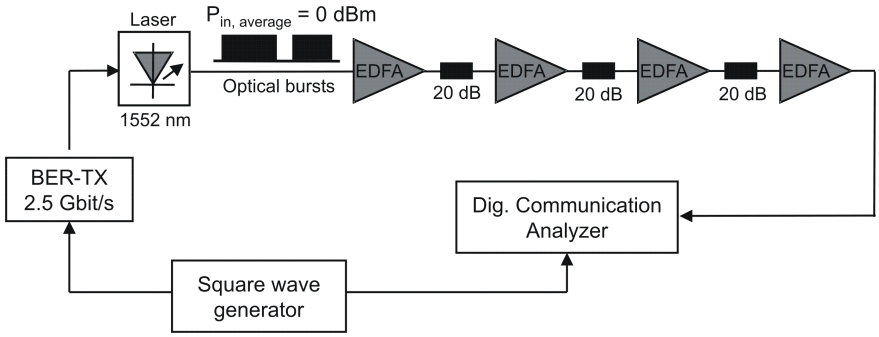

Figure 3.3: Schematic diagram of the experimental setup.

First, the output power transients of a single EDFA are considered. Fig. 3.4 shows the measured transient behaviour of the output power for short bursts with a duration of 40 μs (a and b) and for long bursts 1 ms (c and d). The gap length is chosen either to be equal to the burst length (a and c) or four times the burst length (b and d). The horizontal lines in the figures show the peak output power values and the output power in the stationary case, where the input signal is continuous and has the same power but no gaps.

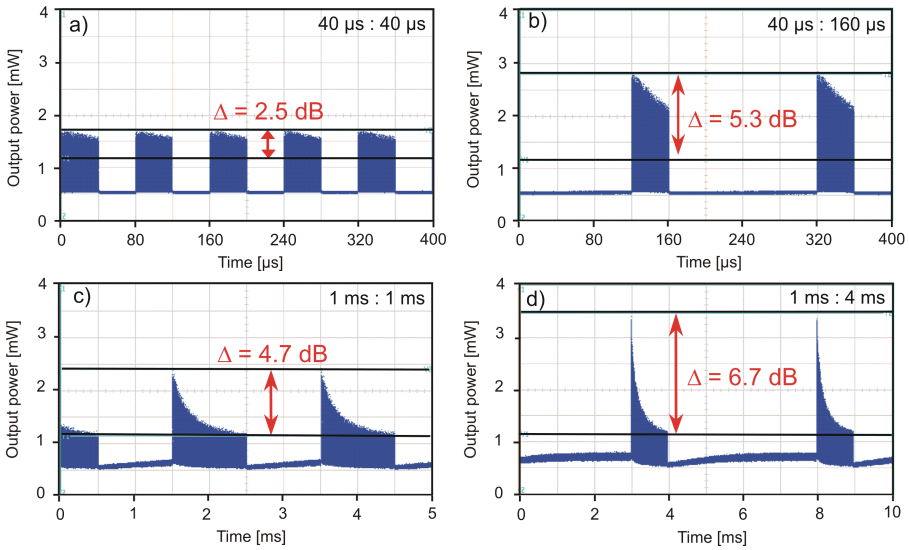

Figure 3.4: Measured power excursions for a burst-gap ratio of a) 40 μs/40 μs; b) 40 μs/160 μs; c) 1 ms/1 ms; d) 1 ms/4 ms.

The power excursion across the output burst can be clearly observed. The power is decreasing along the bursts in all four cases. Comparing Fig. 3.4a with b and c with d, which have the same burst length, the impact of gap length can be seen. The longer the gap is, the higher is the power at the beginning of a burst. This effect can be explained: During the gap period there is no stimulated emission, only spontaneous recombination reduces the number of excited Er-ions, and the number of excited ions increases and consequently the available energy in the cavity due to pumping (EDFA gain) increases. When the burst is switched on, the gain at the beginning of the burst is high and it will then be reduced by stimulated emission. The power variation is rather weak for the short gap lengths (Fig. 3.4a), because for short gaps there is not enough time for the gain recovery and the gain nearly corresponds to the gain with the mean power. With longer gaps (Fig. 3.4b), the peak power is smaller and the average gain is higher. There is more time for the gain to increase to a higher value during the gap. For the longest gap length of 4 ms (Fig. 3.4d) the gain increases to very high values, resulting in very high power overshoots at the beginning of the bursts. Comparing Fig. 3.4a with c and b with d, which have the same burst-gap ratio but different burst length, the longer the burst length is, the faster is the decrease of the power within the burst. During the burst stimulated emission reduces the number of excited ions which results in the decrease of the power within the burst. The longer the burst is, the stronger is the reduction of the number of the excited ions and the faster is the decrease of the power. In the case of long bursts (1 ms) one observes, that the stationary output power value is reached at the end of the burst (Fig. 3.4c, 3.4d).

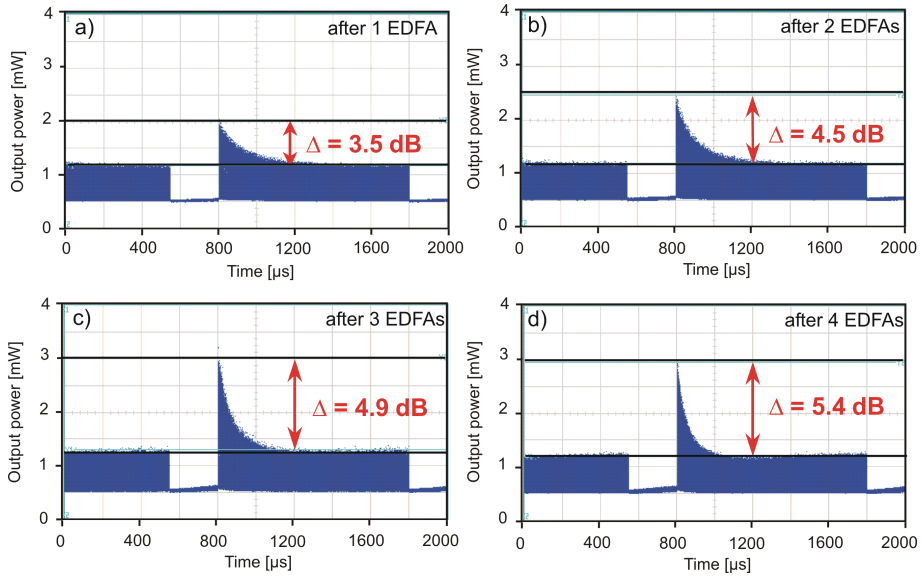

Figure 3.5: Measured power excursions as a function of the number of cascaded EDFAs for a fixed burst-gap ratio at 1 ms/250 μs.

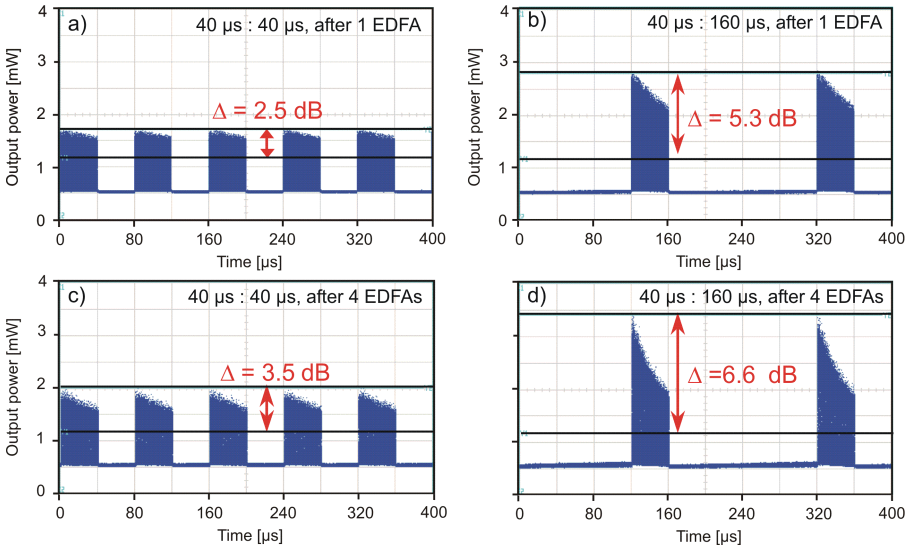

Figure 3.6: Measured power excursions for a) 40 μs/40 μs burst-gap ratio and after 1 EDFA; b) 40 μs/40 μs burst-gap ratio and after 4 EDFAs; c) 40 μs/160 μs burst-gap ratio and after 1 EDFA; d) 40 μs/160 μs burst-gap ratio and after 4 EDFAs

Fig. 3.5 shows the experimental results for a fixed burst-gap ratio at 1 ms/250 μs. Here the number of cascaded EDFAs are varied form 1 to 4. The output power overshoots increase with the number of cascaded EDFAs and the duration of the overshoots become shorter simultaneously. Similar results can also be found in Fig. 3.6, where the burst-gap ratio is 40 μs/40 μs or 40 μs/160 μs and the number of EDFAs is 1 or 4.

3.2.1.2 Numerical Analysis of EDFA Gain Dynamics

1) The Applied Numerical Model for EDFAs

To analyse the gain dynamics in detail, different numerical simulations have been carried out by using the "Dynamic Amplifier EDFA Model" module in the simulation tool "VPITransmissionMaker" (*AmpEDFA_Dynamic*) [80]. This module is based on the numerical model of the EDFA introduced by Sun et al. [81] and Bononi et al. [82].

Usually, optical signals have data contents at frequencies well above the dynamic response frequency of EDFAs. The EDFAs are transparent and quasi linear for such high bit rate systems. However, if these data signals are switched on or off like in the OBS networks, tremendous distortions of the amplifier gain may occur. The signal envelope exhibits strong transients, and interchannel crosstalk can be observed caused by saturation effects.

The "Dynamic Amplifier EDFA Model" module simulates the gain transients by taking the bidirectional signal and pump power propagation into consideration. Detailed descriptions can be found in [80–84]. A summary of all used parameters with their default values can be found in Appendix A.

2) Characteristic Parameters

To analyse the dynamic behaviour of EDFAs with time variable input power, characteristic parameters as shown in Fig. 3.7 can be defined to describe the power variation at the output of an EDFA cascade.

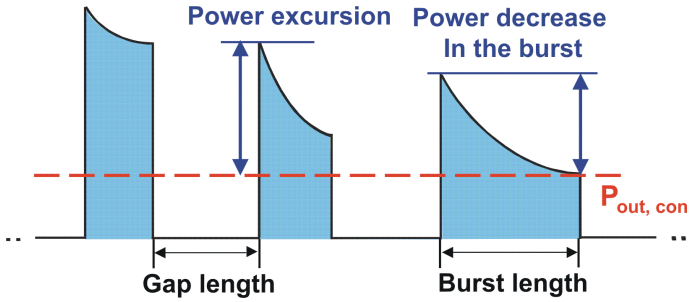

Figure 3.7: Characteristic parameters for describing the power variation after an EDFA cascade in an OBS network.

The dashed line shows the power level $P_{out,con}$ at the output of an EDFA, if a continuous data signal is transmitted. Referring to this output power level another parameter can be defined for burst mode transmission: the so-called *power excursion* at the beginning of the bursts. The experiments have shown that the longer the gap is, the higher increases the gain at the beginning of the next burst, the higher then is the power excursion. A further parameter is the *power decrease* in the burst, which relates to the reduction of the number of excited ions due to stimulated emission. The longer the burst length is, the stronger is the reduction of the number of the excited ions, the stronger is the decrease of the gain and therefore the faster is the decrease of the power. In the case of long bursts the stationary output power value ($P_{out,con}$) is reached at the end of the burst (see Fig. 3.4c, 3.4d on page 31).

3) WDM Burst Transmission after a Single EDFA

To investigate the dynamic behaviour of a single EDFA, a WDM system at Gbit/s bit rates e.g. 10 Gbit/s with up to 8 channels are simulated as shown in Fig. 3.8. The wavelengths is chosen in the 1549 -1556 nm band, with 100 GHz channel spacing. Each channel has an average input power of 0 dBm. The EDFA is operated in saturation and its parameters can be found in Appendix A. Up to 8 channels are multiplexed, attenuated with -28.4 dB (representing the losses of the multiplexer and the fibre) and then amplified with an EDFA. The total output power of the

EDFA is nearly constant independent of the number of WDM channels and the input power, respectively. However, the output power of each single channel depends on the number of existing input channels. The total output power is split into the single channels and the power in a single channel changes everytime, when other channels are switched on or off. This results in a gain change in the existing channels and causes cross-saturation in the EDFA.

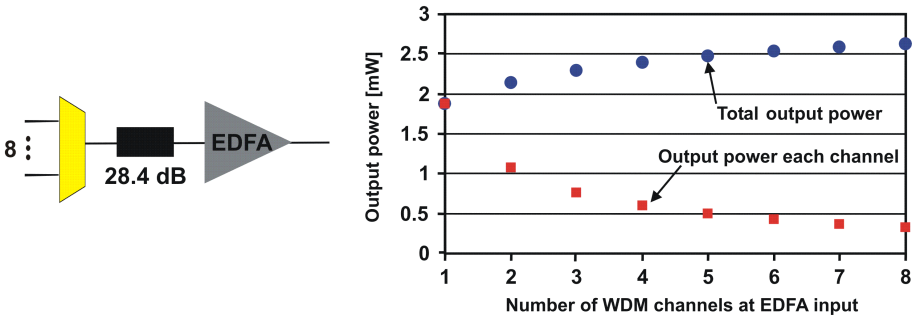

Figure 3.8: EDFA output power versus the number of input WDM channels for WDM transmission after a single EDFA. Each channel has an average input power of 0 dBm.

Then the same simulation setup is used for the eight channel WDM system with random bursty traffic carried by all 8 channels. In Fig. 3.9 the dashed line shows the average total output power of the EDFA, which is measured at the EDFA output including all 8 channels and averaged for all times (including the bursts and the gaps). It is nearly constant due to the operation of the EDFA in the saturation.

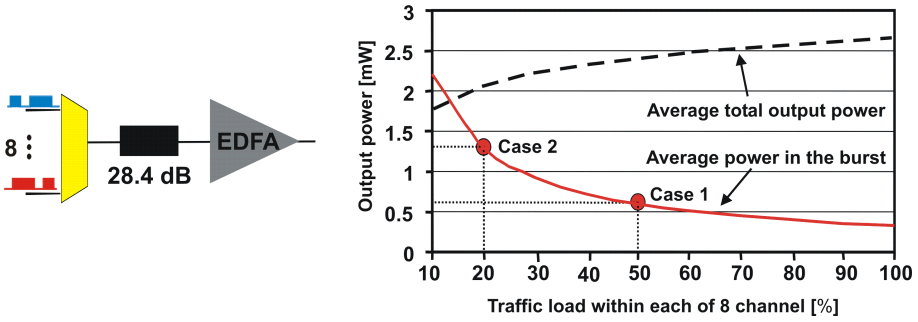

Figure 3.9: Average total output power and average power over the burst at EDFA output versus traffic load within each of 8 channel after an EDFA. Each channel has an average input power of 0 dBm.

The solid line in Fig. 3.9 shows the average power in the burst, which is measured at the EDFA output in one channel and averaged only for the time periods where the bursts are on. The power of each burst is different and depends on the gap

length as shown in the measurements e.g. Fig. 3.4 on page 31. For the *case 1*, where each channel is 50% occupied with bursts, the average power in the burst is almost 0.65 mW. If the load of each channel is only 20% (*case 2*), the average power in the burst increases significantly to 1.3 mW. That means the average power in the burst depends on the traffic load (burst-gap ratio) in the channels.

To explain the cross gain modulation effects between the bursts on different WDM channels in an EDFA, an EDFA with two burst mode input channels with burst peak input power of -28 dBm are simulated numerically. The values for the parameters of the EDFA can be found in Appendix A. The bursts have a duration of 100 μs. The two input channels are chosen at $\lambda_1 = 1554$ nm and $\lambda_2 = 1553$ nm. The two signals at the EDFA output are shown in Fig. 3.10.

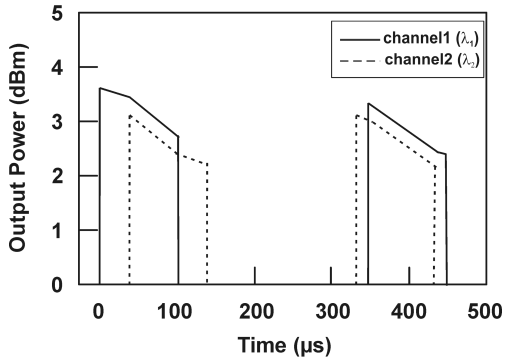

Figure 3.10: Numerical result at an EDFA output for two burst mode input channels with the peak input power -28 dBm each burst.

As the first burst arrives on channel 1 (λ_1) the gain starts to decrease. When the next burst on channel 2 (λ_2) arrives and overlaps the first burst, the gain decreases faster, due to stronger stimulated emission and the power curves become steeper. When overlapping terminates at the end of the first burst, the slope relaxes. When the next bursts arrive, the gain has recovered again during the gap and the same behaviour occurs again.

If a burst arrives at the EDFA input after a long gap of e.g. several ms, a large power excursion will result in the burst at the EDFA output. In Fig. 3.11 the dependence of the power excursion on the burst length is shown for one channel. The power excursion increases with the burst length. This case is surely the worst case in a real network. The traffic in such a network has certain statistics and the power excursion will be in general lower. Nevertheless, large power excursions must be avoided in any cases. In today's optical network, where the EDFAs are operated in saturation, an extra channel with continuous input power should be used to guarantee a basic load in the network.

To show the stabilizing impact of such an extra channel on the power excursions of the other channel, the following simulation was performed. The extra channel is operated with continuous input power at λ_{extra} = 1558 nm. The data burst signal is operated at λ = 1552 nm and is 30 ms delayed with respect to the extra channel. The averaged input power of the data burst channel is 0 dBm. Both signals are multiplexed and attenuated with -28.4 dB (as also used for the other simulations) and then amplified with the EDFA. The input power of this extra channel is adjusted in the simulation in such a way that a constant EDFA output power of 0 dBm is achieved. As shown in Fig. 3.11, using just one extra channel, the power excursion in the burst channel can be reduced dramatically represented by the dashed line.

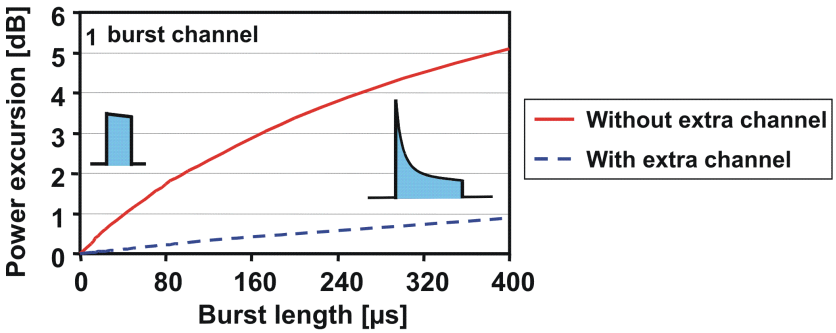

Figure 3.11: Power excursion in the burst versus burst length after an EDFA.

However, the impact of the extra channel depends on the burst lengths and consequently on the traffic load. For WDM burst transmission the power of the extra channel must be adjusted accordingly and this makes this method complex in the practical use. It does also not solve the problem of the dynamic power excursion completely, e.g. if large burst length is used or the traffic load is very low. The effectiveness of this method has to be analysed from case to case and is beyond the scope of this thesis. However to avoid large power excursion after EDFAs, in an OBS network the reservation channel for burst header packets can be used as extra channel.

4) WDM Burst Transmission after an EDFA Cascade

Now the dynamic behaviour of an EDFA cascade is considered. The parameters for simulating the EDFA cascade are adapted from an operated link between Berlin and Darmstadt used by the KomNet project as shown in Fig. 3.12. Details can be found in [9]. The link is composed of seven EDFAs and its length is 756 km. The chain is designed for an 8-channel WDM system using the wavelength band 1549 -1556 nm, with 100 GHz channel spacing and 0 dBm average input power per channel. For the EDFAs parameter values in Appendix A are used, which are typical for EDFAs in the real systems.

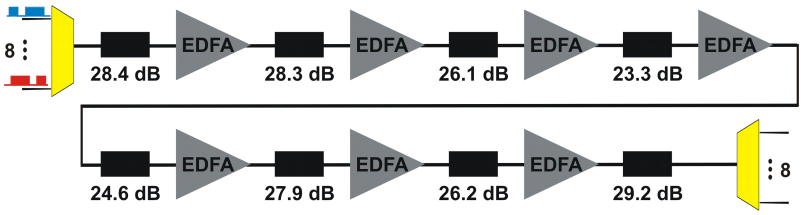

Figure 3.12: Simulation setup for the analysis of the WDM burst transmission after an EDFA cascade.

First the same simulation as for Fig. 3.11 is performed for one burst channel and after the EDFA cascade with 7 EDFAs. Each channel has an average input power of 0 dBm. In Fig. 3.13a the dependence of the power excursion in dB on the burst length after 2, 4, and 7 EDFAs in the cascade is shown. The dependance of the power excursion on the gap length and the number of EDFAs in a cascade are shown in Fig. 3.13b. It can be seen that the power excursion in the burst increases, if the number of amplifiers in a cascade is increased. For the same average input power of 0 dBm, the power excursion at the beginning of the bursts increases with the burst and the gap length.

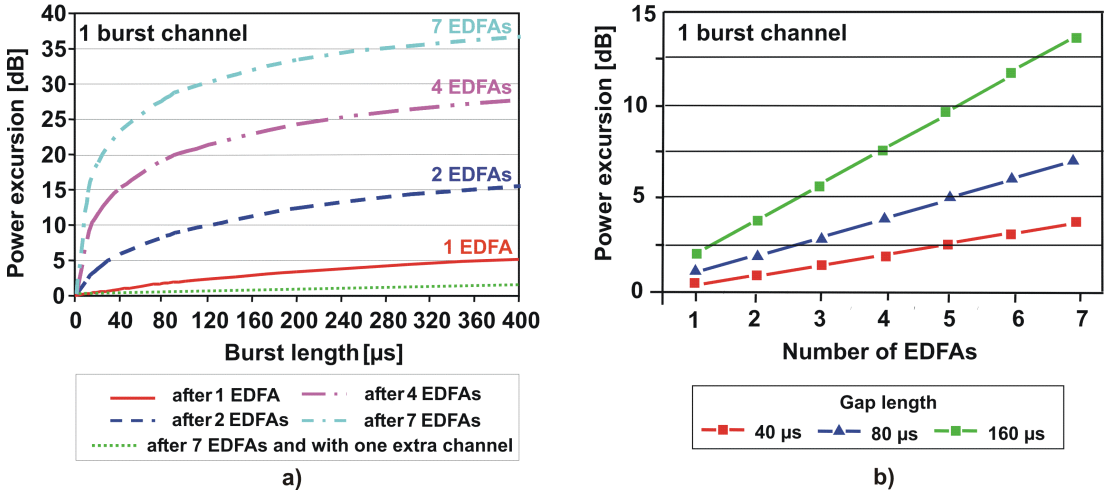

Figure 3.13: Total signal power excursions, a) as function of burst length for different number of cascaded EDFAs, b) as a function of cascaded EDFAs for different gap lengths. Each channel has an average input power of 0 dBm.

Using the same extra channel with continuous power as in the previous single EDFA case, the power excursion after 7 EDFAs can also be reduced significantly (as shown in Fig. 3.13a). The remaining power excursion for a 400 μs burst length after 7 EDFAs here is 2 dB compared to < 1 dB after 1 EDFA by using one extra channel. That means the effectiveness of the extra channel method not only de-

pends on the traffic load in an OBS network, but also depends on the configuration of the transmission link. Like in the single EDFA case, it has to be analysed from case to case.

To find out the typical time constant of the gain changes in an EDFA cascade, the following simulation is performed. For times $t \leq 0$, the system is in a steady state with all 8 channels operating. At time $t = 0$, four of the eight channels are switched off. Fig. 3.14 shows the power variation as a function of time for one of the surviving channels (at 1553 nm) after 1 EDFA, 3, 5, and 7 EDFAs in the cascade.

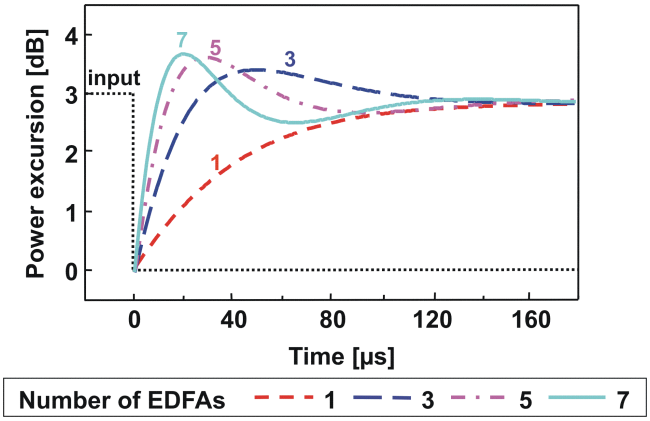

Figure 3.14: Total signal power excursions for one of the surviving channels (at 1553 nm) at the output from numerical simulation along a cascade of seven amplifiers with four of eight channels switched off at $t = 0$.

The response time decreases with the increasing number of cascaded EDFAs. Similar results can also be found numerically calculated in [82] and experimentally measured in [85]. The more EDFAs are in the cascade, the faster is the response time. For 7 EDFAs the response time is clearly reduced to the order of several μs. For a large OBS network, this means that the power variation in the bursts becomes not only larger but also faster along the EDFA cascade.

Finally the eight-channel WDM system as shown in Fig. 3.12 is simulated with random bursty traffic carried by all 8 channels. A burst length of 40 μs is chosen. The gap length is varied to achieve an 0 dBm average input power per channel. For the EDFAs the parameter values in Appendix A are used. Fig. 3.15 shows a simulation result for the output power of one of eight WDM channels (at $\lambda = 1553$ nm), after a cascade of seven EDFAs. The highly varying traffic in the channels and the cross-gain saturation effects in the EDFAs cause significant power excursions of the output bursts. Large power excursions are caused by long gaps in the channels.

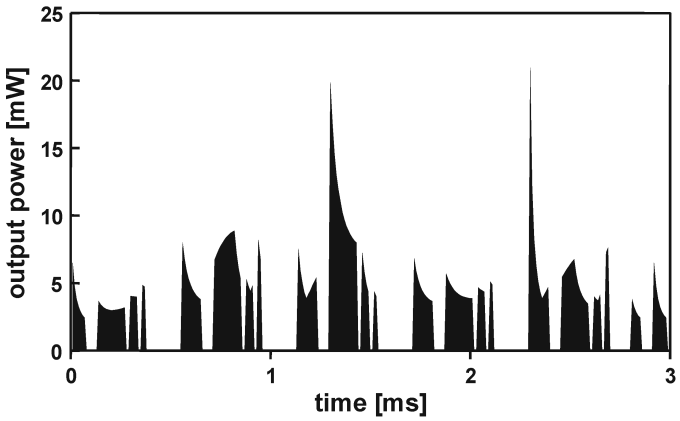

Figure 3.15: Optical power of one of eight burst-mode switched WDM channels after a cascade of seven EDFAs. The burst length of 40 μs is chosen. The gap length is varied to achieve an 0 dBm average input power per channel. For the EDFAs the parameter values in Appendix A are used.

3.2.1.3 Summary

The results from experiments and numerical simulations of this subsection demonstrate that large power excursions occur in WDM channels carrying bursty traffic. Usually, several EDFAs are cascaded in an optical network. In this case, the time constant for gain is decreasing in a chain of X amplifiers according to $1/X$ [86,87]. In addition, the power excursion will accumulate along the EDFA chain [85, 88]. Power excursions of the used channels occur, which result in a decrease of optical signal to noise ratio and a bit error rate increase of the channels.

Moreover, the gain spectrum of conventional EDFAs is dependent on the absolute gain at a particular wavelength. As the gain of an EDFA changes there is a change of the slope of the gain spectrum, too. This dynamic gain tilt results in undesirable variation not only in the gain of signals but also in the gain difference between the WDM channels. A large amount of crosstalk between the channels on the burst level is observed for EDFAs and causes large power excursions as illustrated in Fig. 3.15. The amplitude of the EDFA's output power excursion depends on the channel load, the amount of switched to non-switched power and the length of bursts and gaps. Amplitude and speed of the power excursions increase with the number of cascaded EDFAs.

To ensure proper network operation, it is necessary to stabilize the gain of EDFAs against input power variations in optical switching networks, especially in OBS networks. For an EDFA cascade, fast gain control of EDFAs with response time in the order of microseconds is required.

3.2.2 Comparison of Methods for EDFA Gain Stabilisation

A simple method to reduce the large output power excursions is to fill in the gaps with dummy bursts, especially after long gaps between the bursts. Implementing such filling procedures in real networks is complicated and expensive. An extra channel as saturation control channel can be used to compensate the input power variations. However, as discussed in the last subsection it does not solve the problem completely. The effectiveness of this method depends on the traffic load in an OBS network as well as on the configuration of the transmission link. Therefore, a better solution to stabilize the EDFA gain is the use of a fast gain control with response time in the order of microseconds. Different gain control methods for optical transmission links with an EDFA cascade, which have been proposed, demonstrated, and analyzed in the literature can be classified as shown in Fig. 3.16.

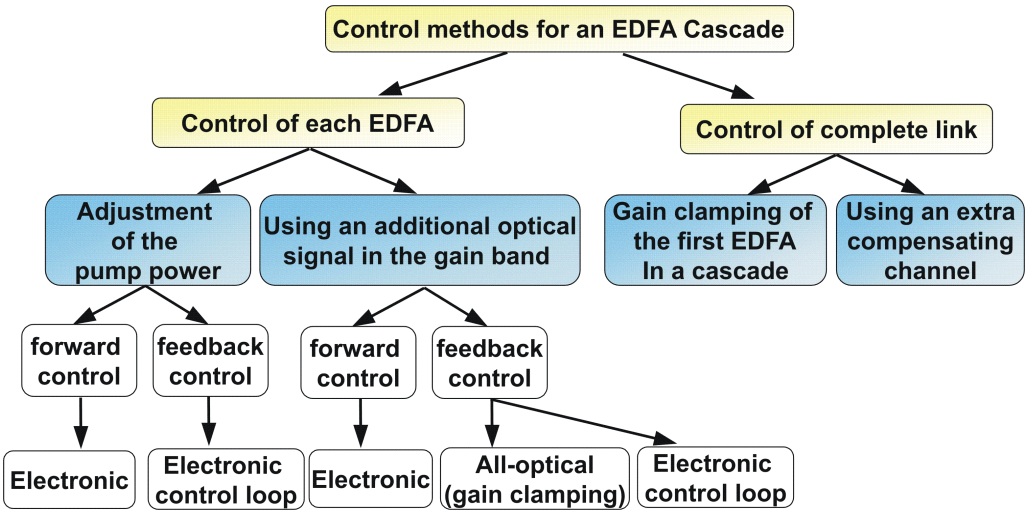

Figure 3.16: Classification of different gain control methods for EDFA cascade.

In the following the different EDFA gain control methods to control the fast power transients of EDFA cascades are compared and their limitations are discussed. An assessment which of the methods is best suited for EDFA cascade in OBS networks is worked out. Details about the individual control methods were published in [89] by the author.

The main criteria for an assessment of different control methods for an EDFA cascade are:

- *The performance of the control*
  An estimate of the required performance could be, that the magnitude of the residual power excursion in the channels is well below 1 dB at the end of an EDFA cascade. The required control response time is proportional to the number of EDFAs in a cascade and is in the order of a microsecond.

- *The cost of the solution*
  Here the cost for implementation (Hardware complexity) as well as the cost for operation and maintenance have to be considered. However, the cost of a solution is hard to estimate. Furthermore, it is only valid for a given time. The discussion here is restricted to remarks on the hardware complexity of the solutions.

There are basically two groups of methods to keep the gain of the EDFAs in a link constant and to minimize power excursions in single wavelength channels. The first group is to *control each EDFA individually* or as the second group to *control the complete link*.

3.2.2.1 Control Each EDFA Individually

In the case where each EDFA in the link is controlled, all EDFAs will be identically configured by using the same control methods as described below. The methods to control the fast power transients of single EDFAs can also be divided into two groups. To control the EDFA gain either the pump power could be adjusted or an extra control channel could be used.

a) Gain Control by Adjustment of the Pump Power

To achieve constant gain for EDFAs it is also possible to adjust the pump power, either by a electronic forward control or using feedback control loop.

Electronic Forward Control
Using the electronic forward control scheme, only a measurement of the input power variation is necessary. The pump power will be adjusted for constant gain, relying on the static characteristic of the amplifier, which has to be determined before. As shown in Fig. 3.17a, for fast gain control of the EDFA, a small part (5%) of the power of the signal channels is tapped at the EDFA input and measured by the pump power control circuit, which adjusts the pump so that the gain is kept constant. This scheme has been proposed and analysed theoretically [90] and demonstrated experimentally in [91] for an 8 channel WDM transmission system. In these experiments the response time of the pump power control circuit was 650 ns. The power excursion of the surviving channel was reduced to 0.17 dB, when 7 of the 8 channels are added or dropped.

The hardware complexity of such an electronic forward control scheme is very low, because only the input power of the EDFA needs to be measured. However, a fast enough modulation input for the pump power has to be implemented in this case. Changes in the amplifier characteristics due to aging or changes in environmental conditions may lead to a degradation of the control performance.

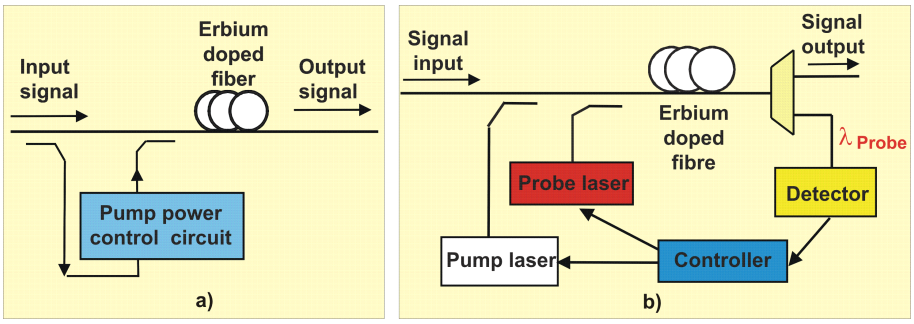

Figure 3.17: Gain control by adjustment of the pump power. a) Electronic forward control, b) Schematic view of a gain block with electronic feedback control [92].

Electronic Feedback Control Loop
Using an electronic feedback control loop, the gain or some parameters proportional to it are continuously measured and the pump power is adjusted to the desired value by a feedback control loop. Examples for gain control using electronic feedback loops have been presented in [92–95].

The schematic view of the electronically controlled gain block proposed in [92] is shown in Fig. 3.17b. It consists of a 980-nm pumped EDFA with a probe laser that is injected into the input of the gain block and measured at the output. The probe laser was at 1572 nm outside the flat gain window used for WDM transmission in this experiment. The control circuit uses negative feedback to the pump current to maintain the EDFA gain constant at the probe laser wavelength. Results are only given for the reduction of gain tilt, but not for the achieved dynamic response. Principally the speed of this control method is determined by the electronic feedback circuit which could be faster than 1 μs.

To measure the gain one can either monitor the power of input and output signals or use an out-of-band probe laser signal for this purpose. A probe signal that has to be created locally means additional expense and complexity. If one just measures the gain of a payload signal one has to take care that it is available all the time. This could be an in band control channel, e.g. the reservation channel in OBS networks.

The main argument against this solution is usually, that it is more complex and needs more electronics than the other methods. This is the case, but on the other hand monitor outputs, which could be used for control purposes, are implemented anyhow in commercial EDFAs. They are equipped with slow automatic gain controls to compensate for slowly changing losses on links and to control gain tilt. So one would only need to upgrade the speed of the monitor receivers, the modulation input for the pump current, and the controller electronics. The cost for this has to be compared with the cost for the implementation of the other methods.

b) Using an Additional Optical Signal in the Gain Band

The second method to control each EDFA in an EDFA cascade individually is to inject an additional optical signal inside the gain bandwidth into the EDFA, in order to control the level of saturation and thereby adjusting the gain. Again adjusting the power in the extra control channel can be achieved by electronic forward control as discussed above or using a feedback control, setting the extra channel power in response to input power changes. The feedback can be implemented electronically as described above or all-optically. If the gain for the extra channel is equal to that of the signal channels (the extra channel is within the flat gain region of the EDFA) the forward control method will keep the optical input power constant. In this case, the method can be used for stabilizing a whole link with an EDFA cascade.

All-optical Feedback Control (Gain Clamping)
The all-optical gain-control technique is widely studied as a potential method to prevent signal power transients due to cross-gain saturation of EDFAs in WDM optical networks [96–101]. Here, an EDFA is made to radiate at a particular wavelength within the EDFA gain bandwidth, which is different from signal wavelengths. The optical feedback (the laser resonator) is usually obtained by two methods:

1. The use of distributed Bragg reflector (DBR) gratings in the fibre at each end of the amplifier, causing reflective feedback at the Bragg wavelength [102–109] as shown in Fig. 3.18a.
2. The use of a ring resonator configuration [110,111] with wavelength selective WDM filters feeding back the lasing wavelength only, as shown in Fig. 3.18b.

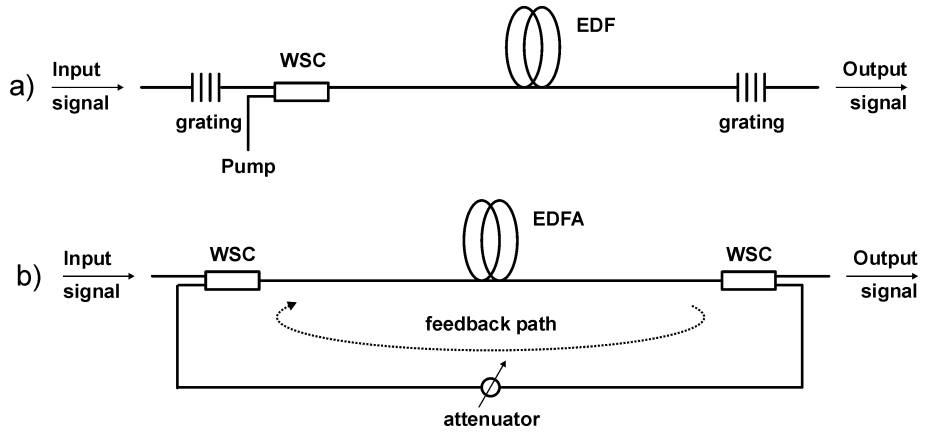

Figure 3.18: Gain clamped amplifier schemes. a) with Fabry Perot laser structure using fibre grating reflectors. b) in a ring laser structure. EDF: erbium-doped fibre, WSC: wavelength selective coupler.

In the first method a constant gain has been achieved by using Bragg gratings in the configuration as shown in Fig. 3.18a [102, 104, 106, 107]. A Fabry-Perot laser structure with two narrow bandpass fibre grating reflectors are placed at the input and the output ends of the amplifier. The lasing wavelength is determined by the center wavelength of the grating reflectors. Laser cavity loss is determined by the peak reflectivity of the grating reflectors and losses between the input and output gratings. With this method a total power transient of a surviving channel as low as 0.3 dB has been achieved, when seven out of eight WDM channels are added or dropped. Additionally, various stabilised gain levels can be achieved by tuning the centre wavelength of one of the inline fibre Bragg gratings, which changes the optical cavity loss [108]. The gain is a monotonously increasing function of the centre wavelength detuning.

Otherwise, gain control can also be achieved by operating the amplifier in a ring-laser configuration as shown in Fig. 3.18b (the second method). The principle of operation is described in [110] theoretically and experimentally. Lasing conditions are controlled by tuning the selected wavelength and varying the attenuation in the feedback loop. This feedback loop can be designed with all-fibre passive components and can be easily implemented in any system using EDFAs. Also countertraveling laser light can be used by placing isolators at the input and the output of the EDFA [88].

For both methods, the gain of the amplifier is clamped to the value corresponding to the laser resonator losses regardless of input signal power level. A decrease of the total signal input power is automatically compensated by an increase of the laser power and vice versa. If each EDFA in a cascade is optically gain-clamped the laser wavelength must be dropped and not propagated to the next amplifier [112–114]. The main advantage of the all-optical gain control by using the laser action in the EDFA is its simple implementation. No intrinsic additional loss for the signal is introduced. However the pump powers required for the controlled operation are quite large. This is because the optical power in the gain band is always at its maximum value (all channels, all bursts on). In contrast to the usual EDFA, the gain cannot be tuned by changing the pump power level, but only by changing the laser resonator losses. Furthermore, the system performance can be degraded due to laser relaxation oscillations [89]. The relaxation oscillations, observed in the laser resonator, give rise to fast oscillations in the signal output power resulting in power excursions which can undershoot the lower gain level and overshoot the higher gain level. The oscillation frequency and damping constants of these oscillations are directly related to the laser cavity loss, the power at the lasing wavelength, the total input power, and the lasing wavelength. The amplitude of the residual power excursions decreases with high pump power and with lower round trip delay. The speed of the optical feedback gain control is limited by the laser relaxation oscillations which are generally in the order of tens of microseconds or slower [97].

3.2.2.2 Control of the Complete Link

To keep the total power on the link constant, two different link control methods can be used. The first one is using a gain clamped amplifier as a first amplifier in a cascade. The signal at the laser output is used as compensating signal for input power variations of the next amplifiers in the cascade. The second method requires an extra compensating channel for the saturating control signal. Both can be implemented at the beginning of the link (the network node) and saves the expenditure for the gain control of the subsequent amplifiers in the link.

a) Gain Clamping of the First EDFA in a cascade

The most investigated link control method is clamping the gain of the first EDFA in the link optically by using a ring laser configuration as shown in 3.18b [112, 113, 115–120]. Special theoretical analysis for burst mode traffic can be found in [121–125].

The output of the first EDFA consists of the amplified data signals and the laser light. The total output power of the first EDFA is nearly constant as explained for single EDFAs. The laser light compensates the power variations in the data channels. Together with the WDM signals the laser light of the first EDFA propagates along the link. The succeeding EDFAs in the link see a constant input power, if the laser signal is within their flat gain region. The gain variation of such EDFAs in the link is suppressed. Because all but the first EDFA are saturated, output power at the end of the chain is not strongly dependent on losses between the amplifiers. The success of this method depends on the EDFA parameters like gain flatness, saturation, and operating point. Different selection of the parameter values can cause over or under compensation in the following EDFAs, with the result that the stabilization of the chain is degraded.

This method is less expensive to implement than controlling each EDFA, since it requires modification of only the first EDFA, but it is sensitive to deviations from gain flatness. Moreover, controlling each amplifier clamps the gain faster and causes smaller residual output power excursions for longer chains. The changes due to the different gains of the signal and compensating channels could accumulate along the EDFA cascade. Therefore gain clamping of only the first EDFA of a cascade seems to be more attractive for short EDFA chains.

Furthermore, Kim et al. [126, 127] have shown experimentally that this all-optical link-control method works only when the channel/burst switching rate is low enough compared to the relaxation oscillation frequency of the gain-clamped EDFA. When the channel/burst switching rate becomes close to the relaxation oscillation frequency, significant power penalties are induced already after a few amplifiers in the controlled link. In the other extreme, where each amplifier in the link is

gain-clamped, the error-free data transmission is always possible even when the channel/burst switching rate becomes close to the relaxation oscillation frequencies of the gain-clamped amplifiers.

Another interesting proposal for an all-optical link control scheme is presented by Bruyère et al. [128]. To achieve gain stabilization in a cascade of EDFAs, a gain-clamped semiconductor amplifier (SOA) is placed before the first EDFA in the amplifier cascade. The laser light of the gain-clamped SOA compensates the variations of the total optical power of the surviving channels effectively up to the output of the amplifier cascade. Because gain-clamped SOAs have intrinsically much faster dynamics (in the nanosecond range) than gain-clamped EDFAs, a gain-clamped SOA could provide a superior solution than EDFA-based schemes for long amplifier cascades.

Link stabilization schemes, where only the first amplifier is optically gain clamped and its laser light serves as a compensating channel for the subsequent amplifiers seem to work only with the required quality for rather short links with only a few cascaded amplifiers. Additionally, this method only works perfect if all channels have the same gain and if the gain spectrum of the EDFAs is really flat. This is fulfilled only approximately in today's broadband EDFAs, where gain equalization is achieved by equalizer filters. In this case the saturation characteristic is different for different channels. How much this effect degrades the performance of the link stabilization schemes quantitatively could be a topic for further investigation. The same problem also occurs with the feed forward control of the pump power.

b) Using an Extra Compensating Channel

A gain control scheme based on the use of an extra WDM channel, compensating the variation of the total optical power and stabilizating all the EDFAs in a link between the network nodes, e.g. OBS core nodes, has been proposed by Zyskind, Sun, and Srivastava et al. [85, 115, 129, 130]. The scheme, illustrated in Fig. 3.19, protects surviving channels on a link by link basis.

The extra control channel is added to the input of the first EDFA in a link (this will commonly be the output EDFA of an OBS core node). The control channel is stripped off at the next node (commonly after its input EDFA). The power of the control channel is adjusted to keep the total power of the control channel and the signal channels constant at the input of the first amplifier. This will maintain a constant channel loading at all EDFA's in the cascade.

In OBS networks, a reservation channel is implemented to carry the burst header packet (BHP) for sending reservation requests to the OBS core nodes. It could be quite attractive to use this channel for compensating the power variations in the

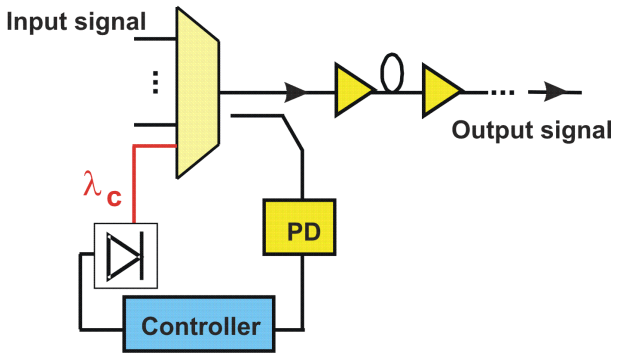

Figure 3.19: Link control by using an extra compensating channel.

payload channels, too. Because of the low data rates on this channel, it should be possible to design a receiver which can tolerate the power variations.

There are also some drawbacks of this compensation method. The maximum power of the compensating channel needed will be drastically increased as the total number of the channels increases. This is also true for the maximum power difference between the compensating signal and the surviving signals. This may cause detrimental nonlinear effects or require a wider flat-gain band. To reduce this problem one could implement one compensating channel for a certain number of WDM-channels (e.g. every eight's channel carries a compensating signal). This again makes the method more complex.

3.2.2.3 Summary

In OBS networks, fast stabilizing the gain of EDFAs is of great importance. There are basically two methods to keep the gain of the amplifiers in a link constant. The first method is to adjust the pump power. This can be done either by using a feedback control loop or by forward control. In the latter case the pump power is changed according to the measured input power, which can be implemented electronically. In the feedback control loop the gain is measured and the pump power is adjusted. This can be implemented all-optically or electronically. The second method is to feed an additional saturating optical signal into the EDFA and thereby adjust the gain. Once again, the power in the additional channel can be adjusted by either feedback or feed forward control. It can also be implemented all-optically (gain-clamped optical amplifier). If the extra channel is within the flat gain region of the EDFA, the feed forward control method keeps the optical input power constant. In this case the method can be used to stabilize a whole link with a EDFA cascade. Also an extra compensating channel can be used to keep the total power on the link constant.

In Tab. 3.2 the performance and hardware complexity of gain control methods for EDFA cascades as discussed above are compared.

	control method	**performance**		**hardware complexity**
		quality (< 1 dB)	achieved speed	
control each EDFA	all-optical feedback	+ (oscillation)	≥ 10 μs [112]	low
	electronic forward control	++	< 1 μs [91]	high
	electronic feedback control	+++	< 10 μs [95]	high
link control	extra control channel	+	1 μs [130]	medium
	gain clamping of first EDFA	- (oscillation, gain flatness)	> 10 μs [112]	low

Table 3.2: Comparison of the gain control methods for EDFA cascades.

At present, there is only very few work published on the fast electronic feedback control of EDFAs, especially no work is dedicated to analyzing cascades of electronically controlled EDFAs. However, this method could still be the most effective way to control the gain of an EDFA cascade in a burst switching environment, if one only considers the technical side. The control should be a feedback loop with the pump power adjusted according to measurements of the amplifier gain using suitable monitor outputs. The gain of the gain block can easily be changed electronically if required. The feedback signal can be filtered electronically, in order to optimise the total dynamic response of the control loop and to avoid the oscillations of gain, observed with the all-optical control method. It makes efficient use of the available pump power (unlike an optically stabilized EDFA where a large part of the pump power is converted into the lasing wavelength). Furthermore it also allows fine control and adjustment of the EDFA gain without sacrificing any of the EDFA transmission bandwidth.

The link control method, which uses an extra channel to compensate the power variations, is less expensive and might fulfill the quality requirements for moderately long amplifier cascades and a moderate number of channels, e.g. possibly a eight-amplifier WDM link carrying seven channels plus one extra link control channel has been demonstrated successfully in [130].

Chapter 4

Design of OBS Core Nodes: Physical Implementations

Without feasible implementations of OBS core nodes, OBS networks will never become a reality. So the focus of this chapter is the physical implementation of OBS core nodes. In Section 4.1 the main functionality and the general structure of such an OBS core node are discussed. The key components in such an OBS node are identified and the requirements for them are then described in Section 4.2. Then different node architectures for building large switch fabrics are given in Section 4.3 in detail. Furthermore, OBS node design requires several performance/complexity trade-offs which will be discussed in Chapter 6 of this thesis in more detail.

4.1 Main Functionality and General Structure of the OBS Core Nodes

Once the IP packets are aggregated into optical bursts at the ingress edge nodes, they will be transmitted in the OBS network through a series of OBS core nodes to a certain destination. As already mentioned in Section 2.3 the main functionality of the OBS core node is forwarding and switching the optical bursts fast and without causing large burst losses during contention. Generally a contention situation in an OBS network can be resolved in the optical layer in one or a combination of the following three domains: wavelength, time, and space domain.

- ***Wavelength Domain - WDM Transmission Technology with Wavelength Conversion***
  In the wavelength domain, WDM technology not only provides increased transmission capacity but also allows for a highly effective contention resolution. If wavelength converters are employed, all wavelengths on a fibre (or within a certain wavelength band) can be shared by all bursts. In teletraffic theory, it is well known that a bundle of k parallel servers each with capacity

c (e.g. channel bit rate b) has a smaller blocking probability and thus a higher utilization than a single server of capacity $k \cdot c$. Using an OBS network based on WDM the burst loss rate on a fibre is lower if the fibre is operated with M wavelength channels at channel bit rate b than with one wavelength channel at bit rate $M \cdot b$ (e.g. a fibre with 16 wavelength channels at 2.5 Gbit/s will have lower burst loss rate than a fibre with one 40 Gbit/s channel). WDM in combination with a wavelength converter in an OBS core node has been investigated intensively for both OPS [32,131–134] and OBS [6,39,62,135–138], also in comparison with other contention resolution schemes. Assuming full wavelength conversion, where every wavelength can be converted into every wavelength, optical bursts can be transmitted on any of the wavelengths of the output fibre. Contention between bursts being sent simultaneously to the same output fibre can then be resolved by using a different wavelength, as long as a free wavelength is available. Therefore, the burst contention can be resolved effectively as shown in Fig. 2.7 on page 21. The need of optical buffering can be reduced or eliminated. Furthermore, this contention resolution scheme does not cause additional loss, burst latency, jitter, and reordering problems. Therefore the wavelength domain should be considered as basic contention resolution domain and the wavelength conversion unit will be an essential part in an OBS core node.

- ***Time domain - Fibre Delay Lines (FDL) Buffer and Burst Segmentation***
  Fibre delay lines (FDLs) offer the possibility of buffering with some similarity to the electronic random access memories (RAMs). A burst can be delayed in the case of contention by using FDLs of a given length. Different kinds of FDL buffer architectures (either in a single or multistage configuration) have been proposed for OPS [22, 26, 29, 30, 35, 139–141]. For OBS many proposals avoid buffers or use only simple FDLs to keep the system significantly less complex than OPS systems [6, 38, 62, 64], other work includes sophisticated buffering concepts [136]. But all of them use FDL buffer in addition to wavelength conversion. Basically two kinds of FDL buffers can be provided in an OBS core nodes:

  - *feed-forward FDL buffer*, where a burst coming out of the buffer goes directly to one of the output ports of the OBS core node;
  - *feedback FDL buffer*, where a burst coming out of the buffer either goes to the output the OBS core node or reenters the space switches and can then be switched to the desired output or to the delay line again.

  Since FDLs rely on the propagation delay in fibres they have, due to the sequential access, much more limitation than electrical RAM. Large buffer capacity needs many and long delay lines. On the physical side this causes

additional losses, and if amplification is applied, additional signal degradation by noise will be caused. Depending on the node architectures, such signal degradation could limit the size and the throughput of OBS core nodes. Furthermore it has also been shown that using FDL buffers the burst loss probability cannot be reduced infinitely. A saturation effect can be observed by a basic delay of $2-3$ times of the mean burst length [64]. Also the sequence in which wavelength conversion and buffering are applied can be exploited to trade off wavelength converter and FDL buffer usage [63]. Such limitations from the network performance could also have strong impact on the design of the OBS core nodes. Therefore the physical as well as traffic performance of the OBS core nodes with FDL-based buffers will be investigated and compared with nodes without buffers later in Chapter 7.

Another time-based contention resolution scheme is *burst segmentation* [142–146]. Here a burst is subdivided in several independent segments. In case of contention, some segments of a burst are either discarded or deflected whereas the remaining part of the burst can still be delivered to the next node. Compared to a solution with the granularity of whole bursts, less bytes are lost. Strategies which realize discarding segments of a burst can be differentiated into head or tail discarding. Head discarding requires the adaption of the offset between header and start of burst. On the other side, tail discarding has to compensate the problem that the header of a burst with discarded tail has already been forwarded to the next node. For reservation of this burst, the next node assumes the wrong (original) length which may result in another contention which is no contention in reality as the burst has been shortened earlier. Other disadvantages of segmentation-based contention resolution are the two introduced overheads. The overhead in Bytes by additional burst headers for every segment, and the overhead in signalling in the OBS core nodes in order to inform succeeding nodes that a burst was shortened. The processing complexity in the core is increasing as a node has to determine what to do in case of a contention and also to manipulate bursts on the data path. This is in contrast to the assumption of transparency and simplicity of OBS. Also smaller transport units require faster switching technology or are less efficient as switching times get more significant. In contrast, the avoidance of small transport units is one of the major drivers for OBS. Therefore, segmentation-based contention resolution will not be considered throughout the rest of this thesis.

- ***Space Domain - Deflection Routing***
  Finally, in meshed networks contention resolution can be also obtained in space by deflection routing, which was considered for both for OPS [147–150] and OBS [65, 151, 152]. If a contention occurs on one output fibre, a burst is sent on another available output fibre of the OBS core node and consequently routed to nodes other than their preferred next-hop nodes. Then it has to

be taken care that the burst will be routed on an alternative path to their destination. Only if there is no alternative, the burst is dropped. That means deflection routing uses the network itself as an extra storage capacity.

There are two main variants of the deflection routing algorithm: first in *deflection routing with alternate routing algorithm*, the optical burst is sent to another output port in order to follow one of a series of pre-calculated alternative routes. If the corresponding output ports from all of these alternative routes are busy, then the burst is dropped off or blocked. The end-to-end delay in the network is limited by the delay of the alternate route with the highest number of hops. However, the disadvantage of the method is a high loss probability at the egress nodes. Since they do not have an alternate route, if a burst finds the output port busy in an egress node, it has to be blocked immediately. Another deflection routing algorithm is the *Random Deflection Routing*. Here the optical burst is send to a randomly selected alternate output port. If the OBS core nodes has the same number of input and output ports, this method is blocking-free, since a burst will always find a free output port (also the node where the burst came from could be included). This is the main advantage of this method. On the other side, since there is no limit to the number of hops through which a burst is transferred, there is no limit for the end-to-end delay as well. In other words, there can be loops. Therefore, high end-to-end delays are possible depending on the network load.

As contention is not resolved locally in a single node but by rerouting overload traffic to neighboring nodes, the effectiveness of this scheme depends strongly on network topology, traffic pattern, and routing strategy. The most important parameter in this context is the connectivity or *nodal degree*, which is a measure of the average number of links per node. The definition for nodal degree is:

$$\text{nodal degree} = \frac{2 \cdot \text{number of (bi-directional) links}}{\text{number of nodes}} \tag{4.1}$$

For big networks, serious delays can be caused. Also it may result in global congestion caused by local congestion and bursts can arrive out of order. Furthermore the implementation of deflection routing depends also on the cascadability of the OBS core nodes, which depends on the physical realisation of such nodes.

As discussed above different contention resolution schemes will have different impact on the performance of the OBS core nodes. To assess the performance of an OBS core node, both technological as well as traffic aspects have to be considered. For the traffic performance the most important parameter is the burst loss rate (or the burst blocking probability). During the last years there are a lot of efforts in the investigations of the optimum dimensioning of an OBS core node, e.g. using

the best combination of contention resolution mechanisms [63–66]. To keep the burst loss rate as low as possible, many concepts, e.g. using optimized combination of wavelength converter pools and FDL buffers [153], using large cascaded FDL buffers [28] and so on, are proposed. However, in this context the physical realisation and limitation of such nodes are still one of the most important open issues. Therefore the main focus of this thesis is the analysis of the physical layer of such OBS core nodes and to find the optimum realisation of such nodes by combining the technological and traffic aspects.

General Structure of an OBS Core Node

In general an OBS node consists of five main building blocks: an input interface, an OBS switch control unit (O/E/O), an optical switch fabric, a wavelength converter unit, and an output interface. The optical switch fabric is generally built with optical space switches. The wavelength converter unit can be placed either at the output or at the input of the nodes as shown schematically in Fig. 4.1.

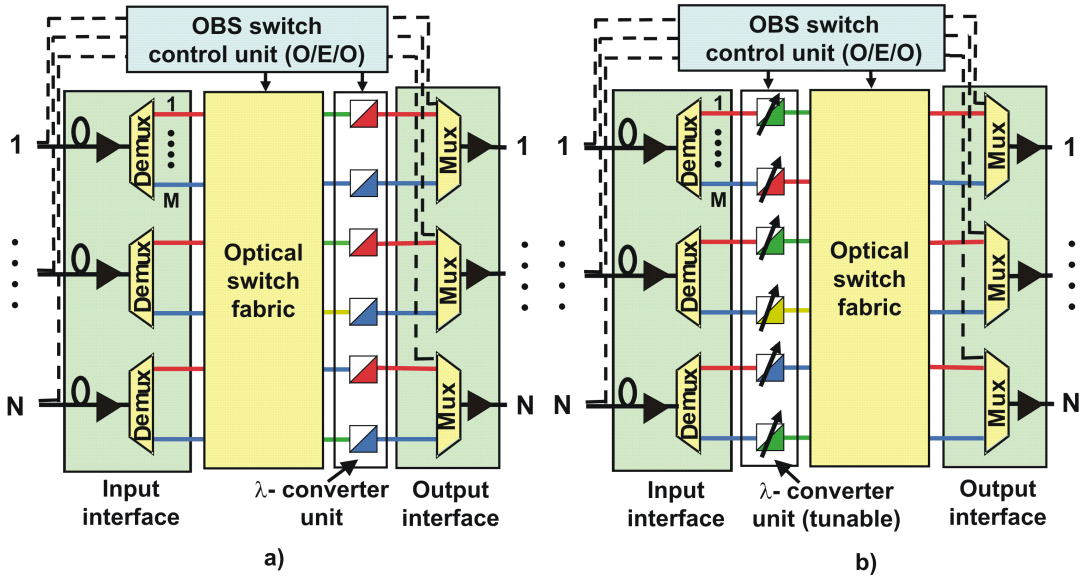

Figure 4.1: OBS nodes with five main building blocks: input interface, OBS switch control unit (O/E/O), optical switch fabric, λ converter unit, and output interface. a) λ converter unit at output with fixed output wavelength and b) λ converter unit at input with tunable output wavelength.

In the figures N indicates the number of in-/output fibres and M the number of wavelengths per fibre without the control wavelength for burst header packets. The fibre delay lines (FDLs) in the input interface are used to delay the data burst while the burst header packets are being processed in the OBS switch control unit (see Section 2.3 on page 20). The incoming signals with data bursts will e.g. be demul-

tiplexed into M wavelengths in the input interface by using WDM demultiplexers and fitted together in the output interface by using WDM multiplexers (Mux). To compensate for splitting losses in the nodes and the losses in the optical switch fabric, EDFAs are required in the input/output interfaces. Like the EDFAs on the transmission links, the EDFAs in the OBS core nodes must be equipped with fast gain control as discussed in Chapter 3. The optical switch fabric and the wavelength converter unit will be controlled by the OBS switch control unit to switch the data bursts to the desired output fibre on the desired output wavelength. For N fibres and M wavelengths per fibre, large NM x NM space switches are required. If the wavelength converters are placed at the output, their output wavelengths can be fixed, unlike wavelength converters at the input, where the output wavelengths must be tunable. With both architectures full wavelength conversion capability can be achieved. Therefore the tuning range of wavelength converters in Fig. 4.1b must cover all the M wavelengths.

With the aim to reducing hardware complexity and cost, OBS nodes with shared wavelength converter pools were also proposed [63, 132]. However, they provide only limited wavelength conversion capability and the technological implementation of such concepts has to be taken into account. Their overall complexity can be higher than that of concepts with full conversion. Furthermore, a high degree of wavelength conversion capability is essential for contention resolution in an OBS network. Therefore this work is looking for node architectures with full wavelength conversion capability. To achieve an acceptable burst loss rate in an OBS network, FDLs can be used additionally. Different structures like FDL pools in a feedback loop, at the input or the output can be used. A detailed analysis of OBS node architectures with FDLs for contention resolution can be found in Chapter 7, where the advantages and disadvantages are discussed for a special implementation of such an OBS core node.

4.2 Key Components in OBS Nodes

This section will concentrate on the key components required for enabling the optical part of the OBS core nodes as shown in Fig. 4.1. The main requirements for them are identified. The existing technologies will be reviewed and discussed in terms of important parameters e.g. such as crosstalk, insertion losses, polarisation and wavelength dependence, and switching speed.

4.2.1 Basic Switch Technologies for Building Optical Switch Fabrics

As shown in Fig. 4.1 the optical switch fabric is the most important part of the OBS core node. Large NM x NM optical switch fabrics are needed for N input/output

fibres and M wavelengths per fibre. The key element in such switch fabrics is the optical space switch. The basic functionality of a space switch is to enable that bursts entering on one input can access a selectable output. The requirements for the space switches suitable for OBS core nodes will be also dependent on the node architecture but generally they must fulfill the following requirements:

- *The ability to build large optical switch fabrics*
  E.g. with $N = 4$ and $M = 64$ a 256 x 256 switch would be needed.
- *Fast switching speed*
  The basic switching elements in the OBS core nodes have to be fast enough to switch the bursts entering on one input to a selectable output. As the bursts have a length in the the μs range depending on the link bit rates, the switching time of the switches should be in the μs or even ns range for efficiency reasons.
- *Low insertion loss or even gain*
  The insertion loss of a switch is the fraction of power (usually expressed in dB) that is lost because of the presence of the switch. Some switches have different losses for different input-output connections. This is an undesirable feature, because it increases the dynamic range of the signals in the network. For such switches, variable optical attenuators to equalize the loss across different paths will be needed.
- *Low crosstalk*
  Switches are not ideal. Even if input x is nominally connected to output y, some power from input x may appear at the other outputs. For a given switching state or interconnection pattern, and output, the crosstalk is the ratio of the power at that output from the desired input to the power from all other inputs. Usually, the crosstalk of a switch is the worst-case crosstalk over all outputs and interconnection patterns.
- *Wavelength independence* (in the EDFA wavelength range)
- *Polarisation independence* (low Polarisation-dependent loss (PDL))
- *High extinction (on/off) ratio*
  The extinction ratio of an on/off switch is the ratio of the output power in the on-state to the output power in the off-state. This ratio should be as high as possible.
- *Multi-wavelength operation and bit-rate transparency*
- *Simple implementation and compactness*

While the switching speed determines the application area of the systems, the other requirements put some constraints on the dimensions of the switching nodes, which will be considered separately in Chapter 6.

In Tab. 4.1 different technologies to realise optical switch fabrics are compared. Most of the values were derived from data sheets for commercially available products.

Technology	**performance**					**Ref.**
	Size	Switching time	Insertion loss [dB]	Crosstalk [dB]	PDL loss [dB]	
Optomechanical	16 x 16	$<$ 10 ms	3	$<$ -55	0.2	[154]
2D MEMS	32 x 32	$<$ 10 ms	1.7-6.9	$<$ -60	0.11-0.16	[155]
3D MEMS	350 x 350	$<$ 10 ms	6 ± 1	$<$ -60	0.4	[156, 157]
	160 x 160	$<$10 ms	$<$ 2	$<$ -55	0.5	[158]
Thermo-optic						
Silica	8 x 8	$<$ 10 ms	8	$<$ -35	0.5	[159]
Polymer	16 x 16	$<$ 10 ms	6	$<$ -30	0.4	[160]
Liquid Crystal	2 x 2	$<$ 10 ms	1.5	$<$ -35	0.1	[161]
Bubble	32 x 32	$<$ 10 ms	7.5	$<$ -50	0.3	[162]
Acousto-optic	1 x N	$<$ 3 μs	6	$<$ -35		[163]
Electro-optic						
$LiNbO_3$	8 x 8	$<$ 10 ns	9	$<$ -35	0.5	[164]
InP	1 x 2	$<$ 10 ns		$<$ -25		[165]
SOA		1 ns	~ 0	$<$ -50	$<$ 1	[166]

Table 4.1: Comparison of different optical switching technologies. Most of them are commercially available.

Comparing the switches in Tab. 4.1 with regard to their suitability for OBS core nodes, only acousto-optic switches, integrated electro-optic switches ($LiNbO_3$ or InP based), and semiconductor optical amplifier (SOA) switches can be used for OBS due to the required fast switching time in the range of μs [167, 168]. Unfortunately, they all have some shortcomings.

Acousto-optic Switches

The operation of acousto-optic switches is based on the acousto-optic effect, i.e., the interaction between sound and light. The principle of operation of a polarization-insensitive acousto-optic switch is as follows: First, the input signal is split into its two polarized components (TE and TM) by a polarization beam splitter. Then, these two components are directed to two distinct parallel waveguides. A surface acoustic wave is subsequently created. This wave travels in the same direction as the lightwaves because of an acousto-optic effect in the material, which is equivalent to a moving grating, phase-matched to an optical wave at a selected wavelength. A signal that is phase-matched is "flipped" from the TM to the TE mode (and vice versa), so that the polarization beam splitter that resides at the output directs it to the lower output. A signal that was not phase-matched exits on the upper output. It is even possible to switch several different wavelengths simultaneously, as it is possible to have several acoustic waves in the material with different frequencies

at the same time. The major drawback of this device is the relatively large insertion losses and large crosstalk. Furthermore the switching speed of acousto-optic switches is limited by the speed of sound and is in the order of μs, which may be too slow for OBS if high link bit rates ($\geq$ 40 Gbit/s) are used.

Electro-optic Switches
An electro-optic switch uses a directional coupler whose coupling ratio is changed by varying the refractive index of the material in the coupling region. Commonly used materials are lithium niobate $LiNbO_3$ and InP. Swiching is accomplished by applying an appropriate voltage to the electrodes. The refractive index of the substrate changes by an electrical voltage. The change in the refractive index manipulates the light through the appropriate waveguide path to the desired port. Therefore, an electro-optic switch is capable of changing its state extremely rapidly, typically in less than 1 ns. The switching time limit of such a switch is determined by the capacitance of the electrode configuration. Their disadvantages are high insertion loss, large crosstalk and a possible polarization dependence. Polarization independence can be achieved but at the cost of a higher driving voltage, which in turn limits the switching speed. Larger switches can be realized by integrating several small 2 x 2 switches on a single substrate, which leads to high loss. E.g. a monolithically integrated 4 x 4 space switch matrix has been fabricated on InP with 16 electro-optic switches [169]. The achievable crosstalk was in the range of $10 - 15$ dB for TE polarization and the loss in the order of 15 dB.

Semiconductor Optical Amplifier (SOA) Switches
SOAs are versatile devices that are used for many purposes in optical networks. An SOA can be used as an on/off gate by varying the bias current to the device. If the bias current is lowered to nearly zero, no population inversion is achieved, and the device absorbs input signals. If the bias current is increased, it amplifies the input signals. The combination of amplification in the on-state and absorption in the off-state makes this device capable of achieving very high extinction (on/off) ratios ($>$ 50 dB). The switching speed is in the order of 1 ns. Larger switches can be fabricated by integrating SOAs with passive couplers. Additionally, the advantages of SOAs are loss compensating capabilities (the gain), and broad amplification bandwidth. Contrary to the acousto-optic and electro-optic switches, where large insertion losses [170, 171] occur, no additional amplifiers are required in the OBS nodes if SOAs are used as on/off gates. The gain of the SOAs can be used to compensate the splitting losses in the nodes. Therefore, in comparison with other fast switches the SOA gate is one of the most attractive candidates for building large optical switch fabrics in OBS core nodes.

However, the biggest disadvantages of SOA gates are power consumption and noise. Therefore SOAs operated with low bias current and optimized for low noise figure are required. Furthermore, many implementations of gates in a WDM network

require gating for multiple channels simultaneously, which increases the total input power to the gate. E.g. the gain of almost 30 dB at 200 mA bias current for low-input signal powers is reduced with increasing signal power [172]. The performance for a conventional SOA will be severely degraded by extinction ratio degradation due to the gain saturation for high input powers. Additionally, the SOA gain varies with the input power leading to cross-gain modulation between the individual WDM channels. Owing to the fast response of the SOA, the modulation will take place on the bit level. These disadvantages of an SOA will cause signal degradation through the OBS core node. For a proper evaluation of today available SOA gates a detailed investigation is very important for the evaluation of SOA-based OBS nodes. Therefore, the performances of different presently available commercial SOAs are analysed in the next chapter experimentally as well as numerically.

4.2.2 The Wavelength Converter and its Regenerative Capability

Having addressed the space switches, another key component in OBS core nodes is the wavelength converter. A wavelength converter is a device that converts data from one incoming wavelength to another outgoing wavelength. As already mentioned before, the ability to switch in the wavelength domain in OBS networks is the most effective contention resolution method. Using converters not only reduces the burst loss rate in OBS core nodes significantly, it also enables flexible network management and more efficient restoration and protection switching [173, 174]. By eliminating or relaxing the wavelength continuity constraint, wavelengths may be assigned to the signals locally at each node. Using wavelength conversion routing and wavelength assignment can be strongly simplified. Therefore many research projects [8, 22, 175] have considered the use of the wavelength converters in their switch block architectures. These examples underline the importance of developing efficient and practical all-optical wavelength converters.

Based on the range of wavelengths that they can handle at their inputs and outputs, the wavelength converters can be classified into four groups:

1. A *fixed-input, fixed-output wavelength converter* takes in a fixed-input wavelength and converts it to a fixed-output wavelength.
2. A *variable-input, fixed-output wavelength converter* takes in a variety of wavelengths but converts the input signal to a fixed-output wavelength.
3. A *fixed-input, variable-output wavelength converter* takes in a fixed-input wavelength and converts it to a variety of wavelengths.
4. A *variable-input, variable-output wavelength converter* can convert any input wavelength to any output wavelength.

Depending on the node architecture, different converters are required. As shown in Fig. 4.1 for OBS core nodes variable-input, fixed-output wavelength converters or variable-input, variable-output wavelength converters are required either at the output or at the input of the nodes. The tunable range of the output wavelength could be unlimited or limited. That means the wavelength converter can convert the input wavelength to any output wavelength (unlimited) or can only convert to a limited group of output wavelengths.

Additional to other applications where wavelength converters are desirable, another important point in an OBS network is: Different signals entering the optical nodes have been transmitted over different distances and amplified by a different number of EDFAs. Consequently, parameters as power levels, signal-to-noise ratios, timing jitter and dispersion will differ for the incoming signals making it impossible to optimise the receiver or to be within the input power dynamic range (IPDR) of the optical components. This is not a problem for a network with electrical nodes since the optical transmitted distance is constant and well defined. Replacing the electrical nodes with optical nodes will result in poorer quality for the traffic which has travelled over longer transmission distance. This leads to a demand for regenerators. Therefore, a wavelength converter which could also provide the same degree of regenerative capability becomes desirable.

Generally there are two types of wavelength converters: 1) O/E/O wavelength converters and 2) all-optical wavelength converters. All-optical wavelength converters can be differentiated in those based on cross modulation effects and those based on non-linear optical four wave mixing.

1) O/E/O wavelength converter

The optoelectronic approach is perhaps the simplest, most obvious, and most practical method today to realise wavelength conversion. The straightforward implementation of a converter is a detector followed by an electronic amplifier, optionally an electronic 3R signal regeneration stage, and a transmitter with the desired new output wavelength as realised in transceivers/transponders. These devices are highly integrated modules including an opto-electronic section with laser diodes and photo diodes as well as driver electronics and electrical receiver amplifiers. Most receivers do not usually care about the input wavelength, as long as it is in the 1550 nm window. The laser is usually a fixed-wavelength laser. Therefore such devices have usually an variable-input and fixed-output. If a tunable transmitter laser is used the output wavelength will be tunable. Suitable receiver structures and modulators allow a choice of the modulation format (e.g. intensity modulation (IM), differential-phase-shift keying (DPSK)) at the receiver and transmitter side.

Currently transceivers/transponders which enable low-cost transmission up to 10 Gb/s are commercially available from vendors such as e.g. JDS Uniphase [154]

and Intel [176]. Here compact devices with standardized interfaces are provided, where all the optical components are integrated and the electrical interface is used for signal conditioning. A bit rate up to 40 Gbit/s also seems to be achievable. 3R regeneration (re-amplification, reshaping and re-timing) can be provided simultaneously. However, re-timing is a bit rate specific function and transponders performing O/E/O conversions are usually optimized for a specific signal bit rate and transmission format, mainly intensity modulation.

2) All-optical wavelength converters

A lot of effort has been and is still put into all-optical wavelength conversion, where the signal is kept in the optical domain throughout the conversion. The main driver of the concept is the hope, that all-optical wavelength conversion can be implemented at considerably lower cost, as compared to the optoelectronic solution. However all proposed solutions are still under investigation and the technical status which is achieved with O/E/O conversion is not yet reached with optical alternatives. In the following, only the techniques are addressed, which show certain potential for practical implementation.

a) Wavelength conversion by cross gain and phase modulation in SOAs

In such converters the intensity modulation of the input signal is detected and a second input signal is modulated by using this information. The active zone of SOAs is used for detection and modulation simultaneously. Such converters have the same disadvantages as O/E/O converters in terms of transparency. Bit rate transparency can only be offered up to a maximum bit rate given by the modulation bandwidth. These converters are not "format transparent"; they can only be used for intensity modulated signals, as they rely on the non-linear gain curve of the SOA in the cross gain modulation (XGM) converter and non-linear transfer function for the interferometers in cross phase modulation (XPM) converter.

a1) XGM wavelength converter

Wavelength conversion based on cross gain modulation (XGM) in SOAs is the simplest technique to realise all-optical wavelength conversion. It relies on gain saturation as the input power in the SOA is increased. The modulated input signal at wavelength λ_{in}, and a CW signal at λ_{out} are injected in the SOA. The high optical power in the marks of the signal at λ_{in} causes depletion of carriers in the SOA leading to gain saturation. The CW light at λ_{out} experiences this change in the SOA gain. So CW light traversing the SOA together with a mark will experience a lower gain than the light traversing with a space and vice versa. Consequently, the information is transferred from λ_{in} to λ_{out}, but the converted signal is inverted compared to the input signal. Co-propagated and counter-propagated signals can be used as shown in Fig. 4.2. The modulation bandwidth for using co-propagating signals and CW light is higher than for the counter-propagating scheme [177]. Additionally, the noise figure is higher for counter-propagation since the carrier

density will be lower in the part of the SOA where the CW light enters. This is due to the amplified input signal, coming from the opposite direction causing a strong saturation and therefore a higher noise figure than for the co-directional case. However, the counter-propagation scheme has several advantages from the system perspective. The filter at the output can be avoided making the converter simpler and more cost-effective. As there is no filter the output wavelength can easily be tuned and it is possible to convert to the same wavelength. The highest demonstrated bit rate today is 40 Gbit/s [178, 179].

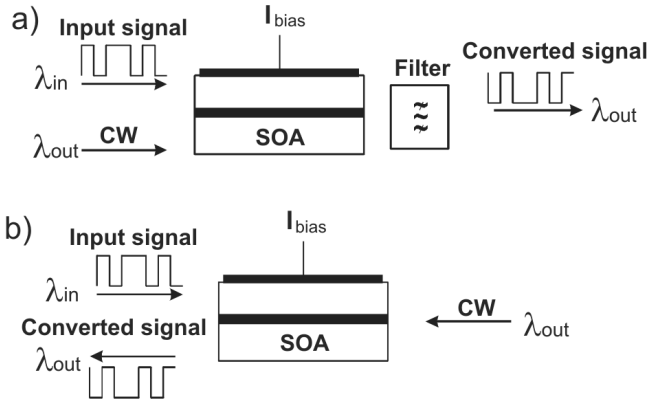

Figure 4.2: Wavelength conversion by XGM in a SOA. a) The signal and CW light co-propagate, hence a filter is used to remove the remaining signal at λ_{in}. b) No filter is needed for counter-propagation of the signal and the CW light.

The disadvantage of XGM converters is the insufficient quality of the output signal. The converted signal is inverted compared to the input signal, which causes additional effort for use in a system. Another drawback is the wavelength dependent conversion. Conversion from lower to higher frequencies (longer to shorter wavelengths) give better extinction ratios because the differential gain is higher at the high frequency (short wavelength) side of the gain peak. So conversion to lower frequencies (longer wavelengths) reduces the extinction ratio and limits the cascadability of XGM converters [180]. Conversion to the same wavelength can only be achieved with counter-propagated signals which unfortunately have a higher noise figure. Since the technique is optically controlled, it requires an optical power level that is high enough to induce the necessary gain modulation. The high optical power levels cause the converted signals to be strongly chirped, thus reducing the transmission distance over dispersive standard fibre. For this reasons, XGM converters cannot be used in optical networks.

a2) XPM wavelength converter

The wavelength converter based on cross phase modulation (XPM) in SOAs is the most promising all-optical solution. The dependency of the refractive index in SOAs on the carrier density and hence on an optical input signal is the basis

of cross-phase modulation (XPM). To make use of the XPM, the SOAs have to be placed in an interferometer structure. The most promising realisations of such interferometric wavelength converters (IWCs) are the integration of SOAs in a Mach-Zehnder interferometer (MZI) [181–185] and a Michelson interferometer (MI) [186, 187] as shown in Fig. 4.3.

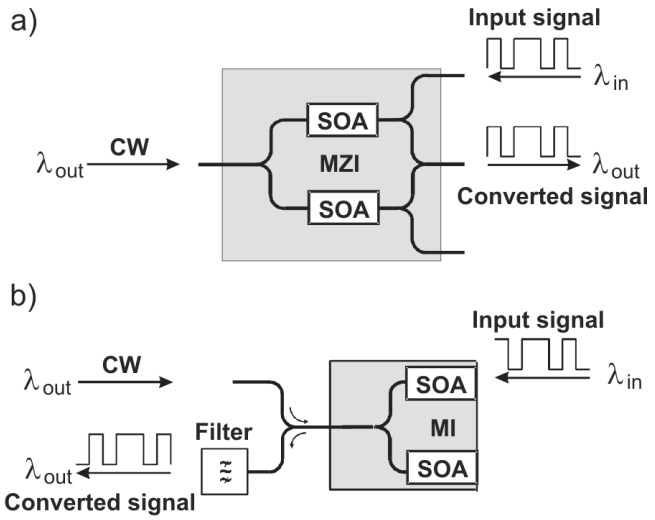

Figure 4.3: Wavelength conversion by XPM in a) Mach-Zehnder interferometer, and b) Michelson interferometer. The Mach-Zehnder interferometer is here operated with counter-propagating signal and CW light.

In a symmetric Mach-Zehnder interferometer (MZI) as shown in Fig. 4.3 a), the MZI is formed by splitters and the input signal is fed to only one of the SOAs through an additional coupler. The carrier density in the upper SOA is modulated. Hereby, the refractive index in the SOA is modulated causing the phase of the CW light propagating in the upper SOA to be modulated according to the bit pattern of the signal. The other half of the CW light propagates through the lower SOA and experiences no phase modulation. At the output, the CW light from the two SOAs interfere either constructively or destructively depending on the phase difference between the two SOAs and is thus controlled by the input signal. The signal and CW light can also co-propagate in the MZI resulting in the same drawbacks and advantages as for the XGM converter: the modulation bandwidth is larger but a filter is needed at the output, and conversion to the same wavelength as the input signal is not possible.

In a Michelson interferometer (MI) (Fig. 4.3 b)) a CW signal at λ_{out} is coupled to the input arm of the power splitter and splits equally between the two interferometer arms. The light is subsequently amplified and partly reflected at the SOA outputs. Depending on the phase-delay between the two arms, the reflected

CW-signal will be combined constructively or destructively at the input arm of the power splitter. The phase-delay of one of the interferometer arms can be controlled by an input signal at λ_{in} inserted to one of the SOAs directly. Therefore, at the output of the coupler, the CW signal at λ_{out} can be modulated according to the data at λ_{in}. A filter for blocking the input signal at λ_{in} is required, and conversion to the same wavelength as the input signal is not possible.

Compared to XGM converters the interferometric wavelength converters are more efficient, because much lower signal power is required to achieve a large phase shift compared to a large gain shift, which is required in XGM converters. Additionally, this method also produces a better extinction ratio [188–190]. Depending on the selected operating point of SOAs the output signal of interferometric wavelength converters can be inverted or not inverted.

b)Wavelength conversion based on non-linear mixing (coherent conversion)
With coherent wavelength conversion techniques based on nonlinear optical wave mixing such as four wave mixing (FWM) in the SOAs and in optical fibres, and difference frequency generation (DFG) based methods in periodically poled $LiNbO_3$ (PPNL), an exact copy of the input signal is generated at the desired output wavelength by mixing with a pump signal. The optical field (magnitude and phase) is transferred to output frequencies independent of the modulation of the input signal. Such converters are universal, as only the carrier frequency of the input signal changes. Conversion of multi channels at the same time is allowed. Moreover, among the all-optical techniques conversion by FWM and DFG is transparent to the modulation format and is thus capable of converting analogue signals and signals with phase modulation formats.

However, such converters impose still a lot of challenges, mainly due to the poor conversion efficiency [191,192]. As the signal-to-noise ratio is inversely proportional to the conversion efficiency, it is troublesome to cascade several of these converters, especially at high bit rates where a high signal-to-noise ratio is necessary. The conversion efficiency depends also strongly on wavelength and the gain of the additional amplifier must be readjusted by changing of in-/output wavelength. Due to the transparency all signal degradations will be accumulated if such converters are cascaded. Additional disadvantages are the polarisation sensitivity and the required high pump power. Also the pump wavelength has to be adjusted by using a tunable pump source [191] to achieve the required output wavelength. Further analyses of FWM and DFG converters can be found in [191–196].

Comparing the different types of the wavelength converters, only coherent wavelength conversion techniques can be used if complete transparency is required. These converters are able to convert even phase modulated (e.g. differential phase shift keying (DPSK) and differential quadrature phase shift keying (DQPSK)) sig-

nals. Conversion of phase modulated signals can also be achieved using O/E/O converters, using suitable receivers and transmitters. However the conversion is then restricted to the special modulation format. Also if the bit rate of the signal is far above 40 Gbit/s, coherent converters may be the only solution, due to the speed limitations of the other methods. At present such converters are still under research and rather far away from system applications.

If the requirements are restricted to the conversion to intensity modulated signals with a data rate up to 40 Gbit/s, O/E/O converters or optical XPM converters can be used. From today's point of view the O/E/O converter is the only one which can provide the full 3R regeneration capability in combination with wavelength conversion. The main disadvantage of this solution is its complexity and cost. The required optoelectronic devices are expensive, especially at high bit rates. However, the alternative in the optical domain is also not so simple and inexpensive. The optical XPM converter will be only preferred, if it can operate stably and the manufacturing is much more cost-efficient than using transceivers/transponders for high bit rates. Also the comparison of operational costs might be an essential issue.

As the obtained solutions for all-optical wavelength converters are still under development and not yet mature enough for commercial use, in the following, only O/E/O wavelength converters will be considered, especially in Chapter 6, where the maximum size of the OBS nodes are evaluated.

4.2.3 Passive Components

In OBS core nodes large scale multiplexers/demultiplexers are needed in the input/output interfaces as shown in Fig 4.1. A M x 1 multiplexer combines signals at different M wavelengths on its input ports onto a common output port, and a 1 x M demultiplexer performs the opposite function. For both applications the arrayed waveguide gratings (AWGs) are the preferable solution to provide large number of wavelengths (M). An AWG has lower loss, flatter passband, and is easier to realise on an integrated-optic substrate, e.g. Silicon. Today AWGs are widely used in WDM transmission systems and up to 80 channels are commercially available [197].

Depending on the architecture of optical switch fabric, large wavelength independent splitters and combiners could be necessary in the OBS nodes. A 1 x X splitter could be used to split the input signal with one or several wavelengths into X parts, and a X x 1 combiner performs the opposite function. For large OBS core node, large scale splitters/combiners are needed, too. The number of the ports X should be in the range of 64, 128 or even larger. As the theoretical basic loss of such splitters/combinier increases with the increasing number of ports ($10 \log X$ dB), low insertion loss is essential.

To fabricate such large-scale optical splitters/combiners several realisations have been proposed. First method is to cascade a large number of 2 x 2 fused-fibre couplers. This method is costly as well as time consuming and the splitter is physically large. So from today's point of view following two methods are most promising.

First several Y-branch element can be cascaded to achieve large scale splitters and combiniers [198–200]. As shown schematically in Fig. 4.4a in a Y-branch element the width of the single mode input side waveguide is doubled in the taper waveguide which is connected to two output side waveguides. The disadvantage of Y-branches based splitters/combiniers is the large scattering losses. In [201] a one-chip integrated 1 x 128 optical power splitter is fabricated by using silica waveguide technology. It contained 127 Y-branch elements cascaded in seven stages and 128 output waveguides. The average measured excess loss of the splitter was 3.2 dB including fibre-waveguide coupling loss. The standard deviation of the loss was 0.63 dB. The maximum and minimum total losses of this splitter are 25.9 dB and 22.2 dB (theoretically 21.1 dB due to $X = 128$), respectively.

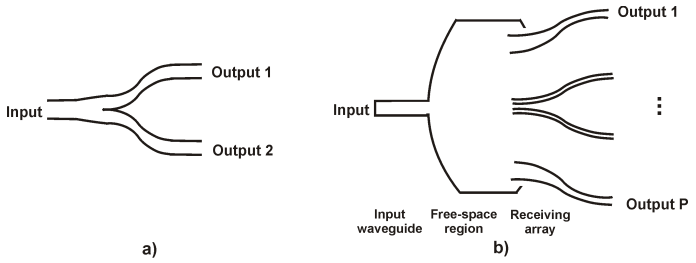

Figure 4.4: Schematic design of optical power splitter/combiner. a) Y-branch element. b) Radiative design.

The second method is based on a radiative design like fabricated in an array waveguide grating (AWG). Here Si/SiO_2 based glass waveguides or InP can be used. As shown in Fig. 4.4b, the input waveguide radiates its power into the planar free-space region, which is a dielectric slab placed between the input waveguide and the receiving array of P waveguides. The efficiency of the device is given by the ratio of the power coupled into the waveguides and the total input power. The power radiated outside the receiving array aperture and the power loss due to the nonzero gaps between the waveguides reduce the efficiency. Using InP the splitter/combiner can be integrated with other optoelectronic components. However, the polarisation sensitivity increases and the fibre-waveguide coupling is more difficult. A 1 x 16 radiative power splitter based on InP has been demonstrated in [200]. The straight waveguide losses are well below 1 dB/cm. Good uniformity (2.6 dB for TE and 4 dB for the TM mode) and excess loss below 3 dB have been achieved.

4.3 Architectures for Building Optical Switch Fabrics

As discussed in the last section, today in comparison with other fast switches the SOA gate is one of the most attractive candidates for building large optical switch fabrics in OBS core nodes. Such SOA gates ensure fast switching times of $\sim$ 1 - 10 ns [202], a high on/off ratios ($>$ 50 dB [202]), and they can provide a gain of $\sim$ 30 dB [203] to compensate the losses in the switch fabrics. Moreover, a polarization independent SOA can be realised and it also has a very large optical bandwidth of more than 50 nm [203]. An integrated board compatible with a 16 x 16 SOA gates with $M = 16$ (throughput of 2.56 Tbit/s) has been reported [204, 205]. Therefore, in the following the focus is on OBS core node architectures with SOAs as on/off gates.

To avoid additional burst losses in an OBS core node, the optical switch fabric should be nonblocking. That means an unused input port can be connected to any unused output port. A nonblocking switch can be divided into strict and rearrangeably nonblocking. Strict nonblocking means a switch is nonblocking regardless of the applied connection rule. Here any unused input can be connected to any unused output, without rerouting any existing connection. A rearrangeably nonblocking switch may require rerouting of connections to achieve the nonblocking property. While rearrangeably nonblocking architectures use fewer switches, they require a more complex control algorithm to set up connections. The other drawback of rearrangeably nonblocking switches is that existing connections will be disrupted, even temporarily, to accommodate a new connection. In such case, additional burst losses can be caused. Therefore strict nonblocking switch fabrics are preferred for the OBS core nodes.

Generally, to realise large strict nonblocking NM x NM optical switch fabrics, two different architectures can be used:

1) Building Large Switch Fabrics by Cascading Small Switching Elements

In this context, a 2 x 2 switch with 4 SOAs as illustrated in Fig. 4.5a can be used as the basic switching element. To build large switch fabrics for an OBS node, nonblocking multistage structures comparable with electric switching matrices, e.g. crossbar architecture can be used. In Fig. 4.5b a 4 x 4 nonblocking crossbar switch realised using 16 2 x 2 switches is shown. The interconnection between the inputs and the outputs is achieved by appropriately setting the states of the 2 x 2 switches. A NM x NM crossbar switch is made of $(NM)^2$ 2 x 2 switches, where $4 \cdot (NM)^2$ SOAs are required. That means large number of 2 x 2 switch elements and SOAs respectively are needed to build a large switch fabric.

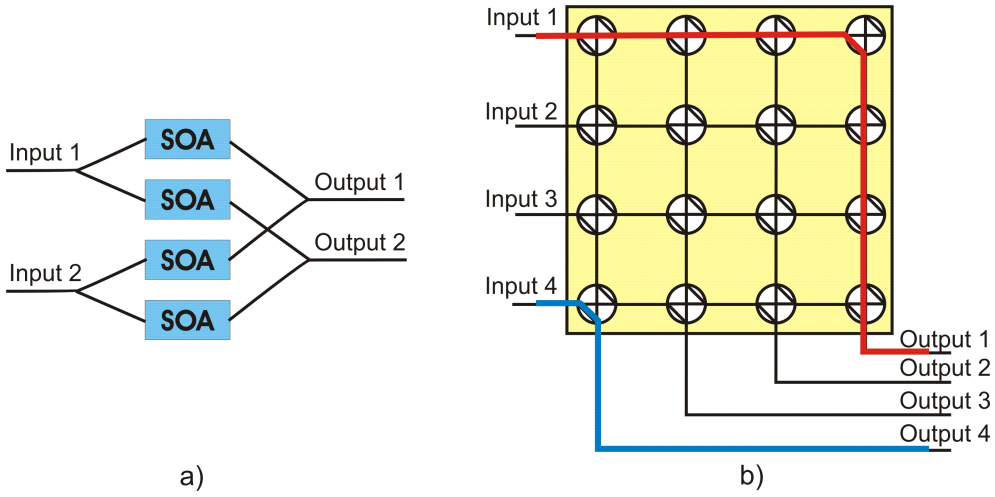

Figure 4.5: a) A 2 x 2 optical switch with 4 SOAs. b) 4 x 4 switch realised with 16 2 x 2 switches (64 SOAs) interconnected in the corssbar architecture.

Furthermore, the length of the signal paths within such crossbar architectures is not the same, the shortest path length is 1, while the longest path length is 2NM-1. This implicits different number of the cascaded SOAs in the different signal paths. To overcome the disadvantages of the crossbar switch fabric and to reduce the required number of basic switching elements and SOAs respectively, other multistage architectures like Beneš, Spanke-Beneš, Spanke, and Clos-architectures can also be used [174].

However, photonic switches are analogue and signal regeneration is not implicitly performed. Signal degradation like high losses and the noise of the SOAs will be accumulated in a multistage architecture and limits the size of the switch. To reduce cost and avoid accumulation of signal degradation the number of cascaded SOAs in the signal path must be as low as possible. Therefore, using SOAs as on/off gates one-stage switch architecture with only one SOA in the signal path is preferred.

2) Single-stage Broadcast-and-Select Architecture

The classical Broadcast-and-Select switch is based on passive $1/(NM)$ splitting of N WDM input signals, each with M wavelengths, followed by active selection at each of the NM outputs. Such Broadcast-and-Select switches have a straightforward capability for multicasting. Their biggest drawback is the high splitting losses which have to be compensated by using additional amplifiers. The decreasing signal quality by adding the amplified spontaneous emission (ASE) noise limits the scalability of such Broadcast-and-Select switches.

For strictly non-blocking Broadcast-and-Select architectures several one-stage architectures have been investigated for OPS [8, 22, 167, 175, 206]. For OBS this concept has been adapted as shown in Fig. 4.6 for the Broadcast-and-Select (BAS) node (a) and the Tune-and-Select (TAS) node (b) [207, 208]. The node has N input/output fibres and M wavelengths per fibre. They are strictly nonblocking and have multicast capability. As shown in Fig. 4.6, for both nodes N^2M SOA gates are required.

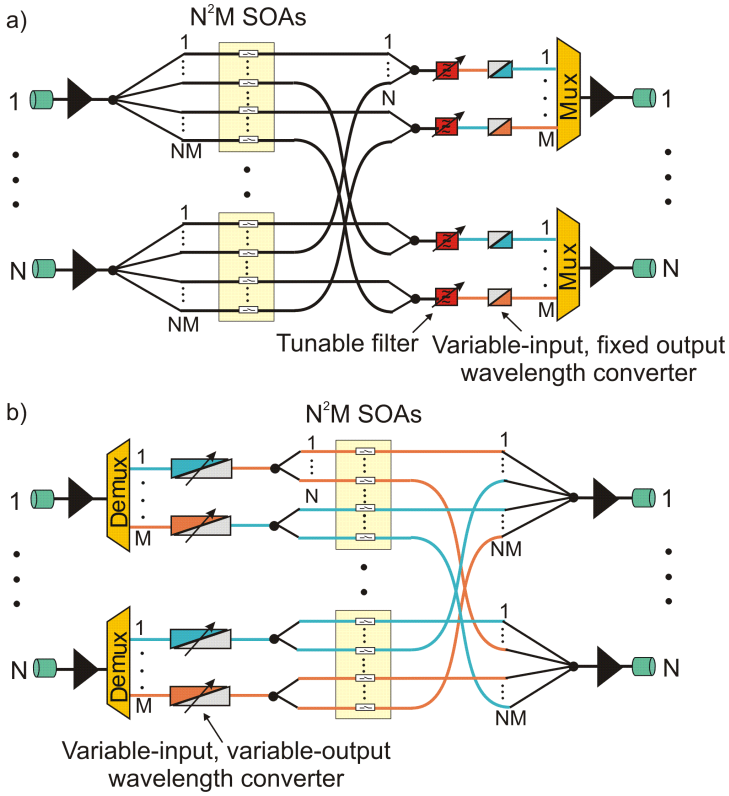

Figure 4.6: OBS core nodes with SOAs as basic switching elements. a) broadcast-and-select (BAS) node, b) tune-and-select (TAS) node. For simplicity no OBS switch control units are shown in both structures.

In the BAS-node the basic switch modules are the SOA gates and the tunable filters for selecting one wavelength. For a node with N fibres and M wavelengths per fibre an input signal is splitted into NM signals (*broadcast*). The following SOA is switched on or off, either one of the M wavelengths has to be switched to the fibre connected to the output of the SOA or not. Afterwards a tunable filter selects this wavelength (*select*) and a wavelength converter with variable-input and fixed-output converts it into the desired output wavelength. Like the SOAs these NM filters must be also tunable in less than 1 μs. Then the wavelength signals are multiplexed to their fibre.

In the TAS-node the basic switch modules are the tunable wavelength converters and the SOA gates. The tunable wavelength converters are used in front of the gates. The input signals are wavelength demultiplexed and the bursts are converted to the desired output wavelength by using the variable-input and variable-output wavelength converters (*tune*). With the following broadcast and select structure, the signal is split up into N signals (splitting loss $1/N$) and is sent towards all output fibres. The bursts are then switched to the desired output fibre, by switching the appropriate SOAs on or off (*select*). At the output of the node, all signals switched to this fibre are combined which also accounts for a power loss of a factor of NM (c.f. splitting factors in Fig. 4.6 b)). For a node with N fibres and M wavelengths per fibre N^2M SOAs and NM variable-input and variable-output wavelength converters with switching times less than 1 μs are required in this node.

Both nodes rely on wavelength converters. For them different implementations can be used as already discussed in the last section. In the BAS node the transmitter output wavelength is fixed, but a tunable optical filter is needed for selecting one of the $1, \ldots, M$ wavelengths in a time range less than 1 μs. The acousto-optical filters with a tuning time in 10 μs range cannot be used and the fast tuneable $LiNbO_3$ electro-optical filters are still under development [209]. In the TAS node the output wavelength of the wavelength converter has to be tunable. For realising tunability of the output wavelength tunable lasers are needed. Several tunable lasers with tuning speeds less than 1 μs have been demonstrated as already discussed in Section 3.1 on page 26.

Several cross connects or optical packet switches using SOAs up to 16x16 [22, 167, 206] and 32x32 [8] in size have been implemented. However, the question is whether large switching nodes can be built for OBS. Depending on the used node architecture, the dimensions of the OBS nodes are additionally determined by the performance of the deployed elements in the nodes. Signal degradation mechanisms like loss, noise, crosstalk, amplifier dynamics and so on limit the maximum size of such nodes. This will be discussed in detail in Chapter 6.

Chapter 5

Investigation of Semiconductor Optical Amplifiers (SOAs) as On/Off Gates

The key element in the OBS core node, which is analysed in this work is the Semiconductor Optical Amplifier (SOA) used as on/off gate. The main reasons to employ SOAs as on/off gates are that the switching speed is sufficiently high, the extinction ratio is high, and that SOAs can compensate for coupling losses. A further advantage is that they can be controlled electronically. Unfortunately, there are several imperfections of SOA gates: polarisation sensitivity, noise, and gain saturation, etc. While the polarisation sensitivity can be minimized technologically, the noise and gain saturation of the SOA gates introduce signal distortions, which will limit the size and the cascadability of the SOA based OBS core nodes.

The objective of this chapter is to investigate the basic characteristics of the today's state of the art SOA gates. First the main requirements for SOAs using for on/off gating application are identified in Section 5.1. Then the recent developments in SOA technology are reviewed in Section 5.2, mainly regarding to the on/off gating application. At present, there are only few SOAs commercially available. The experimental investigations in Section 5.3 will concentrate on two of today commercially available gain-clamped SOAs (GC-SOAs): a gain-clamped SOA from AVANEX (DBR-SOA) and a "linear" optical amplifier (LOA) from Finisar. The principle of the SOA operation as on/off gates is analysed. The static as well as dynamic characteristics of these two GC-SOAs are compared with a conventional SOA experimentally. Finally, in Section 5.4 simple models of the conventional SOA and GC-SOA are developed and validated experimentally. Using these models the limitation of the maximum size and the throughput of the OBS core nodes will be analysed in Chapter 6.

5.1 Main Requirements for SOAs as On/Off Gates

There are three major application areas for the SOAs: as in-line amplifier, on/off gates, and for all-optical signal processing. The requirements for the SOAs depend strongly on the application area of the SOAs. For different applications different parameters should be designed and optimised in a different way. E.g., compared to the SOAs designed for the amplifier application, where a high gain and low noise figure are most important, the SOAs designed for all-optical signal processing require high nonlinearity. Here e.g. increasing the length of a SOA will lead to an improvement in four wave mixing efficiency [210]. However, as the noise figure will increase with the increasing length of the SOA, this will be an impairment for SOA as in-line amplifier and on/off gate. As the main focus of this thesis is using the SOAs as on/off gates in OBS core nodes, the following requirements have to be fulfilled:

1. **Moderate gain**
   The gain requirement for the SOAs as on/off gates is not as stringent as for inline amplification. The gain only should be large enough to compensate the losses in the node.
2. **Low noise figure**
   Amplified spontaneous emission (ASE) has to be kept as low as possible for all applications. Noise is one of the major limiting factors for the size and the cascadability of the SOA based optical nodes. Therefore a low noise figure is an indispensable requirement to keep ASE accumulation low.
3. **High saturation input/output power**
   Usually the required input/output power of the SOAs as on/off gates in an optical node is higher than in the amplifier case, which is caused by the gating of multiple wavelength channels in a WDM system or/and the power budget in the node. Due to the non-linear input-output characteristic of the SOA gates, the SOA gain decreases at high input power. The gain saturation leads to signal distortion and inter symbol interference (ISI) for optical data, decreasing the extinction ratio at the output. To avoid the signal distortion, high saturation input/output power $P_{in,sat}/P_{out,sat}$ is required. This saturation input/output power is defined as the input/output power for which the SOA fibre-to-fibre gain is 3 dB below its unsaturated gain.
4. **Low power consumption, moderate bias current**
   When a SOA is used as optical on/off gate, the amplifier gain is switched on and off by switching the electrical bias current from low to high levels. Therefore a moderate bias current is required to keep the power consumption as low as possible.

5. **Large optical bandwidth, flat gain spectrum**
   The amplifier should provide a large optical bandwidth and the operation should be independent of signal wavelength. That means the gain ripple has to be avoided to ensure a flat gain spectrum in the desired optical gain band. Therefore an ultra-low reflectivity of the facet is required and there should be no resonator in that band. To achieve this, antireflection coating of the facets, combined with angled facets and mode expansion near the facets are usually applied [211–213]. A low residual reflectivity ($R \leq 10^{-4} - 10^{-5}$) to ensure low gain ripple ($\leq 0.5\ dB$) can be achieved.

6. **Low polarisation sensitivity**
   Since the polarization of the optical signal issued from a fibre is usually random and the TE waveguide mode has a higher confinement factor than the TM mode, the SOAs have to be generally polarisation sensitive. To achieve polarisation independence e.g. a tensile strain is generally introduced in the bulk active region and makes the TM material gain higher than that of TE. With high quality epitaxial growth, SOAs of this type routinely exhibit less than 1 dB polarisation dependence across a 50 nm bandwidth [214–216].

7. **Low chirp**
   In the backbone network the signal must be transmitted over a long distance. To facilitate transmission on Standard Single Mode Fibre (SSMF) at high bit rate the signal after the SOAs should be nearly chirp free.

5.2 Recent Developments in SOA Technology

Today, out of many SOA vendors in the past, only few remain active in the market. To the best of our knowledge *Kamelian Ltd.* [166] is the only one that still has different SOAs in its product register. *Finisar Corp.* (acquired *Genoa*) [217] is still selling their linear optical amplifier (LOA), a special type of gain -clamped SOA. Formerly well-know SOA vendors like *Alcatel Optronics*, *Philips Semiconductors*, *Optospeed*, *JDS Uniphases Inc* etc. either do not exist anymore or do not produce SOAs anymore. E.g. SOAs and gain-clamped SOA from *Alcatel Optronics* (was divested to *Avanex* on August 2003) are still available, but not produced anymore. Recently a 4×4 all-optical switch based on SOA gate matrix and passive waveguides on InP substrate is provided by *Fionix Inc.* [218].

However, in the research area there have still been some activities over the last years. Several new proposal on new SOAs and new applications of the SOAs are presented in the literature. In the following different recently proposed and presently commercially available SOAs are first reviewed and then compared regarding to the on/off gating application.

5.2.1 Conventional SOA

The conventional SOA is in principle a semiconductor laser for which the mirrors have been removed by, e.g., anti-reflection (AR) coating in order to prevent oscillation of the Fabry-Perot cavity. To achieve amplification the gain medium has to be inverted, which means that the stimulated emission rate is larger than the stimulated absorption rate. This is obtained by injecting current into the device. The signal is amplified, due to stimulated emission, as it travels along the active waveguide. The gain process is also associated with noise due to spontaneous emission where photons with arbitrary phase and direction are emitted. As mentioned in Section 5.1, using SOA as on/off gate, an amplifier with a flat and ripple free gain profile in a wide optical band (C-band, C+L band respectively) is needed. Therefore the travelling wave (TW) amplifier with low gain ripple ($<$ a few dBs) and the higher bandwidth (up to 3 THz) has to be used. The performance for TW-SOAs depends on the material composition and SOAs based on bulk, multi quantum well (MQW) and quantum dots have been realised, respectively.

1) Bulk SOA
The commercially available SOAs from *Kamelian Ltd.* [166] do not only work in the 1550 nm and in the 1300 nm window, but are also suitable for coarse WDM (CWDM) applications (S- and L-band). A gain up to 20 dB, noise figure less than 7 dB, and polarisation dependence lower than 1 dB can be achieved. The maximum saturation output power is 11 dBm with 250 mA bias current.

In the literature another bulk SOA with higher output saturation power up to 17.6 dBm (1565 nm) with a drive current of 500 mA and a voltage of 1.4 V across the C-band has also been reported [219, 220]. It is a 1.5 mm-long InP-based TW optical amplifier. The device is based on a standard buried hetero-structure design. The active region is 48 nm think and 3 μm wide. The angled waveguide (10 degrees to the crystal axis) allows low coupling losses to fibre and low facet reflectivity without the added complextity of mode expanders. At 20 $^{\circ}C$, the SOA has an unsaturated fibre-to-fibre gain up to 17 dB ($>$ 15 dB), a noise figure below 6 dB (minimum of 5.6 dB at 1550 nm), and the polarisation differential gain is below 1 dB. The fibre coupling loss is 1 dB per facet.

2) Multi Quantum Well SOA
Several multi quantum well (MQW) SOAs (MQW SOAs) were proposed in the literature to achieve high gain and high output saturation power. However, the main drawback of MQW SOAs is the polarisation sensitivity. Recently polarisation insensitive MQW SOAs have been realised where the TE/TM gain difference is eliminated by incorporating strain in the material, but the saturation output power decreased. The following two examples represent the state-of-the-art of MQW SOAs: in [221] a MQW SOA using 16 compensated strain InGaAsP/InGaAs

quantum wells was presented. A high gain up to 27 dB and saturation power up to 17 dBm has been obtained at 240 mA and 700 μm cavity length, respectively. The polarisation sensitivity is less than 1 dB over 85 nm bandwidth. In [211] an angled facet strained MQW semiconductor laser amplifier with integrated mode expanders has been designed and fabricated. A device with a simple single layer antireflection coatings exhibited a maximum of 29 dB fibre-to-fibre gain (at 1540 nm and 250 mA bias current) with a minimum noise figure of 7.2 dB at 26 dB gain and a saturation output power of 7.5 dBm.

3) Quantum Dots SOA

A promising approach to further increase the usable output power is to insert quantum dots (QDs) in the active material [222, 223]. Introducing quantum dots can decrease the optical confinement factor as well as the differential gain due to their complete discrete density-of-states, resulting in high saturation power. The record highest penalty-free output power is now 23 dBm. In addition, QDs are also effective in drastically increasing the bandwidth of SOAs, i.e. the wavelength range where the values of gain, NF, and P_{sat} satisfy the requirements. The most promising quantum-dot SOA is fabricated by *Fujitsu*. Such a QD SOA has a gain larger than 20 dB, NF lower than 7 dB, and 3 dB saturation output power of > 19 dBm, over the record widest bandwidth of 120 nm. A penalty-free output power of 23 dB was realised. But the main drawbacks of this approach are the required large drive current (up to 2 A) and the polarisation dependence [223].

5.2.2 Gain-Clamped SOA (GC-SOA)

Gain clamping is an effective approach in increasing the usable output power and preventing gain saturation. A GC-SOA is a modified version of the conventional SOA where the SOA gain is clamped by an internal laser. It provides a higher saturation input power [202, 214, 224–226]. The principle of the GC-SOA gate is to have an additional light emission within the SOA to adjust the gain of the SOA, i.e., to clamp the gain, relying on the fact that carrier density in a laser is constant when the laser is above threshold. Hereby, a signal coupled to the device will show a constant gain and only power of the laser light will decrease with increasing injected light. Above the point where the laser light is reduced to zero (the laser is switched off), the gain will drop off. The gain is stabilized, but to a lower level compared to the conventional SOA. Furthermore, the gain is clamped by the laser and is difficult to tune. The saturation output power turns out enhanced. Two types of gain-clamped SOAs are commercially available at present: a gain-clamped SOA from *Avanex* (former *Alcatel Optronics*) and a linear optical amplifier (LOA) from *Finisar* (former *Genoa*). In these two GC-SOAs the additional light (laser light) is generated in two different ways.

1) Avanex GC-SOA: Gain-Clamping by Using a Distributed Bragg Reflection (DBR) Laser

One way to achieve gain clamping is accomplished by adding passive distributed Bragg reflector (DBR) regions to each end of a conventional SOA gate while maintaining the anti-reflex (AR) coating of the facets thus allowing a lasing light to exist and absorb the residual gain. The lasing is achieved at the Bragg wavelength, which is designed to be outside the desired gain band (e.g. EDFA window) [171, 214, 224–226].

To simplify writing, in the following the GC-SOA from AVANEX is referred as DBR-SOA. A schematic of the DBR-SOA gate used in the experiments is depicted in Fig. 5.1 showing the device, which basically is a DBR laser with 200 μm passive Bragg regions and a 600 μm active region. Low fiber coupling loss is achieved through optical mode size shaping using a tapered waveguide at the end of the SOA (Fig. 5.1b) in association with transverse evanescent coupling from the upper active SOA towards the passive waveguide.

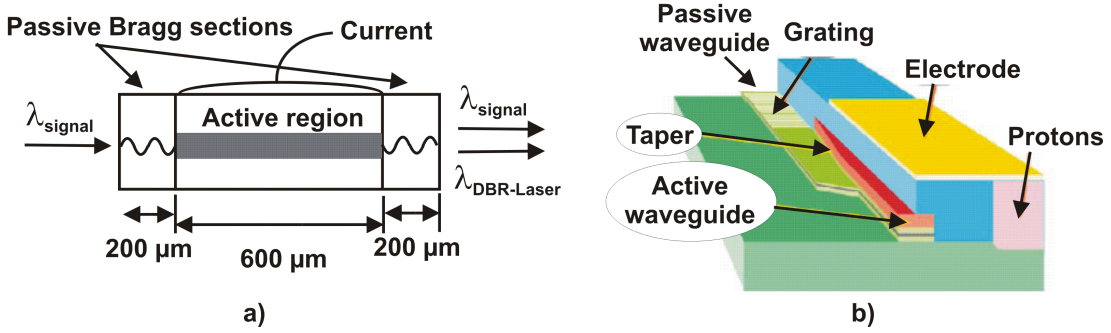

Figure 5.1: a) Schematic view of the 1000 μm long DBR-SOA gate. b) Structure of DBR-SOA fabricated by Avanex with passive waveguide, Bragg regions, active zone, taper and electrode. The passive Bragg regions create lasing at 1508 nm, which clamps the gain [171].

For the DBR-SOA, the internal lasing is at 1508 nm. A gain up to 17 dB can be achieved with -25 dBm input power at 200 mA bias current. The noise figure is lower than 12 dB. The maximum output power is 10 dBm. For moderate input powers the internal laser clamps the gain resulting in a constant gain and a higher saturation power. Increasing the input power causes the amplification for the internal laser to drop and at a certain power level the lasing is switched off and the gain characteristics become similar to what is found for a conventional SOA. The cross-gain modulation can be strongly reduced by the constant gain at lower input power levels [227]. The drawback to the internal laser is that the noise figure for this DBR-SOA is higher owing to the reduced carrier inversion as well as the loss in the input passive Bragg grating adding to the noise figure. Additionally, switching

the laser on and off causes oscillations in the gain at the relaxation frequency of the laser and a power penalty can be caused at a bit rate corresponding to the relaxation frequency [224].

2) Finisar GC-SOA: Gain-Clamping by Using a Vertical Laser
The linear optical amplifier (LOA) produced by Finisar is also an indium-phosphide-based chip amplifier. As shown in Fig. 5.2 schematically a vertical cavity surface emitting laser (VCSEL) is built into the amplifier chip and shares the same active region with the amplifier. The VCSEL has high reflectivity DBR mirrors positioned above and below the active region [217, 228].

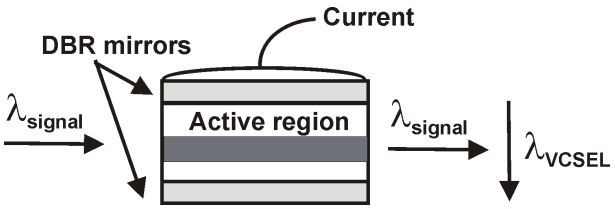

Figure 5.2: Schematic view of a gain-clamped SOA gate with vertical laser which clamps the gain.

The VCSEL operates along the entire length of the amplifier and the lasing action is perpendicular to the propagation of the amplified light. The circulating optical power of the VCSEL overlaps with the amplifier waveguide and keeps the gain of the amplifier constant. The threshold current of the VCSEL is approximately 100 mA and typical operating currents of the LOA are 200 to 300 mA. The amplifier operates across the C-band. A gain up to 17 dB and a saturation output power larger than 13 dBm can be achieved [228–230].

5.2.3 Comparison of Different SOAs and GC-SOAs

In Tab. 5.1 the important parameters for different SOAs are summarized. Among all proposed SOAs, quantum dots SOAs achieve the highest saturation output power P_{sat} and small noise figure NF. Unfortunately, the most critical issues here are the high polarisation dependence and the required high bias current for achieving high gain. For this reason the bulk SOA proposed in [219, 220] could be an interesting alternative for achieving high saturation power P_{sat}.

Comparing commercially available SOAs today, the DBR-SOA from *Avanex* and the LOA from *Finisar* are the most promising amplifiers to be used as on/off gates. All the requirements for gating application (see Section 5.1) could be fulfilled by using both amplifiers. Therefore in the next section these two GC-SOAs will be investigated experimentally and their static as well as dynamic characteristics will be compared with a conventional SOA.

	Gain [dB]	**NF** [dB]	P_{sat} [dBm]	**Current** [A]	**Bandwidth** [nm]	**PDG** [dB]	
Bulk	> 10	< 8	> 8	0.2 - 0.25	C-, S and L-band	< 1	Kamelian [166]
SOA	> 15	< 6	> 17.6	0.5	C-band	< 1	Corning
	> 10	< 7	> 11	0.2			[219, 220]
MQW	> 26		17	0.24	85 (1500 - 1585)	< 1	[221]
SOA	> 26	< 9	> 7.5	0.15 - 0.25	C-band		[211]
QD	> 20	< 7	> 19	1 - 2.5	120 (E- and S-band)	-	Fujitsu
SOA	> 10	< 9	> 19	1 - 2	C-band		[223]
GC-SOA	> 9	< 12	> 10	0.15 - 0.2			Avanex [226]
	> 12	< 8.2	13	0.2 - 0.25	C-band	< 1.8	Finisar [217, 228]

Table 5.1: Comparison of different state of the art SOAs

5.2.4 SOA Arrays

Building large optical switch fabrics with SOA gates, large monolithic integrated arrays of SOA gates could be desirable [172]. The number of discrete components and therefore the packaging cost of the switching matrix could be reduced. Recently a 4×4 all-optical switch based on conventional SOA gates and passive waveguides on InP substrate is commercially available [218]. It operates up to 10 Gbit/s in the wavelength range of 1530 ± 30 nm. The driving current is typically 100 mA. A polarisation dependence loss of < 2.5 dB and a crosstalk of -40 dB can be achieved. The switching speed is in the ns range. It also allows strictly non-blocking operation, multicasting/broadcasting capability and single or multi wavelength switching. 1×4 and 2×2 configurations are also available.

Larger integrated switches based on conventional SOAs have been also reported in the literature. E.g. an optical burst/packet router prototype with throughput of 2.56 Tbit/s was demonstrated by using highly integrated optoelectronic modules with 32 SOA gates (16×16 SOA switches) [204, 205]. Also gain-clamped SOAs can be integrated, e.g. a 8×8 DBR-SOA array has been developed and demonstrated for a 10 Gbit/s WDM switching experiments with 16 wavelengths [231, 232].

5.3 Experimental Investigations of SOA and Gain-Clamped SOA Gates

In this section the two gain-clamped SOAs (the DBR-SOA and the LOA) as described above are investigated experimentally. First the operation principle of the SOA as an on/off gate is analysed. Then the static as well as dynamic characteristics of the DBR-SOAs and the LOAs are compared with a conventional SOA experimentally.

The conventional SOA used here for experiments is a device which was fabricated by *Alcatel Optronics* and based on modified double channel planar buried heterostructure incorporating window structures and a tapered waveguide [203, 214]. It is 450 μm long and has an active layer width and height of 0.7 and 0.4 μm, respectively. The experiments are conducted in a system operating at 10 Gbit/s with an NRZ signal.

5.3.1 Gating Operation Principle

The simplest way to realise an optical gate by the SOAs is to exploit the gain variation with the bias current or the input power. Consequently, two options are possible for fast control of the gate - electrical or optical control. For the electrical control method the gate is opened or closed by varying the bias current to the amplifier, as shown in Fig. 5.3a. The optical input signal passes through the gate if the bias current is high (high gain) and is absorbed if the bias current is low (high loss).

For the optical control method an intensity modulated optical control signal is injected into the SOA as shown in Fig. 5.3b. The wavelength of the signal which has to be gated and the control signal are different. The amplifier gain can be controlled by the optical power, if the power in the control signal is larger than the input saturation power. At low control power levels the SOA gain is high (gate 'on') and at high control power levels the SOA gain is saturated (gate 'off').

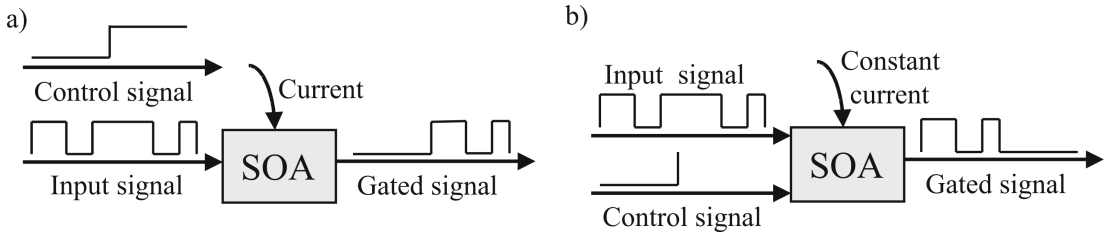

Figure 5.3: Gating operation principle of SOA. a) with electrical control, b) with optical control

With optical control significant faster switching speed e.g. in the picosecond range compared to nanosecond range for electrical control can be achieved [233]. Unfortunately, optical control can only achieve rather limited contrast, because the amplifier can only be bleached out to transparency at the injection wavelength even at high optical power. The on/off ratio is limited to values below 25 dB for realistic control power values [234]. In contrast, with electrically controlled gates a much higher on/off ratio is achievable. In this case, if the injection current is small or zero the active region is strongly absorbing and the input signal is effectively blocked. The achievable on/off ratio depends on the signal wavelength and the

required switching speed. The shorter the wavelength the larger is the achievable on/off ratio. However, by electrically controlled SOA gates, e.g., an on/off ratio larger than 40 dB in a wavelength span of 30 nm with switching speed in several tens of ns can be achieved [234]. Furthermore, the bias current in an optically controlled gate is high (constant) for both the closed and the open state. This results in large power consumption and is additionally a disadvantage for applications like in an OBS network where the gate is closed in longer time intervals (no burst is transmitted). For the OBS core node, a switching time in the ns range and a large on/off ratio are required. Therefore an SOA gate controlled electrically by varying the bias current is preferred and the following investigation will be concentrated on this case.

5.3.2 Static Characteristics

To investigate the static characteristics of the conventional SOA, the DBR-SOA, and the LOA experimentally, the set-up depicted in Fig. 5.4 was used.

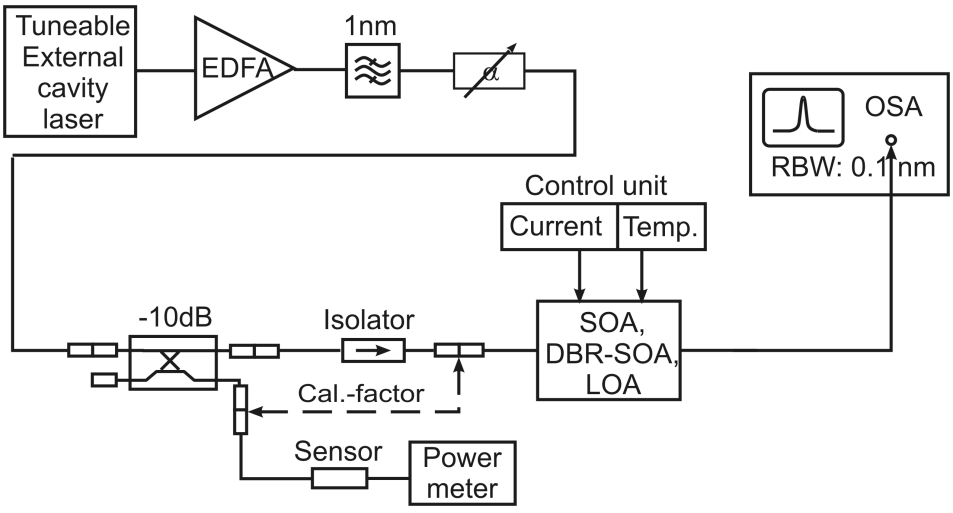

Figure 5.4: Experimental set-up for measuring static characteristics of electrical controlled SOA gate.

The signal source is a tunable external cavity laser. The signal is then amplified and filtered. An attenuator adjusts the required input power for the SOA. To measure the actual input power of the SOA a 10 dB coupler is used. After the SOA/DBR-SOA/LOA the optical signal is analysed with an optical spectrum analyzer. The output characteristics and static on/off ratio for the gates are measured. For all measurements the SOA gates are controlled by current and temperature. The isolator in front of the amplifiers is especially required for the DBR-SOA. It allows only transmission in one direction through it but blocks all transmission in the other direction. In the DBR-SOA, the additional laser light is propagated in the

same direction as the amplified signal. As shown in Fig. 5.5a the laser and the signal wavelengths can be found in the output spectrum of the DBR-SOA, where only the signal wavelength exists at the LOA output (Fig. 5.5b). The isolator prevents therefore the impact of the reflections of the laser light of the DBR-SOA on the measurement.

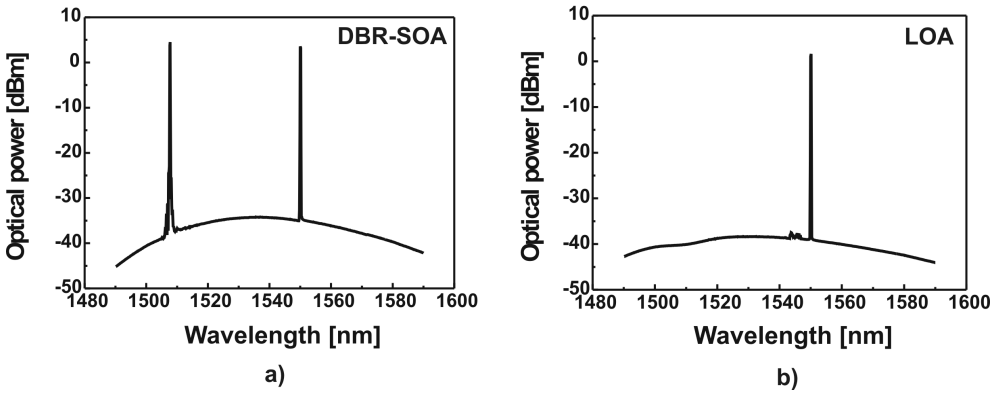

Figure 5.5: Measured output spectrums of the a) DBR-SOA and b) LOA.

A) Gain Dependence on the Bias Current

In the following the static gating performance of the conventional SOA and the GC-SOA gates is described, starting with the dependence on the bias current. In Fig. 5.6a the gain for a conventional SOA gate as a function of the bias current is shown. Here the wavelength is fixed at 1550 nm and the input power is varied. The gain of the conventional SOA increases with increasing bias current, but the maximum achievable gain decreases with increasing input power. This is caused by the gain saturation at large input power values of the conventional SOA, which will be discussed later in details.

In Fig. 5.6b the gain-current characteristics are shown for a conventional SOA, a DBR-SOA and an LOA for an input power of $P_{in} = -15$ dBm. Comparing the three different gates, the largest gain of nearly 25 dB is obtained for the conventional SOA for a supplied bias current of 200 mA. For the DBR-SOA only a gain of 14 dB and nearly 11 dB for the LOA can be achieved. At low bias currents, the semiconductor material (carrier population) is not sufficiently inverted, which yields a net loss (e.g., -5 dB for the SOAs). With increasing bias current maximum inversion is reached and the amplified spontaneous emission (ASE) power increases. Therefore the gain increases with the increasing current and saturates for the conventional SOAs. For the DBR-SOAs and the LOAs the carrier density is clamped above laser threshold, which results in an almost constant gain above a certain bias current (gain-clamping).

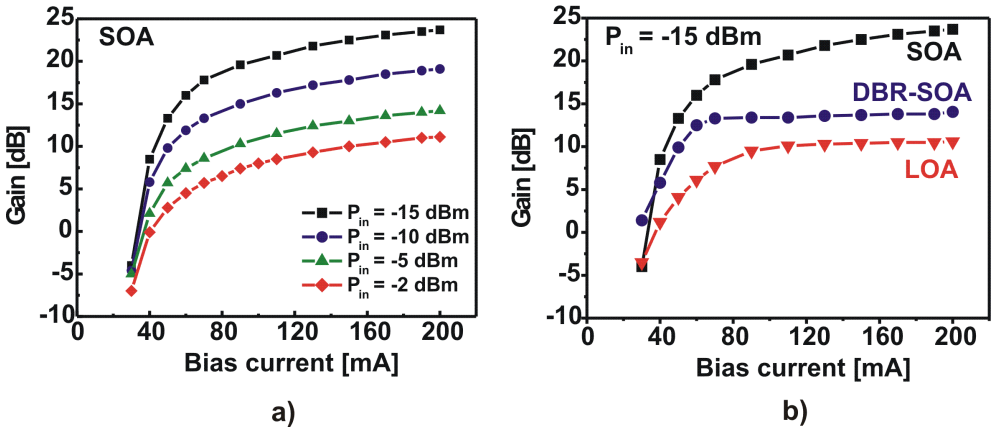

Figure 5.6: Measured values of the gain for the SOA gates versus the bias current. The wavelength is 1550 nm. a) For conventional SOA gate with input power as parameter. b) For the conventional SOA, the DBR-SOA, and the LOA gates with P_{in} = -15 dBm.

Statically, an on/off ratio of $\sim$ 30 dB for the conventional SOA ($\sim$ 15 dB for the DBR-SOA and the LOA) is observed by changing the bias current, e.g., between 30 and 200 mA. The dynamic on/off ratio is determined by the speed in which the inversion can be created or removed, where the removal time is limited by the carrier lifetime. Due to the fast carrier response time in the semiconductor material a dynamic on/off ratio of $\sim$ 50 dB can be obtained within tens of ns [202, 234, 235].

B) Gain and Output Power Dependence on the Input Power

The gain in the SOA gate also depends on the input power, i.e. a low signal input power will see the highest, unsaturated gain whereas the gain will decrease with increasing power levels. This will introduce system impairments since a mark and a space of a binary signal will not be amplified with the same gain and consequently the extinction ratio will degrade. Hence, an essential parameter concerning the SOA gates is the input/output saturation power, i.e. the input/output power where the gain has dropped 3 dB compared to the unsaturated gain. In Fig. 5.7a the measured gain for all three SOAs are shown as a function of the input power with increasing bias current at 1550 nm.

For the conventional SOA the unsaturated gain increases with the bias current and clearly the largest gain is obtained for the smallest input power. On the other hand the input saturation power is decreased by increasing the current. This introduces a trade-off since in a system context both a high gain, i.e. a high bias current but also a high saturation input power are wanted. A high saturation input power will reduce a potential extinction ratio and if multiple channels are gated in the same device cross gain modulation will be minimised.

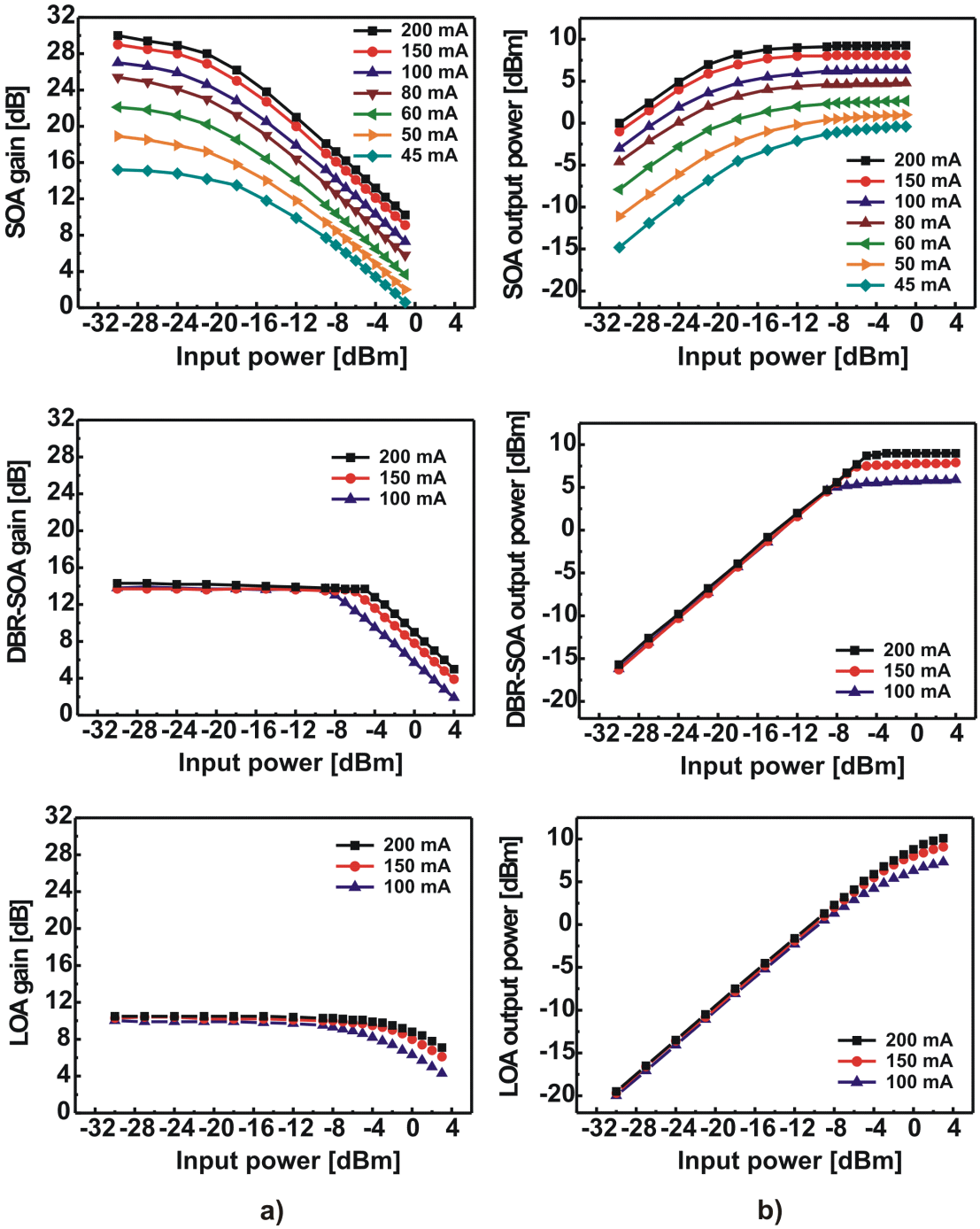

Figure 5.7: The measured characteristics for SOA, DBR-SOA, and LOA gates at 1550 nm with the bias current as the parameter. a) Gain versus input power. b) Output power versus input power.

For the DBR-SOA and the LOA the gain characteristics at 1550 nm as a function of the input power shows a nearly constant gain for lower input power values at bias current larger than 100 mA. The input saturation power is much lower and the maximum gain is much higher for the conventional SOAs. Due to the clamped gain the saturation input power increases from ~ -18 dBm for the conventional SOA gate to ~ -3 dBm for the DBR-SOA gate and to ~ 1 dBm for the LOA gate with 150 mA bias current.

The experiments verify that the gain of the DBR-SOA and the LOA are indeed clamped independent of the current until the amplified signal power level becomes comparable to the power of the lasing mode. Therefore, the extinction ratio degradation due to gain saturation is reduced compared to conventional SOAs. Hence, the saturation input power can be increased slightly to ~ -2 dBm with a bias current of 200 mA for the DBR-SOA gate and to ~ 3 dBm for the LOA gate since the higher bias current yields a higher power in the lasing mode. When the input power is further increased though, the DBR-SOA and the LOA start acting as a conventional amplifier and the gain drops.

Comparing the DBR-SOA and the LOA, larger gain can be reached by using the DBR-SOA. The gain of DBR-SOA drops at a certain input power abruptly, whereas the gain of the LOA decreases gradually. The reason for this different behavior could be found in the different internal laser design which clamp the amplifier gain. Also the different mechanisms how the internal laser is switched off could play an important role, e.g. how fast is the reduction of the power of the lasing mode, respectively.

As discussed in the last section (see Fig. 5.1 and Fig. 5.2 on page 78) the internal laser emission of the DBR-SOA is provided by two passive distributed Bragg reflector (DBR) regions adding to each end of a conventional SOA gate. At a certain input power level the lasing is switched off and the gain characteristics become similar to what is found for a conventional SOA. In the LOA a VCSEL is built into the amplifier chip and share the same active region with the amplifier. The VCSEL operates along the entire length of the amplifier and the lasing action is perpendicular to the propagation of the amplified light. The circulating optical power of the VCSEL overlaps with the amplifier waveguide and keeps the gain of the amplifier constant. The reason for the gain characteristic of the LOAs could be related to the fact that the lasing power of the VCSEL is switched off gradually with increasing input power.

In Fig. 5.7b the corresponding measured output power for all three SOAs are shown as a function of the input power with increasing bias current at 1550 nm. The output/input power relation has a linear characteristic as long as the gain is nearly constant. It saturates when the gain decreases.

c) Noise Figure

As mentioned before the noise figure is one of the most important parameters for the SOA gates used for the OBS core nodes. For the conventional bulk SOA a noise figure of < 8 dB can be achieved [166]. Gain-clamping gives a higher noise figure compared to the conventional SOA [217,226,228]. The additional laser signal saturates the input section of the SOA and results in a reduced carrier inversion and consequently in a higher noise figure. The total noise figure is dominated by the carrier density in the first part of the amplifier. This can be compared to an amplifier cascade where the noise figure of the first amplifier will dominate the total noise figure of the cascade.

Fig. 5.8 shows the noise figure result for the DBR-SOA and the LOA from measurements for a 1550 nm signal as a function of input power. The bias currents are 150 and 200 mA. The coupling losses of ~ 2 dB per facet are included.

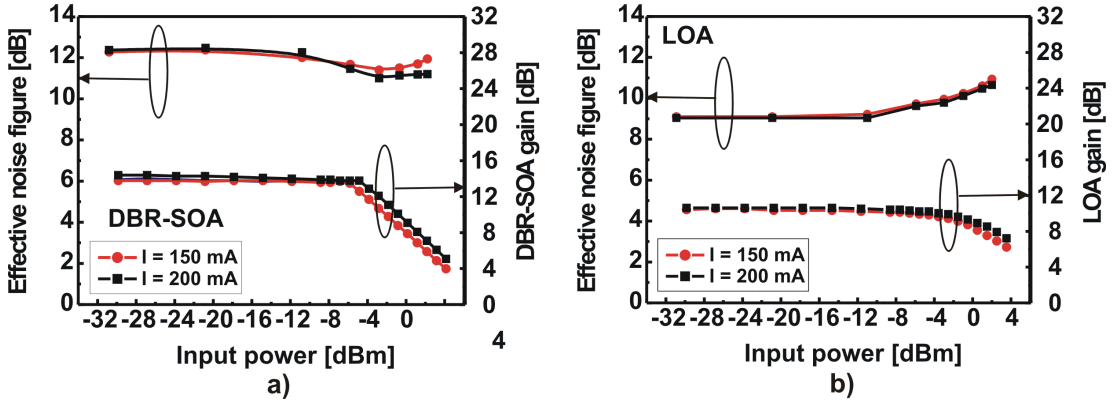

Figure 5.8: The measured noise figure for the DBR-SOA and the LOA gate at 1550 nm versus input power with bias current as parameter.

For the DBR-SOA the noise figure is ~ 11 dB at lower input power and decreases just before saturation occurs (see Fig. 5.7), and then increases. Similar results are also reported in [236,237], where detailed numerical studies of the noise of conventional and gain-clamped SOAs have been performed. For the LOAs a lower noise figure is obtained comparing to DBR-SOA (~ 9 dB at lower input power), and it increases with the increasing input power.

The different noise figure characteristics for the DBR-SOAs and the LOAs could be explained by the different design for the gain clamping in the DBR-SOA and the LOA as shown in the last section in Fig. 5.1 and Fig. 5.2 on page 78. For the DBR-SOA gate the passive Bragg region at the input section causes additional loss that also adds to the noise figure yielding an altogether higher noise figure. The reason for the noise figure decrease for the DBR-SOA just before saturation could

be explained as follows: The DBR-SOA can be thought as a cascade of several smaller subsections. In a cascade of amplifiers, the overall noise figure is primarily determined by the noise figures of the first ones. Hence the noise figure of the DBR-SOA decreases when the first subsections have a better inversion. As the input power increases, the inversion in the first subsections of the DBR-SOA is high due to a weaker lasing signal, the noise figure decreases. As the input power is further increased, the laser turns off and the gain saturates. The noise figure increases again due to the low inversion and low gain.

For the LOA no additional Bragg regions are required resulting in a lower noise figure. The noise figure increases for large input power due to the gain saturation. Additionally, the noise figures for the DBR-SOA as well as the LOA are independent of the bias current.

D) Optical Bandwidth

An important parameter for a gate in an optical burst switched WDM network is the optical bandwidth of the device. In order to ensure a sufficiently high on/off ratio and not to introduce power variations, the gain profile must be flat.

In Fig. 5.9 the gain versus the wavelength with the input power as the parameter is shown for the DBR-SOA (a) and the LOA (b). For a current of 150 mA the 3-dB optical gain bandwidth is > 40 nm for the DBR-SOA and > 50 nm for the LOA, which well covers the EDFA bandwidth of ~ 30 nm. In Fig. 5.9b, the optical bandwidths of the LOA are shown for currents of 150 mA and 200 mA. With increasing current the bandwidth of the material gain increases leading to a larger bandwidth.

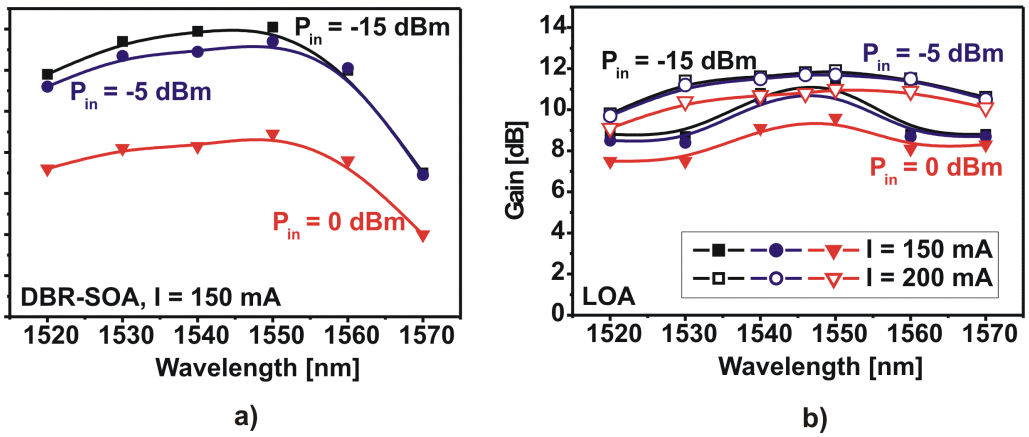

Figure 5.9: The gain versus signal wavelength with the input power as the parameter. a) For the DBR-SOA. b) For the LOA with I = 150 and 200 mA.

5.3.3 Dynamic Performance

To investigate the dynamic performance of the SOA gates experimentally, the set-up depicted in Fig. 5.10 is used. All experiments are performed at 10 Gbit/s with NRZ modulation. The transmitter consists of a DFB laser emitting at 1550 nm and followed by a Mach-Zehnder modulator driven by a 10 Gbit/s PRBS generator. The SOA gates are placed between two variable optical attenuators giving the possibility to vary the input power to the amplifiers and the received power, respectively, to obtain a BER of 10^{-9}. Errors are counted by the 10 Gbit/s BER counter and eye diagrams can be viewed with a spectrum analyser.

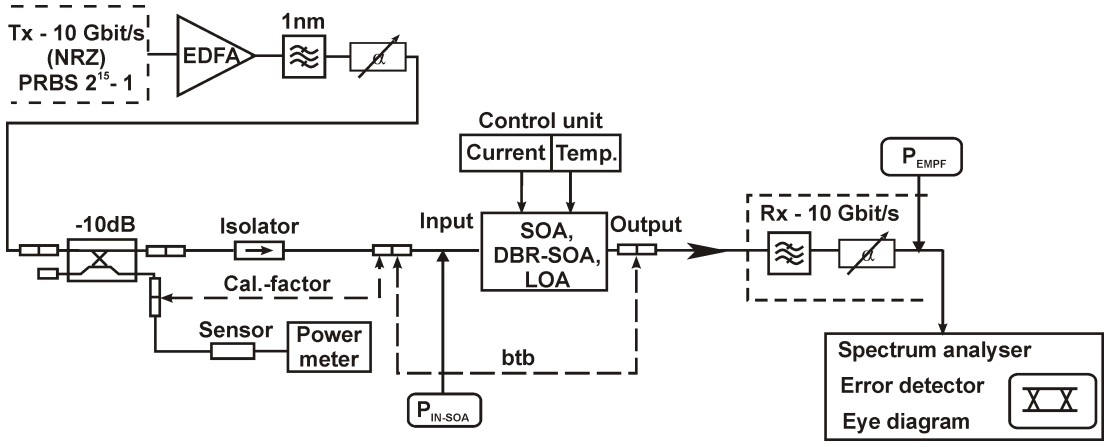

Figure 5.10: Experimental setup for investigation of the dynamic performance of the SOA gates at 10 Gbit/s.

Signal Distortion and Extinction Ratio Degradation of the SOA Gates
For the SOA gates as well as the SOAs used as in-line amplifiers in single wavelength intensity modulated systems there are two types of amplifier induced signal degradations that can influence the system performance significantly. At low input power levels to the SOA the spontaneous noise has the largest influence on the gated signal. At high input power levels, the signal degradation is dominated by gain saturation and results in power excursions on the bit level.

In Fig. 5.11 the input (Fig. 5.11a) and output (Fig. 5.11b-d) signal waveforms after an LOA gate for 10 Gbit/s signal are shown with different average input power levels. The bias current is 200 mA and the wavelength 1550 nm. At -10 dBm input power the LOA is operating in its linear regime giving no waveform distortion (Fig. 5.11b). With increased input power the distortion becomes severe as shown in Fig. 5.11c and d. The amplified pulses have a spike at the leading edges because they experience the full gain whereas the remaining part of the pulse has decreased to saturated level.

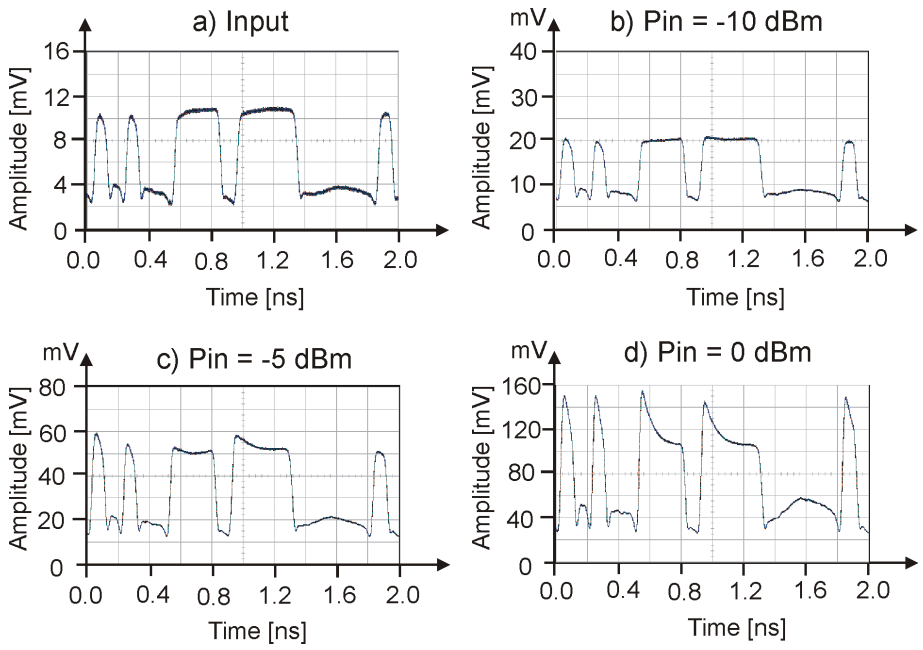

Figure 5.11: Measured PRBS waveforms for increasing average input power levels top the LOA at 10 Gbit/s, bias current is 200 mA. a) Input signal. b) Output signal for P_{in} = -10 dBm. c) Output signal for P_{in} = -5 dBm. d) Output signal for P_{in} = 0 dBm. Note the different scala for y-axis.

For the DBR-SOAs similar results are obtained. Compared to the GC-SOAs, for the conventional SOA the signal distortions occur at much lower input power and the power excursions are much higher. This can be explained by the lower saturation input power and the higher unsaturated gain of the conventional SOAs (see Fig. 5.7 on page 85). Such power excursions will lead to signal distortion and extinction ratio degradation for the amplified signal at the output compared to the input signal. The mechanism behind the extinction ratio degradation can be explained as shown in Fig. 5.12, where the SOA output power is shown as a function of the input power.

Due to the gain saturation, the output versus input power characteristics for the SOA is non-linear. Therefore, an amplified *mark* will experience less gain than an amplified *space* resulting in a smaller extinction ratio at the output compared to the input of the SOA. The reason for this to happen is that the gain dynamics of the SOAs are fast enough to follow the intensity variation of the incoming bit stream [174, 236]. Thus the gain responds in tune with the fluctuations in input power on a bit-by-bit basis. The change of the gain of the SOA gates will lead to power excursions on bit level and reduces the extinction ratio of the output signals.

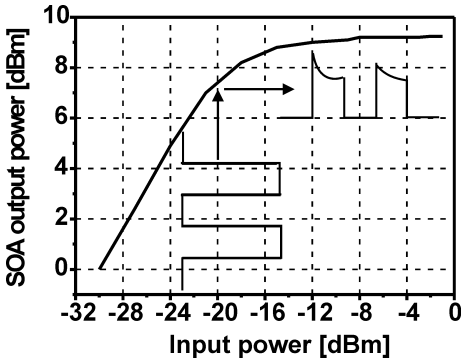

Figure 5.12: Output versus input power characteristics. Due to gain saturation the output pulses have smaller extinction ratio than the input pulses and power excursion occurs at the output.

This is, as discussed in Chapter 3, one of the fundamental differences between the SOA and the EDFA which has a carrier lifetime of the excited states in the ms range and therefore gives the same gain for an amplified *mark* and *space* at Gbit/s bit rates even though it is operated in saturation. Furthermore, when multiple signals at different wavelengths are amplified by a single SOA crosstalk will be produced for the same reason and makes the SOAs unsuitable for amplifying WDM signals. For this reason, amplification of WDM signals by a single SOA must be avoid in an OBS core node based on SOAs.

Receiver Sensitivity Penalty and Dynamic Range of the SOA Gates
As discussed above the gain saturation of the SOAs at high input power level will lead to large signal degradation. The BER increases and the system performance decreases. In this context, the *receiver sensitivity penalty* is a widely used BER quantification criterion to estimate the system performance degradation both in numerical and experimental works. For receiver sensitivity penalty estimation the setup as shown in Fig. 5.10 on page 89 can be used. The receiver sensitivity penalty can be derived from BER measurements of the system in back-to-back (btb) and transmission with SOAs. The measured BER depends on the receiver input power and the receiver sensitivity. By the variation of receiver input power employing different pre-amplifier (EDFA in Fig. 5.10) gains, a BER scan versus the receiver input power (receiver sensitivity) can be realised as illustrated in Fig. 5.13.

For the calculation of the receiver sensitivity penalty, the receiver input power in back-to-back ($P_{receiver,\ btb}$) and transmission with SOAs ($P_{receiver,\ SOA}$) needed for a BER value of 10^{-9} are considered. The receiver sensitivity penalty (RSP) is defined as:

$$RSP[dB] = P_{receiver,SOA}@(BER = 10^{-9}) - P_{receiver,\ btb}@(BER = 10^{-9}) \qquad (5.1)$$

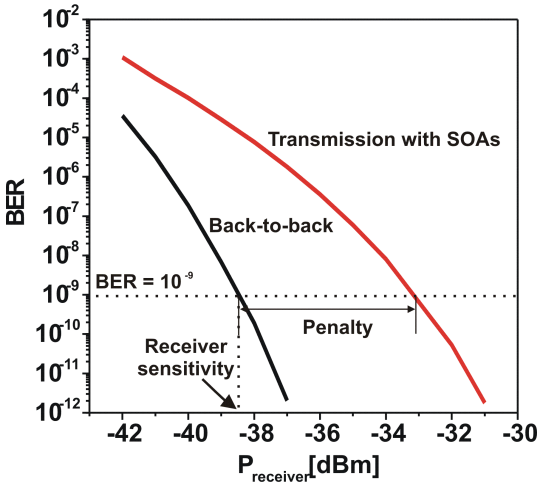

Figure 5.13: Definition of the receiver sensitivity penalty

To estimate the receiver sensitivity penalty result by using different SOA gates, BER measurements are performed for the conventional SOA, the DBR-SOA, and the LOAs. In the Fig. 5.14a the measured BER is shown for the conventional SOA with 200 mA bias current as a function of the receiver input power with the average input power of the SOA as parameter. The corresponding output eyes are shown in Fig. 5.14b. Compared to the btb case, the BER decreases with the increasing average input power of the SOA at lower input power (P_{in} = -25 and -20 dBm, respectively). The resulting receiver sensitivity penalty is mainly caused by the added amplified spontaneous noise and it is therefore larger at lower average input power (2 dB for P_{in} = -25 dBm and 0.5 dB for P_{in} = -20 dBm, respectively). Increasing the average input power of the SOA more and more, the BER and the resulting receiver sensitivity penalty become larger and larger (1 dB for P_{in} = -15 dBm and 4 dB for P_{in} = -12 dBm, respectively). Here the dominating effect is the strong gain saturation and extinction ratio degradation of the conventional SOA at the high input power. The higher the average input power of the SOA is, the larger is the resulting receiver sensitivity penalty and the closer is the corresponding output eye. At low average input power levels the eyes at SOA output and the eye for btb case have the same shape (P_{in} = -25 and -20 dBm in Fig. 5.14b). However, for the increased average input power the amplified pulses have a spike at the leading edge and power excursions occur. The amplified eyes in Fig. 5.14b (P_{in} = -15 and -12 dBm) clearly demonstrate the degradation of the signal quality (extinction ratio) at high average input power levels.

For the DBR-SOA and the LOA driven with 250 mA bias current, the resulting BER as a function of the receiver input power and the corresponding output eye

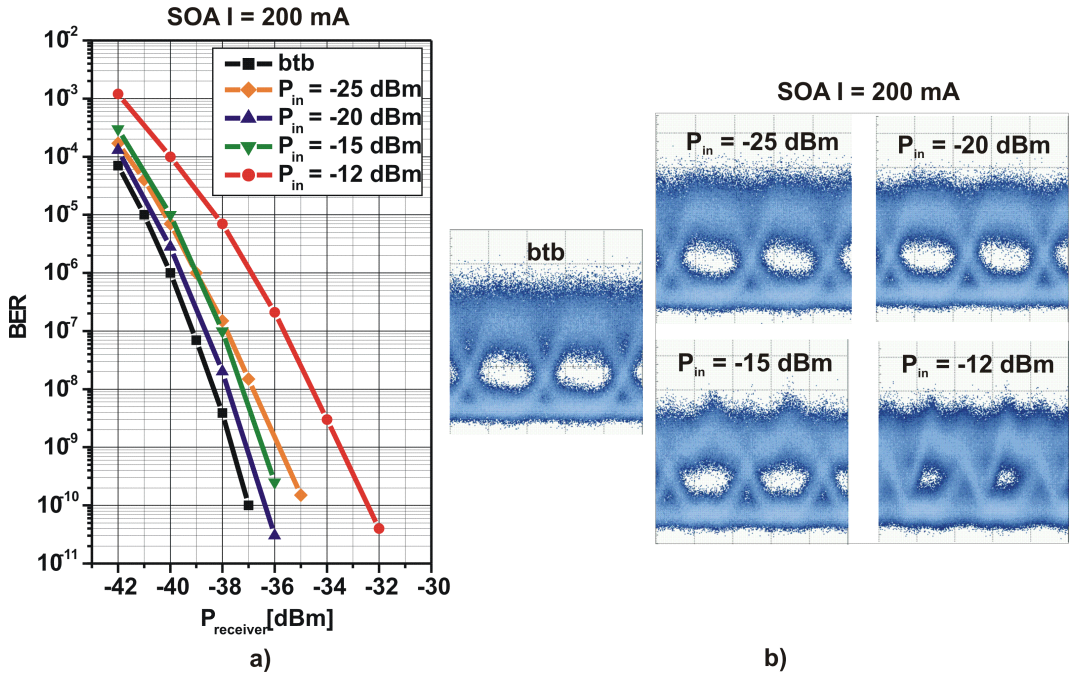

Figure 5.14: a) Measured BER for the conventional SOA with I = 200 mA versus the receiver input power with the average input power of the SOA as parameter. b) Measured corresponding output eye diagrams.

diagrams for the DBR-SOA and the LOA are shown in the Fig. 5.15. The parameters of the average input power levels are -25 dBm, -20 dBm, -15 dBm, and 5 dBm, respectively. Similar to the conventional SOA driven with 200 mA bias current, the BER for the DBR-SOA and the LOA first decreases with the increasing average input power of the SOA as long as the input power levels are low ($P_{in} < -15$ dBm, respectively). Contrary to the conventional SOAs the gain of the DBR-SOA and the LOA is clamped until the internal laser is switched off. Due to the clamped gain the saturation input power is much higher as for the conventional SOA gate (see Fig. 5.7 on page 85). Therefore, the extinction ratio degradation due to gain saturation is reduced compared to conventional SOAs as illustrated in the corresponding eye diagrams. For the DBR-SOA, similar receiver sensitivity penalties as for the conventional SOA result for P_{in} = -25 and -20 dBm, respectively. However, the penalty for P_{in} = -15 dBm is much lower ($\sim$ 0.2 dB for the DBR-SOA compared to 1 dB for the DBR-SOA). If the input power is further increased to P_{in} = 5 dBm, respectively, the DBR-SOA acts as a conventional amplifier and the gain drops. Therefore, the receiver sensitivity penalty increases to almost 5 dB and the output eye has a similar characteristic as the conventional SOA operating at e.g. -15 dBm input power, respectively.

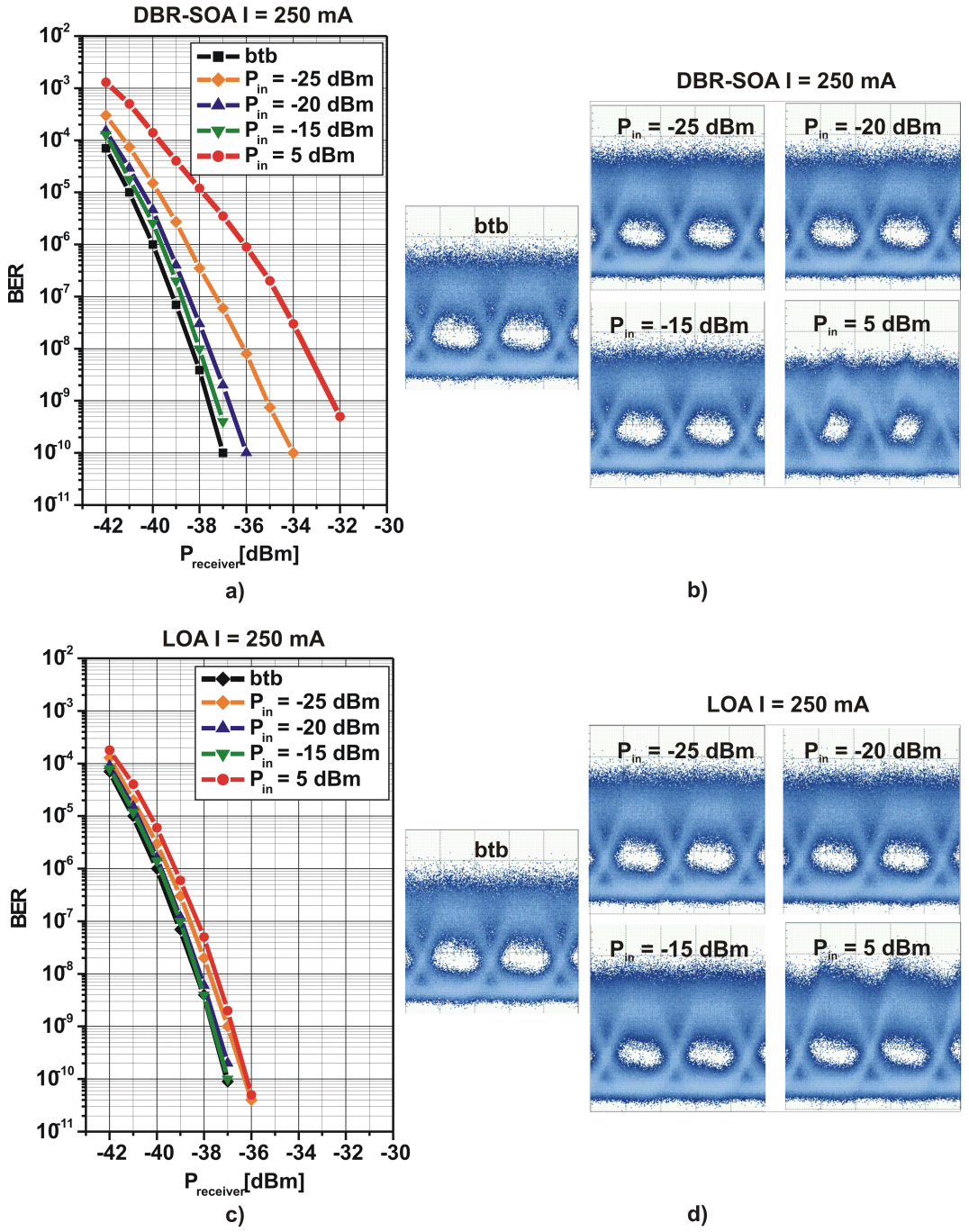

Figure 5.15: Measured BER for a) the DBR-SOA and c) the LOA with I = 250 mA versus the receiver input power with the average input power of the GC-SOAs as parameter. Measured corresponding output eye diagrams for b) the DBR-SOA and d) the LOA.

For the LOA (Fig. 5.15c and d) the receiver sensitivity penalties are less than 1 dB for all four different average input power level. This could be explained by the lower noise figure (see Fig. 5.8 on page 87) and the larger saturation input power (see Fig. 5.7 on page 85) compared to other amplifiers.

For the SOA gates it is also of interest to find the dynamic range where the SOA gates perform satisfactorily. As discussed above the signal degradation imposed by the SOA gates will influence the system performance. The system performance can be evaluated by measuring the receiver sensitivity penalty, which is the power level required at the receiver to obtain e.g. BER = 10^{-9} relative to the power level required without a SOA gate (back-to-back). The dynamic range is then usually defined as the input power range of the SOA gates for which the receiver sensitivity penalty is below 1 dB. At low input power levels the amplified spontaneous noise (ASE) of the SOA gates degrades the signal to noise ratio whereas at high input power levels a penalty is obtained due to the extinction ratio degradation as discussed above.

To compare the input power dynamic range of the three different SOA gates, the conventional SOA is operated with 45 mA as well as 200 mA bias current to obtain the same gain level as the DBR-SOA and the LOA operated with 250 mA. As shown in Fig. 5.16a with a bias current of 45 mA an unsaturated gain of $\sim$ 15 dB can be obtained for an SOA as for the DBR-SOA with 250 mA bias current. With 200 mA bias current similar saturated gain for large input power can be obtained for an SOA as for the DBR-SOA and the LOA with 250 mA bias current.

In Fig. 5.16b the corresponding measured receiver sensitivity penalties at the output of the SOA gates are shown as a function of the average input power of the amplifiers for the conventional SOA, the DBR-SOA, and the LOA at 10 Gbit/s. The limiting factors for the input power dynamic range are a decreasing signal to noise ratio for low input power values and an extinction ratio degradation introduced by the gain saturation for the high input power values. This can be seen in Fig. 5.16b where the receiver sensitivity penalty curves at high input power values start to rise around certain input power values. These input power values are in good correspondence with the saturation input power values of the SOA gates measured in Fig. 5.16a, -22 dBm for the conventional SOA with 45 mA, -16 dBm for the conventional SOA with 200 mA, -2.5 dBm for the DBR-SOA, and > 0 dBm for the LOA, respectively. For the receiver sensitivity power penalty below 1 dB, the allowed input power dynamic range for the conventional SOA with 200 mA at 10 Gbit/s covers -21 to -16 dBm giving a useful dynamic range of 5 dB only. And for SOAs with 45 mA no penalty below 1 dB can be achieved. These experimental results show that, for the conventional SOA to be attractive in realistic systems, it is important to decrease the gain nonlinearity by improving the saturation input power.

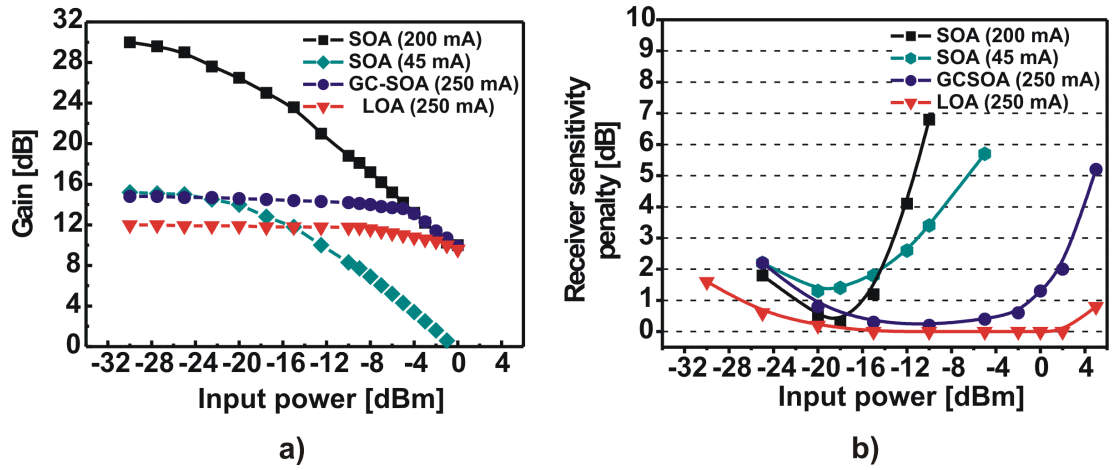

Figure 5.16: Input power dynamic range of the SOA gates, 45 and 200 mA for the SOA, 250 mA for the DBR-SOA and the LOA at 1550 nm and 10 Gbit/s. a) Measured gain versus the input power of the SOA gates. b) Measured penalty versus the input power of the SOA gates.

For a DBR-SOA driven with 250 mA at 10 Gbit/s an input power dynamic range of ∼19 dB measured at 1 dB receiver sensitivity penalty is achieved. Compared to the conventional SOA gate the minimum receiver sensitivity penalty power range for the DBR-SOA is moved to a higher average power level from ∼-16 dBm to ∼-1 dBm. Even a larger input power dynamic range of more than 30 dB can be achieved by using the LOA with 250 mA bias current. The smaller input power dynamic range for the DBR-SOA compared to the LOA could be explained by the lower maximum saturation input power and the laser oscillation in the DBR-SOA. As discussed above the reason therefore could be found in the different internal laser design which clamped the amplifier gain. Also the different mechanisms how the laser is switched off could play an important role, e.g. how fast is the reduction of the power of the lasing mode and the total number of carriers in the cavity. In this context, a detailed analysis of the different internal constructions of the DBR-SOA and LOA are needed, which is out of the scope of this thesis. Summarizing the results from this section, it has been shown that the gain-clamped SOA gates are a very attractive switching device for the OBS networks since larger power variations in single channels and even in multiple channels do not occur in reality.

5.4 Modelling of SOA and GC-SOA Gates

Using SOAs and GC-SOAs as on/off gates in OBS core nodes, the imperfections of the gates will have strong impact on the maximum size and the cascadability of the nodes. As shown in the last section experimentally, signal distortions due

to noise, non-ideal on/off ratio, and the non-linear input-output characteristic etc. of the gates will be introduced. To be able to analyse such physical impairments and their impact on the OBS nodes, numerical models for conventional SOAs and GC-SOAs are required.

The simulations of OBS nodes can be complex and the simulation time increases really fast with e.g. the increasing number of fibres and number of wavelengths per fibre. Therefore the developed SOA/GC-SOA models should be as simple as possible and only the necessary parameters for modelling SOA/GC-SOA as on/off gates with electronic control of the current should be included. The aim was rapid numerical data interpretation, so only fundamental characteristics of SOA/GC-SOA like static and dynamic behaviour should be described correctly. To represent the state of the art SOAs/GC-SOAs as investigated in the previous section the models are validated experimentally.

In the following the simple numerical models for conventional SOAs and GC-SOAs are presented. Both models describe the amplification of signals in the time domain and they can handle arbitrary modulation formats and number of channels. First the fundamental assumptions for both models are summarized in Subsection 5.4.1. The models for conventional SOAs and GC-SOAs are then described in subsection 5.4.2 for conventional SOAs and in subsection 5.4.3 for GC-SOAs separately. To give a more accurate description of the spectral dependence of the gain saturation, for both models the parabolic gain spectrum approximation is used for the material gain. This is described in subsection 5.4.4. In Ssubsection 5.4.5 the static and dynamic characteristics from the simulation are compared with experimental results. A summary of all used equations and the used parameters with their default values can be found in Appendix B.

5.4.1 Fundamental Assumptions

To investigate the static and dynamic behaviour of the SOAs the rate equation for the averaged carrier density is used. In this equation the number of photons in the active region is also included. The number of photons and the output power of the amplifiers can be calculated using the gain and the input power. The following assumptions are made:

- The carrier density n is averaged over the active region of the SOA. This can be justified, if the variation of the carrier density is low in the lateral and transversal direction. It is usually fulfilled for SOAs with moderate gain.
- The propagation effects for the optical field are neglected. This can be justified, as long as the bit length of the input signal is much longer than the optical length of the amplifier. The SOA is viewed as a lumped element with respect to optical power variations within this approximation. E.g. for a 40

Gbit/s optimal signal, the bit length is still two times as long as the optical length of an SOA with 1 mm long active region.

- A fixed distribution of the signal intensity over the transverse section of the active SOA cavity is assumed. The optical field is not totally confined inside the active region. Therefore a transverse optical confinement factor $0 \leq \Gamma \leq 1$ is introduced, which describes the fraction of the lateral power distribution within the active region. This is justified because the transverse field and hence the distribution of the signal intensity in a mono-mode waveguide do not change in the direction of propagation.
- The temperature and polarisation dependence of the gain is also neglected. The first one can be justified with the use of a temperature control. The polarisation dependency can be minimized to 0.5 dB, which can be neglected within the accuracy of the models. The facet reflectivity of the SOA is set to zero, because a facet reflectivity lower than 10^{-5} can be achieved today.

5.4.2 Model for conventional SOAs

5.4.2.1 The Rate Equation for Carrier Density

Under the above assumptions the rate equation for the time variation of carrier density can be written as follows [80, 238]:

$$\frac{dn}{dt} = \frac{I}{eV} - R(n) - \frac{S_s R_{st}(n)}{V} \tag{5.2}$$

The first term on the right hand side depicts the increase in the carrier density by carrier injection, where I is the bias current, e is the elementary charge and $V = L \cdot w \cdot d$ is the volume of the active region. L is the length, w is the width, and d is the thickness of the active region. The second and the third term imply the decrease in the carrier density due to the spontaneous recombination, and the stimulated emission. S_s is the number of photons in the active region. R_{st} represents the stimulated emission rate. The relation between R_{st} and the material gain $g(n)$ is given by

$$R_{st} = v_g \cdot \Gamma g(n) = \frac{c}{n_{\mathit{eff}}} \cdot \Gamma g(n) \tag{5.3}$$

where the v_g is the propagation speed of the signal in the active region with the speed of light in vacuum $c = 3 \cdot 10^8$ m/s and the effective refraction index in InGaAsP/InP $n_{\mathit{eff}} \approx 3.5$. The confinement factor Γ gives the proportion of the optical field inside the active volume.

The carrier recombination rate $R(n)$ is described by a third order polynomial and includes the radiative and non-radiative spontaneous recombinations [239]:

$$R(n) = An + Bn^2 + Cn^3 \tag{5.4}$$

where A, B, and C are constants and related to different recombination mechanisms: Surface and defects state recombinations (An), radiative spontaneous emission (Bn^2), and Auger recombinations (Cn^3).

The propagation of the signal is described by input power P_{in} and the effective gain coefficient g_{eff}:

$$P_s(z) = P_{in} \exp(g_{\mathit{eff}} z) \tag{5.5}$$

The output power P_{out} is then:

$$P_{out} = P_s(L) = P_{in} \exp(g_{\mathit{eff}} L) \tag{5.6}$$

The averaged signal power in the volume $\bar{P}_s$ is determined by averaging the P_s over the length of the active region L:

$$\bar{P}_s = \frac{1}{L} \int_0^L P_s(z) dz = \frac{1}{L} \int_0^L P_{in} \exp(g_{\mathit{eff}}(n) z) dz \tag{5.7}$$

The effective gain coefficient $g_{\mathit{eff}}(n)$, which includes the material gain $g(n)$ as well as the scattering loss α_s in the medium [238], is assumed to be constant :

$$g_{\mathit{eff}}(n) = \Gamma g(n) - \alpha_s \tag{5.8}$$

With the assumption $n(z) = const$ (subsection 5.4.1) the averaged signal power $\bar{P}_s$ in the active region (Eq. 5.7) results in:

$$\bar{P}_s = P_{in} \frac{\exp\left((\Gamma g(n) - \alpha_s) L\right) - 1}{(\Gamma g(n) - \alpha_s) L} \tag{5.9}$$

The number of photons S_s in rate equation Eq. 5.2 and the averaged power $\bar{P}_s$ are related by:

$$S_s = \frac{1}{\hbar\omega} \frac{L}{v_g} \bar{P}_s \tag{5.10}$$

where $\hbar\omega$ is the energy of a single photon and $\frac{L}{v_g}$ the average time a photon is within the volume.

With Eq. 5.3 and Eq. 5.10, the rate equation for carrier density Eq. 5.2 results in

$$\frac{dn}{dt} = \frac{I}{eV} - R(n) - \frac{1}{\hbar\omega} \frac{L}{V} \Gamma g(n) \bar{P}_s \tag{5.11}$$

The gain of the SOA depends also on the number of photons. Two nonlinear effects are spectral-hole burning (SHB) and carrier-heating (CH) [233, 236]. Both are intra band effects and have very short time constants in the range of femtoseconds compared to the pulse lengths in the nanoseconds range. Additionally they are also weak compared to the nonlinearity caused by the carrier density variation. It can be assumed that their impact on the model is only instantaneous and the material gain $g(n)$ in Eq. 5.11 can be extended with a nonlinear factor $\frac{1}{1+\kappa_{nl}\bar{P}_s}$, where the factor κ_{nl} is the so-called gain compression factor [240]. Then the rate equation for carrier density Eq. 5.11 can be written as follows:

$$\begin{aligned} \frac{dn}{dt} &= \frac{I}{eV} - R(n) - \frac{1}{\hbar\omega}\frac{L}{V}\frac{\Gamma g(n)}{1+\kappa_{nl}\bar{P}_s}\bar{P}_s \\ &= \frac{I}{eV} - R(n) - \frac{1}{\hbar\omega}\frac{L}{V}\Gamma g_{nl}(n)\bar{P}_s \\ &\quad \text{with} \quad g_{nl}(n) = \frac{g(n)}{1+\kappa_{nl}\bar{P}_s} \end{aligned} \tag{5.12}$$

For $\bar{P}_s$ in Eq. 5.9 the effect on nonlinear gain is neglected for the power averaging and the material gain $g(n)$ is still used for calculating the averaged power $\bar{P}_s$ with Eq. 5.9.

5.4.2.2 The Resulting Electric Field

The output field of the amplifier $\underline{E}_{out}(t)$ is calculated from the input field $\underline{E}_{in}(t)$ according to

$$\underline{E}_{out}(t) = \underline{E}_{in}(t)\exp\left(\frac{(1+j\alpha_H)\Gamma g_{nl}(n,t)L - \alpha_s L}{2}\right) \tag{5.13}$$

where the α_H is the so-called Henry-factor and represents the coupling between the gain and refractive index of the amplifying medium. It is responsible for the variation of the phase [233]. $\varphi(t) = \alpha_H\Gamma g_{nl}(n,t)L/2$ is the time dependent phase shift between the output field $\underline{E}_{out}(t)$ and the input field $\underline{E}_{in}(t)$.

5.4.2.3 The Steady State

In the case where the system is in steady state, all time-based variations disappear. With $\kappa_{nl}\bar{P}_s \ll 1$, the carrier density (Eq. 5.12) in steady state n_s results in

$$\frac{I}{eV} = R(n_s) + \frac{1}{\hbar\omega}\frac{L}{V}\,\Gamma g_{nl}(n_s)P_{in}\frac{\exp\left((\Gamma g(n_s)-\alpha)L\right)-1}{(\Gamma g(n_s)-\alpha)L}. \tag{5.14}$$

The zero point of this function can be found numerically, e.g., by using Newton-Raphson-Method.

Using Eq. 5.14 the carrier density in steady state n_s can be determined as a function of the input power. The SOA is only linear (n_s independent of P_{in}) as long as the stimulated emission rate is small compared to the spontaneous recombination rate. Therefore low input power is required. For high input power, the carrier density and consequently also the gain decreases. Due to this nonlinear characteristic, the extinction ratio at the SOA output decreases.

The effective lifetime of the carriers τ_e results from the recombination term and depends on the bias point [241]. It describes how fast the SOA reacts to the change of input power or the injection current:

$$\frac{1}{\tau_e(n_s)} = \left.\frac{\partial R(n)}{\partial n}\right|_{n_s} = 3Cn_s^2 + 2Bn_s + A \tag{5.15}$$

This time constant is in the range of nanoseconds. Therefore the carrier density follows the intensity variation of the input signal slightly delayed. Dynamic signal distortion and intersymbol interference (ISI) appear for a pulse frequency around 10 GHz and high input power.

5.4.3 Model for Gain-Clamped SOAs

For the modelling of the gain-clamped SOAs (GC-SOAs) an additional rate equation for photons generated by the additional laser oscillation has to be included.

5.4.3.1 Extension of the Rate Equation for Carrier Density

Both the photons of the signal as well as photons of the laser oscillation contribute to the reduction of the carrier density. Therefore the rate equation for the carrier density of the SOA (Eq. 5.12) can be extended by an additional term:

$$\begin{aligned}\frac{dn}{dt} &= \frac{I}{eV} - R(n) - \frac{1}{\hbar\omega_{signal}}\frac{L}{V}\Gamma g_{nl,\ signal}(n)\bar{P}_{signal} - \frac{1}{\hbar\omega_{laser}}\frac{L}{V}\Gamma g_{nl,\ laser}(n)\bar{P}_{laser} \\ &= \frac{I}{eV} - R(n) - \frac{1}{\hbar\omega_{signal}}\frac{L}{V}\frac{\Gamma g_{signal}(n)}{1+\kappa_{nl}(\bar{P}_{signal}+\eta\bar{P}_{laser})}\bar{P}_{signal} \\ &\quad - \frac{1}{\hbar\omega_{laser}}\frac{L}{V}\frac{\Gamma g_{laser}(n)}{1+\kappa_{nl}(\bar{P}_{laser}+\eta\bar{P}_{signal})}\bar{P}_{laser}\end{aligned} \tag{5.16}$$

The indices *signal, laser* depict the general difference of the signal and laser frequencies and with them the different gains at signal and laser wavelengths. For the nonlinear factor the optical lasing power has to be considered, too. The impact of the respective gain cross saturation is included by factor $0 \leq \eta \leq 1$.

5.4.3.2 The Rate Equation for Photons

The rate equation for photons can be derived from corresponding considerations as for the carrier density Eq. 5.16. The temporal variation of the lasing optical power depends on the gain, the losses and the spontaneous emission:

$$\begin{aligned} \frac{d\bar{P}_{laser}}{dt} &= v_g(\Gamma g_{nl,\ laser}(n) - \alpha_{total})\bar{P}_{laser} + \frac{\hbar\omega_L v_g}{L}\Gamma R_{sp} \\ &= v_g\left(\frac{\Gamma\ g_{laser}(n)}{1+\kappa_{nl}(\bar{P}_{laser}+\eta\bar{P}_{signal})} - \alpha_{total}\right)\bar{P}_{laser} + \frac{\hbar\omega_L v_g}{L}\Gamma R_{sp} \end{aligned} \quad (5.17)$$

Thereby α_{total} includes the total losses, scattering loss and mirror losses. The second term considers the emerging photons per time unit, which are generated by spontaneous emission (analogue to Eq. 5.10). This term can be neglected, if the operation point is above the laser threshold, which is generally fulfilled in GC-SOAs. In the case of low carrier density (e.g., in the case of small pump currents or high signal power) this term makes sure that the laser power will not be infinitesimal. It corresponds to the physical reality that photons generated by spontaneous emission are injected permanently into the resonator.

5.4.3.3 The Condition for Threshold

To evaluate the gain at the threshold the following case is considered: Transmitting light through the resonator, it experiences losses due to scattering or reflection at the mirrors. In order to keep the amplitude of the light constant after a round-trip and the laser starts to oscillate, the threshold gain g_{th} must be as high as the total losses α_{total}:

$$g_{th} = \alpha_{total}, \quad (5.18)$$

After a round-trip of the light, it passes a distance of $2L$ and is reflected with reflection coefficients R_1, R_2:

$$R_1\ R_2\ \exp\left(2L(g_{th}-\alpha_s)\right) = 1 \quad (5.19)$$

From this it follows that the total loss is

$$\alpha_{total} = g_{th} = \frac{1}{2L}\ln\left(\frac{1}{R_1 R_2}\right) + \alpha_s \quad (5.20)$$

5.4.3.4 The Reflection Coefficients

The wavelength sensitive feedback of the resonators is realised with distributed Bragg-reflection structures [242]. At each end of the active zone a Bragg grating is added and its period Λ corresponds to the half of the material wavelength. The laser light will be partly reflected at the two Bragg gratings and this results in a resonant, monomode oscillation in the active medium.

The (amplitude-) reflection coefficients r_l on the left, and r_r on the right side of the Bragg region at the laser wavelength can be calculated with

$$r_l = r_r = \frac{-j\kappa \sinh(\gamma L_{gr})}{\gamma \cosh(\gamma L_{gr}) + \alpha_g \sinh(\gamma L_{gr})} \tag{5.21}$$

$$\gamma^2 = \kappa^2 + \alpha_g^2 \tag{5.22}$$

where L_{gr} is the length of the Bragg region, κ the coupling coefficient and α_g the damping constant of the Bragg region. It is assumed that the laser wavelength corresponds to the Bragg wavelength exactly. The reflection of the signal light at the Bragg gratings is neglected.

Then the power reflection factors R_1, R_2 can be written as:

$$R_{1,2} = r_l^2 = r_r^2 \tag{5.23}$$

5.4.3.5 Modified Field Equations

Due to the additional losses in the Bragg region the averaged signal power in the active region (Eq. 5.9) and the resulting electrical field (Eq. 5.13) should be slightly modified:

$$\bar{P}_{signal,\ s} = P_{signal,\ in}\ \exp(-\alpha_g L_{gr}) \frac{\exp\left((\Gamma g(n) - \alpha_s)L\right) - 1}{(\Gamma g(n) - \alpha_s)L} \tag{5.24}$$

$$\underline{E}_{signal,\ out}(t) = \underline{E}_{signal,\ in}(t) \exp(-\alpha_g L_{gr}) \cdot \exp\left(\frac{(1 + j\alpha_H)\Gamma g_{nl,\ signal}(n,t)L - \alpha_s L}{2}\right) \tag{5.25}$$

5.4.3.6 The Steady State

In the steady state, the rate equation for photons (Eq. 5.17) is

$$v_g(\Gamma g_{nl,\ laser}(n_s) - \alpha_{total})\bar{P}_{laser} = 0 \tag{5.26}$$

Here the spontaneous emission and the nonlinear gain are neglected. It follows that either the laser power $\bar{P}_{laser}$ is 0 (operation below laser threshold) or the gain at the laser wavelength is independent on current:

$$\Gamma g_{nl,\ laser}(n_s) = \alpha_{total} \tag{5.27}$$

Therefore in the rate equation for the carrier density (Eq. 5.16) only the injection current I and the averaged powers $\bar{P}_{signal}, \bar{P}_{laser}$ are independent variables:

$$\frac{I}{qV} = R(n_s) + \frac{1}{\hbar\omega_{signal}} \frac{L}{V} \Gamma g_{nl,\ signal}(n_s)\bar{P}_{signal} + \frac{1}{\hbar\omega_{laser}} \frac{L}{V} \Gamma g_{nl,\ laser}(n_s)\bar{P}_{laser} \tag{5.28}$$

By considering Eq. 5.28, the total power $\bar{P}_{signal} + \bar{P}_{laser}$ in the GC-SOA (except for material parameters) depends only on the current. That means the saturation output power can be varied with the current.

5.4.4 Gain Model for SOAs and GC-SOAs

As the signal and laser wavelengths in GC-SOAs are generally different and even not in the same wavelength window, the most commonly used linear approximation for the gain [233] (neglect the wavelength dependency) cannot be used for the modelling of the GC-SOA. To give a more accurate description of the spectral dependence of the gain the parabolic gain spectrum approximation is used instead for the modelling of material gain [243]. Here a linear dependence of the carrier density and parabolic dependence of the signal frequency are assumed, which gives a good approximation especially for positive values:

$$g(\nu, n) = g_{max}(n) \left[1 - \frac{(\nu - \nu_{max}(n))^2}{(\nu_{tr}(n) - \nu_{max}(n))^2} \right] \tag{5.29}$$

where $g_{max}(n)$ is the maximum gain, $\nu_{max}(n)$ is the frequency for the maximum gain, and $\nu_{tr}(n)$ is the transparent frequency, where the gain is 0. They all depend on the carrier density n. It is assumed that a linear approximation is sufficient to describe the carrier density dependence:

$$\begin{aligned} g_{max} &= g_{max0} + \frac{dg_{max}}{dn}(n - n_0) \\ \nu_{max}(n) &= \nu_{max0} + \frac{d\nu_{max}}{dn}(n - n_0) \\ \nu_{tr}(n) &= \nu_{tr0} + \frac{d\nu_{tr}}{dn}(n - n_0) \end{aligned} \tag{5.30}$$

where g_{max0} is the maximum gain for a reference carrier density n_0. The maximum gain g_{max} increases approximately linear with the carrier density (with the differential gain dg_{max}/dn). The reason for this is that the stimulated emission is proportional to the number of occupied and unoccupied states in the conduction or valance band, respectively; ν_{max0} is the frequency for maximum gain for a reference carrier density n_0; ν_{tr0} is the transparent frequency for a reference carrier density n_0. For increasing carrier density the gain peak shifts to higher frequencies because of the band filling effect [244]. At the same time carrier interaction leads to a decrease of the bandgap energy, which is called bandgap shrinkage [244], the transparent frequency shifts towards lower frequencies.

The values of the parameters in Eq. 5.29-5.30 could be derived from measurements of the gain slope of an amplifier. This would lead to a very extensive study for itself, which is beyond the scope of this work. For this reason the simplest way is used to theoretically calculate the gain, which takes the main features into account.

The main features determining the gain are the band structure, which determines the density of states, and the thermal distribution of electrons and holes at a certain carrier density and temperature. The gain calculation can be shortly described

as follows: to calculate the total transition probability at a certain transition energy, the transition probability for a single interband transition is multiplied by the number of energy and momentum conserving transitions possibilities and the occupation probability of the states participating in the transition. The gain is then proportional to the transition probability from conduction band to valence bands minus that from valence bands to conduction band. Details are described in the chapter "recombination mechanisms in semiconductors" in [239].

The effects of bandfilling are described in [244]. Effects such as bandgap shrinkage, gain broadening due to scattering and particle interaction effects, deviations from momentum conservation, and bandtailing effects, which would be important for a more thorough analysis, are not taken into account. With the assumption of parabolic conduction and valence bands a closed but very complicated formula for the gain can be derived [244]. The bandstructure data (masses of the valence band heavy and light holes and of the conduction band electrons) of InGaAsP is taken from [239]. The gain calculated from this formula for T = 250 K is depicted in Fig. 5.17. From a fit to these curves the parameters given in Tab. 5.2 (optimized for a reference carrier density $n_0 = 1.4 \cdot 10^{24}\ m^{-3}$) are derived. The gain curves using these values with parabolic gain spectrum approximation (Eq. 5.29) are also shown in Fig. 5.17 for comparison.

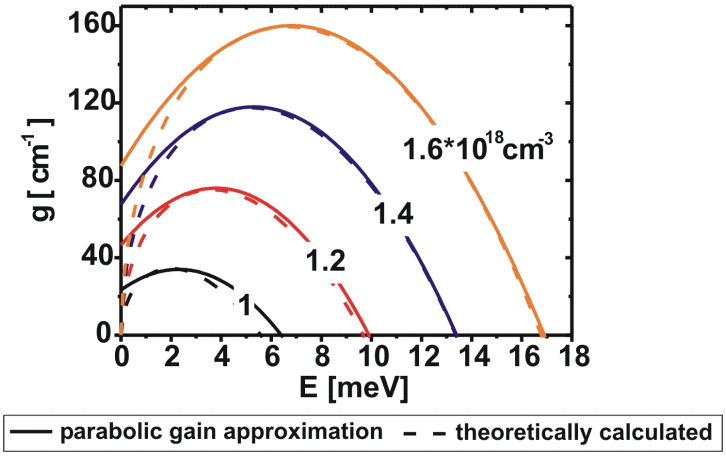

Figure 5.17: Calculation of the material gain of the SOAs versus energy $E = \hbar\nu - W_g$ with the carrier density as a parameter. The parabolic gain spectrum approximation is compared with theoretically calculated gain by using the formula from [244].

Using the parabolic gain spectrum approximation (Eq. 5.29) for the modelling of the SOA gain is more universal compared to the theoretically calculated gain by using the formula from [244]. This gain model can be easier adapted to measured values in literature or from experiments. For the same reason a factor σ in Tab. 5.2 is also introduced as a free factor in the maximum gain g_{max} and in the variation

Description	Parameter	Value
Reference carrier density	n_0	$1.4 \cdot 10^{24}\ m^{-3}$
Maximum gain for n_0	g_{max0}	$\sigma \cdot 1.18 \cdot 10^{4}\ m^{-1}$
Variation of maximum gain	dg_{max}/dn	$\sigma \cdot 21 \cdot 10^{-21}\ m^{2}$
Frequency for maximum gain for n_0	ν_{max0}	$5.3 \cdot 10^{12}$ Hz
Variation of Frequency for maximum gain	$d\nu_{max}/dn$	$7.5 \cdot 10^{-12}$ Hz $\cdot m^3$
Transparent frequency for n_0	ν_{tr0}	$13.4 \cdot 10^{12}$ Hz
Variation of the transparent frequency	$d\nu_{tr}/dn$	$17.5 \cdot 10^{-12}$ Hz $\cdot m^3$

Table 5.2: The used parameters for modelling of the material gain

of maximum gain dg_{max}/dn (see Tab. 5.2). Using this factor the gain model can additionally be fitted by considering several material dependent constants.

5.4.5 Validation of the SOA and GC-SOA Models

In this subsection the basic characteristics of the SOAs and the GC-SOAs are simulated by using the models given in subsection 5.4.2 for the SOA and subsection 5.4.4 for the GC-SOA combined with the gain model described in subsection 5.4.4. Furthermore, the numerical results are compared with the measured data to verify the validity of the developed model. The experimental results for the amplifiers are obtained as described in the previous Section 5.3.

The internal construction and component parameters of the conventional SOA and the DBR-SOA are proposed in several publications e.g. [203, 214] for the conventional SOA and [215] for the DBR-SOA. For the LOA no detailed description of its construction can be found. The parameters determining the dynamic behavior of the LOA are still not well known. Therefore, the theoretical analysis of the gain-clamped SOA is only restricted to the DBR-SOA. Due to the measured eye diagram and Q-factor of the LOA, an even better performance of OBS nodes using LOAs can be expected. Due to the experimental results of the LOA as presented in the previous section, it can be expected that an even better system performance can be achieved by using LOAs instead of DBR-SOAs.

In the following the static as well as the dynamic characteristics of the DBR-SOAs are compared with the conventional SOAs. The values for the amplifier parameters are taken from literature [214, 215] and can be found in Appendix B.

In Fig. 5.18 the static saturation characteristics of the conventional SOA and the DBR-SOA are shown at a signal wavelength of 1550 nm. The conventional SOA is driven with 45 mA and 200 mA and the DBR-SOA with 250 mA bias current, respectively. For both amplifiers very good agreement is obtained between measurements and simulations.

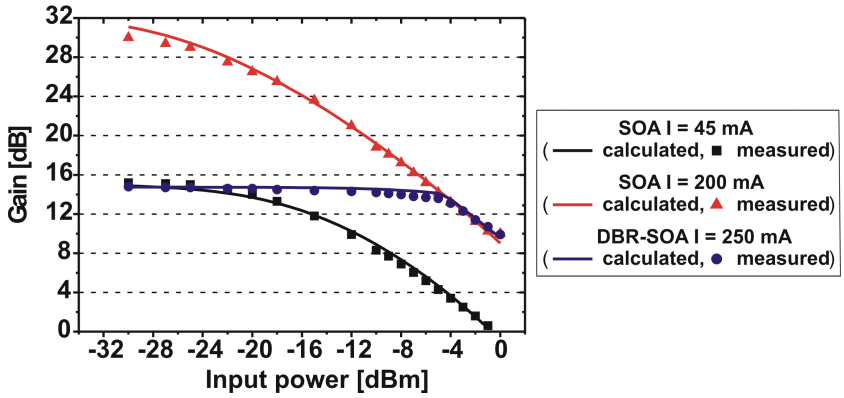

Figure 5.18: Measured and calculated saturation characteristics of the conventional SOA and the DBR-SOA at $\lambda = 1550nm$ versus the input power of the amplifiers. The amplifier parameters can be found in Appendix B.

In Fig. 5.19 the simulated 10 Gbit/s NRZ signals after a conventional SOA and a DBR-SOA and the corresponding eye diagrams for an input power of $-2\ dBm$ are shown.

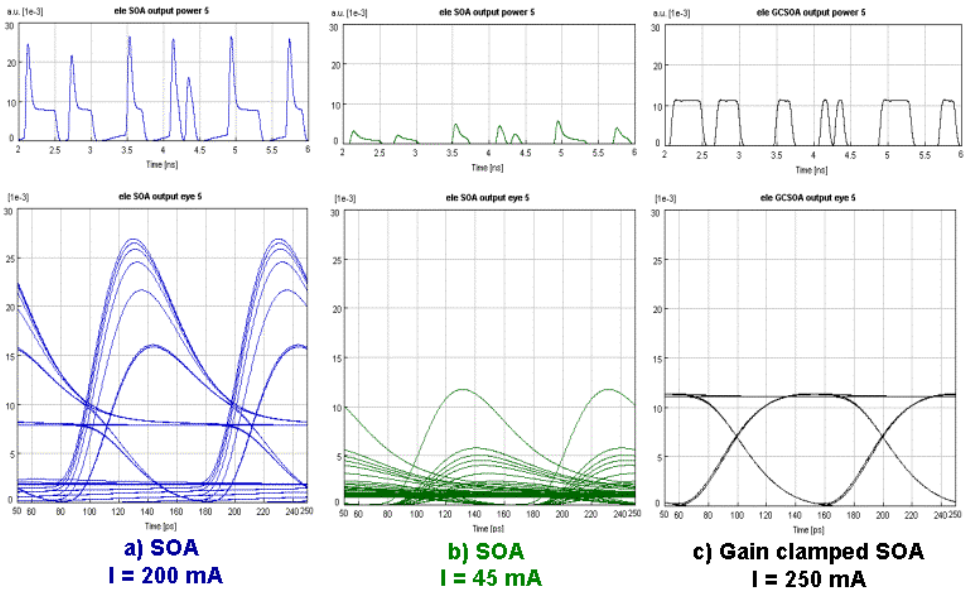

Figure 5.19: The simulated 10 Gbit/s NRZ signal after a conventional SOA and a DBR-SOA and the corresponding eye diagrams for an input power of $-2\ dBm$. The amplifier parameters can be found in Appendix B. a) conventional SOA at I = 200 mA, b) conventional SOA at I = 45 mA. c) DBR-SOA at I = 250 mA.

To point out the impact of SOA gain saturation, the SOA noise is not shown here. If noise is included the eye opening will be much smaller. For both amplifiers the same dynamic behaviour can be found as obtained from the experiments. For a conventional SOA driven at 200 mA bias current the SOA gain decreases dramatically at this input power as shown in Fig. 5.18. So strong signal distortion and intersymbol interference (ISI) due to this gain saturation appear. The amplifier dynamics lead to a decreasing extinction ratio as shown in the eye diagram, which results in an increasing BER (Fig. 5.19a). Driving the conventional SOA with a small bias current (e.g. 45 mA) smaller signal distortion occurs, but only a small gain can be achieved which also leads to a decreasing extinction ratio at the SOA output (Fig. 5.19b). This large signal distortion can be reduced by using DBR-SOA substantially. The gain is stabilised with the laser oscillation inside the SOA. As shown in Fig. 5.19c the remaining signal distortion is much smaller and the eye is sufficiently wide open.

To compare the dynamic behaviour of the amplifiers quantitatively, the receiver sensitivity penalty results from the measurement and the numerical simulation versus the input power of the amplifiers for the conventional SOA and the DBR-SOA are shown in Fig. 5.20. For the simulation the values for parameters like the input power of the SOAs, the gain of the SOA and so on are adapted to the experiment setup as shown in Fig. 5.10 on page 89. The receiver sensitivity penalty (RSP) is then calculated by using the same Eq. 5.1 on page 91. The amplifier parameters can be found in Appendix B. Again very good agreement is obtained between measurements and simulations. Therefore, the SOA and GC-SOA models developed in this chapter are well suitable for the theoretical investigation of the physical limitation of the SOA based OBS core nodes.

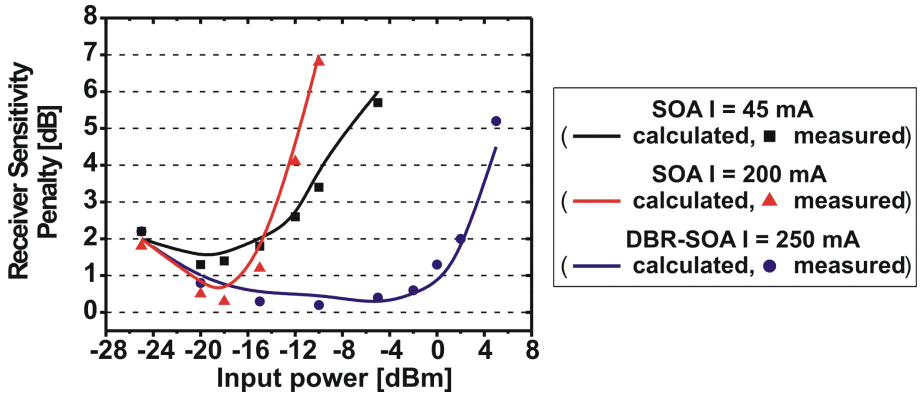

Figure 5.20: Measured and calculated values of the receiver sensitivity penalty versus the input power of the amplifiers for the conventional SOA and the DBR-SOA. The amplifier parameters can be found in Appendix B.

Chapter 6

Physical Evaluation of Selected OBS Node Architectures

In contrary to digital electronic switches, photonic switches are analogue and signal regeneration is not implicitly performed. The signal quality after the OBS core node is accompanied by the impact of distortions due to imperfectness of the multiplexers, splitter/combiner, switches, amplifiers and potentially other devices in the node. Such impairments lead to signal degradation and an increased bit error rate (BER). Therefore the maximum node size and the throughput of such nodes are limited.

As discussed in previous chapters, optical bursts with variable length have a typical duration between a few μs and several 100 μs. Therefore, switching times of burst switching nodes should be below 1 μs. From today's point of view SOA gate is the most promising one for this application. As analysed in Chapter 5 on page 73 the advantages of SOA gates are its high extinction ratio, the gain, and the ability to be electrically controlled. However, the imperfections of such SOA gates are one of the major limiting factors on the size and the cascadability of the SOA based OBS core nodes. Signal distortions will be caused by e.g. noise, non-ideal on/off ratio, and the non-linear input-output characteristic of SOA gates. Especially for high signal input power the gain of conventional SOA decreases. This gain saturation leads to signal distortion and inter-symbol interference (ISI) for optical data, decreasing the extinction ratio at the output. By using gain-clamped SOAs (GC-SOAs) instead of conventional SOA gates the signal distortion and ISI can be reduced substantially, due to the more flat gain profile and the higher saturation input power compared to conventional SOAs.

Based on those investigations of SOA/GC-SOAs the two basic broadcast and select based OBS core node architectures as proposed in Section 4.3 on page 70 will be analysed in the following in terms of maximum size and throughput. The models as developed in Section 5.4 on page 96 are used for this theoretical analysis. The

used parameters and the system environment for the investigation are shown in Section 6.1. A simple power budget analysis in Section 6.2 will show that the so-called "Tune-and-Select" (TAS) switching node is the more promising architecture for OBS applying SOAs, the analysis in the following sections will be focused on the TAS nodes. In Section 6.3 the signal degradation effects in the nodes are analysed. The maximum size and throughput of the nodes are evaluated for three different line rates (2.5, 10, 40 Gbit/s). The impact of several parameters like the amplifier noise figure, amplifier gain, output power of wavelength converters and additional amplifiers on maximum size and throughput are discussed in detail.

6.1 Component Parameters and System Environment

To determine the maximum size and throughput of both BAS and TAS-nodes as shown in Fig. 4.6 on page 70 the component parameters in Tab. 6.1 are used, which, to our best knowledge, represent the today's state-of-the-art for a dynamic application case.

Node	input power	-16 dBm
	output power	0 dBm
EDFA	noise figure	6 dB
	max. gain	30 dB
	max. output power	30 dBm
SOA	noise figure	11 dB
	max. gain	15 dB
	max. output power	11 dBm
	extinction ratio	50 dB
Splitter/Combiner	excess loss	1 - 3 dB
WDM MUX/DeMUX	excess loss	5 dB
	crosstalk	-30 dB
Wavelength converter	input power	-16 dBm
	output power	5 dBm
Delay Line	loss	0.2 dB/km

Table 6.1: Parameter values used for the calculations.

In the analysis a characteristic signal path between two edge nodes with few burst switching nodes in between is considered. This is shown in Fig. 6.1a with the BAS nodes and in Fig. 6.1b with the TAS nodes. The links between the nodes are assumed to be 240 km long and have two inline EDFAs. As discussed in Section 4.2 on page 56 regenerative (O/E/O) wavelength converters are assumed to be used in the OBS core nodes. Therefore the accumulation of signal degradation is avoided. Only the signal path between two neighbouring nodes, i.e. consecutive wavelength converters have to be considered in the analysis.

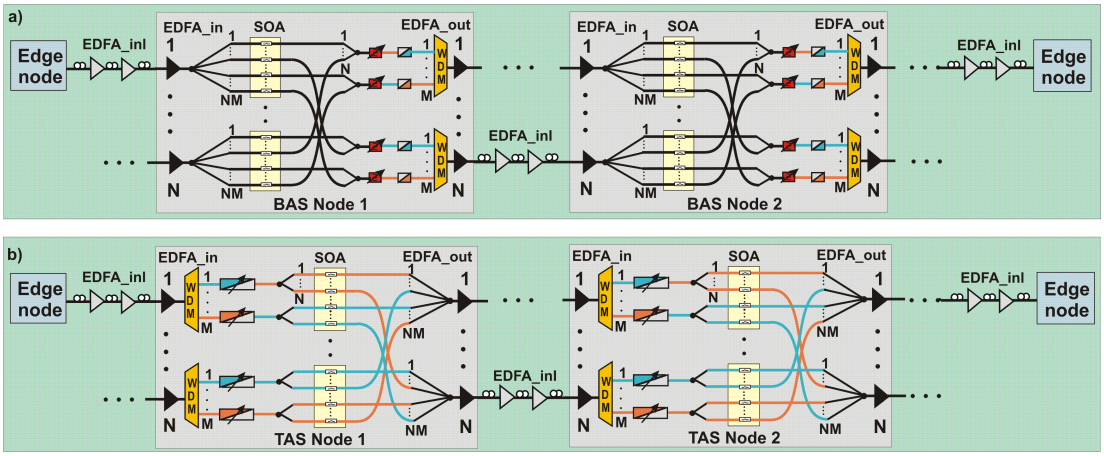

Figure 6.1: Signal path between two edge nodes in an OBS network with many a) BAS nodes, b) TAS nodes.

The topology of real networks is irregular, and a wide variety of network nodes exists, with different number of neighbour nodes (nodal degree), different capacity, asymmetry of traffic, and different ratio of transit to locally generated/terminated traffic. In realistic backbone networks, the highest node degree (number of input/output fibres per node) is typically small e.g. in the order of four [245, 246], therefore in this thesis the evaluation of BAS and TAS nodes will mainly focus on nodes with four input/output fibres.

6.2 Power Budget Analysis

First a simple power budget analysis is performed for both BAS and TAS core node architectures (Fig. 4.6 on page 70). The power levels at and inside the a) BAS and b) TAS nodes at 10 Gbit/s are shown in Fig. 6.2. For both nodes the input power level of the nodes is assumed to be -16 dBm per channel which is the typical power after a transmission of a 80 km optical fibre. The output power level of the nodes is 0 dBm per channel which depicts the optimum input power for fibre transmission at 10 Gbit/s [247, 248]. For wavelength converter an input power of -16 dBm and an output power of 5 dBm per channel are assumed, which are typical receiver power and laser output power at 10 Gbit/s. The two EDFAs at the input and the output of the nodes and the SOA must provide enough amplification of the signal to compensate the losses inside the nodes due to the power budget in the node. With such assumptions and the component parameters as shown in Tab. 6.1 the blue shaded areas in Fig. 6.2 are the most critical areas in the node.

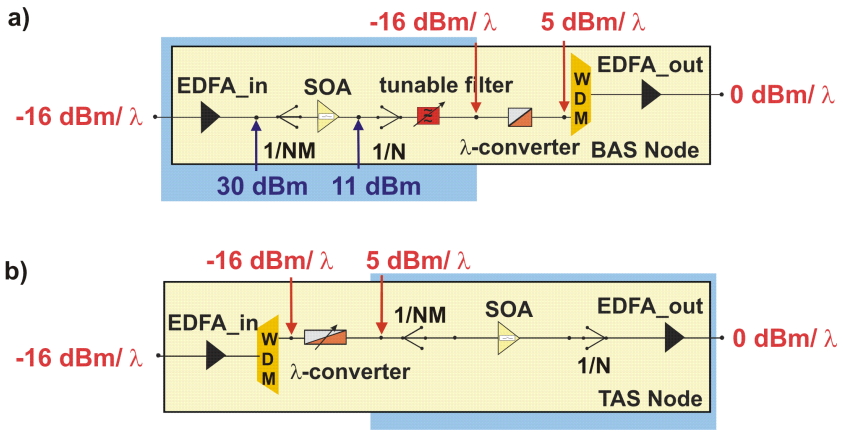

Figure 6.2: Power levels at and inside the a) BAS and b) TAS nodes due to the power budget in the nodes. N: the number of in-/output fibres of the nodes, M: the number of wavelengths per fibre. The power levels valid for all possible N and M of the nodes.

For BAS node the input EDFA and the SOA together must be able to compensate the losses between the node input and the wavelength converter and provide the required receiver power of -16 dBm per channel. But there are two limitations: the maximum output power of EDFA (30 dBm) and of the SOA (11 dBm) cannot be exceeded even operating both amplifiers with their maximum gains. In BAS architecture all M wavelength channels will be passing both amplifiers, therefore these powers are the total output power of the amplifiers. In Fig. 6.3a the following case is considered: as long as the total output power of 30 dBm after the input EDFA is not exceeded, the EDFA provides a gain up to maximum 30 dB. For the SOA using here as on/off gate as well as amplifier there are two limits, the maximum gain should be lower than 15 dB and the total output power below 11 dBm simultaneously. But for a BAS node with 8 wavelength pro fibre at 10 Gbit/s the gain and the corresponding output power as shown in Fig. 6.3a are required. So the maximum size for BAS node due to the power budget in the node is a node with 64 x 64 ports e.g. 4 input/output fibres and 16 wavelengths per fibre. Using additional EDFAs could produce the missing power, but a large number of additional EDFAs (MN^2) are required. Furthermore the amplified noise will be introduced additionally and could also limit the size of the BAS nodes.

Considering the TAS node in the same way, the most critical area in the node due to the power budget is between the output of the wavelength converter (5 dBm/channel) and the output of the node (0 dBm/channel). In Fig. 6.3b the number of the fibres N versus the number of the wavelengths per fibre M is shown. Contrary to the BAS architecture larger nodes can be build with the TAS architecture, if only the power budget in the nodes are considered. TAS nodes with large ports e.g. 1024 x 1024 or 2048 x 2048 can be achieved with 32 fibres and 32 wavelengths per fibre or with 16 fibres and 128 wavelengths per fibre. Additionally,

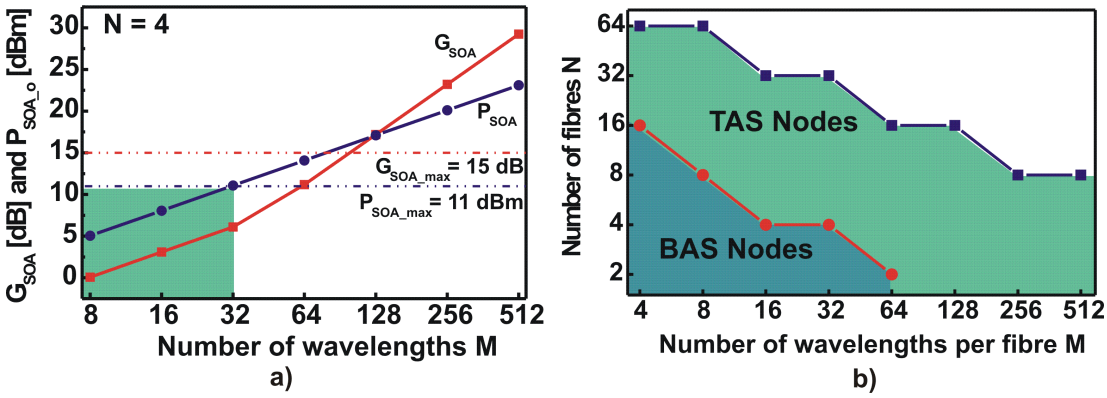

Figure 6.3: Power budget analysis of the BAS and TAS nodes a) The required gain and output power of the SOA in BAS node versus the number of wavelengths for N = 4. b) Maximum number of the fibres N versus the number of the wavelengths M per fiber for the BAS and TAS node due to the power budget in the nodes. Other impairments such as noise and crosstalk are not considered here.

in the BAS architecture the SOA amplifies all M wavelengths instead of only one in the TAS architecture. As already discussed in the previous section, large crosstalk will be produced when multiple signals at different wavelengths are amplified by a single SOA [249]. So comparing both node architectures, the TAS architecture is the more promising one to build large OBS core nodes [207, 208]. Therefore, in the following analysis in terms of maximum size and throughput the focus will be on the TAS nodes with SOAs as on/off gates as shown in Fig. 4.6b on page 70.

6.3 Signal Degradation Mechanisms and their Impacts on Maximum Size of Tune-and-Select (TAS) Nodes

The quality of a signal at the end of a path through the burst switched domain between two edge nodes is affected by several impairments: noise, crosstalk, amplifier saturation, fibre dispersion etc. While the fibre dispersion is an imperfection in the transmission line, which can be compensated to a high degree, the non-ideal optical switching node with SOAs as on/off gates inevitably introduces noise, crosstalk and signal distortion. Furthermore, SOAs will introduce chirp which could also have an impact on the optimised fibre chromatic dispersion compensation in the transmission link. In the following such signal degradation mechanisms will be discussed step by step and their impacts on the maximum size and throughput of the TAS nodes are investigated.

6.3.1 Performance Evaluation Criterions

For the evaluation of optical WDM transmission system various performance criterions can be used. They provide a precise determination and separation of different dominant system limitations. Some of them provide also a good comparison of experimental and numerical investigation, which is useful for the verification of applied numerical models e.g., the receiver sensitivity penalty as used in the previous section. In the following only the criterions are described that are used to determine the maximum size and throughput of the OBS nodes.

6.3.1.1 Optical Signal-to-Noise Ratio

The optical signal-to-noise ratio (OSNR) describes the ratio of optical signal power (P_S) to optical noise power (P_N) in an optical channel:

$$\mathrm{OSNR} = \frac{P_S}{P_N} \tag{6.1}$$

The optical noise around the optical signal reduces the receiver's ability to correctly detect the signal because of the interferences between the optical signal and optical optical noise. For system limited by ASE-noise, OSNR gives a good estimation of the system performance. The OSNR for a single EDFA with constant output power P_{out} is given by:

$$\mathrm{OSNR}_{EDFA} = \frac{P_S}{P_N} = \frac{P_{out}}{P_{ASE}} = \frac{P_{out}}{(\mathrm{NF} \cdot G - 1) \cdot h\nu B_r} \tag{6.2}$$

where P_{ASE} is the ASE noise power of the EDFA, NF is the amplifier noise figure, $h\nu$ is the photon energy (e.g. $1.282 \cdot 10^{-19}$ J at $\lambda = 1550$ nm), B_r is the resolution bandwidth used for OSNR measurement, typically 0.1 nm (12.5 GHz).

Depending on the amplifier infrastructure used in a transmission system, the OSNR values is proportional to the number of the optical amplifiers as well as to the gain flatness of a single amplifier. For a amplified fibre link, with X ideal flat-gain amplifiers, the OSNR value can be calculated as [233]:

$$\begin{aligned} \mathrm{OSNR}[dB] =& P_{out}[dBm] - \alpha \cdot L[dB] - \mathrm{NF}[dB] - 10\log(X)[dB] \\ & - 10\log(h\nu B_r)[dBm] \\ =& P_{in}[dBm] - \alpha \cdot L[dB] - \mathrm{NF}[dB] - 10\log(X)[dB] + 58[dBm] \end{aligned} \tag{6.3}$$

where P_{out} is the signal power at the receiver side, α is the fibre loss, L is the length of the transmission line, and X stands for the number of amplifiers. According to this equation, the dominant limiting parameters for OSNR calculation are the number of amplifiers (total length) and the noise figure NF, because these two parameters determine the ASE-noise accumulation over the distance. Lower noise

figure of the single optical amplifier will result in better OSNR values of the system. For different channel bit rates different OSNR values are required at the end of the transmission link and at the receiver, respectively. OSNR in the range of 15 - 21 dB is required for 2.5 Gbit/s, 22 - 27 dB for 10 Gbit/s, and 30 - 35 dB for 40 GBit/s [233]. The exact values depends on several parameters e.g. the required BER, the nonlinearities on the transmission line and the quality of the receiver. Generally the OSNR is in proportion to the channel bit rate, e.g. if the channel bit rate is increased four times, the OSNR value has to be increased by about 6 dB.

6.3.1.2 Q-Factor

Another parameter that determines system performance is the Q-factor as a specially defined signal-to-noise ratio. It is defined as the difference between mean level of marks and spaces, normalized by the sum of their standard deviation:

$$Q = \frac{\mu_1 - \mu_0}{\sigma_1 + \sigma_0} \tag{6.4}$$

where μ_1, μ_0 and σ_1, σ_0 are the mean levels and standard deviations of marks and spaces, respectively.

Under the assumption that the probabilities of marks and spaces possess a Gaussian statistic with an optimum decision threshold and an optimum sampling point at the receiver side, the relation between Q-factor and BER for amplitude shift keying (ASK) based modulation format is:

$$\mathrm{BER} = \frac{1}{2}\mathrm{erfc}(\frac{Q}{\sqrt{2}}) \approx \frac{1}{Q\sqrt{2\pi}}\exp(-\frac{Q^2}{2}) \tag{6.5}$$

where erfc is the complementary error function.

The OSNR can be used to derive an approximate value for the Q-factor, if the system under investigation shows no significant performance degradation from propagation effects other than noise (such as dispersion and non-linearities), and an infinite extinction ratio is assumed. The relation between Q-factor and OSNR can be approximated by [174, 250, 251]:

$$Q \approx \frac{2 \cdot \mathrm{OSNR}\sqrt{\frac{B_{opt}}{B_{ele}}}}{1 + \sqrt{1 + 4 \cdot \mathrm{OSNR}}} \tag{6.6}$$

where B_{opt} is the bandwidth of the optical filter and B_{ele} is the bandwidth of the electrical post-detection filter. Using the Q-factor definition, the relation between the OSNR and BER can be established according to Eq. 6.6 [252] as:

$$\mathrm{OSNR}(\mathrm{BER} = 10^{-9}) = 22.24 \approx +13.5dB \tag{6.7}$$

6.3.1.3 Bit Error Rate (BER) Evaluation and The Using Approximations

Bit error rate (BER) evaluation is a classical method for performance estimation. It is defined as probability of faulty detected bits, e.g. marks detected as spaces and vice versa. The direct way of calculating BER is to estimate the ratio of corrupt detected bits to the total number of transmitted bits over a statistically significant time period by using the so-called Monte Carlo method. No assumptions about the probability distributions is needed.

However, for optical communication systems BER values of interest are usually very small ($10^{-9} - 10^{-12}$). This makes it difficult to calculate the BER directly as error counting needs to be performed over very long, sometimes impossibly long time intervals. It is even more difficult to estimate the BER via Monte Carlo method from computer simulations. The duration of Monte Carlo simulations is determined by the accuracy and variance of calculated BERs. For a BER variance of 50% at 10^{-9} and an error probability of 5%, 23×10^9 bits have to be simulated [253], which is quite unrealistic with today's computer resources.

Therefore, techniques for approximating the BER are usually applied in computer simulations. Most of these techniques make e.g. certain assumptions about the Probability Density Function (PDF) of amplitude fluctuations of marks and spaces at the detector (statistical techniques). One statistical approach commonly applied is the so-called Gaussian approximation technique, which is based on the assumption that amplitude fluctuations of marks and spaces are Gaussian distributed. In this case the numerical determination of the BER with a reduced number of bits can be realised. As already mentioned above Eq. 6.5 can be used to estimate the BER indirectly by calculating the Q-factor. This approximation enables a good BER estimation, but according to the assumption of a Gaussian distribution independent of the real distribution the predicted BER values are typically higher [251]. Even though disturbances tend to be Gaussian for a reasonably large number of sources (central limit theorem), and thus would imply the validity of the Gaussian approximation, it fails for several practical cases. One reason is that initially Gaussian disturbance are passed through nonlinear elements (fibre, receiver) altering the statistics. Also intra- and interchannel interferences might result in degrading effects, which could not be approximated by additive Gaussian disturbances. E.g. to estimated the BER after the SOA, where signal distortion and ISI are obtained at high input power due to the SOA gain saturation and dynamics.

In such cases the so-called deterministic noise approximation can be used [251]. Here the phases interactions between the noise from optical amplifiers and the WDM signal comb are neglected. The noise is modeled deterministically at the optical receiver. This is possible, for instance, when the noise and signal streams

are modeled to propagate separately from each other over the transmission link using multiple signal representations [80, 251]. The optical signal can be represented by its full time dynamics. It is passed to the receiver as a noise-free signal, however, taking deterministic impairments, such as dispersion, crosstalk, ISI and so on along the optical path into account. Noise is described by wavelength-sensitive values of its power spectral density directly. It is passed along the optical path to obtain a deterministic measure of accumulated noise power spectral density versus wavelength at the receiver input.

The variance of amplitude fluctuation for each bit is determined from the noise accumulated along the optical path together with the photodiode noise. The variance of the pulse amplitude for an arbitrary bit can be written as

$$\sigma^2 = \sigma^2_{signal,\ ASE} + \sigma^2_{ASE,\ ASE} + \sigma^2_{thermal} + \sigma^2_{shot} \tag{6.8}$$

where $\sigma^2_{signal,\ ASE}$ is the variance of the signal-ASE beat noise, $\sigma^2_{ASE,\ ASE}$ is the variance of the ASE-ASE beat noise, $\sigma^2_{thermal}$ is the variance of the thermal noise of the receiver unit including the electrical preamplifier, and σ^2_{shot} is the variance of the shot noise of the receiver unit. Their definition can be found in [80, 251, 252]. The most dominant noise limitation is caused by the signal-ASE noise term, which is dependent on the signal power and ASE-noise of the pre-amplifier. The impact of ASE-ASE noise is governed by the optical filter after the pre-amplifier and it can be efficiently suppressed by tailoring the optical filter bandwidth at the receiver side. The thermal and shot noise terms can be neglected in practically relevant system investigations since they are much smaller than the ASE-noise [254].

Using the deterministic noise approximation, the demand for simulations of long bit streams is dramatically reduced compared to the Gaussian approximation, as there is no numerical uncertainty in determining the amplitude variances. To estimate the BER the calculation method *Average* is used [80]. That means the BER is obtained by calculating all the simulated bits with the formula:

$$\mathrm{BER} = \frac{1}{2N} \sum_{n=0}^{N-1} erfc\left(\frac{\mid p(n) - D \mid}{\sigma(n)}\right) \tag{6.9}$$

where N is the number of simulated bits, p(n) and $\sigma^2(n)$ denote the mean and the variance of bit number n, and D is the decision threshold. An effective Q-factor can be then calculated by using Eq. 6.5:

$$Q_{eff} = \sqrt{2}\mathrm{inverserfc}(2\mathrm{BER}) \tag{6.10}$$

where inverserfc is the inverse complementary error function.

In the following the maximum size and throughput of the TAS nodes will be estimated by using the above discussed criterions. For the noise analysis OSNR and Q-factor are estimated by analytical calculations. For crosstalk consideration a worst case calculation of the Q-factor is performed analytically. To investigate the impact of SOA gain saturation and amplifier dynamics and SOA chirp additionally numerical simulations are done. Here the BERs are calculated by using the deterministic noise approximation and then the corresponding effective Q-factors are estimated. The results presented here can be affected by other impairments. Therefore, to have enough margin for other impairments, Q larger than 10 is taken as the limit of signal degradation. This means, the Q factor of the investigated signal path must be greater than 10 which corresponds to a BER less than BER $= 10^{-22}$ with Gaussian approximation. In the analysis the number of the fibre (N) is hold to a fixed value and the maximum number of the wavelengths per fibre (M) is estimated. The product of the number of fibres N, the maximum number of wavelengths per fibre M and the channel bit rate B gives then the maximum throughput of the TAS nodes for a certain channel bit rate ($N \cdot M \cdot B$). Note that this maximum throughput does not consider dynamic burst traffic but assumes a constant bit stream.

6.3.2 Noise Analysis

In an OBS network, the optical amplifiers (EDFAs and SOAs) are the major noise sources in the signal path between two edge nodes. Only the noise generated by such amplifiers is considered in the analysis. Due to the assumption of 3R wavelength converters, the signal path between two neighbouring nodes, i.e. consecutive wavelength converters as shown in Fig. 6.1b for the TAS nodes is considered. In this case the noise sources are SOAs as well as input and output EDFAs in the TAS nodes and the two inline EDFAs in the transmission links.

Amplified Spontaneous Emission (ASE) Noise

The ASE noise of an individual amplifier can be approximated by a white, Gaussian random process. The power spectral density with a Gaussian distribution at the amplifier output is:

$$\rho_{ASE} = n_{sp} \cdot (G - 1) \cdot h\nu \tag{6.11}$$

where n_{sp} is the spontaneous emission factor, G is the total amplifier gain, $h\nu$ is the photon energy. ASE-noise is superposed in both signal polarisations and the total ASE-noise power P_{ASE} is given by:

$$P_{ASE} = 2 \cdot \rho_{ASE} \cdot B_{tot} = 2 \cdot n_{sp} \cdot (G - 1) \cdot h\nu \cdot B_{tot} \tag{6.12}$$

where B_{tot} represent the total system bandwidth.

The noise performance of amplifiers is usually characterised by the noise figure NF, which is defined as a relation between the OSNR at the input and output of the amplifier:

$$\mathrm{NF} = \frac{\mathrm{OSNR}_{in}}{\mathrm{OSNR}_{out}} \tag{6.13}$$

The OSNR values are defined by signal P_S and noise P_N powers at input ($P_{S,in}$ and $P_{N,in}$) and output ($P_{S,out}$ and $P_{N,out}$), respectively as shown in Eq. 6.1 on page 114.

$$\begin{aligned} \mathrm{NF} &= \frac{P_{S,in}}{P_{S,out}} \cdot \frac{P_{N,out}}{P_{N,in}} \\ &= \frac{1}{G} \cdot \left[1 + \frac{n_{sp} \cdot h\nu \cdot (G-1) \cdot B_{tot}}{P_{N,in}}\right] \end{aligned} \tag{6.14}$$

with

$$P_{S,out} = P_{S,in} \cdot G \tag{6.15}$$

and

$$P_{N,out} = P_{N,in} + (G-1) \cdot n_{sp} \cdot h\nu \cdot B_{tot} \tag{6.16}$$

where $P_{N,in}$ corresponds to the zero point energy W_0 of the quantum mechanic oscillation or vacuum fluctuations defined as [255]:

$$W_0 = \frac{1}{2} \cdot h\nu \cdot B_{tot} = P_{N,in} \tag{6.17}$$

Therefore the NF of an amplifier is given as:

$$\mathrm{NF} = \frac{1}{G} \cdot [1 + 2n_{sp} \cdot (G-1)] \tag{6.18}$$

The NF is typically given in dB and NF $[dB] \approx 10\log(2n_{sp})$ for $G \gg 1$. The minimum NF is 3 dB, as $n_{sp} \geq 1$.

Noise Figure of the Considered Signal Path

To analyse the impact of the ASE-noise on the performance of the TAS nodes, first the noise figure (NF_{TAS}) of the considered signal path as shown in Fig. 6.1b on page 111 with the TAS nodes is estimated. Due to the assumption that regenerative (O/E/O) wavelength converters are used in the TAS nodes, only the signal path between two neighbouring TAS nodes, i.e. consecutive wavelength converters has to be considered in the analysis. The NF_{TAS} of this signal path can be calculated as concatenation of noise figures of signal transmission components (e.g. EDFAs, fibres, splitters, SOAs). The total noise figure NF_{total} of m cascadeded noisy fourpoles is defined as:

$$\mathrm{NF}_{total} = \mathrm{NF}_1 + \frac{\mathrm{NF}_2 - 1}{G_1} + \frac{\mathrm{NF}_3 - 1}{G_1 \cdot G_2} + \ldots + \frac{\mathrm{NF}_m - 1}{G_1 \cdot G_2 \cdots G_{m-1}} \tag{6.19}$$

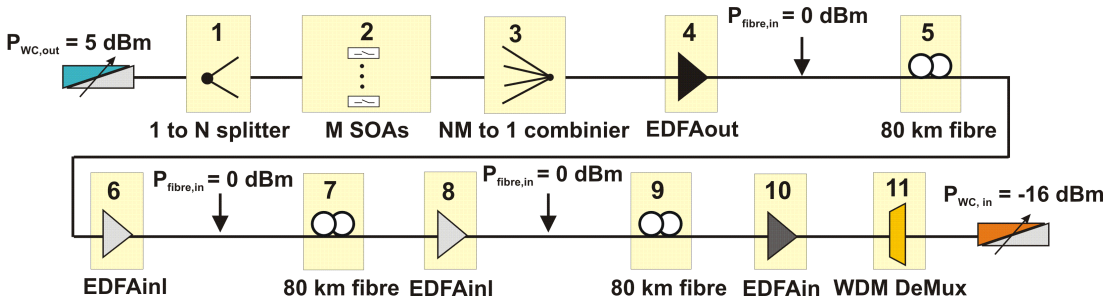

Figure 6.4: The considered signal path for noise figure calculation.

According to the above equation, the NF_{TAS} of the considered signal path with 11 fourpoles as shown in the Fig. 6.4 can be calculated.

For the 1 to N splitter an excess loss of 1 dB and for the NM to 1 combiner an excess loss of 3 dB are assumed. The optical fibres are L = 80 km long and have α = 0.2 dB/km losses. The WDM demultiplexer has an excess loss of 5 dB. The noise figure of the passive components (e.g. fibres, splitters/combiners and the WDM demultiplexer) and its corresponding gain are given by:

$$\mathrm{NF}_1(N) = \frac{1}{G_1} = N \cdot 10^{0.1} \tag{6.20}$$

$$\mathrm{NF}_3(N,M) = \frac{1}{G_3} = NM \cdot 10^{0.3} = 2NM \tag{6.21}$$

$$\mathrm{NF}_5 = \mathrm{NF}_7 = \mathrm{NF}_9 = \frac{1}{G_{fibre}} \tag{6.22}$$

$$\mathrm{NF}_{11} = \frac{1}{G_{11}} = \frac{1}{10^{0.5}} \tag{6.23}$$

where N is the number of the input/output fibres, M is the number of wavelengths per fibre. The G_{fibre} = -16 dB represents the loss of a 80 km long fibre.

The noise figure of the amplifiers is given by:

$$\begin{aligned} \mathrm{NF}_2 &= \mathrm{NF}_{SOAs}(N,M) \\ &= [1 + M \cdot 2n_{sp,\ SOA}(G_{SOA}(N) - 1)] \cdot \frac{1}{G_{SOA}(N)} \end{aligned} \tag{6.24}$$

$$\begin{aligned} \mathrm{NF}_4 &= \mathrm{NF}_{EDFAout}(N,M) \\ &= [1 + 2n_{sp,\ EDFA}(G_{EDFAout}(N,M) - 1)] \cdot \frac{1}{G_{EDFAout}(N,M)} \end{aligned} \tag{6.25}$$

$$\mathrm{NF}_6 = \mathrm{NF}_8 = \mathrm{NF}_{EDFAinl} = [1 + 2n_{sp,\ EDFA}(G_{EDFAinl} - 1)] \cdot \frac{1}{G_{EDFAinl}} \tag{6.26}$$

$$\mathrm{NF}_{10} = \mathrm{NF}_{EDFAin} = [1 + 2n_{sp,\ EDFA}(G_{EDFAin} - 1)] \cdot \frac{1}{G_{EDFAin}} \tag{6.27}$$

The M in Eq. 6.24 is because that in the worst case M of NM SOAs are switched on and the noise powers from M SOAs will be merged after the NM to 1 combiner. Due to the power budget in the TAS node (see previous section), the SOA and output EDFA together have to provide enough gain to compensate the losses between the output of the wavelength converter (5 dBm/channel) and the input of the fibre (0 dBm/channel). Generally the design criterion for low noise is to keep the signal power along the signal path as uniform as possible and not let it decrease too much. The most critical point is the large NM to 1 combiner behind the SOAs with highest loss (1/NM splitting and 3dB excess loss), the SOA gain must be as high as possible, as long as the maximum output power of the SOA (11 dBm/channel) is not exceed. However the noise powers from several (M) SOAs will be merged behind the combiner. Due to the 1 to N splitter, the SOA gain G_{SOA} in Eq. 6.24 depends on the N. The gain of the output EDFA $G_{EDFAout}$ in Eq. 6.25 depends on the N and M. It compensates then the rest of the losses and provides the required input power of the fibre (0 dBm/channel). The gain of the two inline EDFA $G_{EDFAinl}$ in Eq. 6.26 are 16 dB to compensate the fibre loss. The input EDFA has to provide the required input power of the wavelength converter (-16 dBm/channel). As shown in Fig. 6.4 it only has to compensate the loss of the WDM demultiplexer, the gain of the input EDFA in Eq. 6.27 is $G_{EDFAin} = 5$ dB.

Using Eq. 6.19-6.27, the total noise figure $\mathrm{NF}_{TAS}(N, M)$ results in:

$$\begin{aligned}\mathrm{NF}_{TAS}(N,M) = &\frac{\mathrm{NF}_{SOAs}(N)}{G_1} + \frac{\mathrm{NF}_{EDFAout}(N,M) - G_3}{G_1 G_{SOA}(N) G_3} \\ &+ \frac{2\mathrm{NF}_{EDFAinl} + \mathrm{NF}_{EDFAin} - 3G_{fibre}}{G_1 G_{SOA}(N) G_3 G_{EDFAout}(N,M) G_{fibre}} \\ &+ \frac{1 - G_{11}}{G_1 G_{SOA}(N) G_3 G_{EDFAout}(N,M) G_{fibre} G_{EDFAin} G_{11}}\end{aligned} \tag{6.28}$$

and the noise figure $\mathrm{NF}_{fibre\ link}$ is:

$$\mathrm{NF}_{fibre\ link} = \frac{2\mathrm{NF}_{EDFAinl} - 2G_{fibre} + 1}{G_{fibre}} \tag{6.29}$$

For four input/output fibres, the total noise figure NF_{TAS} of the considered signal path is calculated by using the above equations. In Fig. 6.5 not only the NF_{TAS} of the considered signal path as function of the number of wavelengths M per fibre is shown, but also the noise figures for the different amplifiers (SOAs, EDFA at the output of the TAS nodes, and EDFA at the input of the TAS nodes) and for the fibre link with 3 fibre sections each 80 km and two inline EDFAs. The total noise figure NF_{TAS} of the considered signal path grows up with the number of wavelengths per fibre. The noise figure of the SOAs increases with increasing number of wavelengths per fibre. This is because that the noise powers from M SOAs will be merged after the combiner. The noise figures for the output EDFAs of

the TAS nodes is almost constant. For the input EDFAs and the fibre link the noise figures are independent on the number of wavelength. If the number of wavelength is smaller than 32, the noise generate by the inline EDFAs represents the largest part of the noise. For large M the total noise caused by amplifiers in the cascade are mainly determined by the SOA noise. For TAS nodes with more input/output fibres (e.g. N = 8, 16), the total noise figure NF_{TAS} of the considered signal path increases, too. Similar results as shown in Fig. 6.5 are obtained. It results that low-noise SOAs are very important for such SOA based switching node.

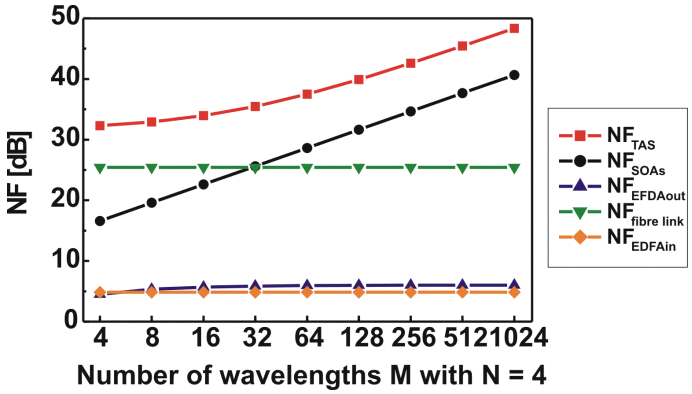

Figure 6.5: The total noise figure NF_{TAS} and noise figures for the different amplifiers and the fibre link as function of the number of wavelengths M per fibre with N = 4.

OSNR of the TAS node

The OSNR of the TAS node can be calculated with Eq. 6.1, where the optical signal power at the receiver (input of the wavelength converter) is P_S = -16 dBm and the total optical noise power (P_N) at the receiver is given by the sum of the noise powers of the different amplifiers in the considered signal path (Fig. 6.4):

$$P_N = M \cdot P_{N,\ SOA}(N) + P_{N,\ EDFAout}(N,M) + 2 \cdot P_{N,\ EDFAinl} + P_{N,\ EDFAin} \quad (6.30)$$

where the noise power of the amplifiers can be calculated as:

$$P_{N,\ SOA}(N) = 2n_{sp,\ SOA} \cdot (G_{SOA}(N) - 1) \cdot h\nu \cdot B_r \cdot \frac{P_S}{P_{out,\ SOA}(N)} \quad (6.31)$$

$$P_{N,\ EDFAinl} = 2n_{sp,\ EDFA} \cdot (G_{EDFAinl} - 1) \cdot h\nu \cdot B_r \cdot \frac{P_S}{P_{out,\ EDFAinl}} \quad (6.32)$$

$$P_{N,\ EDFAin} = 2n_{sp,\ EDFA} \cdot (G_{EDFAin} - 1) \cdot h\nu \cdot B_r \cdot \frac{P_S}{P_{out,\ EDFAin}} \quad (6.33)$$

$$P_{N,\ EDFAout}(N,M) = 2n_{sp,\ EDFA} \cdot (G_{EDFAout}(N,M) - 1) \cdot h\nu \cdot B_r \cdot \frac{P_S}{P_{out,\ EDFAout}}$$

with $P_{out,SOA}(N) = P_{WC,out} \cdot G_1 \cdot G_{SOA}(N)$ ($P_{WC,out}$ = 5 dBm), $P_{out,EDFAout} = P_{out,EDFAinl} = P_{fibre,in}$ = 0 dBm, and $P_{out,EDFAin} = P_{fibre,in} \cdot G_{11} \cdot G_{EDFAin}$.

In Fig. 6.6 the OSNR of the TAS node in dB is shown as a function of the number of wavelengths M for different number of the input/output fibres.

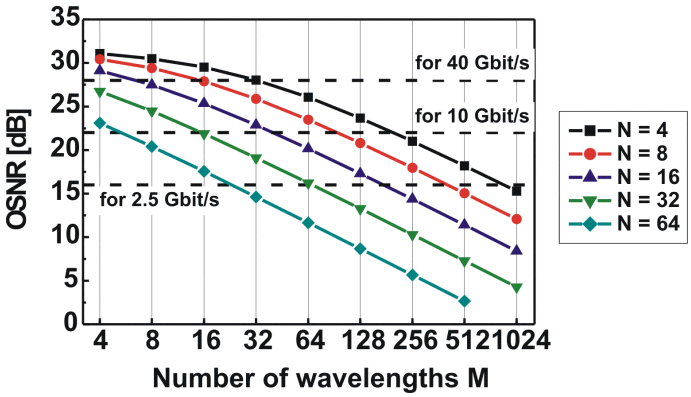

Figure 6.6: The OSNR of the TAS node as function of the number of wavelengths M for different number of the input/output fibres N.

With the increasing number of the wavelengths the OSNR of the nodes decreases due to the increasing noise power. The larger the TAS nodes (large N and M values) is, the lower is the resulting OSNR value of the TAS node. In Fig. 6.6 the OSNR limits for the signal degradation caused by ASE noise at different channel bit rate are also shown. E.g. if OSNR = 22 dB is used as the limit for 10 Gbit/s, a TAS node with 4 input/output fibres can be built with 128 wavelengths per fibre. With OSNR = 16 dB for 2.5 Gbit/s, OSNR = 22 dB for 10 Gbit/s, and OSNR = 28 dB for 40 Gbit/s as the limits, which corresponds to a Q-factor ≥ 10 according to Eq. 6.6, the maximum number of wavelengths per fibre and the maximum throughput of the TAS nodes versus the number of fibres at three different bit rates are shown in Fig. 6.7.

With the increasing number of fibres the maximum number of wavelengths decreases due to the increasing noise powers, mainly from M SOAs. Furthermore, the maximum number of wavelengths decreases with the increasing bit rate. But for all three bit rates the same maximum throughput (5.12 Tbit/s) can be achieved for TAS nodes with up to 32 input/output fibres at 2.5 and 10 Gbit/s by considering the ASE noise of the amplifiers. At 40 Gbit/s the maximum throughput of the TAS nodes decreases to 2.56 Tbit/s with 32 input/output fibres. At 2.5 and 10 Gbit/s the maximum throughput decrease also to 2.56 Tbit/s, but for nodes with even more input/output fibres, e.g. N = 64. However, such large fibre number is not realistic in the backbone networks [245, 246]. These results can be easily explained by the required OSNR of the TAS node. Increasing the channel bit rate four times, the required OSNR values has to be increased about 6 dB and the resulting maximum number of the wavelengths per fibre decreases around factor 4.

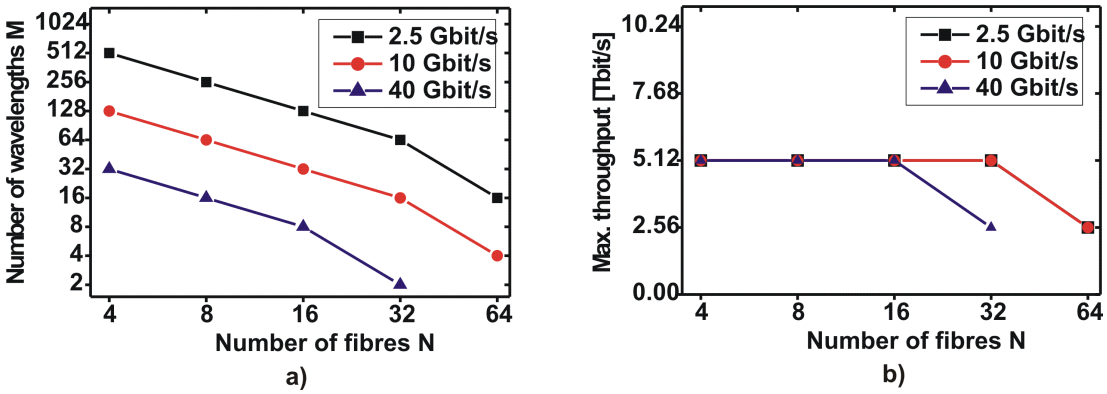

Figure 6.7: Calculated maximum number of wavelengths per fibre (a) and maximum throughput of TAS nodes (b) versus the number of fibres at three different bit rates. Only ASE noise is considered here.

For the results in Fig. 6.5 - 6.7 the standard value for the parameters as shown in Tab. 6.1 on page 110 are used. Several parameters e.g. the noise figure of the amplifiers and the SOA gain could have strong impact on the maximum size and throughput of the TAS nodes. In the following, their impact on the size of the TAS nodes will discussed in detail.

Variation of Noise Figure of the SOA

As shown in Fig. 6.5, the total noise figure NF_{TAS} of the considered signal path is mainly determined by the SOA noise. Consequently the amplifier noise from the SOA gates has the largest impact on the maximum of wavelengths M of a TAS node, especially for large M. If the noise figure of SOAs is reduced to 9 dB, which is typically achievable with the LOA as discussed in Chapter 5 on page 87, compared to SOAs with $NF_{SOA} = 11$ dB higher OSNR values can be achieved at large M as shown in the Fig. 6.8a. Generally the OSNR increases linear with the decreasing NF as shown in Eq. 6.3 on page 114, e.g. if the NF is increased/decreased 1 dB, the OSNR value is decreased/increased 1 dB, too. For 2.5 Gbit/s a TAS node with four in-/output fibres can be built with 1024 wavelengths. That means 10.24 Tbit/s maximum throughput can be achieved for the TAS nodes with four in-/output fibres. However, such large number of the wavelengths per fibres are not practicable in a real system. For 10 and 40 Gbit/s the same maximum number of the wavelengths (256 for 10 Gbit/s and 32 for 40 Gbit/s) can be achieved as with $NF_{SOA} = 11$ dB. Reduced the NF of the SOA to 7 dB, higher OSNR values can be obtained due to the reduced noise power of the M SOAs. For 10 Gbit/s a TAS node with N = 4 can be built with 256 wavelengths and for 40 Gbit/s the maximum number of the wavelength is M = 64. That means a maximum throughput up to 10.24 Tbit/s can be achieved with TAS nodes with N = 4 by using an advanced low noise figure.

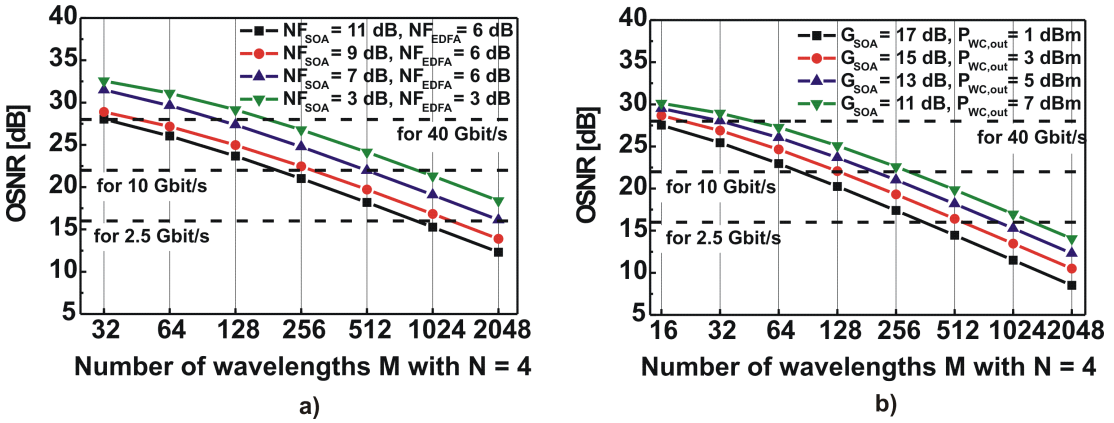

Figure 6.8: The OSNR of the TAS nodes with four in-/output fibres as function of the number of wavelengths M for a) different noise figures of SOA and EDFA, b) different SOA gain.

However, there are still fundamental physical boundaries which limit the size of the TAS nodes: A noise figure better than 3 dB is not possible for SOAs and EDFAs. If all EDFAs and SOAs in the system had noise figures equal to 3 dB, the maximum achievable throughput of a TAS-node at all three bit rates is 20.48 Tbit/s by considering noise as limitation for signal degradation. However, this represents only a fundamental physical boundary. As shown in Fig. 6.8a very large number of wavelengths per fibre are required, which is hardly practicable in a real system.

Variation of SOA Gain

The demand for the SOA gain to be as high as possible is not sufficient to guarantee automatically large-sized switching nodes. The SOA gain in TAS nodes with a fixed number of input/output fibres (e.g. N = 4) depends on the input power of the SOAs (output power of wavelength converters $P_{WC,out} = 5$ dBm) and the maximum output power of the SOAs $P_{out,max,SOA} = 11$ dBm (see Fig. 6.4). Using the parameters in Tab. 6.1 on page 110 a TAS node with 4 input/output fibres can be built with 256 wavelengths per fibre at 10 Gbit/s by considering noise as the limitation for signal degradation. For this node only an SOA gain of $\sim$ 13 dB is required.

By holding the maximum SOA output power constant, the SOA gain can be increased by decreasing the output power of the wavelength converter and consequently decreasing the input power of the SOA. E.g. a SOA gain of 15 dB is required, if the output power of the wavelength converter is $P_{WC,out} = 3$ dBm. Large SOA gain results also in large noise power. As shown in Fig. 6.8b, the maximum number of wavelengths will decrease to e.g. 16 at 40 Gbit/s due to the decrease of the OSNR value of the TAS node from $\sim$ 28 dB to $\sim$ 26 dB for 32 wavelengths per fibre. If the output power of wavelength converter $P_{WC,out}$ is further increased to 1

dBm (17 dB SOA gain is required), the resulting OSNR value is e.g. $\sim$ 20 dB for 128 wavelengths per fibre. In this case the maximum throughput of the TAS nodes with 4 input/output fibres will decreased to 2.56 Tbit/s at 10 Gbit/s, respectively. The reason therefor is that a decrease of the output power results in a decreasing SOA input power. Large SOA gain is then required to compensate the losses in the TAS nodes, which results in large noise and leads to smaller TAS nodes. This behaviour indicates that not the large SOA gain, but large input power of SOAs and large output power of wavelength converters respectively are important for achieving large TAS nodes with high maximum throughput.

On the other hand if the SOA gain is reduced from 13 dB to 11 dB, the input power of the SOA is raised from -2 dBm to 0 dBm. Better OSNR value ($\sim$ 23 dB for M = 256, $\sim$ 20 dB for M = 512) is achieved due to the lower SOA noise power. This results in a maximum throughput of 10.24 Tbit/s at 10 Gbit/s. Same maximum throughput can also be achieved at 2.5 Gbit/s, but not for 40 Gbit/s. It indicates that with increasing bit rate per channel, components with a better performance are needed. However, the input power of the SOAs cannot be raised arbitrarily due to the gain saturation of the SOAs as already discussed in the Chapter 5.

Fig. 6.8 also indicates that the OSNR values decrease almost linear with the increasing SOA gain and the NF of the SOAs. Increase the SOA gain or SOA NF about 1 dB, the OSNR of the TAS node decreases about 1 dB, too. As already shown in Fig. 6.7a on page 124 the achievable maximum number of the wavelengths per fibre is almost in proportion to the OSNR value. E.g. if the OSNR value of the TAS node is decreased about 6 dB by increasing the SOA gain or the SOA NF about 6 dB or increasing the channel bit rate four times, the achievable maximum number of the wavelengths per fibre is decreased about four times.

6.3.3 Crosstalk Consideration

In addition to noise, crosstalk is the other impairment which will limit the size of the TAS nodes additionally [207, 208, 256]. Two major crosstalk sources are considered in the analysis and a worst case calculation is performed. The first source is the WDM demultiplexer with M-1 interfering signals. Due to the different centre frequency of the interfering signals with wavelengths 1, ..., M, only a power addition of interfering signals caused by crosstalk has to be considered. The second source of crosstalk is the non ideal extinction ratio of the SOA gates. For TAS N-1 switched-off amplifiers have the same input wavelength as the considered channel with the consequence of coherent crosstalk. Here the field of the interfering signal is added together [249]. For Q-factor calculation by considering the impact of noise and crosstalk the Q-factor definition in Eq. 6.4 on page 115 is used. The electrical signal mean level of the marks μ_1 and of the spaces μ_0 are calculated as follow:

$$\mu_1(N) = 2 \cdot P_S \cdot \frac{e}{h\nu} \cdot \left[1 - (N-1) \cdot \sqrt{X_{SOA}}\right] \tag{6.34}$$

$$\mu_0(M) = 2 \cdot P_s \cdot \frac{e}{h\nu} \cdot (M-1) \cdot X_{Demux} \tag{6.35}$$

where P_S is the optical signal power at the receiver (input of the wavelength converter with $P_S = -16$ dBm). X_{SOA} is the non ideal extinction ratio of the SOA gates and the factor $(N-1)\sqrt{X_{SOA}}$ in Eq. 6.34 is resulting from the consideration of the field addition of the $N-1$ coherent crosstalk signals from the SOAs. $(M-1)X_{Demux}$ in Eq. 6.35 takes then the power addition of the $M-1$ incoherent crosstalk signals from the WDM demultiplexer into account.

The standard deviations of the spaces σ_0 is assumed to be 0, where the standard deviations of the markes σ_1 is calculated by:

$$\sigma_1(N,M) = 2 \cdot \frac{e}{h\nu} \sqrt{2P_s \cdot P_N(N,M) \cdot \frac{B_e}{B_o}} \tag{6.36}$$

where $P_N(N,M)$ is the total optical noise power at the receiver and is given by Eq. 6.30 for the TAS nodes on page 122, B_e is the electrical and B_o the optical bandwidth.

In Fig. 6.9 the Q-factor for increasing number of wavelengths M and different bit rates are shown. The $X_{Demux} = -30$ dB is used for the crosstalk of the WDM demultiplexer and $X_{SOA} = -50$ dB is used for non ideal extinction ratio of the SOA gates, which is achievable with the state-of-the-art components as discussed in Chapter 4.

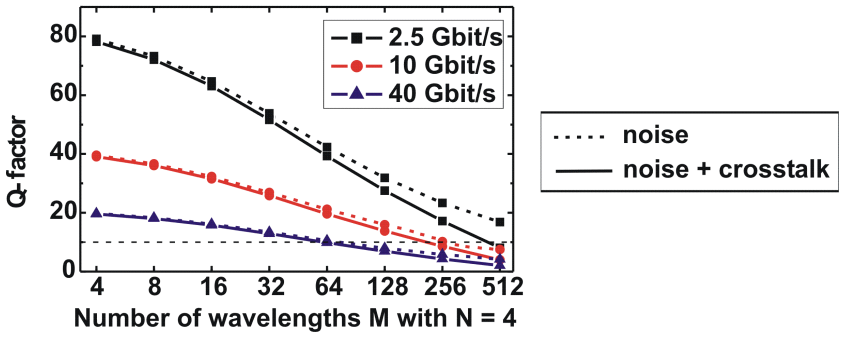

Figure 6.9: The calculated Q-factor versus the maximum number of wavelengths per fibre by considering noise and crosstalk for the TAS nodes with 4 input/output fibres at three different bit rates. A crosstalk of the WDM demultiplexer of -30 dB and a -50 dB non ideal extinction ratio of the SOA gates are assumed.

The dashed line is for ASE noise only and the solid line for noise and crosstalk. As shown in Fig. 6.5 on page 122 the total noise figure of the considered signal path with the TAS nodes increases with the number of wavelengths. It determines the decreasing of the OSNR values of the TAS nodes as shown in Fig. 6.6 on page 123 and also the Q-factor. Together with crosstalk the Q-factor become smaller especially for large number of wavelengths M, but the signal degradation is dominated by the noise. With Q = 10 as the limit of signal degradation, large TAS nodes can still be built by using the standard parameters as shown in Tab. 6.1 on page 110 (see Fig. 6.10a).

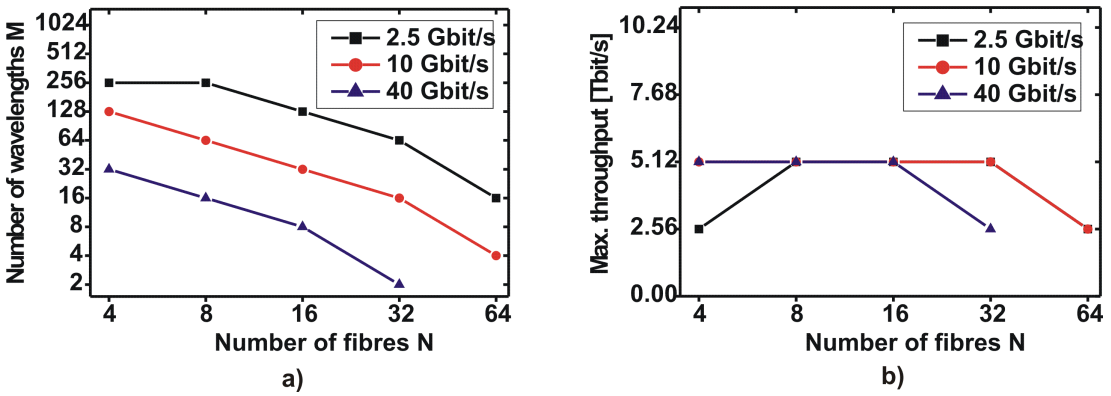

Figure 6.10: Calculated maximum number of wavelengths per fibre (a) and maximum throughput of TAS nodes (b) versus the number of fibres at three different bit rates. ASE noise and crosstalk are considered here. Using SOAs with noise figure of 11 dB.

Compared to the results, where only the noise is considered as signal degradation (Fig. 6.7 on page 124), the maximum number of the wavelengths per fibre reduces by about a factor of two for the TAS nodes with 4 input/output fibres at 2.5 Gbit/s, if the impact of the crosstalk is considered additionally. This is mainly due to the large number of wavelengths, and consequently strong impact of the crosstalk from WDM demultiplexer with M-1 interfering signals. For other TAS nodes the same number of wavelengths can be achieved as only considering the noise. A maximum throughput up to 5.12 Tbit/s can be achieved for all three bit rates.

To achieve larger maximum throughput, e.g. 10.24 Tbit/s, several parameters can be varied as discussed above in the noise analysis. E.g. using SOAs with a small noise figure of 9 dB instead of 11 dB or increasing the SOA gain about 2 dB, the OSNR of the TAS nodes will decreased 2 dB, too. It results in an increasing number of wavelengths about factor two and e.g. a TAS node with 4 input/output fibres and 256 wavelengths per fibre can then be build at 10 Gbit/s. In Fig. 6.11 the calculated maximum number of wavelengths per fibre (a) and maximum throughput of TAS nodes (b) versus the number of fibres at three different bit rates are

shown for a system with noise figures equal to 3 dB for all EDFAs and SOAs. It represents the fundamental physical limits of the TAS node size by considering noise and crosstalk as limitation for signal degradation: the maximum achievable throughput of the TAS nodes is 10.24 Tbit/s at 2.5 Gbit/s , 20.48 Tbit/s at 10 Gbit/s and 40.96 Tbit/s at 40 Gbit/s. For a TAS node with 4 input/output fibres the maximum achievable throughput is 5.12 Tbit/s at 2.5 Gbit/s, 10.24 Tbit/s at 10 Gbit/s and 20.48 Tbit/s at 40 Gbit/s.

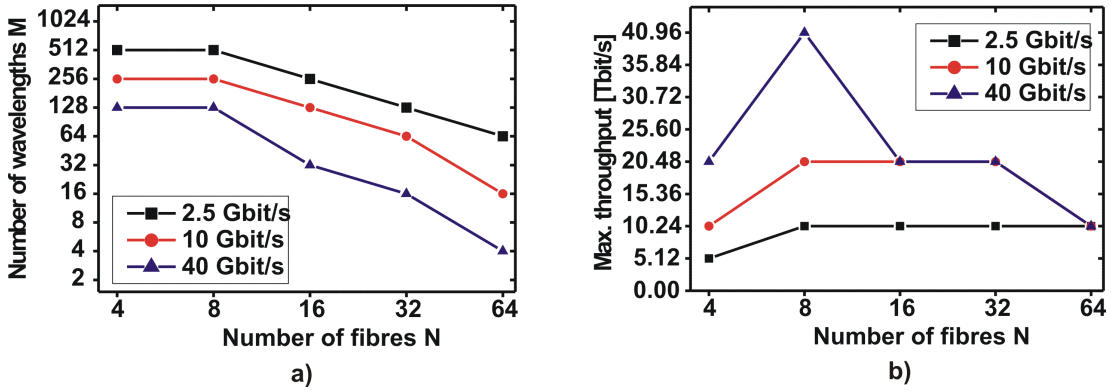

Figure 6.11: Calculated maximum number of wavelengths per fibre (a) and maximum throughput of TAS nodes (b) versus the number of fibres at three different bit rates. ASE noise and crosstalk are considered here. Using SOAs and EDFAs with noise figure of 3 dB.

6.3.4 Impact of Additional Amplifiers

The use of additional amplifiers to overcome the losses in the nodes seems to be an option to increase the maximum number of wavelengths per fibre. Cascading many SOAs has to be avoided due to signal degradations caused by noise and gain saturation. Thus only EDFAs can be used as additional amplifiers. Due to the cost the number of additional EDFAs must be limited and their position in the node is very important. Placing the additional EDFAs behind the SOA gates are not resulting in better noise performance. An improvement can only be achieved, if additional EDFAs are placed in front of the SOA gates.

The drawback of this is the large number of additional EDFAs (NM at least), which can be avoided by increasing the input power of the SOAs (decreasing the SOA gains), as discussed in previous subsection. However, the input power of the SOAs is limited by gain saturation of the SOA gate caused by high input power and leads to signal distortions as discussed in Chapter 5. The impact of SOA gain saturation and amplifier dynamics on the maximum size of TAS nodes will be investigated later in more detail.

6.3.5 Regeneration Capability of Wavelength Converter

As assumed so far, if 3R-regenerating wavelength converters are used in the TAS nodes, the previously achieved results remain valid also for many cascaded OBS core node sections between two edge nodes. To achieve this opto-electronical wavelength converter as discussed in Chapter 4 can be used. If all-optical wavelength converters are used instead, the 3R regeneration is not implemented and the cascadability of the TAS nodes is limited. An investigation of the regeneration capacity of different all-optical wavelength converters is beyond the scope of this thesis.

In the following TAS nodes with linear wavelength converters are investigated to give an estimation of their impact on the cascadability of the TAS nodes. In a linear wavelength converter the incoming signal is only amplified (e.g. from -16 dBm input power to 5 dBm output power with a noise figure of 3 dB) but not fully 3R regenerated, so that the signal degradation is accumulated and the number of cascaded nodes is limited. Therefore, the maximum size of the TAS nodes depends on the number of the passing nodes. To investigated the cascadability of the TAS nodes with a linear wavelength converter, the signal path as shown in Fig. 6.12 is considered. It consists an edge node with a WDM multiplexer and an output EDFA, a transmission link with two inline EDFAs and k cascaded TAS nodes.

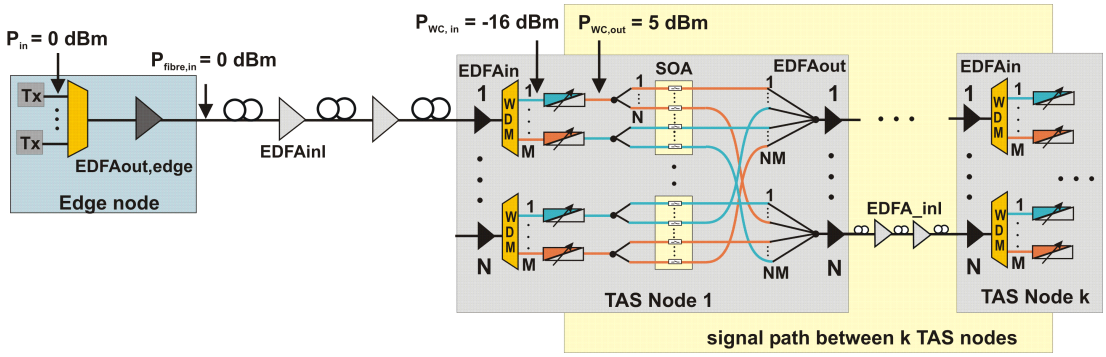

Figure 6.12: The considered signal path for the cascadability calculation of the TAS nodes with linear wavelength converter.

First the impact of noise is investigated by calculating the OSNR of the signal path with k TAS nodes by using Eq. 6.1, where the optical signal power at the receiver (input of the wavelength converter) is P_S = -16 dBm and the total optical noise power ($P_{N,\ cascade}(N,M)$) at the receiver is given by the sum of the noise powers of the different amplifiers in the considered signal path as shown in Fig. 6.12:

$$\begin{aligned} P_{N,\ cascade}(N,M) = {} & P_{N,\ EDFAout,\ edge} + 2 \cdot P_{N,\ EDFAinl} \\ & + P_{N,\ EDFAin} + k \cdot [(P_{N,\ WC} + P_N(N,M)] \end{aligned} \tag{6.37}$$

where the noise power $P_{N,\ EDFAinl}$ is given by Eq. 6.32, $P_{N,\ EDFAin}$ is given by Eq. 6.33, and $P_N(N, M)$ is given by Eq. 6.30 for the TAS node on page 122. The other noise power can be calculated as:

$$P_{N,\ EDFAout,\ edge}(N) = 2n_{sp,\ EDFA} \cdot (G_{EDFA,\ edge} - 1) \cdot h\nu \cdot B_r \cdot \frac{P_S}{P_{out,\ EDFAedge}} \quad (6.38)$$

$$P_{N,\ WC} = 2n_{sp,\ WC} \cdot (G_{WC} - 1) \cdot h\nu \cdot B_r \cdot \frac{P_S}{P_{WC,\ out}} \quad (6.39)$$

with $P_{out,\ EDFAedge}(N) = P_{fibre,\ in} = 0$ dBm. $G_{EDFA,\ edge}$ is 5 dB to compensate the loss of the WDM multiplexer, if a $P_{in} = 0$ dBm is assumed. $P_{WC,\ out}$ is 5 dBm, G_{WC} is 21 dB ($P_{WC,in} = -16$ dBm and $P_{WC,\ out} = 5$ dBm), and $n_{sp,\ WC}$ is assumed to 3 dB and $P_{WC,\ out} = 5$ dBm.

Using the above equations the OSNR of the cascaded TAS nodes is calculated for different number k of cascaded TAS nodes. In Fig. 6.13 the calculated OSNR values of k cascaded TAS nodes as function of the number of wavelengths M for the TAS nodes with four in-/output fibres (a) and with eight in-/output fibres (b) are shown.

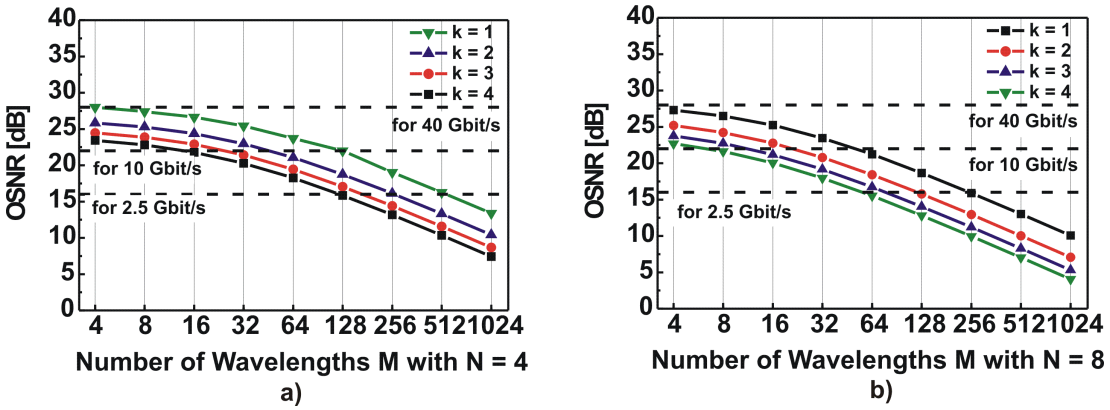

Figure 6.13: The OSNR of k cascaded TAS nodes as function of the number of wavelengths M for the TAS nodes a) with 4 in-/output fibres, b) with 8 in-/output fibres.

The OSNR decreases with the increasing number of the cascaded TAS nodes. For $k = 1, 2, 4$ the resulting OSNR values are reduced by 3 dB each time. To investigate the impact of noise and crosstalk on the cascadability, the Q-factor is then calculated by using the Q-factor definition in Eq. 6.4 on page 115. The electrical signal mean level of the marks μ_1 and of the spaces μ_0 are calculated with Eq. 6.34 and 6.35 on page 127. The standard deviations of the spaces σ_0 is assumed to be 0 and the standard deviations of the markes σ_1 is calculated with Eq. 6.36 on page 127 where the $P_N(N, M)$ in Eq. 6.36 is now $P_{N,cascade}(N, M)$ (Eq. 6.37).

With Q = 10 as the limit of signal degradation, the maximum number of the wavelengths per fibre is calculated for different number k of the cascaded TAS nodes. The results are summarised in Tab. 6.2 for three different bit rates.

N	Bit rate	M			
	[GBit/s]	1 TAS node	2 TAS nodes	3 TAS nodes	4 TAS nodes
4	2.5	512	256	128	64
	10	128	32	16	8
	40	4	-	-	-
8	2.5	256	128	64	32
	10	32	16	8	4
	40	2	-	-	-

Table 6.2: Maximum number of wavelengths per fibre (M) for TAS nodes with 4 or 8 input/output fibres (N) versus number of cascaded nodes for three different bit rates by considering noise and crosstalk.

In an OBS network with 4 cascaded TAS nodes in a signal path without 3R-regeneration the largest node is e.g. N = 4 and M = 8 at 10 Gbit/s. In other words, at 10 Gbit/s if an OBS network is built with TAS node with 4 input/output fibres and 8 wavelength per fibre, the maximum number of hops in a signal path without 3R regeneration must be lower than 4. The higher the bit rate, the smaller is the achievable maximum size of the TAS nodes without 3R regeneration, especially for 40 Gbit/s 3R regeneration is essential even for cascading 2 TAS nodes. Therefore, in the following the analysis of TAS nodes will only be concentrated on nodes with regenerative (3R) wavelength converters, so the accumulation of signal degradation is terminated at each wavelength converter.

6.3.6 Impact of SOA Gain Saturation and Amplifier Dynamics

SOA dynamic behaviour leads to further impairments which cause signal distortion and limit the size of TAS nodes. As already discussed in the Chapter 5, the input-output characteristic of the conventional SOA gate is non-linear. The gain decreases for high input signal power. For TAS node e.g. with 4 input/output fibres the SOA has an input power about -2 dBm, which is required due to the power budget in the node. A lower input power would require a higher SOA gain which results in high amplifier noise and lead to much smaller TAS nodes. However, at this input power a conventional SOA is in the saturation as shown in Fig. 5.18a on page 107. For optical signals with data rates above 2.5 Gbit/s the gain saturation leads to signal distortion and ISI. The extinction ratio for the output signal is decreased, which results in an increasing BER. As also shown in the Chapter 5, the signal distortion and the ISI can be reduced substantially by using the GC-SOAs instead of the conventional SOA gates. The gain is stabilised with laser oscillations inside the SOA gate. The gain of GC-SOA is clamped to a fixed

value by the power in the lasing mode, i.e. the laser oscillation creates what can be thought of as a carrier reservoir that shrinks when the input power is increasing and vice versa thus clamping the carrier density in the active region.

However, such remaining signal distortion could still have some impact on the signal quality at the output of the TAS nodes [257]. Therefore in this subsection the analysis of TAS nodes is extended to the analysis of SOA gain saturation and dynamic in addition to the impact of noise and crosstalk. Different SOAs (conventional SOAs or GC-SOAs) will have different impact on the maximum wavelengths per fibre and the maximum throughput of the TAS nodes. Three different types of SOAs are compared. The *reference SOA* is defined by a static gain versus current characteristic, and a noise figure of 11 dB determining the amount of amplified spontaneous emission. It is used for (ideal) reference and does not show any dynamics (no ISI, no chirp). The *conventional SOA* and the *gain-clamped SOA (GC-SOA)* are used to describe real SOAs. For them the rate equation models as developed in previous chapter 5 is used. The modelling parameters can be found in Appendix B.

The simulations of a signal path between two TAS nodes are done with *VPItransmissionMaker*^{TM} *WDM* of *VPIsystems*^{TM} [80]. The SOA/GC-SOA model is developed in *Microsoft Visual C* and included in *VPItransmissionMaker*^{TM} *WDM* by using a Co-simulation interface [258]. As an extension to the previous analysis, dispersion compensated fiber links between two TAS nodes are used. The used system configuration is shown in Fig. 6.14.

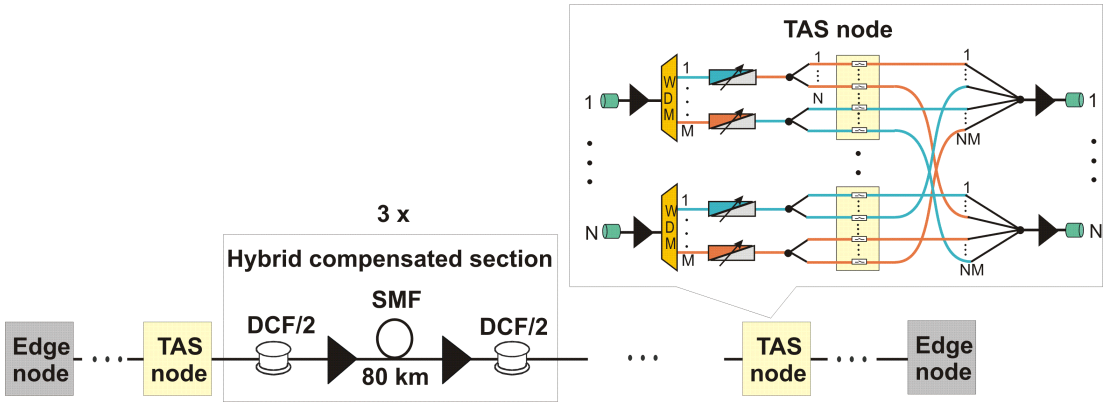

Figure 6.14: Investigated system configuration with TAS nodes and hybrid compensated fiber links.

It consists of a transmission link between two edge nodes with several TAS nodes in the link. Like previous calculations 3R regenerating wavelength converters are assumed. Each fibre link consists of three hybrid compensated fibre sections where the dispersion compensation is split into two sections of equal dispersion (dispersion

compensating fibre (DCF)) placed before and after the standard single mode fibre (SSMF). Two EDFAs are used to compensate the fibre losses. The modelling parameters of SSMF and DCF are taken from Corning data sheets and are shown in Tab. 6.3.

	α [dB/km]	D [ps/nm/km]	S_0 [ps/nm^2/km]	A_{eff} [μm^2]	n_2 [$10^{-20} W^{-1} m^2$]
SSMF	0.19 @ 1550 nm	17.3 @ 1550 nm	0.092	85	2.2
DCF	0.49 @ 1550 nm	-100 @ 1550 nm	-0.375	20	2.6

Table 6.3: The modelling parameters of SSMF and DCF

The α is the attenuation, D the dispersion, S_0 the dispersion slope, A_{eff} the effective core area, and n_2 the nonlinear refractive index of the fibre, respectively. The input power in the standard single mode fibre and in the second dispersion compensating fibre in the hybrid compensated fibre sections are fixed to $P_{in,\ SSMF}$ = 0 dBm and $P_{in,\ DCF}$ = -2 dBm to achieve the optimal system performance at 10 Gbit/s with NRZ signal as shown in [259]. The analysis is done for a TAS node with four in-/output fibers and the standard components parameters as shown in Tab. 6.1 on page 110 is used. The BER at the end of the signal path is then estimated by using a deterministic BER estimator as described on page 117. With such a deterministic BER estimation method the signal and noise propagate separately. The optical noise from EDFAs and SOAs are described using the optical *Noise Bins*. The noise is assumed to have Gaussian statistics and the total noise is given by the the sum of the statistical independent noise sources of the signal-ASE beat, ASE-ASE beat, shot noise (including a contribution from the dark current) and thermal noise in the receiver. The noise in the electrical signal is calculated analytically from the noise spectral density of the optical *Noise Bins* and the equivalent filter bandwidths specified at the BER estimator. The noise free signal, including ISI degradation, propagates separately and is sampled in the BER estimator. The BER is estimated for each of the bits in the bit stream by using Eq. 6.9 on page 117. Then an effective Q-factor is calculated by using Eq. 6.10 on page 117.

Fig. 6.15 shows the calculated effective Q-factor versus the number of wavelengths M for TAS node with four input/output fibers (N = 4) for the three different SOA gates and three different channel bit rates. The *reference SOA* is an SOA with a static gain about 14 dB and a noise figure of 11 dB. The results for this SOA correspond to the results achieved until now by analytical considerations of the noise and crosstalk. The *conventional SOA* and the *gain-clamped SOA (GC-SOA)* are used to describe real SOAs. The bias current of the conventional SOA is I = 200 mA and I = 250 mA for GC-SOA. With these bias currents, the same gain (approx. 14 dB) can be achieved for an input signal at P_{in} = -2 dBm. The hybrid compensated fibre link has full dispersion compensation, that is performed

according to the following rule:

$$D_{SSMF} \cdot L_{SSMF} + D_{DCF} \cdot L_{DCF} = 0 \tag{6.40}$$

where D_{SSMF}, D_{DCF} are the chromatic dispersion values of transmission and compensating fibres, respectively, and L_{SSMF}, L_{DCF} the lengths of these fibres. This rule can be fulfilled by placing DCFs in different positions within a transmission line. Three basic dispersion compensation schemes can be distinguished: the pre-, hybrid- and post-compensation. In pre- and post-compensation the DCFs are placed before or after the SSMF fibre. In hybrid-compensation 50% of the SSMF dispersion is compensated before the SSMF and the other 50% is compensated afterwards.

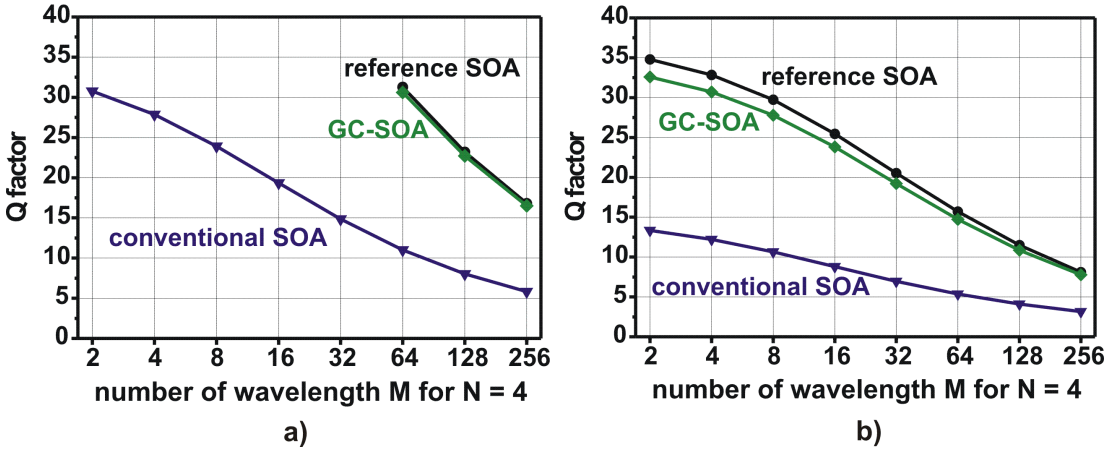

Figure 6.15: Calculated effective Q-factor from numerical simulations as function of the number of wavelengths M for TAS with N = 4 by considering noise, crosstalk, and SOA gain dynamics. a) at 2.5 Gbit/s, b) at 10Gbit/s. Three different SOA types are considered.

The use of conventional SOAs without any gain clamping results in severe signal degradation due to dynamic gain saturation and ISI. The Q-factor is decreased dramatically. For a Q-factor greater than 10 (BER $\geq 10^{-22}$), only very small TAS nodes can be achieved by using conventional SOAs (e.g. 8 wavelengths per fiber for TAS nodes with N = 4 at 10 Gbit/s, respectively). Using gain-clamped SOAs (e.g. DBR-SOA as discussed in Chapter 5) instead similar results can be achieved as reference SOA, where SOA gain dynamics is neglected and only ASE noise and crosstalk are considered. For 2.5 and 10 Gbit/s the same TAS node size can be achieved (256 wavelengths at 2.5 Gbit/s, 128 at 10 Gbit/s) [257, 260]. If such gain-clamped SOAs are used, the maximum size and throughput of TAS nodes are mainly limited by ASE noise and crosstalk. For moderate number of wavelengths per fibre the ASE noise is the dominating effect.

6.3.7 Analysis of SOA Chirp and its Impact on Dispersion Tolerance

In this subsection the analysis of TAS nodes is extended to the analysis of the impact of SOA chirp on the dispersion compensation characteristic of the fibre link. For such investigations the system configuration as shown in Fig. 6.14 is used. The number of possible wavelengths M for TAS nodes with four in /output fibers is fixed to 128. A typical chirp factor of $\alpha = 5$ is used for the conventional SOA and the GC-SOA. The input power of the SOA gates P_{in} = -2 dBm is chosen, which corresponds to the input power of a TAS node with 4 input/output fibres. The bias current of the conventional SOA is I = 200 mA and I = 250 mA for GC-SOA. With these bias currents, the same gain (approx. 14 dB) can be achieved for an input signal at P_{in} = -2 dBm. The *reference SOA* has no chirp and a static gain about 14 dB, a noise figure of 11 dB are used. Here only the signal path between two TAS nodes are considered by assuming the use of the 3R-regenerating wavelength converters. That means 3 hybrid compensated fibre sections each 80 km are cascaded. The modelling parameters in Tab. 6.3 are used for the SSMF and DCF. The effective Q-factor at the end of the signal path is estimated for the three SOA types operating with a 10 Gbit/s NRZ signal for different compensation ratio (CR), which is defined as:

$$\mathrm{CR} = \frac{-D_{DCF} \cdot L_{DCF}}{D_{SSMF} \cdot L_{SSMF}} \tag{6.41}$$

Using the fibre parameters in Tab. 6.3, the length of the DCF in the hybrid compensated sections varies according to L_{DCF} [km] $= 13.84 \cdot CR$. If the hybrid compensated fibre link is not full dispersion compensated, the remaining dispersion D_{rest} can be calculated according to the following rule:

$$\begin{aligned} D_{rest}[ps/nm] = {} & D_{SSMF}[\mathrm{ps/nm/km}] \cdot L_{SSMF}[km] \\ & + D_{DCF}[\mathrm{ps/nm/km}] \cdot L_{DCF}[km] \cdot \mathrm{CR} \end{aligned} \tag{6.42}$$

If the CR varies from 80% to 110%, the remaining dispersion D_{rest} is between 276.8 ps/nm and -138.4 ps/nm, respectively. Fig. 6.16 shows the calculated effective Q-factor for a TAS node with N = 4 and M = 128 versus the compensation ratio of the links. The simulation was done for a channel bit rate at 10 Gbit/s with NRZ signal and for three different SOA types.

For NRZ modulation the Q-factor achieved for the conventional SOA is much lower as compared to the reference SOA and the GC-SOA. A TAS node with four in-/output fibers cannot be built with 128 wavelengths each fiber by using a conventional SOA, as also shown in Fig. 6.15. But very similar performance is achieved for the reference SOA and the GC-SOA. This is due to the effective reduction of dynamic gain saturation. The curves for the GC-SOA and conventional SOA are shifted to lower values of the compensation ratio, which implies that both SOAs

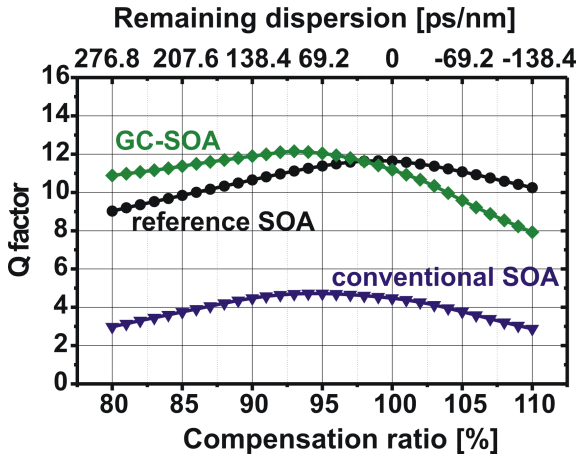

Figure 6.16: Calculated effective Q-factor for a TAS node with N = 4 and M = 128 versus the compensation ratio of the links. The simulation was done for a channel bit rate at 10 Gbit/s with NRZ signal and for three different SOA types: reference SOA, conventional SOA (I = 200 mA) and GC-SOA (I = 250 mA). The same average input power $P_{in,SOA}$ = -2 dBm is used.

provide some degree of dispersion compensation due to SOA chirp. For compensation ratio below 97 % the Q-factor achieved with the GC-SOA is even higher than that for the reference SOA. The tolerance against non ideal dispersion is the same as for the reference SOA. That means the GC-SOA chirp has only a slight impact on the dispersion compensation characteristic of the link [260].

The physical investigations of the TAS nodes in this chapter have shown that the quality of a signal at the end of a path through the burst switched domain between two edge nodes is affected by several impairments. The non-ideal optical switching node with SOAs as on/off gates introduces noise, crosstalk, chirp, and signal distortion. Such signal degradation mechanisms are discussed step by step and their impacts on the maximum size and throughput of the TAS nodes are investigated. From today's technology point of view fast and large OBS core nodes can be built with TAS node architecture. But conventional SOAs are not suitable to be used as switching gates. By using GC-SOAs as on/off gates in TAS nodes, the remaining signal distortion due to gain saturation and dynamics only slightly decrease of the maximum size of the nodes compared to the reference SOA (no gain dynamics, no chirp, only noise and crosstalk are introduced). The maximum size and throughput of the TAS nodes will be limited mainly by noise and crosstalk and large switching nodes with up to 10.24 Tbit/s maximum throughput can be build, if optimized components e.g. GC-SOA with small noise figure are used. Furthermore, regenerative (3R) wavelength converters should be used to avoid the accumulation of signal degradation.

Chapter 7

Physical and Traffic Evaluation of Selected OBS Node Architectures

As discussed in the previous chapter the maximum size and throughput of an OBS node is limited by signal degradations, which are introduced by several physical impairments. Additional to such physical limitations another limiting factor for the throughput of such OBS nodes is the burst loss in the case of contention [256, 261].

A contention situation occurs in an OBS core node when two or more bursts try to leave the node at the same time on the same output fibre and the same wavelength. In electric packet switched networks contention is resolved by the store and forward technique. The packet is stored as long as contention exists. This is not possible in optical networks because no large and flexible optical random access memory (RAM) exists. As already mentioned in Chapter 2 (Section 2.3.1) a key characteristic of OBS networks is the use of one-pass reservation scheme. That means the network resources are reserved for each individual burst but are not acknowledged before sending the data bursts. Therefore during contention situations burst loss can be severe. To keep the burst losses as low as possible three different contention resolution methods in three different domains can be used, the wavelength conversion in the wavelength domain, fibre delay lines (FDLs) in the time domain, and deflection routing in the space domain (see Chapter 4 on page 51).

While the effectiveness of deflection routing depends strongly on network topology and traffic pattern, the effectiveness of the other two contention resolution schemes depend mainly on the OBS core node architectures. In an OBS core node the burst loss rate B can be reduced by using many wavelengths per fibre in combination with wavelength conversion and optionally by FDLs as buffers. Otherwise the burst loss rate (B) is the lower, the lower the utilization of the WDM channels is. For a given maximum acceptable burst loss rate (B), the maximum utilization of WDM channels depend on the node architecture as well as the burst reservation scheme. The product of maximum utilization and maximum throughput gives then

the effective throughput of the node for dynamic traffic. That means the effective throughput of an OBS node is not only determined by the physical impairments, which limits the maximum size and consequently the maximum throughput of the nodes, but also by the burst losses. To estimate the effective throughput of an OBS node both physical as well as traffic performance must be considered.

In this chapter the physical analysis of maximum size and throughput of the Tune-and-Select (TAS) node architecture introduced in the previous chapter is extended. First in Section 7.1 based on the result from the physical analysis in Chapter 6 a traffic analysis of TAS nodes is performed additionally. The effective throughput of the node is determined for a burst loss rate of $B \leq 10^{-6}$. Then with the objective to increase the achievable effective throughput of the nodes, three different variations of TAS nodes are considered in Section 7.2: TAS nodes with wavelength converters of limited tuning range (TAS-LTR), TAS nodes with dedicated FDL buffer per output (TAS-dFDL), and shared FDL buffer per node (TAS-shFDL)) are compared with basic TAS nodes. Here not only the maximum size of such nodes is calculated, but also the effective throughput. Finally, in Section 7.3 this chapter is summarised by giving some concluding remarks.

7.1 Effective Throughput of the TAS Nodes

To evaluate the effective throughput of the TAS nodes, a traffic analysis is performed in addition to the physical evaluation as shown in the previous chapter. First the maximum utilization of an output fibre of an TAS node is calculated for a burst loss rate B $\leq 10^{-6}$ based on the maximum number of wavelengths per fibre. Then the result from the physical analysis of the TAS node is combined with the results from the traffic analysis. The product of the maximum utilization and the maximum throughput gives the effective throughput of the nodes.

7.1.1 Traffic Analysis of the TAS nodes

The burst loss performance of the OBS networks has been studied extensively using either simulation or simple analytical models [6, 39, 42, 48, 50, 136]. Typically, an output port of an OBS node has been analysed by assuming Poisson arrivals and no buffering [39, 42, 48, 50, 136]. Under these assumptions, an output port of an OBS node can be modeled by a finite number of servers, each representing a wavelength channel, with no buffer. Then, the probability that a burst designated to this output port is lost can be obtained from the well-known *Erlang loss formula* [262, 263].

A TAS node has N input/output fibres and each fibre supports M + 1 wavelength channels, where one wavelength channel is used as reservation channel for signaling (transmission and processing of the burst header packets) as discussed in Chapter 4

on page 55. The other M wavelength channels carry data bursts. With the following three assumptions,

1. The burst header packets and in consequence data bursts arrive at the OBS node according to independent Poisson processes with arrival rate $r_{arrival}$.
2. Burst transmission times on each fibre link are independent and exponentially distributed with a common mean $h = 1/\mu$.
3. Full wavelength conversion is performed, i.e., a burst can change to any wavelength in case the wavelength it arrives on is currently occupied on the outgoing fibre.

the burst loss probability (burst loss rate) B on each fibre link of the TAS nodes is the same and is given by using the well-known *Erlang loss formula* with:

$$B(A, M) = \frac{A^M/M!}{\sum_{i=0}^{M} A^i/i!} \tag{7.1}$$

where A is the offered traffic load and M the number of wavelengths per output fibre. Therefore A/M is the normalized offered traffic, which corresponds to the utilization of an output fibre of the TAS node.

Eq. 7.1 shows that the burst loss probability is depending on the offered traffic load A and the number of wavelengths per fibre M. Fig. 7.1a depicts the burst loss probability B versus the number of wavelength M with the utilization of an output fibre A/M as parameter.

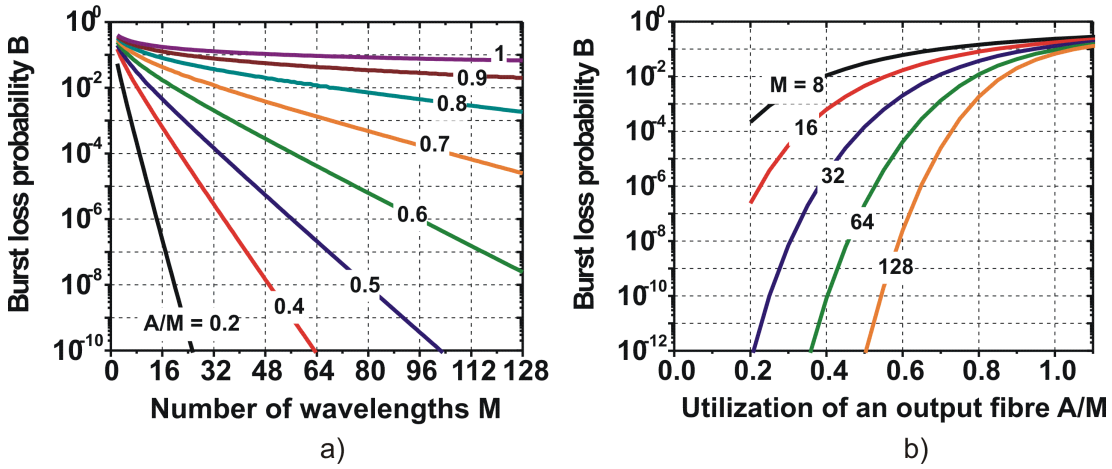

Figure 7.1: Burst loss probability B on each fibre link of the TAS nodes versus a) the number of wavelengths M with the utilization of an output fibre A/M as parameter, b) the utilization of an output fibre A/M with M as parameter.

It can be seen that a greater number of wavelengths yields an dramatic decrease in burst losses B, e.g., if M increased from 16 to 128 in a scenario with $A/M = 0.6$, B is decreased by about six orders of magnitude. That means the greater the number of wavelengths, the greater the probability that a request can find a wavelength which is not occupied at the moment. The slope of the decrease depends on A/M. If A/M approaches 1, the slope is very small resulting in a hardly reduced loss probability with increasing number of wavelengths. In Fig. 7.1b, the burst loss probability B is depicted against the utilization A/M with the number of wavelengths M as parameter. E.g. for a burst loss probability of 10^{-4}, it is possible to operate an OBS network with 60% utilization if the underlying WDM technology supports 64 optical channels/fibre. This shows that it is possible to operate an OBS network at high utilization if the number of wavelength channels per fibre is sufficiently large, even without any buffering. In this figure, also overload situations with $A/M > 1$ are depicted. It can be seen that an increased A/M also yields an increased loss probability. For higher overload, B approaches roughly the same value despite the number of wavelengths, i.e., a higher M does not yield a lower B in higher overload situations. For smaller values of A/M it can be seen that a reduced A/M results in a decrease in B. The slope of this decrease depends on the number of wavelengths. A low loss probability can only be achieved by a large number of wavelengths and A/M which is controlled far below 1.

In an OBS network, the burst loss probability is also depending on the burst reservation mechanism used in the network. The offered traffic A relevant for loss computation is different for different reservation mechanism. Recently, several reservation mechanisms have been proposed in literature [6, 11]. The objective of such reservation mechanisms is to achieve optimal utilization of the output wavelength channels per fibre and low contentions. The optimum is to keep the output wavelength channel just reserved for the length of the burst. Based on their way of indicating the end of a burst and the time when allocation of a WDM channel starts, they can be classified mainly into three groups [39].

The simplest approach for reservation of a wavelength channel is to indicate the end of a burst by an additional trailing control packet or using an in-band terminator (IBT). In both cases the network nodes only need to know whether a wavelength channel is currently available or not. The complexity in both edge and core nodes is very low. A mechanism that follows that principle is *Just-In-Time (JIT)* reservation [11]. Upon arrival of the reservation request and a wavelength channel is immediately allocated if available. Otherwise, the request is rejected and the corresponding data burst is discarded. The wavelength channel remains allocated until burst transmission has finished. The drawback of this method is its low efficiency as losses also occur in cases without any transmission conflict between different bursts on the same wavelength. As shown in Fig. 7.2a only *burst 3* can be accepted. At the time of arrival of the BHP 1 and 2 the end of the actual

bursts (a, b) on that wavelength are not known, *burst 1* and *2* have to be discarded although there would be no contention.

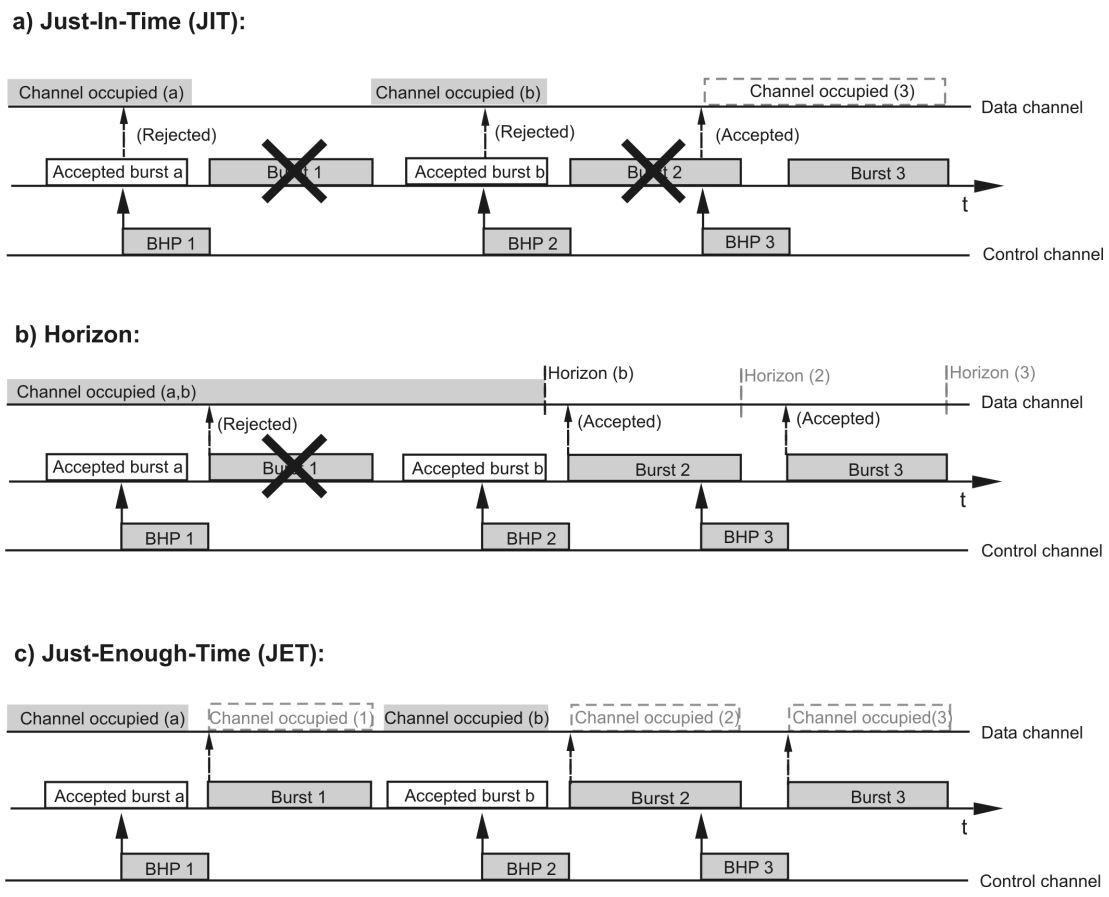

Figure 7.2: Comparison of three different reservation mechanisms in terms of efficiency.

An improvement to schemes like JIT can be achieved by using reserve-a-limited-duration (RLD) based mechanisms. They require the sender to add the burst length in the BHP. A wavelength channel is only allocated for a limited duration so that subsequent burst transmission requests with a start time greater than the finishing time of an allocated burst may be accepted. That means the basic offset interval of a burst may overlap the transmission phase of a previously accepted burst. The *Horizon* mechanism proposed by Tuner in [6] as well as the very similar *Latest Available Unscheduled Channel mechanism (LAUC)* proposed by Xiong et al. in [38] are representatives of RLD-based mechanisms. In Horizon and LAUC wavelength channel state information is enhanced by the so-called *reservation horizon*, i.e., the time until which the wavelength is allocated. When a control packet arrives, the wavelength channel with largest reservation horizon which is before the start time of the new burst is reserved. The end of the new burst is then the

new reservation horizon of the corresponding wavelength. Thus, unlike IBT (*burst 2* in Fig. 7.2b) can be accepted, although there is an overlap of the request (BHP 2) and the previous burst b. So the blocking probability of bursts can be reduced and the channel can be used more effective than by IBT. The difference between Horizon and LAUC is that the minimization of the emerging gap is only an option in Horizon, whereas it is mandatory for LAUC. However, as also depicted in Fig. 7.2b, *burst 1* cannot be accepted in a gap between two already reserved bursts as the reservation mechanism is not aware that this gap exists. The disadvantage of RLD-based mechanisms is the increase of the system complexity.

Even higher efficiency can be achieved by using reserve-a-fixed-duration (RFD) approach. The wavelength channel is allocated for a fixed duration corresponding to the burst transmission time. One proposal of the RFD-based mechanism is *just-enough-time (JET)*, devoloped by Qiao and Yoo [5, 62]. It is also the most commonly used reservation mechanism in an OBS network due to its high efficiency. It considers the exact predeterminated start and end times of each burst for reservation. In contrast to Horizon, RFD-based reservation mechanisms are able to detect situations where no transmission conflict occurs although the start time of a new burst is earlier than the finishing time of the already accepted burst. That leads to most efficient utilization of resources. There are lots of information like starting and finishing times of all accepted bursts has to be stored and processed which makes such a system rather complex. But they allow to reserve newly arriving bursts in gaps between other already reserved bursts, e.g., *burst 1* in Fig. 7.2c can be transmitted. The blocking probability of bursts can be reduced in comparison to RLD and JIT.

For Horizon and JET, the offered traffic A relevant for loss computation is simply the product of arrival rate $r_{arrival}$ and the mean transmission time h of a data burst. So the loss probability of a burst is given for Horizon and JET by

$$P_{Loss,\ Horizon} = P_{Loss,\ JET} = B(r_{arrival} \cdot h, M) = \frac{(r_{arrival} \cdot h)^M / M!}{\sum_{i=0}^{M} (r_{arrival} \cdot h)^i / i!} \qquad (7.2)$$

Note, that Horizon and JET have the same performance under above given assumptions as the scenario where a burst is reserved in between two already reserved bursts does not occur in the single node case with constant offset time δ. The offset time δ is the time between the burst header packets and the data bursts for reservation and switching operations (see Chapter 2 on page 20.)

If Just-in-time (JIT) is used the system behaves like a loss system with increased offered traffic, resulting in the loss probability:

$$P_{Loss,\ JIT} = B(r_{arrival} \cdot (h+\delta), M) = \frac{[r_{arrival} \cdot (h+\delta)]^M / M!}{\sum_{i=0}^{M} [r_{arrival} \cdot (h+\delta)]^i / i!} \tag{7.3}$$

The reason for this behavior is that each request blocks a channel for an interval whose length is the sum of basic offset δ and burst transmission time h. The increased load leads to a higher loss probability of JIT compared to JET and Horizon, e.g. a JET/Horizon system with 16 wavelength channels is even better than a 32 wavelength channel system using JIT if $\delta > 1.7$h [60]. Therefore, in the following analysis JET reservation mechanism is used for reservation of wavelength channels on the output fibre of the TAS nodes. For a given maximum number of wavelengths M (from the physical analysis) and an allowable fixed burst loss rate e.g. B $\leq 10^{-6}$, the maximum utilization A/M of an output fibre can be calculated by using the Eq. 7.1.

As already shown in Fig. 7.1, the calculated maximum utilization (Eq. 7.1) of an output fibre as a function of the number of wavelengths M with the allowable fixed burst loss rate B as parameter is depicted in Fig. 7.3. It can be seen that for different burst loss rate different utilization of an output fibre can be achieved. The larger the acceptable burst loss rate in an OBS network is, the larger is the utilization for a fixed number of wavelengths. For a fixed burst loss rate up to 100 wavelength channels the maximum utilization increases dramatically with the number of wavelengths. Then the slope of the increase slows down and e.g. only $\sim 80\%$ the wavelength channels (400 in total) of an output fibre can be used to guarantee a burst loss rate of B $\leq 10^{-8}$.

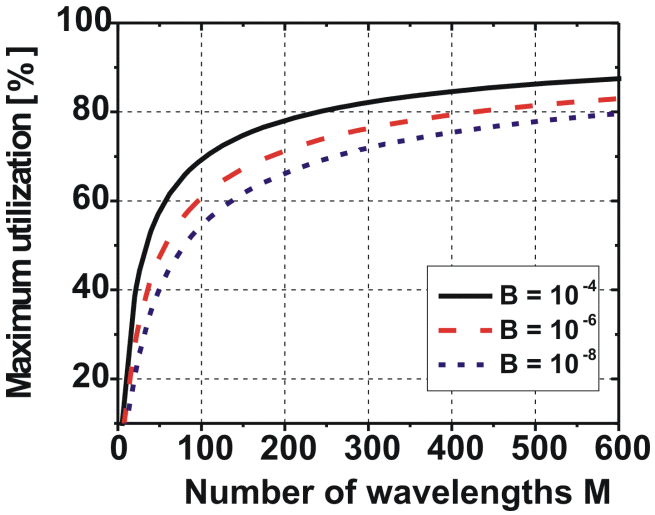

Figure 7.3: The calculated maximum utilization A/M in % of an output fibre versus the number of wavelengths M with burst loss probability as parameter.

7.1.2 Estimation of the Effective Throughput of the TAS nodes

a)Results From the Physical Analysis:

To determine the maximum number of wavelengths per fibre of the TAS nodes a physical analysis as shown in previous Chapter 6 is done by using the component parameters as shown in Tab. 6.1 on page 110. The usable capacity in the fibre is directly dependent on the operating windows in the different bands and the spectral efficiency of the WDM systems, which can be defined as the ratio of the bit rate per channel to the channel spacing. The higher the spectral efficiency is, the higher is the capacity that can be packed into a single fibre. The spectral efficiency of WDM system today is typically 0.4 bit/s/Hz [246]. This means new systems will have 10 Gbit/s channels spaced 25 GHz and 40 Gbit/s channels spaced 100 GHz. For 2.5 Gbit/s channels the channel spacing is 12.5 GHz due to available optical filters leading to a lower spectral efficiency of 0.2 bit/s/Hz. If only the C-band is used the available number of wavelengths per fiber is 320 for 2.5 Gbit/s channel bit rate, 160 for 10 Gbit/s channel bit rate, and 40 for 40 Gbit/s channel bit rate. For C- and L-band the available number of wavelengths per fibre is doubled (640 for 2.5 Gbit/s, 320 for 10 Gbit/s, and 80 for 40 Gbit/s). In the following, the maximum number of wavelengths M and hence the maximum throughput of the TAS nodes are determined within these constraints for 2.5/10/40 Gbit/s channel bit rate. In contrast to the previous analysis, the number of wavelengths is varied between 4 and 640 in steps of 2 instead of multiple of two. With a Q-factor greater than 10, the maximum number of wavelengths per fibre and the maximum throughput of TAS nodes versus the number of fibres at three different bit rates are shown in Fig. 7.4. The number of input/output fibres is varied from N = 3 to N = 10.

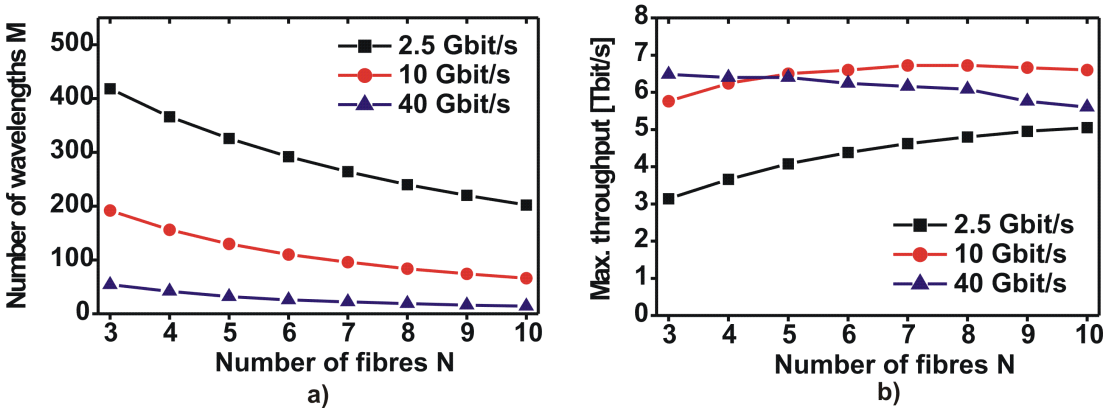

Figure 7.4: Results form the physical analysis as shown in previous Chapter 6: the calculated maximum number of wavelengths per fibre (a) and the maximum throughput (b) of TAS nodes versus the number of fibres at three different bit rates.

With the increasing bit rate the number of wavelength channels per fibre decreases due to the increasing BER for the same TAS node with same input/output fibres. For all three bit rates, the maximum number of wavelengths of TAS-nodes decreases with the increasing number of input/output fibres. The resulting maximum throughput of the nodes increases at 2.5 and 10 Gbit/s with the increasing number of input/output fibres. Up to 5 Tbit/s maximum throughput can be achieved at 2.5 Gbit/s for a TAS node with 10 input/output fibres. Compared to 2.5 Gbit/s larger maximum throughput among 6 - 7 Tbit/s can be achieved at 10 Gbit/s for all TAS nodes. At 40 Gbit/s similar maximum throughput can be achieved as at 10 Gbit/s, but it decreases with the increasing number of input/output fibres. The maximum available number of wavelengths per fiber (C- and L-band) can never be achieved by any TAS nodes.

b) Combining the Results From the Physical and Traffic Analysis:

Combining the results from Fig. 7.4 and Fig. 7.3 the effective throughput of the TAS nodes can be calculated. Fig. 7.5a shows then the resulting effective throughput of TAS nodes versus the number of input/output fibres at three different bit rates for a burst loss rate B $\leq 10^{-6}$.

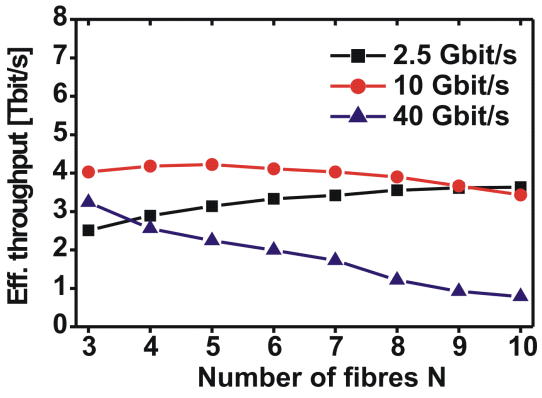

Figure 7.5: The calculated maximum and effective throughput of TAS nodes versus the number of input/output fibres at three different bit rates for a burst loss rate B $\leq 10^{-6}$.

The maximum throughput resulting from the physical analysis as shown in Fig. 7.4b is also shown here for comparison. For all three bit rates the effective throughput is much lower than their maximum throughput. Comparing the achievable maximum and effective throughput at each bit rate, it can be seen, that nodes at 2.5 Gbit/s are the most efficient ones. Due to the large number of wavelengths per fibre the maximum utilization on an output fibre is much higher ($\sim$ 70 - 80 %) than at 10 and 40 Gbit/s. Similar to maximum throughput the effective throughput increases also with the number of input/output fibres at 2.5 Gbit/s. Up to about 3.6 Tbit/s effective throughput (5 Tbit/s maximum throughput) can be achieved

at 2.5 Gbit/s for a TAS node with 10 input/output fibres. Compared to the other two bit rates the largest effective throughput among 4 Tbit/s can be achieved at 10 Gbit/s. For 40 Gbit/s the achievable effective throughput decreases dramatically with the increasing number of input/output fibres, due to the small number of wavelengths and therefore small utilization on the output fibre. So TAS node at 40 Gbit/s is very inefficient and compared to the other two bit rates it is only meaningful for a network with small node degree. Using TAS node architecture the largest achievable effective throughput of TAS nodes is about 4 Tbit/s for a burst loss rate of $B \leq 10^{-6}$.

7.2 Variations of the TAS Nodes and Their Maximum Size and Effective Throughput

As shown in the previous section, the largest achievable effective throughput of an OBS nodes with SOA-based TAS architecture is 4 Tbit/s for a burst loss rate of $B \leq 10^{-6}$. To increase the achievable effective throughput of the nodes, two different methods can be used. Either the maximum size and hence the maximum throughput of the nodes should be increased or the burst losses should be reduced by using additional contention resolution schemes as discussed in Chapter 4 e.g. in the time domain using optical delay lines (FDL) as buffers. As the efficiency of such methods depends also on the used node architecture, three different variation of TAS nodes are considered in this section. Their performance, not only the maximum size but also the effective throughput will be compared with TAS nodes.

7.2.1 TAS with Wavelength Converters of Limited Tuning Range

A variant of the TAS node is a TAS architecture with wavelength converters of limited tuning range (TAS-LTR) as shown in Fig. 7.6b. This node architecture is very similar to a TAS node as shown in Fig. 7.6a. The main difference compared to a TAS node is the wavelength converters in TAS-LTR do not have full wavelength conversion capability and each wavelength converter can only convert input signals to few output wavelengths with x < M e.g. x = 8, 16, 32, 64 etc. Using such wavelength converters the large 1 to NM output combiners in the TAS nodes can be replaced with smaller output combiners and WDM multiplexers. This results in low splitting losses. Also, less noise contributions (from x SOAs instead from M SOAs for TAS) are disturbing the transmitted signals. Furthermore, a converter with a smaller tuning range may be easier to realise. It is expected that simpler and larger sized nodes can be built with the TAS-LTR architecture, but the utilization of WDM channels will be smaller compared to the TAS node because of the limited tuning range of the wavelength converters [256, 261].

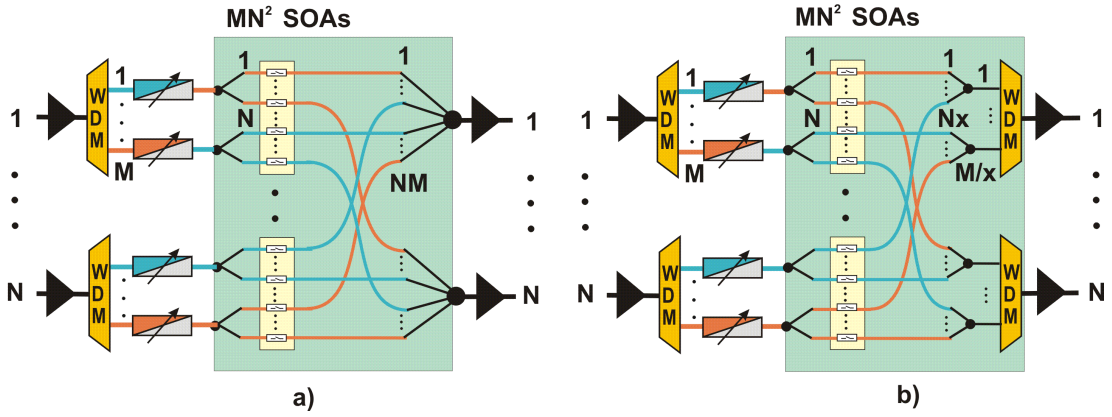

Figure 7.6: OBS core nodes. a) Tune-and-select (TAS) node. b) TAS node with wavelength converters of limited tuning range (TAS-LTR).

Variation of tuning range

Variation of the tuning range of the wavelength converter will result in a different maximum size of a TAS-LTR node. Fig. 7.7 shows the maximum and effective throughput for TAS-LTR nodes with 4 input/output fibres, but for the different tuning ranges x and at different channel bit rates. The number of wavelengths per converter x is varied from 8 to 128. The number above the bar diagrams are the maximum number of wavelength per fibre. Due to the lower number of SOAs contributing to the noise in front of the next wavelength converter of the neighbouring node (from x SOAs instead from M SOAs for TAS) larger nodes can be built with this architecture compared to the basic TAS architecture.

The maximum number of C- and L-band wavelengths and highest achievable maximum throughput can be reached for all bit rates, but the wavelength converters have different tuning ranges. For 2.5 Gbit/s (M = 640) and 10 Gbit/s (M = 320) the tuning range must be between 8 and 64 and for 40 Gbit/s (M = 80) the tuning range is 8 and 16.

On the other hand the limited number of the wavelengths per converter x leads to small utilization of an output fibre to guarantee a burst loss rate of $B \leq 10^{-6}$ (see Fig. 7.3 on page 145). The maximum utilization of an output fibre is calculated with Eq. 7.1 and as shown in Fig. 7.7 the achievable effective throughput is reduced dramatically due to the small utilization and depends on the possible tuning range of the wavelength converters. The largest effective throughput of the TAS-LTR nodes with 4 input/output fibres ($\sim$ 7 Tbit/s) can be achieved at 10 Gbit/s with a tuning range of x = 64.

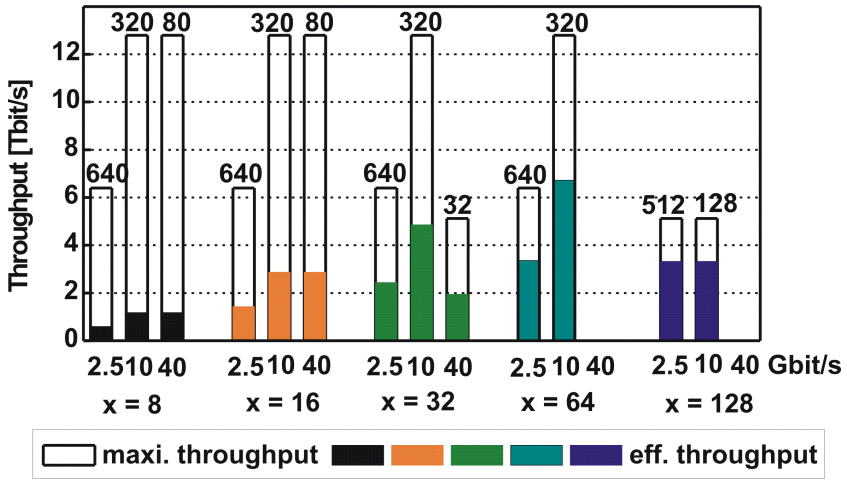

Figure 7.7: The maximum and effective throughput for TAS-LTR node (N = 4) different tuning range (x) and channel bit rate. The number above the bar diagrams are the maximum number of wavelength (M) per fibre.

There is an optimal tuning range for the wavelength converters to achieve the highest effective throughput: x = 64 for 2.5 and 10 Gbit/s and x = 16 for 40 Gbit/s. At 2.5 and 40 Gbit/s similar effective throughput ($\sim$ 3.5 Tbit/s at 2.5 Gbit/s, $\sim$ 3 Tbit/s at 40 Gbit/s) can also be achieved as with basic TAS architecture, but the hardware complexity of this architecture is much lower, as the same number of SOAs are needed but the wavelength converters only have to have much smaller tuning range, 64 instead of $\sim$ 250 for TAS at 2.5 Gbit/s and 16 instead of $\sim$ 50 for TAS at 40 Gbit/s. As shown in Chapter 3, the realisation of such tunable wavelength converters/lasers is much more realistic and such fast tunable lasers accessing 16 [264] and 32 [265] ITU channels with 100 GHz spacing in ns range have been already demonstrated. At 10 Gbit/s higher effective throughput can be achieved than as with basic TAS architecture ($\sim$ 7 Tbit/s instead $\sim$ 4 Tbit/s).

7.2.2 TAS with FDL Buffer

To reduce the burst loss rate FDL buffers can be used solely for contention resolution in the time domain additionally to wavelength conversion in the wavelength domain (see Chapter 4). Adding such FDL buffers in a TAS node in a simple way two different architectures can be used [256, 261, 266]:

1) TAS with Dedicated FDL Buffer per Output (TAS-dFDL)

First modification of the TAS node with WDM fibre delay line (FDL) buffer is a node provides one WDM fibre delay line (FDL) per output fibre. It is called TAS with dedicated FDL (TAS-dFDL) and is depicted in Fig. 7.8a. A TAS node

with an FDL per input fibre is also feasible, but comparatively unfavorable due to higher losses in front of the SOA. Such FDLs can carry several wavelength channels simultaneously and are used for contention resolution to reduce burst loss rate [35, 64, 141]. Drawbacks of this node are higher splitting losses and larger switching arrays with $2 \cdot M \cdot (N-1)^2$ SOA gates. The number of WDM FDLs per output fibre can be extended, but the size of the TAS-dFDL node will be reduced due to the increase of splitting losses. In this case additional EDFA could be required to compensate the splitting losses and fibre attenuation.

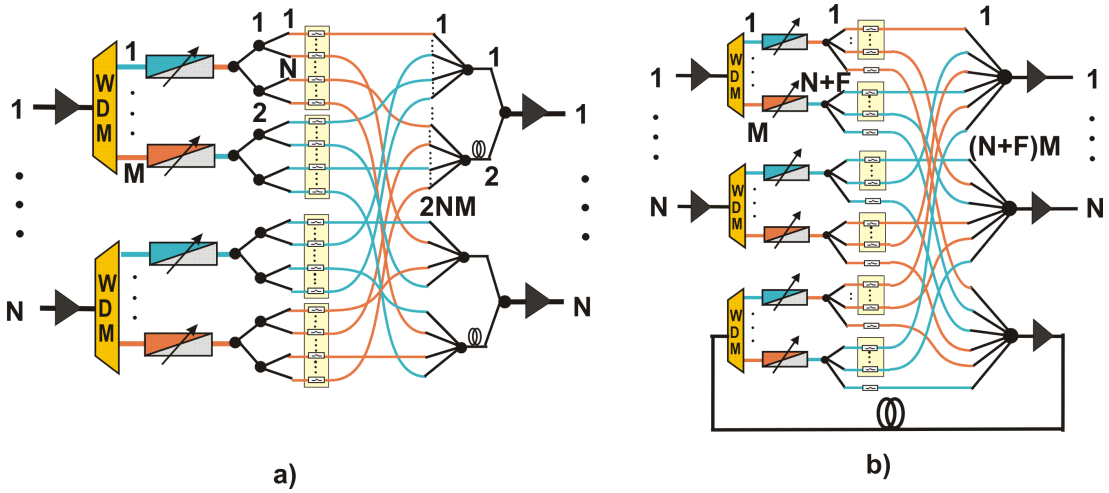

Figure 7.8: OBS core nodes with FDL buffer. a) TAS node with dedicated FDL buffer per output (TAS-dFDL). b) TAS node with shared FDL buffer per node (TAS-shFDL).

2) TAS with Shared FDL Buffer per Node (TAS-shFDL)

Another modification of the basic TAS architecture uses an FDL buffer shared among all the output fibres of the node. It is called TAS with shared FDL buffer (TAS-shFDL) and is depicted in Fig. 7.8b for F = 1. The FDL buffer consists of one (F=1) or several (F > 1) feedback FDLs of different lengths. The delay of the shortest FDL in the buffer is called basic delay b. In all investigations made here, the delays of the longer FDLs are integer multiples of the basic delay b, i.e. FDL i has delay $i * b$, $i = 1, \ldots, F$.

Compared to the TAS architecture not only more SOA gates - $M \cdot (N-1+F)^2$ instead of $M \cdot N^2$ in TAS - but also more tunable wavelength converters ($M \cdot (N+F)$) are needed. Here TAS-shFDL nodes with up to F = 4 feedback FDLs are considered. With the increasing number of feedback FDLs, the number of SOAs and the complexity of a TAS-shFDL node increase, too. However, there is still M noise contributions from the SOAs, if the use of 3R regenerating wavelength converters is assumed. Similar as in the basic TAS nodes and the TAS-dFDL nodes, at the

same time only M bursts can be transmitted on M wavelengths to one output fibre, that means in the worst case NM SOAs are switched on in a node and M noise contributions will be combined to one output fibre.
Both node architectures with FDLs (TAS-dFDL and TAS-shFDL) apply the same number of wavelengths in the FDL and on the output fibre. This is not necessary but a reasonable assumption. The FDLs can carry several wavelength channels simultaneously. In contrast to the TAS-dFDL architecture, the TAS-shFDL architecture requires an additional EDFA in each feedback loop to compensate splitting loss and fibre attenuation. Depending on the kind of wavelength converter, the TAS-shFDL architecture allows for multiple re-loops. This is not considered in the following.

When using FDL buffers in OBS nodes, the physical length of the FDL has to be considered. Several physical constraints like attenuation, chromatic dispersion and non-linear effects etc. limit the length of the FDLs. To simplify the physical investigation of such FDL buffers, dispersion compensated FDL is assumed, if necessary. However due to the FDL buffers, the node complexity is already increased due to the increasing number of the SOAs. The maximum length of the FDL should be then limited by the requirement, that no more than one EDFA is required to compensate the fibre attenuation of the FDLs. That means, all FDLs used for contention resolution have to be shorter than e.g. a typical EDFA span of 80 km. It limits the maximum FDL delay to e.g. about 260 μs. As shown in [64], FDL delays should be in the order of a few mean burst durations. In an FDL buffer with 4 FDLs, e.g., a delay of 8 mean burst durations for the longest FDL is a good choice. From the 260 μs it can be derived that the mean burst length has to be shorter than 10 kbyte, 40 kbyte and 160 kbyte for 2.5, 10 and 40 Gbit/s line-rate, respectively. Thus, mean burst lengths in the order of Mbytes cannot be realistically stored in FDL buffers with only one EDFA.

7.2.2.1 Traffic Performance Analysis of TAS Nodes with FDL Buffers

For the TAS and TAS-LTR nodes the utilization of an output fibre for a burst loss rate B $\leq 10^{-6}$ is calculated analytically and is insensitive to burst length distribution. In contrast to such an analysis, the utilization of an output fibre for the TAS architectures with FDL buffers is evaluated by discrete event simulation. Control packets of bursts arrive in a stream according to a Poisson process. Only one service class is considered and the offset between control packet and burst is assumed to be the same for all bursts. Burst length is negative-exponentially distributed with mean 12.5 kbyte, i.e. a mean transmission time h of 40 μs, 10 μs and 2.5 μs for 2.5, 10 and 40 Gbit/s channel bit rate, respectively. The term load refers to offered load per wavelength and is given with respect to the capacity of a wavelength channel. Destination of bursts is uniformly distributed over all N = 4 output fibres. Also, selection of the wavelength on which a burst arrives to the

node follows a uniform distribution. The same number of wavelength channels per output fibre and per FDL is used. All graphs include 95 %-confidence intervals based on the batch simulation method [266].

For load 0.8 and 16 and 32 wavelength channels, Fig. 7.9a depicts the impact of the basic FDL delay on burst loss probability. As the delays are normalized to the mean burst transmission time, the results apply for all bit-rates. All scenarios show that increasing the FDL delay reduces burst loss probability until a lower bound is reached for a basic delay in the range of 2 to 3 mean burst transmission times. For lower loads, this lower bound is only reached for larger delays which is not shown here. Similar results were published for TAS-dFDL in [64]. As increasing the basic FDL delay beyond 2 mean burst transmission times yields diminishing improvements in loss probability and considering the physical constraints on FDL length discussed above, this value is used as FDL delay for TAS-dFDL and basic delay for TAS-shFDL.

For TAS-shFDL nodes, Fig. 7.9b shows the impact of the number of FDLs F in the buffer for different basic FDL delays b. An increased number of FDLs in the buffer leads to a significantly reduced burst loss probability which could be motivation to employ FDL buffers with several FDLs. Again, it can be seen that increasing the basic delay beyond 2 mean burst transmission times has no significant impact.

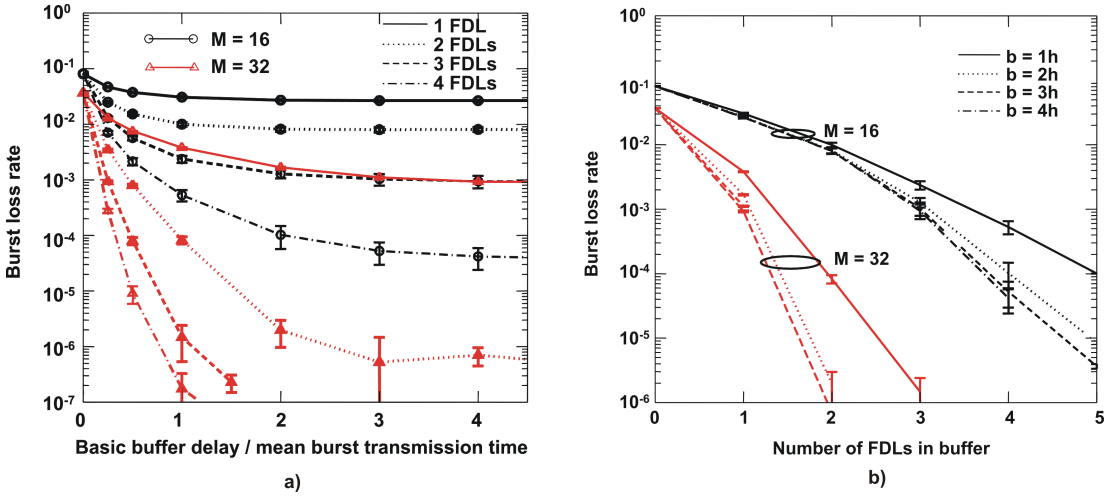

Figure 7.9: a) Impact of basic FDL delay on burst loss probability. b) Impact of number of FDLs in the buffer on burst loss probability (M=16 and M=32, offered load 0.8) [266].

Fig. 7.10 depicts the burst loss probability versus the offered load per wavelength for 16 wavelength channels and different node configurations. Due to the improved contention resolution capability, multi-FDL buffers have a lower loss probability for

a given offered load. The utilization for B = 10^{-6} used in the integrated analysis is extracted as indicated by the arrows. For a burst loss rate of B = 10^{-6}, the utilization A/M(1-B) approximately equals A/M.

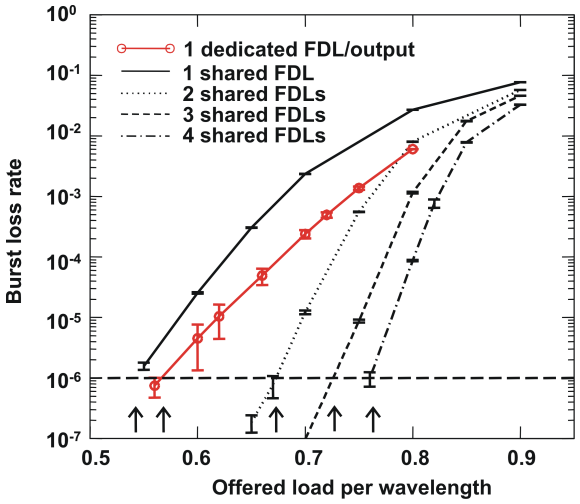

Figure 7.10: Burst loss probability versus the offered load per wavelength (utilization of an output fibre) for TAS-dFDL and TAS-shFDL with $1, \ldots, 4$ FDLs (M = 16) [266].

7.2.2.2 Maximum Throughput of TAS Nodes with FDL Buffers

If one WDM FDL per output fibre is used to reduce burst losses during contention, only small nodes can be built due to higher splitting losses and losses of the delay line. The delay lines in the TAS-dFDL node have a delay of two mean burst transmission times which corresponds to 16/4/1 km of fibre for 2.5/10/40 Gbit/s. As introduced above, the ith FDL in a TAS-shFDL node with F FDLs has a delay of $2 * i$ times the mean burst transmission times, $i = 1 \ldots F$. The calculation of the maximum number of wavelengths is done for nodes with 4 input/output fibre and Q equal 10 is taken as limit of signal degradation. Compared to basic TAS nodes TAS nodes with a dedicated FDL per output fibre (TAS-dFDL) can only be built with much smaller number of wavelengths: M = 212 for 2.5 Gbit/s line-rate, M = 76 for 10 Gbit/s line-rate and M = 16 for 40 Gbit/s line-rate. These values result in a maximum throughput of 2.12 Tbit/s for 2.5 Gbit/s line-rate, 3.04 Tbit/s for 10 Gbit/s line-rate and 2.56 Tbit/s for 40 Gbit/s line-rate.

In TAS nodes with shared FDL buffer (TAS-shFDL) the signals going through the FDLs are fully regenerated after passing the feedback loop due to the regenerative (3R) wavelength converters assumed. To compensate the fibre attenuation and the splitting losses in the feedback loop additional EDFAs must be used. For FDL lengths considered here only one EDFA is needed per loop and no fibre dispersion

compensation is required. To calculate the maximum size of a TAS-shFDL node two signal paths have to be considered separately: First, the signal path between the wavelength converter at the input of the node and the wavelength converter in the feedback loop; Second, the signal path between the wavelength converter in the feedback loop and the input wavelength converter in the downstream node. Primarily, the second path limits the size of TAS-shFDL nodes. The resulting maximum number of wavelengths and the maximum throughput of TAS-shFDL nodes with 4 input/output fibres are shown in Tab. 7.1 for different bit-rates and number of FDLs F varied from 1 to 4. Due to the lower losses in the second signal path (no FDL power loss; a smaller splitting loss for F $<$ 4) larger nodes can be built with this architecture compared to the TAS-dFDL architecture.

Number of FDLs in TAS-shFDL (length of FDL)	2.5 Gbit/s	10 Gbit/s	40 Gbit/s
F = 1 (16/4/1 km for 2.5/10/40 Gbit/s)	M = 312 3.12 Tbit/s	M = 120 4.80 Tbit/s	M = 28 4.48 Tbit/s
F = 2 (32/8/2 km for 2.5/10/40 Gbit/s)	M = 280 2.80 Tbit/s	M = 104 4.16 Tbit/s	M = 24 3.84 Tbit/s
F = 3 (48/12/3 km for 2.5/10/40 Gbit/s)	M = 252 2.52 Tbit/s	M = 88 3.52 Tbit/s	M = 20 3.20 Tbit/s
F = 4 (64/16/4 km for 2.5/10/40 Gbit/s)	M = 228 2.28 Tbit/s	M = 80 3.20 Tbit/s	M = 16 2.56 Tbit/s

Table 7.1: Maximum number of wavelengths and maximum throughput of TAS-shFDL for different number of FDLs F and different line bit-rates with $Q > 10$.

From Tab. 7.1 it can be seen that the increasing number of FDLs in a TAS-shFDL node results in a smaller number of wavelengths and consequently in a smaller maximum throughput. The maximum throughput of a specific node architecture e.g. TAS-dFDL and TAS-shFDL is almost in the same range for a line bit-rate of 10 and 40 Gbit/s, but not for a line bit-rate of 2.5 Gbit/s at which the maximum throughput is smaller due to crosstalk of a large number of WDM channels.

7.2.2.3 Effective Throughput of TAS Nodes with FDL Buffers

Now, the effective throughput of TAS nodes with FDL buffers that can be achieved under dynamic traffic in the presence of a burst loss probability of B $\leq 10^{-6}$ is calculated.

While the application of FDLs in an OBS node (TAS-dFDL and TAS-shFDL) in general and increasing the number of FDLs in a TAS-shFDL node specifically shows that the burst loss rate B is effectively reduced and the utilization in the traffic performance evaluation is improved, the physical analysis indicates that both options reduce the node size and the maximum throughput. Also, the impact of the bit-rate which had no influence on the performance analysis above is essential when

looking at maximum throughput. Thus, the question arises whether the effective throughput, i.e. the product of utilization and maximum throughput, increases or decreases when using more complex FDL buffers.

Fig. 7.11 shows the number of wavelengths as well as the maximum and effective throughput for a node with 4 input/output fibres combining results of the physical and the traffic performance evaluation for 10 Gbit/s and 40 Gbit/s channel bit rates.

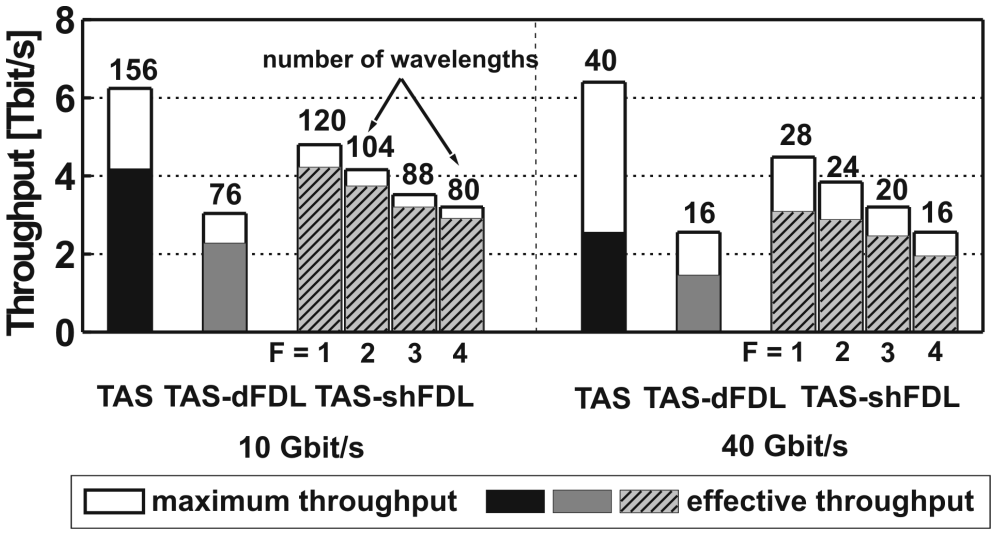

Figure 7.11: Maximum and effective throughput of TAS, TAS-dFDL and TAS-shFDL nodes with 4 input/output fibres at 10 Gbit/s and 40 Gbit/s.

The maximum throughput of all architectures is in the range from 3 to 6 Tbit/s. The highest maximum throughput (about 6 Tbit/s for 10 and 40 Gbit/s line-rates) can be achieved with the basic TAS node architecture. With TAS-dFDL and TAS-shFDL, only rather small nodes can be built due to higher splitting losses and losses of the delay line. Comparing respective architectures, it can be seen that increasing the channel bit rate from 10 to 40 Gbit/s yields nearly the same maximum throughput, but smaller achievable number of wavelengths. The utilization of WDM channels decreases which results in lower effective throughput at 40 Gbit/s channel bit rate. Hence, due to cost, migration to 40 Gbit/s is only advantageous if the number of wavelength channels on the fibre has to be strictly minimized, i.e. cost for lighting and operating them is high compared to the node cost. For both channel bit rates, maximum throughput is highest for TAS and lowest for TAS-dFDL while the TAS-shFDL architectures lie in between.

Regarding the effective throughput, both utilization and achievable node size have to be considered. For the TAS-shFDL architectures, increasing the number of FDLs reduces burst loss probability but also limits node size. Both effects are balanced that increasing the number of FDLs hardly changes the utilization and the effective throughput actually decreases. In comparison with TAS, only TAS-shFDL with a single FDL can achieve higher effective throughput for 10 Gbit/s bit rate. For 40 Gbit/s, the utilization of TAS is only 40% and therefore TAS-shFDL architectures with up to 3 FDLs achieve a higher effective throughput. The TAS-dFDL architecture always has the lowest effective throughput. As has been mentioned above when introducing the TAS node architectures, a TAS-dFDL node and a TAS-shFDL node with 2 FDLs have approximately the same number of SOAs. However, when looking at maximum and effective throughput, the TAS node with shared FDL buffer performs significantly better.

7.3 Comparison of Different Node Architectures

In Fig. 7.12 the maximum and effective throughput for the four different nodes with 4 input/output fibres with 10 and 40 Gbit/s line-rates are compared by using the standard parameters as shown in Tab. 6.1. For TAS-LTR the tuning ranges of the wavelength converters are set to 64 wavelengths for 10 Gbit/s and 16 for 40 Gbit/s to achieve the the highest maximum and effective throughput of this node architecture. For TAS nodes with shared FDL buffer only one FDL feedback loop is used to achieve the highest maximum and effective throughput of this node architecture.

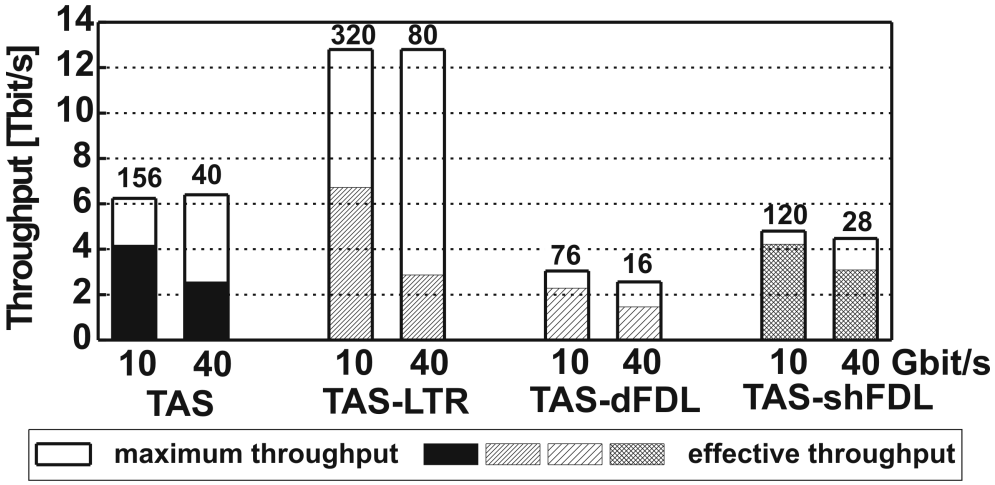

Figure 7.12: The maximum and effective throughput for different node architectures with 4 input/output fibres at 10 and 40 Gbit/s.

The maximum size and throughput of these nodes are calculated for a Q-factor of 10. For all four node architectures, the maximum throughput of each node architecture is almost identical for a bit rate of 10 and 40 Gbit/s. But for a bit rate of 2.5 Gbit/s the maximum throughput is smaller due to crosstalk of large number of WDM channels. Among the studied node architectures, the highest maximum throughput (12.8 Tbit/s) can be achieved with TAS-LTR because only x SOAs instead of M SOAs contribute to the noise in one channel. With basic TAS nodes a maximum throughput ~ 6 Tbit/s can be achieved. With TAS-dFDL and TAS-shFDL, only rather small nodes ($\sim 3-4$ Tbit/s) can be built due to higher splitting losses and losses of the delay line.

The effective throughput is defined as the throughput at burst loss rate B $\leq 10^{-6}$ for dynamic traffic. Just-enough-time (JET) reservation strategy is used for wavelength channels on the output fiber and in the FDL buffer. For a buffered burst the output wavelength channel is reserved by using pre-reservation method. For all studied architectures, 40 Gbit/s is less efficient due to a smaller achievable number of wavelengths. The highest effective throughput can be achieved for a bit rate of 10 Gbit/s. As expected the TAS-LTR node architecture has the lowest efficiency in comparison with other architectures. But with this architecture the largest effective throughput of about 7 Tbit/s can be achieved for 10 Gbit/s. For 40 Gbit/s the largest effective throughput (~ 4 Tbit/s) can be achieved with TAS-shFDL node architecture with one FDL feedback loop. The best efficiency can be achieved by TAS nodes with FDL buffers among the architectures studied. The highest utilization has the TAS-shFDL at 10 Gbit/s with above 85 %. With TAS-dFDL node only a small number of wavelengths is allowed due to the high splitting losses of such node architectures. Consequently the maximum achievable effective throughput is rather small: about 2 Tbit/s at 10 Gbit/s and about 1 Tbit/s at 40 Gbit/s.

Architectures with FDL buffers have an improved utilization and better efficiency but can only be built smaller by considering technological constraints. Regarding maximum and effective throughput they do not scale significantly better than the TAS architecture without FDLs - the node with dedicated buffer even has a lower throughput. Remarkably, increasing the number of FDLs in the shared buffer hardly changes the utilization due to the reduced node size, thus leading to decreased maximum and effective throughput. It can be concluded that studying architectural options only from the technological or only from the traffic performance point of view does not provide balanced results. Consequently, there is a need for integrated analysis.

Chapter 8

Conclusions

This work represents a contribution to the investigation of Optical Burst Switching (OBS) networks. Recently, there have been major efforts to adapt the OBS concept to WDM-based optical networks. In this context, the required complexity and technical feasibility of an OBS network are investigated in this work. Different physical and technological constraints in an OBS network are analysed by considering available and expected technologies in the short and long term.

First, the impact of OBS on optical transmission is analysed, and the required key components and subsystems to upgrade the existing WDM transmission links are identified. The experimental and numerical investigations of the dynamic behaviour of EDFAs shows that the highly changing traffic in the channels and the cross-gain saturation effects of the EDFA cause significant power excursions of the output bursts. There is a large amount of crosstalk between the channels on the burst level, and optical signal-to-noise ratios, as well as bit error rates, may deteriorate considerably. The amplitude of the EDFA's output power excursion depends on the channel load, the amount of switched to non-switched power and the length of bursts and gaps. The amplitude and speed of power excursions increase with the number of cascaded EDFAs. To ensure proper network operation, fast gain stabilisation of EDFAs in the microsecond range is required. At present, the best gain control method of an EDFAs cascade is a fast electronic gain control for each amplifier.

Without feasible implementations of OBS core nodes, OBS networks will never become a reality. Thus, the main focus of this work is the physical implementation of OBS core nodes. Different OBS core node architectures are designed and evaluated in terms of feasibility and performance. To build large OBS core nodes, fast optical space switches with a switching time of less than 1 μs are essential. The choice of today's commercially available optical space switches is extremely limited. SOAs seem to be the only promising ones to be used as on/off gates in the OBS core nodes, where the gain is switched on and off electronically. However, the

gain of conventional SOA decreases for high signal input power, which is required due to the power budget in the OBS core nodes. This gain saturation and the fast gain dynamics of the conventional SOAs lead to signal distortion and ISI for optical data. The performance of the nodes based on such switches decreases, and only very small node size can be achieved. To overcome this size limitation, gain-clamped SOAs (GC-SOAs) can be used. Therefore, two GC-SOAs available today commercially are investigated experimentally. A simple model for such SOAs is also developed and validated experimentally.

From today's technology point of view, fast and large OBS core nodes can be built with the so-called Tune-and-Selected (TAS) node architecture. To evaluate the maximum size of such OBS core nodes, characteristic optical signal paths within such nodes are investigated by considering different signal degradation mechanisms such as noise, crosstalk, SOA gain saturation and dynamics, SOA chirp and so on. Here, conventional SOAs are not suitable to be used as switching gates due to their large nonlinear distortion caused by gain saturation and dynamics. By using GC-SOAs as on/off gates in TAS nodes, the maximum size and throughput of the TAS nodes will be limited mainly by noise and crosstalk, and large switching nodes with up to 10.24 Tbit/s maximum throughput can be built, if optimized components like GC-SOAs with small noise figures are used. Furthermore, regenerative (3R) wavelength converters should be used to avoid the accumulation of signal degradation.

In the final part of the work, an integrated evaluation of OBS core nodes is presented by considering the physical and the traffic performance. In addition to physical limitations, burst losses in the case of contention are another limiting factor for the throughput of the OBS core nodes. To estimate the effective throughput of an OBS core node, both signal degradation and burst losses must be considered. To show the benefit of such an integrated evaluation, the analysis is extended to different variations of TAS nodes, which aim at increasing maximum throughput (TAS with wavelength converters of limited tuning range, TAS-LTR) or improvement of effective throughput (TAS with fibre delay line (FDL) either per output, TAS-dFDL or per node, TAS-shFDL). The major conclusion of this investigation is that studying OBS node architectures only from the technological or only from the traffic performance point of view does not provide balanced results. E.g. architectures with FDL buffers have an improved utilization and better efficiency, but can only be built smaller by considering technological constraints. Regarding maximum and effective throughput, they even have a lower throughput than the TAS architecture without FDLs. Remarkably, increasing the number of FDLs in the shared buffer per node hardly changes the utilization due to the reduced node size, thus leading to decreased maximum and effective throughput. Consequently, to provide a better and more balanced view on the design of OBS nodes, an integrated analysis is essential.

Summarising the main results from this work, OBS will only be a feasible solution for the optical network if the following essential optical technologies and building blocks are available:

- WDM technology, wavelength converters, and tunable lasers are essential for an OBS network. Large numbers of wavelengths (> 100) should be able to be transmitted on a optical fibre. The wavelength converter should have regeneration capability to avoid the accumulation of signal degradation. The tuning speed of the tunable laser must be in the μs range.
- Burst-capable receiver with large dynamic range, fast adjustment of receiver decision threshold, and fast clock recovery.
- Gain-stabilised EDFAs. The response time of the control method must be in the μs range.
- Large and fast optical switch fabrics for building the OBS core nodes.

Regarding the design of the OBS core nodes, the following general design guidelines are derived:

- If SOAs are used as basis switching elements in the nodes, gain-clamped SOAs have to be used.
- The maximum size of the nodes is mainly determined by amplifier noise and crosstalk between the WDM channels. While the crosstalk limitation only plays a role for a very large number of wavelengths per fibre, the noise dominates in all cases. Therefore, the amplifiers used in the nodes must have a low noise figure.
- For such noise-limited nodes, the achievable maximum number of wavelengths per fibre is in proportion to the optical signal-to-noise ratio (OSNR) of the node. E.g. it decrease about four times, if the OSNR value of the node is decreased about 6 dB.
- To provide a better and more balanced view on the design of OBS core nodes, an integrated analysis considering the physical and the traffic performance is essential, which enable a better understanding of performance limitations in such optical networks.

Future work should extend the integrated analysis to OBS node architectures applying other technologies, e.g. arrayed waveguide gratings (AWG). Furthermore, different modulation formats could be investigated regarding OBS network design. The characteristics of the signal which passes the OBS core nodes will depend on the modulation format, if e.g. SOAs are used as switching gates. In this context a comparison of NRZ and RZ modulation formats can be found in [260]. As the pattern dependence originated by different recovery times of zeros and ones can be neglected with DPSK/RZ-DPSK modulation [267–269], an OBS network with such advanced modulation format could provide better performance than using a conventional modulation format such as NRZ or RZ.

Appendix A

Parameters for Numerical Anaysis of EDFA Gain Dynamics

To analyse the gain dynamics of EDFAs by numerical simulations, the "Dynamic Amplifier EDFA Model" module (*AmpEDFA_Dynamic*) in the simulation tool "VPITransmissionMaker" [80] is used. In this appendix the used parameters for this module, its simulation names in "VPITransmissionMaker", and its values for the simulations in Section 3.2 on page 33 are listed.

Parameters	**Simulation name**	**Values**
Length of the active fibre L	FiberLength	15 m
Core radius of the active fibre r_c	CoreRadius	1.4 μm
Numerical aperture of the active fibre n_a	NumerAperture	0.28
Dopant density N_{dop}	DopantDensity	$5 \cdot 10^{24}\ 1/m^3$
Lifetime of Erbium ions in the excited state τ	FluorescenceTime	10 ms
Relative number of excited Erbium ions at initialisation instance ρ_0	InitialInversion	0.78
Forward pump power at the beginning of fibre P_f	FwdPumpPower	10 mW
Backward pump power at the end of fibre P_b	BkdPumpPower	0 mW
Forward pump wavelength λ_{pf}	FwdPumpWavelgth	980 nm
Backward pump wavelength λ_{pb}	BkwdPumpWavelgth	1480 nm

Table A.1: Using model parameters for the EDFA modelling

Appendix B

Parameters for SOA/GC-SOA Modelling

For the modelling of the conventional SOAs and the gain-clamped SOAs, the models developed in Section 5.4 on page 96 are used. To investigate the impact of SOA gain saturation and amplifier dynamic (ISI) both models are included in the simulation tool "VPITransmissionMaker" by using a Co-simulation interface [80]. In this appendix the used parameters for both models, its simulation names in "VPITransmissionMaker", and its values for the simulations in Section 5.4 on page 106 and in Section 6.3 on page 132 are listed.

The parameter values in Tab. B.1 are used for the conventional SOA and the parameter values in Tab. B.2 are used for the GC-SOA, which is adapted to the DBR-SOA. The most using values for the amplifier parameters are taken from literature [214, 215] and validated experimentally as done in Section 5.4.

Parameters	**Simulation name**	**Values**
Injection current I	InjectionCurrent	200 mA
Length of active zone L	Length	600 μm
Width of active zone w	Width	1 μm
Height of active zone d	Height	0.2 μm
Optical confinement factor Γ	OptConfinement	0.4
Internal losses α_s	InternalLosses	26680/m
Henry factor α_H	IndexToGainCoupl	5
Recombination coefficient A	RecombConstA	$1.2 \cdot 10^8 \cdot 1/s$
Recombination coefficient B	RecombConstB	$7 \cdot 10^{-16} \cdot m^3/s$
Recombination coefficient C	RecombConstC	$5 \cdot 10^{-41} \cdot m^6/s$
Gain factor σ	Sigma	2.8
Gain compression factor κ_{nl}	Kappa	2
Cross saturation factor η	Alpha	0

Table B.1: Using model parameters for the conventional SOA

Parameters	**Simulation name**	**Values**
Injection current I	InjectionCurrent	250 mA
Length of active zone L	Length	600 μm
Width of active zone w	Width	1 μm
Height of active zone d	Height	0.2 μm
Optical confinement factor Γ	OptConfinement	0.4
Internal losses α_s	InternalLosses	4000/m
Henry factor α_H	IndexToGainCoupl	5
Recombination coefficient A	RecombConstA	$1.2 \cdot 10^8 \cdot 1/s$
Recombination coefficient B	RecombConstB	$7 \cdot 10^{-16} \cdot m^3/s$
Recombination coefficient C	RecombConstC	$5 \cdot 10^{-41} \cdot m^6/s$
Bragg section length L_{gr}	LengthBraggSection	200 μm
Laser wavelength λ_L	LasingWavelength	1508nm
Bragg wavelength λ_B	BraggWavelength	1508nm
couple coefficient κ	CouplingCoeffBragg	1000/m
Losses in Bragg section α_g	LossBraggSection	6500/m
Gain factor σ	Sigma	2.8
Gain compression factor κ_{nl}	Kappa	2
Cross saturation factor η	Alpha	0

Table B.2: Using model parameters for the DBR-SOA

Bibliography

[1] K. Fukuchi et al., "10.92-Tbit/s triple-band/ultra-dense optical-repeated transmission experiment," in *Proceedings of Optical Fiber Communication Conference (OFC)*, Anaheim, California, USA, March 2001, number PD24.

[2] F.M. Chiussi and A. Francini, "Scalable electronic packet switches," *IEEE Journal on Selected Areas in Communications*, vol. 21, no. 4, pp. 486–500, May 2003.

[3] M.E. Crovella and A. Bestavros, "Self-similarity in World Wide Web traffic: evidence and possible causes," *IEEE/ACM Transactions on Networking*, vol. 5, no. 6, pp. 835–846, December 1997.

[4] R. Inkret, A. Kuchar, and B. Mikac, "Final report: Advanced infrastructure for photonic networks: Extended final report of cost action 266," *http://www2.cordis.lu/cost/src/266 indivpage.htm*, 2003.

[5] C. Qiao and M. Yoo, "Optical Burst Switching (OBS) - a new paradigm for an optical Internet," *Journal of High Speed Networks*, vol. 8, no. 1, pp. 69–84, January 1999.

[6] J.S. Turner, "Terabit Burst Switching," *Journal of High Speed Networks*, vol. 8, no. 1, pp. 3–16, January 1999.

[7] R. Ryf et al., "1296-port MEMS transparent optical crossconnect with 2.07 Petabit/s switch capacity," in *Proceedings of Optical Fiber Communication Conference (OFC)*, Anaheim, California, USA, 2001, number PD28.

[8] M.W. Chbat et al., "Towards wide-scale all-optical transparent networking: The ACTS OPtical Pan-European (OPEN) project," *IEEE Journal on Selected Areas in Communications*, vol. 16, no. 7, pp. 1226–1244, September 1998.

[9] K.-D. Langer and J. Vathke, "KomNet-optical transport and networking technologies for the boradband Internet," in *Proceedings of the International Conference on Transparent Optical Networks (ICTON 2001)*, June 2001, pp. 183–190.

[10] D. Stoll et al., "Metropolitan DWDM: A dynamically configurable ring for the KomNet field trial in Berlin," *IEEE Communications Magazine*, vol. 39, no. 2, pp. 106–113, February 2001.

[11] C. Qiao and M. Yoo, "Choices, features and issues in Optical Burst Switching," *Optical Networks Magazine*, vol. 1, no. 2, pp. 37–44, April 2000.

[12] T.S. El-Bawab et al., "The evolution to optical switching-based core networks," *Optical Networks Magazine*, pp. 7–18, March/April 2003.

[13] C.H. Xin and C.Qiao, "A comparative study of OBS and OFS," in *Proceedings of Optical Fiber Communication Conference (OFC)*, Anaheim, California, USA, March 2001, number ThG7-1.

[14] I. De Miguel, M. Düser, and P. Bayvel, "Traffic load bounds for optical burst-switched networks with dynamic wavelength allocation," in *Proc. of the IFIP TC6 5th International Working Conference on Optical Network Design and Modelling (ONDM 2001)*, Vienna, February 2001.

[15] M. Düser and P. Bayvel, "Bandwidth utilization and wavelength re-use in WDM optical burst-switched packet networks," in *Proc. of the IFIP TC6 5th International Working Conference on Optical Network Design and Modelling (ONDM 2001)*, Vienna, February 2001.

[16] M. Düser and P. Bayvel, "Analysis of a dynamically wavelength-routed optical burst switched network architecture," *IEEE Journal of Lightwave Technology*, vol. 20, no. 4, pp. 574–585, April 2002.

[17] M. Renaud et al., "Network and system concepts for optical packet switching," *IEEE Communications Magazine*, vol. 35, no. 4, pp. 96–102, April 1997.

[18] S. Yao, B. Mukherjee, and S.Dixit, "Advances in photonic packet switching: An overview," *IEEE Communications Magazine*, vol. 38, no. 2, pp. 84–94, February 2000.

[19] D.K. Hunter and I. Andonovic, "Approaches to optical internet packet switching," *IEEE Communications Magazine*, vol. 38, no. 39, pp. 116–122, September 2000.

[20] T.S. El-Bawab and J.D. Shin, "Optical packet switching in core networks: Between vision and reality," *IEEE Communication Magazine*, vol. 40, no. 9, pp. 60–65, September 2002.

[21] F. Masetti et al., "High speed, high capacity ATM optical switches for future telecommunications transport network," *IEEE Journal on Selected Areas in Communications*, vol. 14, no. 5, pp. 979–998, June 1996.

[22] C. Guillemot et al., "Transparent optical packet switching: The European ACTS KEOPS project approach," *IEEE Journal of Lightwave Technology*, vol. 16, pp. 2117–2134, December 1998.

[23] L. Dittmann et al., "The European IST project DAVID: A viable approach toward optical packet switching," *IEEE Journal on Selected Areas in Communications*, vol. 21, no. 7, pp. 1026–1040, September 2003.

[24] K.G. Vlachos et al., "STOLAS: Switching technologies for optically labeled signals," *IEEE Optical Communications*, pp. 9–15, November 2003.

[25] K. Claffy, G. Miller, and K. Thompson, "The nature of the beast: Recent traffic measurements from an internet backbone," in *Proceedings of the annual meeting of the Internet Society 1998 (INET'98)*, Caida, 1998, http://www.caida.org/outreach/papers/1998/Inet98/index.xml.

[26] D. K. Hunter, W. D. Cornwell, T. H. Gilfedder, A. Franzen, and I. Andonovic, "SLOB: A switch with large optical buffers for packet switching," *IEEE Journal of Lightwave Technology*, vol. 15, no. 10, pp. 1725–1736, October 1998.

[27] A. Carena et al., "OPERA: An optical packet experimental routing architecture with label swapping capability," *IEEE Journal of Lightwave Technology*, vol. 16, no. 12, pp. 2135–2145, December 1998.

[28] F. Callegati, "Optical buffers for variable length packets," *IEEE Communications Letters*, vol. 4, no. 9, pp. 292–294, September 2000.

[29] L. Tančevski et al., "Optical routing of asynchronous, variable length packets," *IEEE Journal on Selected Areas in Communications*, vol. 18, no. 10, pp. 2084–2093, October 2000.

[30] I. Chlamtac et al., "CORD: Contention resolution by delay lines," *IEEE Journal on Selected Areas in Communications*, vol. 14, no. 5, pp. 1014–1029, June 1996.

[31] F. Callegati et al., "Architecture and performance of a broadcast and select photonic switch," vol. 4, no. 3, pp. 266–284, July 1998.

[32] P.B. Hansen, S.L. Danielsen, and K.E. Stubkjaer, "Optical packet switching without packet alignment," in *Proceedings of European Conference on Optical Communication (ECOC)*, Madrid, Spain, September 1998, number WdD13, pp. 591–592.

[33] S. Bjornstad, D. R. Hjelme, and N. Stoli, "A scalable optical packet switch for variable length packets employing shared electronic buffering," in *Proceedings*

of European Conference on Optical Communication (ECOC), Copenhagen, September 2002.

[34] F. Callegati and W. Cerroni, "Time-wavelength exploitation in optical feedback buffer with trains of packets," in *Proceedings of SPIE OptiComm 2002*, Boston, USA, July 2002, http://www.caida.org/outreach/papers/1998/Inet98/index.xml, pp. 274–285.

[35] D.K. Hunter, M.C. Chia, and I. Andonovic, "Buffering in optical packet switches," *IEEE Journal of Lightwave Technology*, vol. 16, no. 12, pp. 2081–2094, December 1998.

[36] S.R. Amstutz, "Burst switching - an introduction," *IEEE Communications Magazine*, vol. 21, pp. 36–42, 1983.

[37] S.R. Amstutz, "Burst switching - an update," *IEEE Communications Magazine*, vol. 27, no. 6, pp. 50–57, 1989.

[38] Y. Xiong, M. Vanderhouth, and C.C. Cankaya, "Control architecture in optical burst switched WDM networks," *IEEE Journal on Selected Areas in Communications*, vol. 18, no. 10, pp. 1838–18510, October 2000.

[39] K. Dolzer, C.M. Gauger, J. Späth, and S. Bodamer, "Evaluation of reservation mechanisms for optical burst switching," *AEÜ International Journal of Electronics and Communications*, vol. 55, no. 1, pp. 18–26, January 2001.

[40] A. Ge, F. Callegati, and L.S. Tamil, "On optical burst switching and self-similar traffic," *IEEE Communications Letters*, vol. 4, no. 3, pp. 98–100, March 2000.

[41] G. Hu, K. Dolzer, and C.M. Gauger, "Does burst assembly really reduce the self-similarity," in *Proceedings of Optical Fiber Communication Conference (OFC)*, 2003, vol. 1, pp. 124–126.

[42] K. Dolzer and C.M. Gauger, "On burst assembly in optical burst switching networks - a performance evaluation of Just-Enough-Time," in *Proceedings of the 17th International Teletraffic Congress (ITC 17)*, Salvador da Bahia, Brazil, September 2001, pp. 149–160.

[43] K. Dolzer, "Assured Horizon - a new combined framework for burst assembly and reservation in optical burst switched networks," in *Proceedings of the European Conference on Networks and Optical Communications (NOC 2002)*, Darmstadt, Germany, June 2002.

[44] G. Eilenberger, "Optische Paketnetze - Alles optisch, oder?," in *Beiträge zur 2. ITG Fachtagung Photonische Netze*, Dresden, Germany, March 2001, pp. 109–114.

[45] I. Baldine, G. Rouskas, H. Perros, and D. Stevenson, "JumpStart: A Just-In-Time signalling architecture for WDM burst switched networks," *IEEE Communications Magazine*, vol. 40, no. 2, pp. 82–89, February 2002.

[46] F. Callegati, H.C. Cankaya, Y. Xiong, and M. Vandenhoute, "Design issues of optical IP routers for Internet backbone applications," *IEEE Communications Magazine*, vol. 37, no. 12, pp. 124–128, December 1999.

[47] Y. Xu, P.N. Lamy, E.L. Varma, and R. Nagarajan, "Generalized MPLS-based distributed control architecture for automatically switched transport networks," *Bell Labs Technical Journal*, pp. 33–49, January 2001.

[48] S. Verma, H. Chaskar, and R. Ravikanth, "Optical burst switching: A viable solution for Terabit IP backbone," *IEEE Network*, vol. 14, no. 6, pp. 48–53, November 2000.

[49] K. Dolzer, "Assured Horizon - an efficient framework for service differentiation in optical burst switched networks," in *Proceedings of the SPIE Optical Networking and Communications Conference (OptiComm 2002)*, Boston, USA, July 2002.

[50] M. Yoo, C. Qiao, and S. Dixit, "Optical burst switching for service differentiation in the next-generation optical Internet," *IEEE Communications Magazine*, vol. 39, no. 2, pp. 98–104, February 2001.

[51] C.M. Gauger, "Viability and performance of optical burst switching," in *Proceedings of the 9th European Conference on Networks and Optical Communications (NOC)*, Eindhoven, NL, June/July 2004.

[52] X. Yu et al., "Traffic statistics and performance evaluation in optical burst switched networks," *IEEE Journal of Lightwave Technology*, vol. 22, no. 12, pp. 2722–2738, December 2004.

[53] X. Yu, Y. Chen, and C. Qiao, "Study of traffic statistics of assembled burst traffic in optical burst switched networks," in *Proc. of Opticomm*, 2002, pp. 149–159.

[54] S. Oh and M. Kang, "A burst assembly algorithm in optical burst switching networks," in *Proceedings of Optical Fiber Communication Conference (OFC)*, March 2002, number ThGG112, pp. 771–773.

[55] A. Zalesky et al., "Performance analysis of an OBS edge router," *IEEE Photonics Technology Letters*, vol. 16, no. 2, pp. 695–697, February 2004.

[56] R. Rajaduray, D.J. Blumenthal, and S. Ovadia, "Impact on burst assembly parameters on edge router latency in an optical burst switching network," in *Proceedings of IEEE LEOS 2003*, October 2003, vol. 1, pp. 56–57.

[57] K. Dolzer, W. Payer, and M. Eberspächer, "A simulation study on traffic aggregation in multi-service networks," in *Proc. of the IEEE Conference on High Performance Switching and Routing (ATM 2000)*, Heidelberg, June 2000, pp. 157–165.

[58] K. Dolzer and W. Payer, "On aggregation strategies for multimedia traffic," in *Proc. of the 1st Polish-German Teletraffic Symposium (PCTS 2000)*, Dresden, September 2000.

[59] C.M. Gauger, "Trends in optical burst switching," in *Proceedings of the SPIE ITCom Conference*, Orlando, FL, September 2003.

[60] K. Dolzer, *Mechanisms for Quality of Service Differentiation in Optical Burst Switched Networks*, Ph.D. thesis, Institut für Kommunikationsnetze und Rechnersysteme, Universität Stuttgart, 2004.

[61] S. Junghans and C.M. Gauger, "Architectures for resource reservation modules for optical burst switching," in *Beiträge zur 4. ITG Fachtagung Photonische Netze*, Leipzig, Germany, Mai 2003, pp. 109–117.

[62] C. Qiao, "Labeled Optical Burst Switching for IP-over-WDM integration," *IEEE Communications Magazine*, vol. 38, no. 9, pp. 104–114, September 2000.

[63] C. Gauger, "Performance of converter pools for contention resolution in optical burst switching," in *Proceedings of the SPIE Optical Networking and Communications Conference (OptiComm 2002)*, Boston, July 2002.

[64] C. Gauger, "Dimensioning of FDL buffers for optical burst switching nodes," in *Proceedings of the 6th IFIP Working Conference on Optical Network Design and Modeling (ONDM 2002)*, Torino, February 2002.

[65] Y. Chen, H. Wu, D. Xu, and C. Qiao, "Performance analysis of optical burst switched node with deflection routing," in *Proc. IEEE International Conference on Communication (ICC)*, Anchorage, May 2003.

[66] H.Q. Ngo, D. Pan, and C. Qiao, "Nonblocking WDM switches based on arrayed waveguide grating and limited wavelength conversion," in *IEEE Infocom 2004*, Hongkong, March 2004, vol. 4, www.ieee-infocom.org/2004/technicalprogram.htm.

[67] *ADC, http://www.adc.com.*

[68] *http://www.agilty.com.*

[69] *Intune, http://www.intune-technologies.com.*

[70] J. E. Simsarian et al., "Fast switching characteristics of a widely tunable laser transmitter," *IEEE Photonics Technology Letters*, vol. 15, pp. 1038–1040, August 2003.

[71] A. Bhardwaj, J. Gripp, J.E. Simsarian, and M. Zirngibl, "Long-term wavelength switching measurements with random schedules on fast tunable lasers," in *Proceedings of European Conference on Optical Communication (ECOC)*, 2002, number 11.5.3.

[72] C.C. Renaud, M. Düser, B. Puttnam, T. Lovell, P. Bayvel, and A.J. Seeds, "Nanosecond switching time, uncooled, zero frequency error DWDM source," in *Proceedings of Optical Fiber Communication Conference (OFC)*, Los Angeles, 2004, number WL3.

[73] F. Kano and Y. Yoshikuni, "Frequency control and stabilization of broadly tunable SSG-DBR lasers," in *Proceedings of Optical Fiber Communication Conference (OFC)*, 2002, number ThV3.

[74] G. Alibert et al., "Subnanosecond tunable laser using single electroabsorption tuning super structure grating," *IEEE Photonics Technology Letters*, vol. 9, pp. 895–897, July 1997.

[75] A. Bergonzo et al., "Widely vernier tunable external cavity laser including a sampled fiber bragg grating with digital wavelength selection," *IEEE Photonics Technology Letters*, vol. 15, pp. 1144–1146, August 2003.

[76] M. Kauer et al., "16-channel digitally tunable external-cavity laser with nanosecond switching time," *IEEE Photonics Technology Letters*, vol. 15, no. 3, pp. 371–373, March 2003.

[77] K. Shrikhande et al., "Performance demonstration of a fast-tunable transmitter and burst-mode packet receiver for HORNET," in *Proceedings of Optical Fiber Communication Conference (OFC)*, 2001, number ThG2.

[78] H. Nishizawa et al., "Design of a 10-gb/s burst-mode optical packet receiver module and its demonstration in a WDM optical switching network," *IEEE Journal of Lightwave Technology*, vol. 20, no. 7, pp. 1078–1083, July 2002.

[79] M. Duelk et al., "Fast packet routing in a 2.5 Tb/s optical switch fabric with 40 Gb/s duobinary signals at 0.8 b/s/Hz spectral efficiency," in *Proceedings of Optical Fiber Communication Conference (OFC)*, Atlanta, Georgia, USA, March 2003, number PD8-1.

[80] *VPTsystems, Photonic Modules Reference Manual, 2005.*

[81] Y. Sun, G. Luo, J.L. Zyskind, A.A.M. Saleh, A.K. Srivastava, and J.W. Sulhoff, "A model for gain dynamics in erbium-doped fibre amplifiers," *Electronics Letters*, vol. 32, no. 16, pp. 1490–1491, August 1996.

[82] A. Bononi and L.A. Rusch, "Doped-fiber amplifier dynamics: A system perspective," *IEEE Journal of Lightwave Technology*, vol. 16, no. 5, pp. 945–956, May 1998.

[83] Y. Sun, J.L. Zyskind, and A.K. Srivastava, "Average inversion level, modeling, and physics of erbium doped fiber amplifiers," *IEEE Journal of Selected Topics in Quantum Electronics*, vol. 3, no. 4, pp. 991–1012, August 1997.

[84] S.R. Chinn, "Simplified modeling of transients in gain-clamped erbium-doped fiber amplifiers," *IEEE Journal of Lightwave Technology*, vol. 16, no. 6, pp. 1095–1100, June 1998.

[85] Y. Sun and A.K. Srivastava, "Dynamic effects in optically amplified networks," in *Proceedings of Optical Amplifiers and Their Applications*, Victoria, Canada, July 1997, number MC4, pp. 44–47.

[86] J.L. Zyskind, Y. Sun, A.K. Srivastava, J.W. Sulhoff, A.J. Lucero, C. Wolf, and R.W. Tkach, "Fast power transients in optically amplified multiwavelength optical networks," in *Proceedings of Optical Fiber Communication Conference (OFC)*, February 1996, number PDP31.

[87] Y. Sun, A.K. Srivastava, J.L. Zyskind, J.W. Sulhoff, C. wolf, and R.W. Tkach, "Fast power transients in WDM optical networks with cascaded EDFAs," *Electronics Letters*, vol. 33, no. 4, pp. 313–314, February 1997.

[88] Q. Yu and C.C. Fan, "Simple dynamic model of all-optical gain-clamped erbium-doped fiber amplifiers," *IEEE Journal of Lightwave Technology*, vol. 17, no. 7, pp. 1166–1171, July 1999.

[89] H. Feng, E. Patzak, and J. Saniter, "Methods for stabilizing the gain of EDFAs in burst switching optical networks," *Photonic Network Communications*, vol. 4, no. 2, pp. 151 – 166, May 2002.

[90] C.R. Giles, E. Desurvire, and J.R. Simpson, "Transient gain and cross talk in erbium-doped fiber amplifiers," *Optical Letters, Optical Society of America*, vol. 14, no. 16, pp. 880–882, August 1989.

[91] S.Y. Park, H.K. Kim, G.Y. Lyu, S.M. Kang, and S.-Y. Shin, "Dynamic gain and output power control in a gain-flattened erbium-doped fiber amplifier," *IEEE Photonics Technology Letters*, vol. 10, no. 6, pp. 787–789, June 1998.

[92] N.E. Jolley, F. Davis, and J. Mun, "Out-of-band electronic gain clamping for a variable gain and output power EDFA with low dynamic gain tilt," in *Proceedings of Optical Fiber Communication Conference (OFC)*, Dallas, USA, February 1997, number WF7, pp. 134–135.

[93] J. Drake, A. Tipper, A. Ford, B. Flintham, and K.P. Jones, "A comparison of practical gain and transient control techniques for erbium doped fiber amplifiers," in *Optical Amplifiers and Their Applications*, 1998, pp. 163–165.

[94] K.P. Jones, B. Flintham, J. Drake, and H. Lebreton, "Gain control and transient suppression in long wavelength band EDFA modules," in *Proceedings of European Conference on Optical Communication (ECOC)*, Nice, France, September 1999, pp. 152–153.

[95] N. Suzuki, K. Shimizu, T. Kogure, J. Nakagawa, and K. Motoshima, "Optical fiber amplifiers employing novel high-speed AGC and tone-signal ALC functions for WDM transmission systems," in *Proceedings of European Conference on Optical Communication (ECOC)*, Munich, Germany, September 2000, pp. 179–180.

[96] J. Chung, S.Y. Kim, and C.J. Chae, "All-optical gain-clamped EDFAs with different feedback wavelengths for use in multiwavelength optical networks," *Electronics Letters*, vol. 32, no. 23, pp. 2159–2161, November 1996.

[97] G. Luo, J.L. Zyskind, Y.Sun, A.K. Srivastava, J.W. Sulhoff, and M.A. Ali, "Relaxation oscillations and spectral hole burning in laser automatic gain control of EDFAs," in *Proceedings of Optical Fiber Communication Conference (OFC)*, Dallas, USA, February 1997, number WF4, pp. 130–131.

[98] G. Luo, J.L. Zyskind, Y.Sun, A.K. Srivastava, J.W. Sulhoff, C. Wolf, and M.A. Ali, "Performance degradation of all-optical gain-clamped EDFA's due to relaxation-oscillations and spectral-hole burning in amplified WDM networks," *IEEE Photonics Technology Letters*, vol. 9, no. 10, pp. 1346–1348, October 1997.

[99] H.X. Dai, J.Y. Pan, and Ch. Lin, "An optical gain control of in-line EDFA for hybrid AM/digital WDM systems," in *Proceedings of Optical Fiber Communication Conference (OFC)*, February 1997, pp. 133–134, Dallas, USA.

[100] H.X. Dai, J.Y. Pan, and Ch. Lin, "All-optical gain control of in-line erbium-doped fiber amplifiers for hybrid analog/digital WDM systems," *IEEE Photonics Technology Letters*, vol. 9, pp. 737–739, 1997.

[101] G. Luo, J.L. Zyskind, J.A. Nagel, and M.A. Ali, "Experimental and theoretical analysis of relaxation-oscillations and spectral hole burning effects in all-optical gain-clamped EDFA's for WDM networks," *IEEE Journal of Lightwave Technology*, vol. 16, no. 4, pp. 527–533, April 1998.

[102] E. Delevaque, T. Georges, J.F. Bayon, M. Monerie, P. Niay, and P. Bernage, "Gain control in erbium-doped fibre amplifiers by lasing at 1480 nm with photoinduced bragg gratings written on fibre ends," *Electronics Letters*, vol. 29, no. 12, pp. 1112–1114, June 1993.

[103] J.F. Massicott, S.D. Willson, R. Wyatt, J.R. Armitage, R. Kashyap, D. Williams, and R.A. Lobbett, "1480nm pumped erbium doped fibre amplifier with all optical automatic gain control," *Electronics Letters*, vol. 30, no. 12, pp. 962–964, June 1994.

[104] A. Yu and M.J. O'Mahony, "Properties of gain controlled erbium doped fiber amplifiers by lasing," *Electronics Letters*, vol. 31, no. 16, pp. 1348–1349, 1995.

[105] B. Landousies, T. Georges, E. Delevaque, R. Lebref, and M. Monerie, "Low power transient in multichannel equalised and stabilised gain amplifier using passive gain control," *Electronics Letters*, vol. 32, no. 20, pp. 1912–1913, September 1996.

[106] Y.X. Zhao, J. Bryce, and R. Minasian, "Gain clamped erbium-doped fiber amplifiers - modeling and experiment," *IEEE Journal of Selected Topics in Quantum Electronics*, vol. 3, no. 4, pp. 1008–1012, August 1997.

[107] A. Yu and M.J. O'Mahony, "Design and modeling of laser-controlled erbium-doped fiber amplifiers," *IEEE Journal of Selected Topics in Quantum Electronics*, vol. 3, no. 4, pp. 1013–1018, August 1997.

[108] S.Y. Ko, M.W. Kim, D.H. Kim, S.H. Kim, J.C. Jo, and J.H. Park, "Gain control in erbium-doped fibre amplifiers by tuning centre wavelength of a fibre Bragg grating constituting resonant cavity," *Electronics Letters*, vol. 34, no. 10, pp. 990–991, May 1998.

[109] C.H. Kim, H. Yoon, S.B. Lee, C.-H. Lee, and Y.C. Chung, "All-optical gain controlled bidirectional add-drop amplifier using fiber bragg gratings," *IEEE Photonics Technology Letters*, vol. 12, no. 7, pp. 894–896, July 2000.

[110] M. Zirngibl, "Gain control in erbium-doped fiber amplifiers by an all-optical feedback loop," *Electronics Letters*, vol. 27, no. 7, pp. 560–561, March 1991.

[111] E. Desurvire, M. Zirngibl, H.M. Presby, and D. DiGiovanni, "Dynamic gain compensation in saturated erbium-doped fiber amplifiers," *IEEE Photonics Technology Letters*, vol. 3, no. 5, pp. 453–455, May 1991.

[112] D.H. Richards, J.L. Jackel, and M.A. Ali, "A theoretical investigation of dynamic all-optical automatic gain control in multichannel EDFAs and EDFA cascades," *IEEE Journal of Selected Topics in Quantum Electronics*, vol. 3, no. 4, pp. 1027–1036, August 1997.

[113] D.H. Richards, J.L. Jackel, and M.A. Ali, "Multichannel EDFA chain control: A comparison of two all-optical approaches," *IEEE Photonics Technology Letters*, vol. 10, no. 1, pp. 156–158, January 1998.

[114] L. Poti, A. Bononi, and N. Oriente, "Impulse response measurement of balanced chains of EDFAs in a recirculating loop," in *Proceedings of European Conference on Optical Communication (ECOC)*, Nice, France, September 1999, pp. 150–151.

[115] J.L. Zyskind, A.K. Srivastava, Y. Sun, J.C. Elison, G.W. Newsome, R.W. Tkach, A.R. Chraplyvy, J.W. Sulhoff, T.A. Strasser, J.R. Pedrazzani, and C. Wolf, "Fast link control protection for surviving channels in multiwavelength optical networks," in *Proceedings of European Conference on Optical Communication (ECOC)*, Oslo, Norway, September 1996, number ThC.3.6, pp. 49–52.

[116] J.L. Jackel and D.H. Richards, "All-optical stabilization of multiwavelength EDFA chains: A network level approach," in *Proceedings of LEOS'96*, Boston, MA, 1996, number PDP2.2.

[117] J.L. Jackel and D. Richards, "All-optical stabilization of cascaded multichannel erbium doped fiber amplifiers with changing numbers of channels," in *Proceedings of Optical Fiber Communication Conference (OFC)*, Dallas, USA, February 1997, pp. 84–85.

[118] M. Karásek and J.C. van der Plaats, "Protection of surviving channels in a cascade of pump-loss controlled gain-locked EDFAs," *International Journal of Optoelectronics*, vol. 12, no. 3, pp. 105–112, June 1998.

[119] M. Karásek and F.W. Willems, "Suppression of dynamic cross saturation in cascades of over pumped erbium-doped fiber amplifiers," *IEEE Photonics Technology Letters*, vol. 10, no. 7, pp. 1036–1038, July 1998.

[120] M. Karásek and J.A. Vallés, "Analysis of channel addition/removal response in all-optical gain-controlled cascade of erbium-doped fiber amplifiers," *IEEE Journal of Lightwave Technology*, vol. 16, no. 10, pp. 1795–1803, October 1998.

[121] L. Tančevski, A. Bononi, and L.A. Rusch, "Output power and SNR swings in cascades of EDFAs for circuit and packet-switched optical networks," *IEEE Journal of Lightwave Technology*, vol. 17, no. 5, pp. 733–742, May 1999.

[122] A. Bononi, L. Tančevski, and L.A. Rusch, "Fast dynamics and power swings in doped-fiber amplifiers fed by highly variable multimedia traffic," in *Proceedings of Optical Fiber Communication Conference (OFC)*, February 1998, vol. 2, pp. 213–214, San Jose, USA.

[123] A. Bononi, L. Tančevski, and L.A.Rusch, "Large power swings in doped-fiber amplifiers with highly variable data," *IEEE Photonics Technology Letters*, vol. 11, no. 1, pp. 131–133, January 1999.

[124] M. Karásek, A. Bononi, L.A. Rusch, and M. Menif, "Gain stabilization in gain clamped EDFA cascades fed by WDM burst-mode packet traffic," *IEEE Journal of Lightwave Technology*, vol. 18, no. 3, pp. 308–313, March 2000.

[125] M. Karásek and M. Mennif, "Effect of EDFA cross-gain saturation on the transmission of packetized burst-mode data over WDM," in *Optical Network Design and Modelling*, February 2000, pp. 110–123.

[126] S.Y. Kim, J. Chung, and B. Lee, "Effects of relaxation oscillations on transmission performances in the all-optical link-controlled EDFA cascade," *Optical Amplifiers and Their Applications*, pp. 48–51, July 1997, Victoria, Canada.

[127] S.Y. Kim, J. Chung, and B. Lee, "Dynamic performance of the all-optical gain-controlled EDFA cascade in multiwavelength optical networks," *Electronics Letters*, vol. 33, no. 17, pp. 1475–1477, August 1997.

[128] F. Bruyère, A. Bisson, and L.Noirie, "Gain stabilization of EDFA cascade using clamped-gain SOA," in *Proceedings of Optical Fiber Communication Conference (OFC)*, San Jose, CA, USA, February 1998, pp. 166–167.

[129] A.K. Srivastava, Y. Sun, J.L. Zyskind, J.W. Sulfoff, C. Wolf, and R.W. Tkach, "Fast gain control in an erbium-doped fibre amplifier," *Optical Amplifiers and Their Applications*, vol. 5, no. PDP4, pp. 24–27, Monterrey, CA 1996.

[130] A.K. Srivastava, J.L. Zyskind, Y. Sun, J. Ellson, G. Newsome, R.W. Tkach, A.R. Chraplyvy, J.W. Sulfoff, T.A. Strasser, C. Wolf, and J.R. Pedrazzani, "Fast-link control protection of surviving channels in multiwavelength optical networks," *IEEE Photonics Technology Letters*, vol. 9, no. 12, pp. 1667–1669, December 1997.

[131] S.L. Danielsen, P.B. Hansen, and K.E. Stubkjear, "Wavelength conversion in optical packet switching," *IEEE Journal of Lightwave Technology*, vol. 16, no. 12, pp. 2095–2108, December 1998.

[132] V. Eramo and M. Listanti, "Packet loss in a bufferless optical WDM switch employing shared tunable wavelength converters," *IEEE Journal of Lightwave Technology*, vol. 18, no. 12, pp. 1818–1833, December 2000.

[133] D.K. Hunter et.al, "WASPNET: A wavelength switched packet network," *IEEE Communications Magazine*, vol. 37, no. 3, pp. 120–129, March 1999.

[134] G. Castanon, L. Tančevski, S. Yagnanarayanan, and L. Tamil, "Asymmetric WDM all-optical packet switched routers," in *Proceedings of Optical Fiber Communication Conference (OFC)*, Atlanta, Georgia, USA, March 2000, vol. 1, pp. 53–55.

[135] K. Dolzer and C. M. Gauger, "On burst assembly in optical burst switching networks - a performance evaluation of Just-Enough-Time," in *Proceedings of the 17th International Teletraffic Congress (ITC 17)*, Salvador, Brazil, December 2001, pp. 149–160.

[136] M. Yoo, C. Qiao, and S. Dixit, "QoS performance in IP over WDM networks," *IEEE Journal on Selected Areas in Communications*, vol. 18, no. 10, pp. 2062–2071, October 2000.

[137] S. Yao, B. Muhkerjee, S. J. B. Yoo, and S. Dixit, "All-optical packet-switched networks: a study of contention-resolution schemes in an irregular mesh network with variable-sized packets," in *Proceedings of SPIE OptiComm 2000*, Dallas, October 2000.

[138] H. L. Vu and M. Zukerman, "Blocking probability for priority classes in optical burst switching networks," *IEEE Communications Letters*, vol. 6, no. 5, pp. 214–216, May 2002.

[139] Z. Haas, "The staggering switch: An electronically controlled optical packet switch," *IEEE Journal of Lightwave Technology*, vol. 11, no. 5, pp. 925–936, May/June 1993.

[140] L. Tančevski, A. Ge, and G. Castanon, "Optical packet switch with partially shared buffers: Design principles," in *Proceedings of Optical Fiber Communication Conference (OFC)*, March 2001, vol. 2.

[141] F. Callegati and W. Cerroni, "Wavelength allocation algorithms in optical buffers," in *Proceedings of IEEE Int. Conf. Communications (ICC '01)*, June 2001, vol. 2, pp. 499–503.

[142] M. Neuts et al., "Performance analysis of optical composite burst switching," *IEEE Communications Letters*, vol. 6, no. 8, pp. 346–348, August 2002.

[143] Z. Rosberg et al., "Burst segmentation benefit in optical switching," *IEEE Communications Letters*, vol. 7, no. 3, pp. 127–129, March 2003.

[144] V.M. Vokkarane and J.P. Jue, "Prioritized routing and burst segmentation for QoS in optical burst switched networks," in *Proceedings of Optical Fiber Communication Conference (OFC)*, Anaheim, USA, March 2002, pp. 221–222.

[145] V.M. Vokkarane and J.P. Jue, "Prioritized burst segmentation and composite burst-assembly techniques for QoS support in optical burst-switched metworks," *IEEE Journal on Selected Areas in Communications*, vol. 21, no. 7, pp. 1198–1209, September 2003.

[146] V.M. Vokkarane and J.P. Jue, "Burst segmentation: an approach for reducing packet loss in optical burst switched networks," *Optical Networks Magazine*, pp. 81–89, November/December 2003.

[147] F. Forghierri, A. Bononi, and P. R. Prucnal, "Analysis and comparison of hot-potato and single-buffer deflection routing in very high bit rate optical mesh networks," *IEEE Transaction Communications*, vol. 43, no. 1, pp. 88–98, January 1995.

[148] G. Castanon, L. Tančevski, and L. Tamil, "Routing in all-optical packet switched irregular mesh networks," in *Proc. IEEE GLOBECOM '99*, December 1999, pp. 1017–1022.

[149] F. Brogonovo, L. Fratta, and J. Bannister, "Unslotted deflection routing in all-optical networks," in *Proc. IEEE GLOBECOM '93*, December 1993, vol. 1, pp. 119–125.

[150] J. Fehrer, J. Sauer, and L. Ramfelt, "Design and implementation of a prototype optical deflection network," in *Proc. ACM SIGCOMM*, 1994, vol. 24, pp. 191–200.

[151] C.-F. Hsu, T.-L. Li, and N.-F. Huang, "Performance analysis of deflection routing in optical burst-switched networks," in *Proc. IEEE Infocom*, New York, June 2002.

[152] X. Wang, H. Morikawa, and T. Aoyama, "Deflection routing protocol for burst switching WDM mesh networks," in *Proc. SPIE Terabit Optical Networking: Architectures, Control and Management Issues*, Boston, November 2000.

[153] C.M. Gauger, "Optimized combination of converter pools and FDL buffers for contention resolution in optical burst switching," in *Proceedings of the 7th IFIP Working Conference on Optical Network Design and Modelling (ONDM 2003)*, 2003.

[154] *JDS Uniphase, http://www.jdsu.com.*

[155] L.Y. Lin, E.L. Goldstein, and R.W. Tkach, "On the expandability of free-space micromachined optical cross connects," *IEEE Journal of Lightwave Technology*, vol. 18, no. 4, pp. 482–489, April 2000.

[156] J.I. Dadap et al., "Modular MEMS-based optical cross-connect with large port-count," *IEEE Photonics Technology Letters*, vol. 15, no. 12, pp. 1773 – 1775, December 2003.

[157] K. Bergman, "Overview of high capacity optical cross-connects," in *Proceedings of the 14th Annual Meeting of the IEEE LEOS 2001*, November 2001, vol. 1, pp. 224 – 225.

[158] *Glimmerglass, http://www.glimmerglass.com.*

[159] *NEL NTT Electronics Corp., http://www.nel-world.com.*

[160] *Dupont Photonix, http://www.photonics.dupont.com.*

[161] *SpectraSwitch, http://www.spectraswitch.com.*

[162] *Agilent Technologies, http://www.agilent.com.*

[163] *Light Management Group, Inc., http://www.lmgr.net/data05.htm.*

[164] *Lynx Photonic Networks, http://www.lynxnetworks.com.*

[165] *Yokogawa Electric Corporation, http://www.yokogawa.com.*

[166] *Kamelian, www.kamelian.com.*

[167] M.J. Potasek, "All-optical switching for high bandwidth optical network," *Optical Networks Magazine*, vol. 3, no. 6, pp. 30–43, November/December 2002.

[168] G.I. Papadimitriou, Ch. Papazoglou, and A.S. Pomportsis, "Optical switching: Switch fabrics, techniques, and architectures," *IEEE Journal of Lightwave Technology*, vol. 21, no. 2, pp. 384–405, February 20032.

[169] P.J. Duthie, N. Shaw, M. Wale, and I. Bennion, "Guided wave switch array using electro-optical and carrier depletion effects in indium phosphide," *Electronics Letters*, vol. 27, no. 19, pp. 1747–1748, 1991.

[170] H. Herrmann et al., "Advanced integrated, acousto-optical switches, add-drop multiplexers and WDM cross-connects in $LiNbO_3$," in *Proceedings of European Conference on Optical Communication (ECOC)*, Stockholm, Sweden, September 1997, pp. 578–581.

[171] M. Bachmann et al., "Crosstalk-reduced DOS with high fabrication tolerances designed for InGaAsP/InP," in *Proceedings of European Conference on Optical Communication (ECOC)*, Oslo, Norway, September 1996, vol. 3, pp. 261–264.

[172] M. Renaud, M. Bachmann, and M. Erman, "Semiconductor optical space switches," *IEEE Journal on Selected Topics in Quantum Electronics*, vol. 2, no. 2, pp. 277–288, June 1996.

[173] K. Sato, S. Okamoto, and H. Hadama, "Network performance and integrity enhancement with optical path layer technologies," *IEEE Journal on Selected Areas in Comminications*, vol. 12, no. 1, pp. 159–170, January 1994.

[174] R. Ramaswami and K.N. Sivarajan, *Optical Networks: A Practical Perspective.*, Morgan Kaufmann Publishers, Inc., San Francisco, California, 1998.

[175] P. Gambini et al., "Transparent optical packet switching: Network architecture and demonstrators in the KEOPS project," *IEEE Journal on Selected Areas in Communications*, vol. 16, no. 7, September 1998.

[176] *Intel, http://www.intel.com.*

[177] C. Joergensen et al., "All-optical wavelength conversion at bit rates above 10 Gbit/s using semiconductor optical amplifiers," *IEEE Journal of Selected Topics in Quantum Electronics*, vol. 3, pp. 1168–1180, October 1997.

[178] S.L. Danielsen et al., "Bit error rate assessment of 40 Gbit/s all-optical polarisation independent wavelength converter," *Electronics Letters*, vol. 32, no. 18, pp. 1688 – 1689, August 1996.

[179] C. Joergensen et al., "40 Gbit/s all-optical wavelength conversion by semiconductor optical amplifiers," *Electronics Letters*, vol. 32, no. 4, pp. 367–368, February 1996.

[180] X. Zheng, F. Liu, and A. Kloch, "Experimental investigation of the cascadability of a cross-gain modulation wavelength converter," *IEEE Photonics Technology Letters*, vol. 12, no. 3, pp. 272–274, March 2000.

[181] C. Joergensen et al., "Wavelength conversion by optimized monolithic integrated mach-zehnder interferometer," *IEEE Photonics Technology Letters*, vol. 8, no. 4, pp. 521–523, April 1996.

[182] L.H. Spiekman et al., "All-optical mach-zehnder wavelength converter with monolithically integrated preamplifiers," *IEEE Photonics Technology Letters*, vol. 10, no. 8, pp. 1115–1117, August 1998.

[183] J. Leuthold et al., "All-optical mach-zehnder interferometer wavelength converters and switches with integrated data- and control-signal separation scheme," *IEEE Journal of Lightwave Technology*, vol. 17, no. 6, pp. 1056–1066, June 1999.

[184] H.J. Song, J.S. Lee, and J.I. Song, "Signal up-conversion by using a cross-phase-modulation in all-optical SOA-MZI wavelength converter," *IEEE Photonics Technology Letters*, vol. 16, no. 2, pp. 593–595, February 2004.

[185] M.L. Masanovic et al., "Design and performance of a monolithically integrated widly tunable all-optical wavelength converter with independent phase control," *IEEE Photonics Technology Letters*, vol. 16, no. 10, pp. 2299–2301, October 2004.

[186] F. Ratovelomanana et al., "Monolithic integration of a Michelson all-optical wavelength converter," in *Proceedings of Optical Fiber Communication Conference (OFC)*, March 1996, pp. 124–125.

[187] S.L. Danielsen et al., "All optical wavelength conversion schemes for increased input power dynamic range," *IEEE Photonics Technology Letters*, vol. 10, no. 1, pp. 60–62, January 1998.

[188] D. Wolfson et al., "Experimental and theoretical investigation of electro-optic and all-optical implementations of wavelength converting 2R-regenerators," in *Proceedings of Optical Fiber Communication Conference (OFC)*, March 1998, number WB3, pp. 103–105.

[189] D. Wolfson et al., "All-optical 2R regeneration at 40 Gbit/s in an SOA-based Mach-Zehnder interferometer," in *Proceedings of Optical Fiber Communication Conference (OFC)*, March 1999, number PD36.

[190] B. Mikkelsen et al., "Opto-electronic and all-optical wavelength translators and their cascadability," in *Proceedings of Optical Fiber Communication Conference (OFC)*, March 1999, pp. 146–148.

[191] D.F. Geraghty et al., "Wavelength conversion for WDM communication systems using four-wave mixing in semiconductor optical amplifiers," *IEEE Journal of Selected Topics in Quantum Electronics*, vol. 3, no. 5, pp. 1146–1155, October 1997.

[192] R.B. Lee et al., "Cascaded wavelength conversion by four-wave mixing in a strained semiconductor optical amplifier at 10 Gb/s," *IEEE Photonics Technology Letters*, vol. 9, no. 6, pp. 752–754, June 1997.

[193] S. Diez et al., "Four-wave mixing in semiconductor optical amplifiers for frequency conversion and fast optical switching," *IEEE Journal of Selected Topics in Quantum Electronics*, vol. 3, no. 5, pp. 1131–1145, October 1997.

[194] J. Yu et al., "40-Gb/s all-optical wavelength conversion based on a nonlinear optical loop mirror," *IEEE Journal of Lightwave Technology*, vol. 18, no. 7, pp. 1001–1006, July 2000.

[195] M.C. Cardakli et al., "All-optical time-slot-interchange and wavelength conversion using difference-frequency-generation and FBGs," in *Proceedings of Optical Fiber Communication Conference (OFC)*, March 2000, vol. 4, pp. 196–198.

[196] N. Antoniades et al., "An architecture for a wavelength-interchanging cross-connect utilizing parametric wavelength converters," *IEEE Journal of Lightwave Technology*, vol. 17, no. 7, pp. 1113–1125, July 1999.

[197] *ANDevices Inc. ANDevices Inc., http://www.andevices.com.*

[198] S. Kobayashi et al., "Novel waveguide Y-branch for low-loss 1 x N splitters," in *Proceedings of Optical Fiber Communication Conference (OFC)*, 1992, vol. 1.

[199] Y. Shani et al., "Buried Rib passive waveguide Y junctions with sharp vertex on InP," *IEEE Photonics Technology Letters*, vol. 3, 1991.

[200] M. Zirngibl et al., "Efficient 1 x 16 optical power splitter based on InP," *Electronics Letters*, vol. 28, no. 13, pp. 1212–1213, June 1992.

[201] H. Takahashi, Y.Ohmori, and M. Kawachi, "Design and fabrication of silica-based integrated-optic 1 x 128 power splitter," *Electronics Letters*, vol. 27, no. 23, pp. 2131–2133, November 1991.

[202] D. Chiaroni et al., "High performance semiconductor optical amplifier gate for fast WDM packet switching," in *Proceedings of European Conference on Optical Communication (ECOC)*, September 1995, vol. 1.

[203] B. Mikkelsen et al., "High performance semiconductor optical amplifiers as in-line- and pre-amplifiers," in *Proceedings of European Conference on Optical Communication (ECOC)*, Florence Italy, September 1994, vol. 2, pp. 710–713.

[204] N. Sahri et al., "A highly integrated 32-SOA gates optoelectronic module suitable for IP multi-terabit optical packet routers," in *Proceedings of Optical Fiber Communication Conference (OFC)*, Marcoussis, France, 2001, vol. 4.

[205] F. Masetti et al., "Design and implementation of a multi-Terabit optical burst/packet router prototype," in *Proceedings of Optical Fiber Communication Conference (OFC)*, Anaheim, California, USA, March 2002, vol. 1, pp. FD11 – FD13.

[206] D. Chiaroni et al., "Physical and logical validation of a network based on all-optical packet switching systems," *IEEE Journal of Lightwave Technology*, vol. 16, no. 12, pp. 2255–2264, December 1998.

[207] H. Feng, E. Patzak, and J. Saniter, "Physikalische Grenzen von Broadcast and Select-Schaltknoten für Optical Burst Switching," in *Proceedings of 3. ITG-Fachtagung Photonische Netze*, Leipzig, Germany, April 2002.

[208] H. Feng, E. Patzak, and J. Saniter, "Size and cascadability limits of SOA based burst switching nodes," in *Proceedings of European Conference on Optical Communication (ECOC)*, Kopenhagen, September 2002.

[209] D. Sadot and E. Boimovich, "Tunable optical filters for dense WDM networks," *IEEE Communications Magazine*, vol. 36, pp. 50–55, January 1998.

[210] D.D. Marcenac, A.E.Kelly, D.Nesset, and D.A.O. Davies, "Bandwidth enhancement of wavelength conversion by semiconductor optical amplifier cascade," *Electronics Letters*, vol. 31, no. 17, pp. 1442–1443, January 1995.

[211] A.E. Kelly et al., "Low noise figure (7.2 dB) and high gain (29 dB) semiconductor optical amplifier with single layer AR coating," *Electronics Letters*, vol. 33, no. 6, pp. 536–538, March 1997.

[212] D. Sigogne et al., "1.55 μm polarisation insensitive InGaAsP strained MQW optical amplifier integrated with short spot-size converters," *Electronics Letters*, vol. 32, no. 15, pp. 1403–1405, July 1996.

[213] K. Morito et al., "High saturation output power (+17 dBm) 1550 nm polarisation insensitive semiconductor optical amplifier," in *Proceedings of European Conference on Optical Communication (ECOC)*, 2000, vol. 1, pp. 39–41.

[214] P. Dousierre et al., "1.55 μm polarization independent semiconductor optical amplifier with 25 dB fiber to fiber gain," *IEEE Photonics Technology Letters*, vol. 6, no. 2, pp. 170–172, February 1994.

[215] M. Bachmann, P. Doussière, J.Y. Emery, R. NǴo, F. Pommereau, L. Goldstein, G. Soulage, and A. Jourdan, "Polarisation-insensitive clamped-gain SOA with integrated spot-size convertor and DBR gratings for WDM applications at 1.55μm wavelength," *Electronics Letters*, vol. 32, no. 22, pp. 2076–2078, 1996.

[216] L.H. Spiekman, G.N. van den Hoven, T. van Dongen, M.J.H. Sander-Jochem, J.J.M. Binsma, J.M. Wiesenfeld, A.H. Gnauck, and L.D. Garrett, "Recent advances in WDM applications od semiconductor optical amplifiers," in *Proceedings of European Conference on Optical Communication (ECOC)*, Munich, Germany, September 2000, pp. 35–38.

[217] *Finisar, www.finisar.com.*

[218] *Fionix, Inc., http://www.fionix.com.*

[219] A. Borghesani et al., "High saturation power (>16.5 dBm) and low noise figure (<6 dB) semiconductor optical amplifier for C-band operation," in *Proceedings of Optical Fiber Communication Conference (OFC)*, 2003, number ThO, pp. 534–536.

[220] M.H. Hu et al., "Outband optical modulation technique for measuring intrinsic dynamics of semiconductor optical amplifier," in *Proceedings of Optical Fiber Communication Conference (OFC)*, 2004, number MF44.

[221] A. Ougazzaden et al., "Atmospheric pressure MOVPE growth of high performance polarisation insensitive strain compensated MQW InGaAsP/InGaAs optical amplifier," *Electronics Letters*, vol. 31, no. 15, pp. 1242–1244, April 1995.

[222] M. Sugawara, "Quantum-dot semiconductor optical amplifiers," in *Proceedings of Optical Fiber Communication Conference (OFC)*, March 2003, pp. 537–539.

[223] T. Akiyama et al., "An ultrawide-band (120 nm) semiconductor optical amplifier having an extremely-high penalty-free output power of 23 dBm realized with quantum-dot active layers," in *Proceedings of Optical Fiber Communication Conference (OFC)*, 2004, number PDP12.

[224] L. Lablonde, I. Valiente, P. Lamouler, E. Delevaque, S. Boj, and J.C. Simon, "Experimental and theoretical investigation of a gain clamped semiconductor optical amplifier," in *Proceedings of European Conference on Optical Communication (ECOC)*, Florence, Italy, September 1994, pp. 2.715–2.718.

[225] G. Soulage, P. Doussiere, A. Jourdan, and M. Sotom, "Clamped gain travelling wave semiconductor optical amplifier as a large dynamic range optical gate," in *Proceedings of European Conference on Optical Communication (ECOC)*, Florence, Italy, September 1994, pp. 1.451–1.454.

[226] P. Doussiere et al., "1550 nm polarisation independent DBR gain clamped SOA with high dynamic input power range," in *Proceedings of European Conference on Optical Communication (ECOC)*, Oslo, September 1996, vol. 3, pp. 169–172.

[227] J.C. Simon et al., "Travelling wave semiconductor optical amplifier with reduced nonlinear distortions," *Electronics Letters*, vol. 30, no. 1, pp. 49–50, January 1994.

[228] D.A. Francis, S.P. DiJaili, and J.D. Walker, "A single-chip linear optical amplifier," in *Proceedings of Optical Fiber Communication Conference (OFC)*, Anaheim, California, USA, March 2001, number PD13.

[229] E. Tangdiongga et al., "Performance analysis of linear optical amplifiers in dynamic WDM systems," *IEEE Photonics Technology Letters*, vol. 14, no. 8, pp. 1196–1198, August 2002.

[230] J.J.J. Crijns et al., "8 cascaded linear optical amplifiers in a 200-km 8 x 10-Gb/s, metro WDM ring featuring static and dynamic switching of channels," in *Proceedings of European Conference on Optical Communication (ECOC)*, September 2002, number 6.4.6.

[231] F. Dorgeuille et al., "First array of 8 GC-SOA gates for large-scale WDM space switches," in *Proceedings of European Conference on Optical Communication (ECOC)*, Madrid, Spain, September 1998, pp. 255–256.

[232] F. Dorgeuille et al., "1.28 Tbit/s throughput 8 x 8 optical switch based on gain-clamped semiconductor optical amplifier gates," in *Proceedings of Optical Fiber Communication Conference (OFC)*, 2000, vol. 1.

[233] E. Voges and K. Petermann, *Optische Kommunikationstechnik*, Springer Verlag, Berlin/Heidelberg, 2002.

[234] T. Durhuus, *Semiconductor Optical Amplifiers: Amplification and Signal Processing*, Ph.D. thesis, Technical University of Denmark, Dept. of Eletromagnetic Systems, January 1995.

[235] C. Joergensen, *Optical Amplification and Processing in High-Capacity Photonic Networks*, Ph.D. thesis, Technical University of Denmark, Dept. of Eletromagnetic Systems, March 1997.

[236] J.L. Pleumeekers et al., "Longitudinal spatial hole burning and associated nonlinear gain in gain-clamped semiconductor optical amplifiers," in *IEEE Journal of Quantum Electronics*, May 1998, vol. 34, pp. 879–886.

[237] G. Giuliani and D. D'Alessandro, "Noise analysis of conventional and gain-clamped semiconductor optical amplifiers," *IEEE Journal of Lightwave Technology*, vol. 18, no. 9, pp. 1256–1263, September 2000.

[238] R. Ludwig, *Experimental Investigations on Semiconductor Laser Amplifiers for Optical Communications*, Ph.D. thesis, Elektrotechnik und Informatik der Technischen Universität Berlin, 1992.

[239] G.P. Agrawal and N. K. Dutta, *Long-Wavelength Semiconductor Lasers*, Van Nostrand Reinhold Company Inc., New York, 1986.

[240] K. Petermann, *Laser diode modulation and noise*, Kluwer Academic, Dordrecht/Boston/London, 1988.

[241] J. Hörer and E. Patzak, "Large-signal analysis of all-optical wavelength conversion using two-mode injection-locking in semiconductor lasers," *IEEE Journal of Quantum Electronics*, vol. 33, no. 4, pp. 596–608, April 1997.

[242] W. Harth and H. Grothe, *Sende- und Empfangsdioden für die Optische Nachrichtentechnik*, Teubner-Studienskripten, Stuttgart, 1984.

[243] I.D. Henning et al., "Performance predictions from a new optical amplifier model," *IEEE Journal of Quantum Electronics*, vol. 21, no. 6, pp. 609–613, Juni 1985.

[244] B.R. Bennett, "Carrier induced change in refractive index of InP, GaAs, and InGaAsP," *IEEE Journal of Selected Topics in Quantum Electronics*, vol. 26, pp. 113 – 122, Janunary 1990.

[245] J.M. Simmons, "Analysis of wavelength conversion in all-optical express backbone networks," in *Proceedings of Optical Fiber Communication Conference (OFC)*, 2002, number TuG2, pp. 34–36.

[246] O. Gerstel, R. Ramaswami, and S. Foster, "Merits of hybrid networking," in *Proceedings of Optical Fiber Communication Conference (OFC)*, 2002, number TuG1, pp. 33–34.

[247] C. Caspar, "Dispersions-Management für transparent WDM-Weitverkehrsnetze," in *Beiträge zur 2. ITG Fachtagung Photonische Netze*, Dresden, Germany, March 2001, pp. 179–183.

[248] C. Peucheret, N. Hanik, R. Freund, L. Molle, and P. Jeppesen, "Optimization of pre- and post-dispersion compensation schemes for 10-Gbits/s NRZ links using standard and dispersion compensating fibers," *IEEE Photonics Technology Letters*, vol. 12, no. 8, pp. 992–994, August 2000.

[249] T. Gyselings et al., "Crosstalk analysis of multiwavelength optical cross connects," *IEEE Journal of Lightwave Technology*, vol. 17, no. 8, pp. 1273–1283, August 1999.

[250] E. Desurvire et al., *Ebium-Doped Fiber Amplifiers - Device and System Developments*, John Wiley & Sons, Inc, 2002.

[251] A. Richter, *Timing Jitter in Long-haul WDM Return-to-Zero Systems*, Ph.D. thesis, Elektrotechnik und Informatik der Technischen Universität Berlin, 2002.

[252] A. Hodžić, *Investigations of high bit rate optical transmission systems employing a channel data rate of 40 Gb/s*, Ph.D. thesis, Elektrotechnik und Informatik der Technischen Universität Berlin, 2004.

[253] R. Freund, *On Computer Aided Modeling of Photonics Systems and Networks*, Ph.D. thesis, Technische Universität Ilmenau, 2002.

[254] G.P. Agrawal, *Nonlinear Fiber Optics*, Academic Press, 3. Edition, 2001.

[255] K. Petermann, *Einführung in die optische Nachrichtentechnik*, Vorlesungsskript, Technische Universität Berlin, 2003.

[256] H. Buchta, E. Patzak, J. Saniter, and C.M. Gauger, "Maximal and effective throughput of optical switching nodes for optical burst switching," in *Proceedings of 4. ITG-Fachtagung Photonische Netze*, Leipzig, Germany, May 2003.

[257] H. Buchta, E. Patzak, J. Saniter, and F. Raub, "Impact of SOA gain saturation and dynamics on the throughput of optical burst switching nodes," in *Proceedings of Optical Fiber Communication Conference (OFC)*, Los Angeles, USA, February 2004.

[258] R. Elschner, "Untersuchung des dynamischen Sättigungsverhaltens von gain-clamped optischen Halbleiterlaserverstärkern beim Einsatz als Schalter für optische Burst-Schaltknoten," Studienarbeit, Technische Universität Berlin, 2002.

[259] N. Hanik et al., "Extension of all-optical network-transparent domains based on normalized transmission sections," *IEEE Journal of Lightwave Technology*, vol. 22, no. 6, pp. 1439–1453, June 2004.

[260] H. Buchta and E. Patzak, "Impact of modulation formats and SOA chirp on the throughput of SOA based OBS nodes," in *Proceedings of Optical Fiber Communication Conference (OFC)*, Anaheim, California, USA, March 2005.

[261] H. Buchta, E. Patzak, J. Saniter, and C.M. Gauger, "Limits of effective throughput of optical burst switches based on semiconductor optical amplifiers," in *Proceedings of Optical Fiber Communication Conference (OFC)*, Atlanta, Georgia, March 2003.

[262] P.J. Kühn, *Teletraffic Theory and Engineering*, Lecture at University Stuttgart, 2002/2003.

[263] L. Kleinrock, *Queueing Systems - Volume I: Theory*, John Wiley & Sons, New York, 1975.

[264] J.E. Simsarian et al., "A widely tunable laser transmitter with fast, accurate switching between all channel combinations," in *Proceedings of European Conference on Optical Communication (ECOC)*, Copenhagen, Denmark, September 2002, number 3.3.6.

[265] J. Gripp et al., "4x4 demonstration of a 1.2 Tb/s (32 x 40 Gb/s) optical switch fabric for multi-Tb/s packet routers," in *Proceedings of European Conference on Optical Communication (ECOC)*, Copenhagen, Denmark, September 2002, number PD2.4.

[266] C.M. Gauger, H. Buchta, E. Patzak, and J. Saniter, "Performance meets technology - an integrated evaluation of OBS nodes with FDL buffers," in *Proceeding of the first International Workshop on Optical Burst Switching (WOBS 2003)*, Dallas/TX, October 2003.

[267] X. Wei, Y. Su, X. Liu, J. Leuthold, and C. Chandrasekhar, "10 Gb/s RZ-DPSK transmitter using a saturated SOA as power booster and limiting amplifier," *IEEE Photonics Technology Letters*, vol. 16, no. 6, pp. 1582–1584, Juny 2004.

[268] L.C. Chen K. Chan, C.-K. Chan and F. Tong, "Mitigation of pattern-induced degradation in SOA-based all-optical OTDM demultiplexers by using RZ-DPSK modulation format," *IEEE Photonics Technology Letters*, vol. 15, no. 9, pp. 1264–1266, 2003.

[269] P.S. Cho and J.B. Khurgin, "Suppression of cross-gain modulation in SOA using RZ-DPSK modulation format," *IEEE Photonics Technology Letters*, vol. 15, no. 1, pp. 162–164, 2003.